# INVESTIGATION ON COUPLING ORGANIC RANKINE CYCLE WITH A SHALLOW GROUND-BASED COOLING SYSTEM


By

Montaser Mahmoud

B.Sc.Eng, M.Sc.Eng


A thesis submitted for the degree of Doctor of Philosophy


Department of Mechanical Engineering and Aeronautics

School of Mathematics, Computer Science and Engineering

City, University of London


August 2022

Supervisors

Dr. Sumsun Naher

Dr. Mohamad Ramadan

# Preface

This research study depicts original work which has not been previously submitted in City University of London or any other university. The study was carried out in the Department of Mechanical Engineering and Aeronautics, School of Mathematics, Computer Science and Engineering, City University of London during the period 2019 to 2022. This research was supervised by Dr. Sumsun Naher and Dr. Mohamad Ramadan. This work has been disseminated through the following publications.

**Journal Papers:**

- Montaser Mahmoud, Mohammad Alkhedher, Mohamad Ramadan, Keith Pullen, Abdul-Ghani Olabi, Sumsun Naher, Experimental investigation into the potential of using a shallow ground-cooled condenser in Lebanon, Energy Conversion and Management, Volume 264, 2022, 115729, ISSN 0196-8904, https://doi.org/10.1016/j.enconman.2022.115729.
- Montaser Mahmoud, Mohamad Ramadan, Keith Pullen, Mohammad A. Abdelkareem, Abdul Ghani Olabi, Sumsun Naher, An Investigation on Nano-Enhanced Phase Change Materials: Carbon-Based Nanoparticles, Key Engineering Materials, Volume 922, 2022, ISSN 1662-9795, https://doi.org/10.4028/p-m17i9f.
- Montaser Mahmoud, Mohammad Alkhedher, Mohamad Ramadan, Sumsun Naher, Keith Pullen, An investigation on organic Rankine cycle incorporating a ground-cooled condenser: Working fluid selection and regeneration, Energy, Volume 249, 2022, 123742, ISSN 0360-5442, https://doi.org/10.1016/j.energy.2022.123742.
- Montaser Mahmoud, Mohamad Ramadan, Sumsun Naher, Keith Pullen, Abdul-Ghani Olabi, $CO_2$ – Based transcritical Rankine cycle coupled with a ground-cooled condenser, Thermal

Science and Engineering Progress, Volume 25, 2021, 100948, ISSN 2451-9049, https://doi.org/10.1016/j.tsep.2021.100948.

- Montaser Mahmoud, Mohamad Ramadan, Keith Pullen, Mohammad Ali Abdelkareem, Tabbi Wilberforce, Abdul-Ghani Olabi, Sumsun Naher, A review of grout materials in geothermal energy applications, International Journal of Thermofluids, 2021, 100070, ISSN 2666-2027, https://doi.org/10.1016/j.ijft.2021.100070.
- Montaser Mahmoud, Mohamad Ramadan, Sumsun Naher, Keith Pullen, Mohammad Ali Abdelkareem, Abdul-Ghani Olabi, A review of geothermal energy-driven hydrogen production systems, Thermal Science and Engineering Progress, Volume 22, 2021, 100854, ISSN 2451-9049, https://doi.org/10.1016/j.tsep.2021.100854.
- Montaser Mahmoud, Mohamad Ramadan, Sumsun Naher, Keith Pullen, Abdul-Ghani Olabi, The impacts of different heating systems on the environment: A review, Science of The Total Environment, Volume 766, 2021, 142625, ISSN 0048-9697, https://doi.org/10.1016/j.scitotenv.2020.142625.
- Montaser Mahmoud, Mohamad Ramadan, Sumsun Naher, Keith Pullen, Ahmad Baroutaji, Abdul-Ghani Olabi, Recent advances in district energy systems: A review, Thermal Science and Engineering Progress, Volume 20, 2020, 100678, ISSN 2451-9049, https://doi.org/10.1016/j.tsep.2020.100678.
- Montaser Mahmoud, Mohamad Ramadan, Abdul-Ghani Olabi, Keith Pullen, Sumsun Naher, A review of mechanical energy storage systems combined with wind and solar applications, Energy Conversion and Management, Volume 210, 2020, 112670, ISSN 0196-8904, https://doi.org/10.1016/j.enconman.2020.112670.

- Abdul Ghani Olabi, Montaser Mahmoud, Bassel Soudan, Tabbi Wilberforce, Mohamad Ramadan, Geothermal based hybrid energy systems, toward eco-friendly energy approaches, Renewable Energy, Volume 147, Part 1, 2020, Pages 2003-2012, ISSN 0960-1481, https://doi.org/10.1016/j.renene.2019.09.140.

**Chapters:**

- Montaser Mahmoud, Mohamad Ramadan, Keith Pullen, Mohammad A. Abdelkareem, Abdul H. Alami, Abdul-Ghani Olabi, Sumsun Naher, Using Nanoparticles for Thermal Enhancement of Phase Change Materials, Encyclopedia of Smart Materials, Elsevier, Volume 3, 2022, Pages 281-287, ISBN 9780128157336, https://doi.org/10.1016/B978-0-12-815732-9.00111-X.
- Montaser Mahmoud, Keith Pullen, Mohamad Ramadan, Ahmad Baroutaji, Mohammad A. Abdelkareem, Abdul-Ghani Olabi, Sumsun Naher, Phase Change Materials Integrated Into Solar Parabolic Collectors, Encyclopedia of Smart Materials, Elsevier, Volume 2, 2022, Pages 613-620, ISBN 9780128157336, https://doi.org/10.1016/B978-0-12-815732-9.00084-X.
- Montaser Mahmoud, Mohamad Ramadan, Keith Pullen, Mohammad A. Abdelkareem, Ahmad Baroutaji, Abdul-Ghani Olabi, Sumsun Naher, Advances in Shape-Stabilized Phase Change Materials, Encyclopedia of Smart Materials, Elsevier, Volume 4, 2022, Pages 326-333, ISBN 9780128157336, https://doi.org/10.1016/B978-0-12-815732-9.00094-2.
- Montaser Mahmoud, Mohamad Ramadan, Keith Pullen, Mohammad A. Abdelkareem, Abdul H. Alami, Abdul-Ghani Olabi, Sumsun Naher, Foam-Based Composite Phase Change Materials, Encyclopedia of Smart Materials, Elsevier, Volume 4, 2022, Pages 343-351, ISBN 9780128157336, https://doi.org/10.1016/B978-0-12-815732-9.00083-8.
- Montaser Mahmoud, Mohamad Ramadan, Keith Pullen, Mohammad A. Abdelkareem, Tabbi Wilberforce, Abdul-Ghani Olabi, Sumsun Naher, Waste Heat Recovery Applications

Incorporating Phase Change Materials, Encyclopedia of Smart Materials, Elsevier, Volume 2, 2022, Pages 513-521, ISBN 9780128157336, https://doi.org/10.1016/B978-0-12-815732-9.00074-7.

- Montaser Mahmoud, Mohamad Ramadan, Sumsun Naher, Keith Pullen, Mohammad A. Abdelkareem, Ahmad Baroutaji, Abdul-Ghani Olabi, Investigation on the Use of Phase Change Materials in Geothermal Energy Applications, Encyclopedia of Smart Materials, Elsevier, Volume 4, 2022, Pages 352-361, ISBN 9780128157336, https://doi.org/10.1016/B978-0-12-815732-9.00059-0.
- Montaser Mahmoud, Mohamad Ramadan, Sumsun Naher, Keith Pullen, Abdul-Ghani Olabi, Advances in Grout Materials in Borehole Heat Exchangers, Encyclopedia of Smart Materials, Elsevier, Volume 4, 2022, Pages 334-342, ISBN 9780128157336, https://doi.org/10.1016/B978-0-12-815732-9.00053-X.

**Conferences:**

- Montaser Mahmoud, Mohamad Ramadan, Keith Pullen, Abdul-Ghani Olabi, Sumsun Naher, An investigation on the effect of configuration on the performance of organic Rankine cycle incorporating a ground-cooled condenser, 13th International Conference on Sustainable Energy & Environmental Protection, SEEP, 13-16 September 2021, University of Natural Resources and Life Science, Vienna (BOKU), Austria.
- Montaser Mahmoud, Keith Pullen, Mohamad Ramadan, Abdul-Ghani Olabi, Sumsun Naher, Optimizing ground-cooled condenser in a Rankine cycle using phase change materials, 7th International Conference on Materials Science and Smart Materials, 4-6 August 2021, Brunel University London, UK.

- Montaser Mahmoud, Mohamad Ramadan, Keith Pullen, Abdul-Ghani Olabi, Sumsun Naher, An investigation on nano-enhanced phase change materials: Carbon-based nanoparticles, 7th International Conference on Materials Science and Smart Materials, 4-6 August 2021, Brunel University London, UK.
- Montaser Mahmoud, Mohamad Ramadan, Sumsun Naher, Keith Pullen and Abdul-Ghani Olabi. A review on mechanical energy storage systems combined with wind and solar applications. 12th International conference on Sustainable Energy and Environmental Protection, 18-21 November 2019, Sharjah University, UAE.
- Montaser Mahmoud, Mohamad Ramadan, Sumsun Naher, Keith Pullen and Abdul-Ghani Olabi. An investigation on the environmental impact of different heating systems: A review. 12th International conference on Sustainable Energy and Environmental Protection, 18-21 November 2019, Sharjah university, UAE.
- Montaser Mahmoud, Mohamad Ramadan, Sumsun Naher, Keith Pullen and Abdul-Ghani Olabi. An investigation on the effect of burning coal, natural gas, and wood on the environment. 6th International conference on material science and smart materials. July 2019 23-26. Aston University, UK.

## Declaration

I hereby certify that this research, which I now submit for assessment on the program of study leading to the award of Doctor of Philosophy is entirely my own work. This is an original work which has not been investigated before. All information used from previous studies have been cited to avoid breaching the copyright law.

# Dedication

This thesis is dedicated to my family for supporting me and providing all requirements to help me achieving my goals.

# Acknowledgements

First, I would like to thank my supervisors, Dr. Sumsun Naher and Dr. Mohamad Ramadan. They have always helped and supported me with all needed information, directions, motivations, and advice. I am grateful for their help and appreciate every moment they spent for supporting me. I would like also to thank Prof. Abdul-Ghani Olabi and Prof. Keith Pullen for their guidance and assistance in research publications. Their experience in the research domain has helped me developing my skills and improving immensely my thesis and publications.

# Abstract

In this research, a new power system is proposed which is formed of an organic Rankine cycle combined with a shallow ground-cooled condenser. The aim is to investigate a ground-based cooling system to enhance the performance of the power cycle in terms of net output power. This combination is beneficial for power generation, especially in summer because the ground is more effective than that of the ambient air as a heat sink for the condenser due to its lower temperature. A primary heat rejector is also added to the cycle to ensure stability, avoid heat accumulation, and provide coolth compensation. The study includes experimental, analytical, and numerical investigations under several cycle conditions (temperatures and pressures) and working fluids ($CO_2$, R123, R124, and R245fa). The experimental study was employed to examine the potential of shallow geothermal energy in Bekaa-Lebanon. The data collected from the experimental study was used as an input to the analytical and numerical analyses to assess the daily and annual performance. The software used are Engineering Equation Solver, Visual Basic and ANSYS Mechanical APDL. A cost analysis was carried out to evaluate the capital cost and payback period of the proposed system. The highest cycle's performance was achieved while using R123 in which the net output power was enhanced by 31.5% considering a waste heat source (diesel generator) with exhaust gas temperature of 500°C and mass flow rate of 150 kg/hr. Based on the numerical simulations, the soil thermal interference radius was evaluated as ~0.32 m after 8 hours of operation which is considered as the maximum operating duration of the diesel generator. The corresponding average capital cost and payback period of the proposed system were estimated as £34,941 and 3.7 years, respectively.

# Table of Contents

# List of Tables

# List of Figures

| **Nomenclature** | |
|---|---|
| ŋ | efficiency |
| $\dot{m}$ | mass flow rate (kg/s) |
| $\dot{Q}$ | heat transfer rate (W) |
| $\dot{W}$ | power (W) |
| $\Delta T_{lm}$ | logarithmic mean temperature difference |
| $A$ | area ($m^2$) |
| $D$ | diameter (m) |
| $h$ | heat transfer coefficient ($W/m^2.K$) |
| $k$ | thermal conductivity (W/m.K) |
| $L$ | length (m) |
| $L_r$ | characteristic length (m) |
| $n_c$ | number of coil turns |
| $Nu$ | Nusselt number |
| $p$ | pressure (MPa) |
| $p_c$ | coil pitch (m) |
| $Pr$ | Prandtl number |
| $r$ | radius (m) |
| $Ra$ | Rayleigh number |
| $Re$ | Reynolds number |
| $T$ | temperature (°C) |
| $t$ | time (hour) |
| $U$ | overall heat transfer coefficient ($W/m^2.K$) |
| $\sigma$ | stress (MPa) |
| *Abbreviations* | |
| ACR | auxiliary cooling ratio |
| AMIS® | abatement of mercury and hydrogen sulphide (in Italian language) |
| ANN | artificial neural network |
| ASHP | air source heat pump |
| ASME | American Society of Mechanical Engineers |
| BHE | borehole heat exchanger |
| BTES | borehole thermal energy storage |
| CLSM | controlled low-strength material |
| COP | coefficient of performance |
| CTRC | $CO_2$-based transcritical Rankine cycle |
| DCV | directional control valve |
| DG | deep geothermal |
| EAHE | earth-air heat exchanger |
| EES | Engineering Equation Solver |
| EGS | enhanced geothermal system |
| ESC | extremum seeking control |

| | |
|---|---|
| FL | fuzzy logic |
| GCS | ground cooling system |
| GE | geothermal energy |
| GHE | ground heat exchanger |
| GSHP | ground source heat pump |
| HDPE | high-density polyethylene |
| HGCHP | hybrid ground coupled heat pump |
| HGSHP | hybrid ground source heat pump |
| HVAC | heating, ventilating, and air conditioning |
| IDEC | indirect-direct evaporative cooling |
| LNG | liquefied natural gas |
| MDS | marine dredged soil |
| MPC | model predictive control |
| MPCM | microencapsulated phase change material |
| NCG | non-condensable gases |
| ORC | organic Rankine cycle |
| PCM | phase change materials |
| PEM | proton exchange membrane |
| PVT | photovoltaic thermal |
| RES | renewable energy source |
| SAGSHP | solar assisted ground source heat pump |
| TES | thermal energy storage |
| TRT | thermal response test |
| *Subscripts* | |
| $c$ | coil |
| $g$ | ground |
| $p$ | pump |
| $t$ | turbine |

# Chapter 1. Introduction

As the population of our planet increases, so does the need and demand for energy [1]. Until recently, this demand has been met mostly through the consumption of traditional fossil-based fuels. The consumption of these fuels has been shown to be directly linked to global warming, pollution, and a deterioration of air quality [2, 3]. A recent report published by the World Health Organization (WHO) released in May 2018 states that "*90 percent of people worldwide breathe polluted air*" [4]. There are also some other major issues that are influenced by energy-related systems such as $CO_2$ emissions, sea level rises and weather changes. Therefore, governments around the world are increasingly investing in renewable energy sources (RESs) as possible replacements of fossil-based fuels avoiding their harsh effects on the environment [5]. RESs can meet a significant portion of the energy demand without the harmful greenhouse gases and the associated pollution. One of the issues affecting most RESs is their stochastic and intermittent nature. The energy source is not available all the time, and sometimes it is not sufficient even when available. This is highly noticeable in solar and wind energy systems where it will be necessary to add energy storage systems [6, 7] especially in micro-grids and small district energy systems [8].

This is where geothermal energy (GE) has an advantage over most other RESs, its availability is approximately deterministic and independent of ambient conditions. It is attracting large interest from researchers and practitioners these days. As a renewable thermal energy resource, the potential of GE is estimated to be around ~40 million MW of generated power and is expected to remain a sustainable resource within the foreseeable future [9]. Several studies are available that underline the various advantages of utilizing this resource that provides near-constant heat and power [10]. While it may be geographically limited, wherever geothermal energy is present it is usable all the time at approximately the same level. GE has the added advantage of attaining lower operating cost compared to traditional systems [11, 12]. Another advantage of GE is that the energy reservoir (ground) can be a heat source as well as a heat sink depending on the need. Compared to air, soil has a much higher heat capacity. As a result, seasonal variations of deep soil temperature in the ground are much lower than that of the surrounding ambient air. At depths higher than about 20 meters, soil temperature becomes approximately constant year-round. This makes deep earth warmer than ambient air in the winter and cooler in the summer. Ground heat exchangers (GHEs) have been designed to leverage this air-to-soil differential to condition the ambient air temperature.

There are three different configurations of GHEs: vertical, horizontal, and coiled. The suitable type of GHE depends mainly on the available space and soil conditions. The horizontal configuration is typically constructed at a depth around 1.5 meters, while the vertical type reaches depths more than 50 meters [13]. Under appropriate circumstances, it is possible to create a combination of vertical and horizontal configurations that can produce better thermal performance and acceptable cost [14]. The GHE is usually surrounded by grout material (such as cement or a mixture of sand and bentonite) to protect ground water and improve heat transfer rate [15, 16]. Shallow geothermal energy is typically used in hybrid combinations because it is considered as a low-grade source of energy. GE has unequivocal potential for hybridization with different renewable resources. This helps achieving tangible operational cost reduction, low greenhouse gases emissions [17], enhanced efficiency, low fuel consumption, ground heat compensation and extended power plants lifespan [18].

### 1.1 Problem Statement

One of the main problems facing power cycles is the low efficiency in summer due to the high temperature of coolant compared to that of winter at the condenser's level when using ambient air as a cooling source. This makes the expansion of working fluid limited in the turbine leading to a decrease in the output power and efficiency. This problem is also more significant when the heat source temperature is not so high such as in most waste heat recovery systems which is considered in the current study. Another choice for cooling a power cycle is to use a cooling system to supply cold water to the condenser. However, this is still not a perfect replacement for the air-cooling system since it will consume additional amount of power instead of being supplied. This requires using a constant low temperature heat sink (ex: shallow geothermal energy). In this research, investigation on the use of ground cooling system will be carried out presenting its contribution to enhancing organic Rankine cycles. This is a new technology that will be introduced in this study to avoid the negative effect of high ambient air temperatures.

### 1.2 Aim and Objectives

The aim of this research study is to enhance the organic Rankine cycle using a shallow ground heat exchanger to increase its performance in terms of output power and cost. The ground will be used as a heat sink while the source of energy will be the exhaust gas of an engine. At the first stage, it is recommended to use underground water as a heat sink since it can extract heat from the working fluid better than that of soil. However, investigating the effect of using soil as a heat sink is also included in this research assuming that shallow underground water is not available in many regions. The following are the main objectives:

- Explore the effectiveness of incorporating ground-cooled condenser while studying the influence of cycle and heat source conditions.
- Investigate the potential of shallow geothermal energy in Bekaa-Lebanon by measuring the ground temperature reaching a depth of 2 m.

- Perform parametric and optimization studies to find the best operating temperature, pressure, configuration and working fluid.
- Study the feasibility of using the proposed system based on data collected from a real application.
- Compare the output power of the proposed and conventional systems to estimate the fuel savings and calculate the expected payback period.

### 1.3 Research Structure

This thesis contains 8 chapters namely, introduction, literature review, ground-cooled condenser investigation using EES, experimental study for ground temperature measurement, parametric study for system optimization, simulation of ground thermal distribution, waste heat recovery: application, and conclusions and future work. Figure 1.1 presents an overview of the methodology followed in this thesis. The first chapter presents an introduction to the current work, problem statement, objectives, and outline. Chapter 2 includes all details related to geothermal energy involving applications, heat exchangers, grout materials and hybrid geothermal energy systems. The main concept of ground-cooled condenser is explained in Chapter 3. The setup used and experimental data analysis are presented in Chapter 4 including a comparison between ground and ambient air temperatures in Bekaa-Lebanon during 2020. The optimization of the proposed system is exhibited in Chapter 5. It includes selecting the suitable working fluid and comparing the different configurations. The numerical simulations are presented in Chapter 6 using ANSYS software to evaluate the soil thermal interference radius. Chapter 7 aims to apply the concept presented in this research to a real application to check its economic and thermodynamic feasibility. The final conclusions are presented in Chapter 8 in addition to some recommendations that can be applied to the proposed system as a future work.

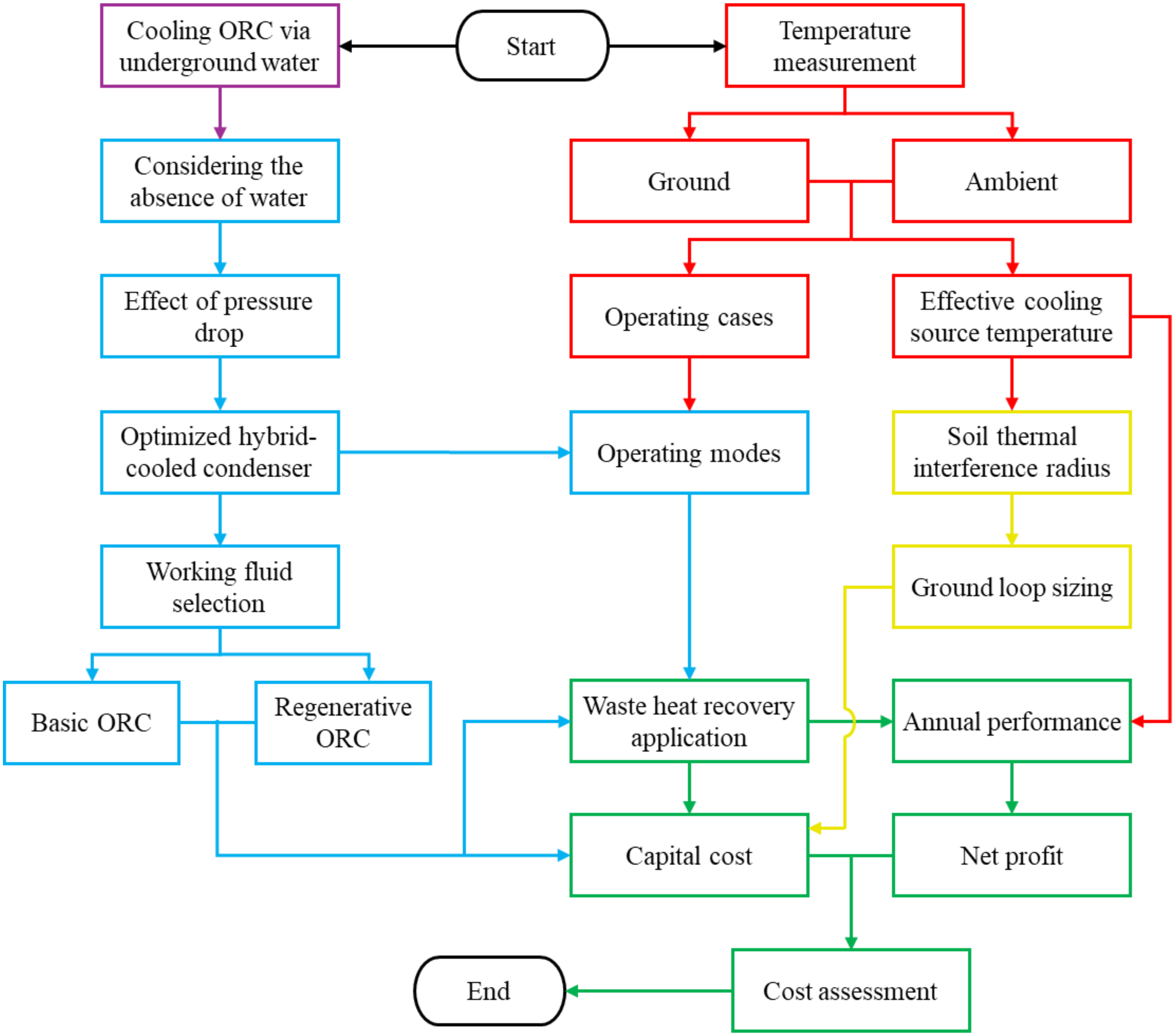


Figure 1.1: Thesis flow chart; Chapter 3 (purple), Chapter 4 (red), Chapter 5 (blue) Chapter 6 (yellow), and Chapter 7 (green)

# Chapter 2. Literature Review

GE has a wide variety of utilizations and can provide different types of outputs such as heating, cooling, and electricity. The adoption of GE-based systems helps reducing the dependency on fossil fuels and non-renewable resources while increasing the penetration of renewable energy. In other words, this encourages the use of natural resources and as a matter of fact, the environmental impacts will be significantly decreased and mainly due to the very low emissions resulting from GE systems. Furthermore, GE is characterized by stability which cannot be obtained from other renewable sources, and that is due to the independency from the atmospheric conditions.

The weight of scientific research on GE has been growing rapidly and can be clearly noticed from the evolution of the number of research papers with time. It can be easily recognized that the use of GE for heating holds the lion's share among the existing applications followed by cooling. Another interesting application that seems to be attracting increasing attention is hybridization in which GE is combined with other energy systems.

Several parameters affect the performance of GE systems depending on the considered application. The most effective parameters are soil properties (thermal conductivity, specific heat, density, temperature, etc.), depth, circulating fluid and ambient conditions. Figure 2.1 shows the main parameters that influence the efficiency of geothermal systems. To optimize the design of the system, these parameters should be analysed to avoid any failure.

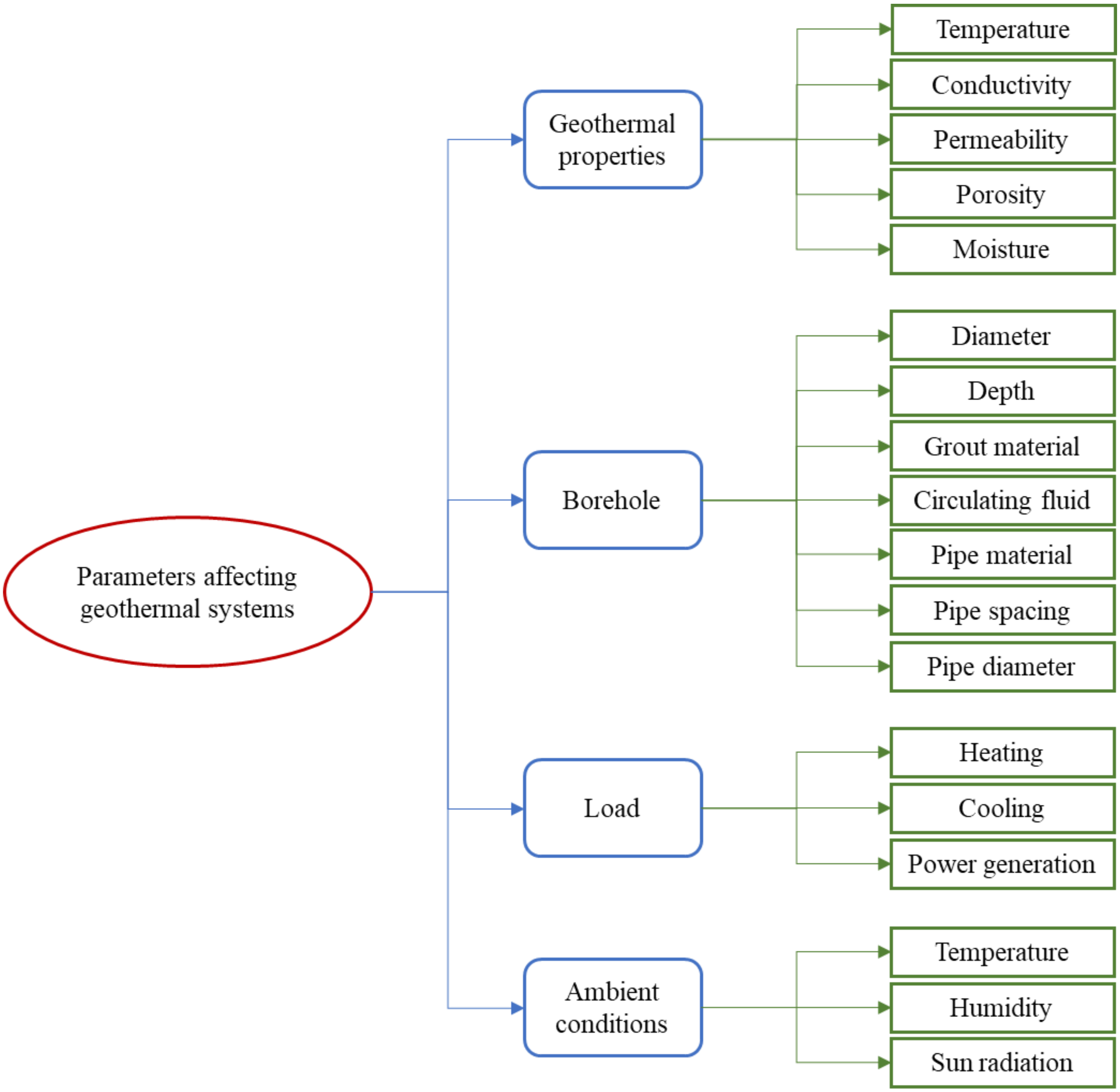


Figure 2.1: Parameters affecting geothermal energy systems

The major problem faced by GE systems is the high capital cost. The capital cost of this system must cover the installation and all materials used including pipes, grout material, turbomachines, working fluid, etc. Additional expenses maybe included if there is no free space enough within the owner's land. Therefore, the pre-study must involve the space needed for construction. In addition, it is necessary to ensure that the materials will not be damaged because it is difficult to perform the maintenance when needed which is also quite expensive. In fact, people are still afraid of using GE systems due the unexpected results that may appear later after installation because of the high dependency on several hidden underground factors. Thus, it is very essential to perform an accurate pre-study to avoid unforeseen troubles such as thermal pollution or unbalance.

### 2.1 Geothermal Energy Applications

The direct use of geothermal energy has exhibited a rapid increase in the past two decades. Indeed, the number of countries using geothermal energy has increased from 28 in 1995 to 82 countries in 2015 [19]. GE is mainly used for heating, cooling, power generation and hydrogen production. Several utilizations have also been introduced to GE such as energy storage, water desalination, bathing and swimming, aquaculture, snow melting and other uses.

#### 2.1.1 Heating and cooling

GE can be used for heating and cooling by the help of two different techniques: ground source heat pump (GSHP) [20] and earth-air heat exchanger (EAHE) [21]. The GSHP depends on the refrigeration cycle (see Figure 2.2) while the EAHE is based on circulating air under the ground via fan (see Figure 2.3). Each type offers various advantages based on different points of interest. The GSHP is more frequently used and has several advantages compared to the air source heat pump (ASHP) such as low energy consumption, stability, no need for supplemental heat at low outside temperatures, less use of refrigerant and no specific unit location. On the other hand, the high capital cost seems to be the major disadvantage of the GSHP which is 30% to 50% more than that of conventional air unit.

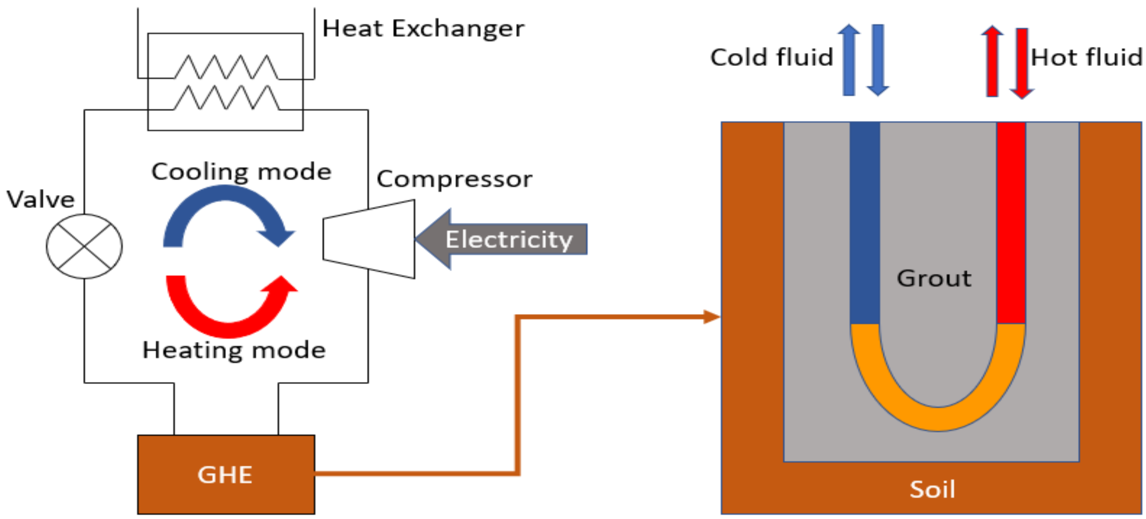


Figure 2.2: The ground source heat pump (GSHP) in heating and cooling modes

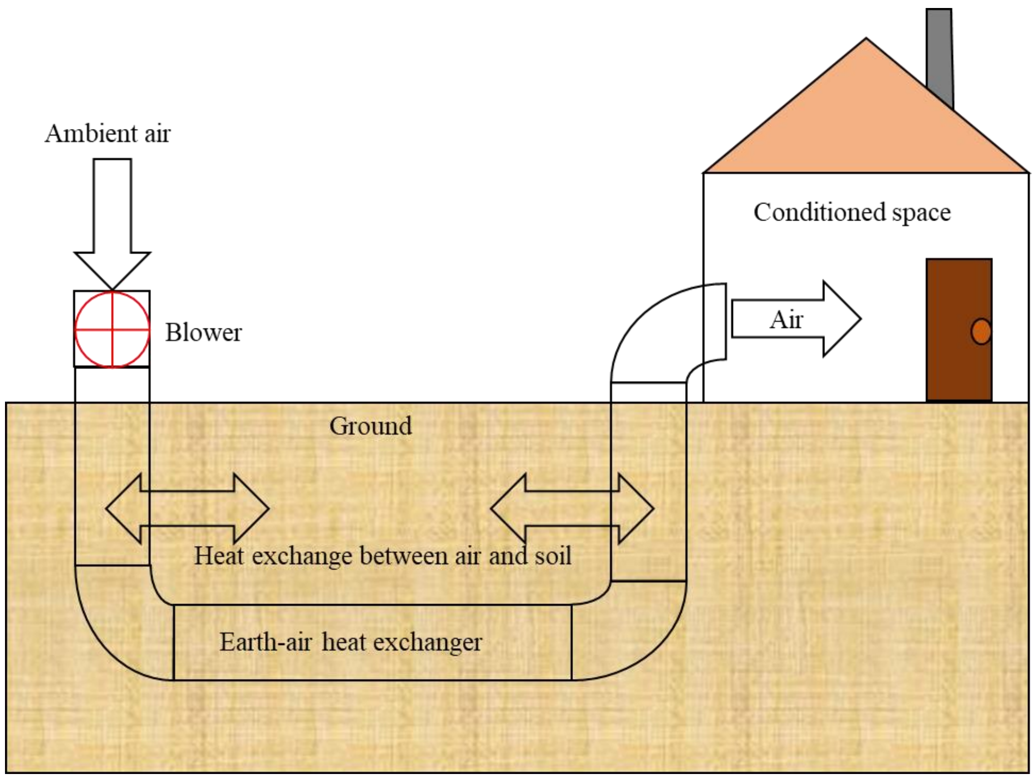


Figure 2.3: Earth-air heat exchanger (EAHE) system

Since 1990s, the number of geothermal heat pump installations have increased rapidly worldwide especially in US, China, Sweden, Germany, Japan, Switzerland, and Canada. From these previous installations, researchers found that pre-installation studies and accurate estimations are necessary for optimizing the considered system to conserve the hydrogeological conditions of the ground [10].

In Aljubury and Ridha [22], an experimental setup was constructed to increase the performance of the air-conditioning system by using the ground water as a working fluid (see Figure 2.4). It was reported that when the water flow rate increased from 1 to 4 L/s, the evaporative efficiency increased from 79.5% to 84.4%. As a result, using the ground water as a working fluid was found to be very powerful for cooling and ventilation applications.

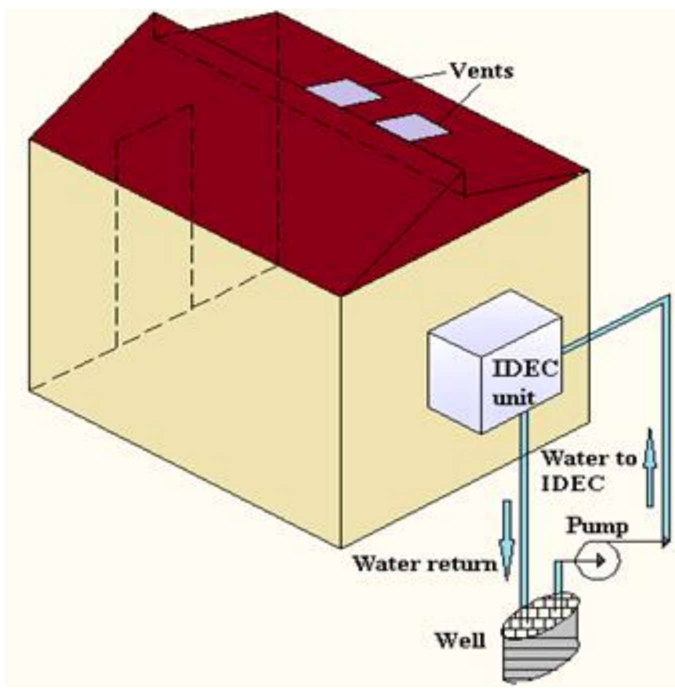


Figure 2.4: Using well water to activate the indirect-direct evaporative cooling (IDEC) system, reproduced from [22]

### 2.1.2 Power generation

Various power cycles can be utilized to generate power from the ground source even though it is considered as a low enthalpy source in most cases. Deep GE can be used as a source for power generation plants using an organic Rankine cycle (ORC) as an example. One of the common GE systems that are used for power generation is the enhanced geothermal system (EGS) [23, 24] (see Figure 2.5). The role of this system is to extract heat from hot dry rocks to benefit from GE with depths of several thousand meters. It relies on creating an artificial reservoir which means that there is no specific path for the fluid. It is only required to inject cold fluid into the reservoir and extract it then using a production pipe.

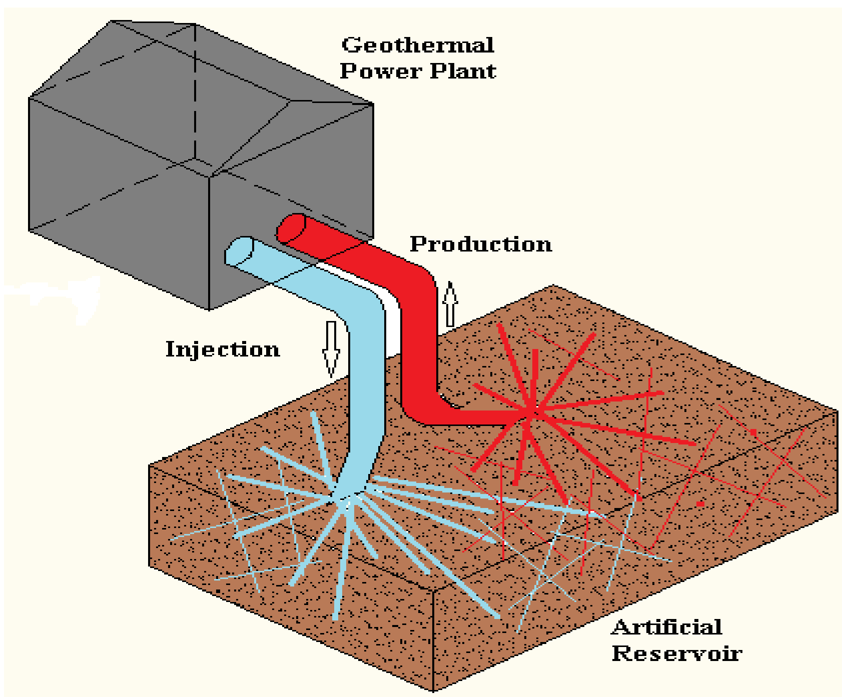


Figure 2.5: Conceptual diagram showing the enhanced geothermal system

Replacing conventional plants with geothermal plants is an attractive proposal for implementing eco-friendly systems [25]. Geothermal power plants (GPPs) produce far lower emissions as compared to fossil fuels for the same given load. However, GE is usually considered as a low-grade energy source and generally suffers from low energy extraction efficiency. Additional sources of energy can be combined through a hybrid system to improve the efficiency and meet the requirements that geothermal energy may not be able to deliver alone [26, 27]. These systems will be discussed in detail in section 2.5. Recently, GE based power plants have been frequently used due to their reliability in terms of net output power and efficiency. GPPs are usually found in four different forms: dry steam, binary, single and double flash cycle. These are the basic cycles that have been passed through several upgrades and investigated in various research articles and studies. For example, one of the recently attractive technologies is the production of hydrogen using GE-driven systems [28]. The choice of which cycle to use is directly restricted to the operating and available geothermal conditions. Dry steam and flash cycles are used when the hydro geothermal fluid is available in the form of steam and hot liquid, respectively. In Hernández *et al.* [29], the single and double flash cycles were compared to conclude that the former produces a maximum net output power less than that of the double flash cycle. The main difference between the two cycles is that the double flash cycle uses two separators instead of one and operates at different pressure ratios. The most used binary GPPs are the subcritical and transcritical organic Rankine cycle (ORC) [30, 31]. This is due to the specifications of these binary plants that could fit most geothermal conditions (see Figure 2.6). In Mosaffa and Zareei [32], a flash-binary cycle was introduced to combine the two main concepts previously used in GPPs. It was deduced that this combination can maximize the net output power which is mainly based on replacing the flash separator with a two-phase expander.

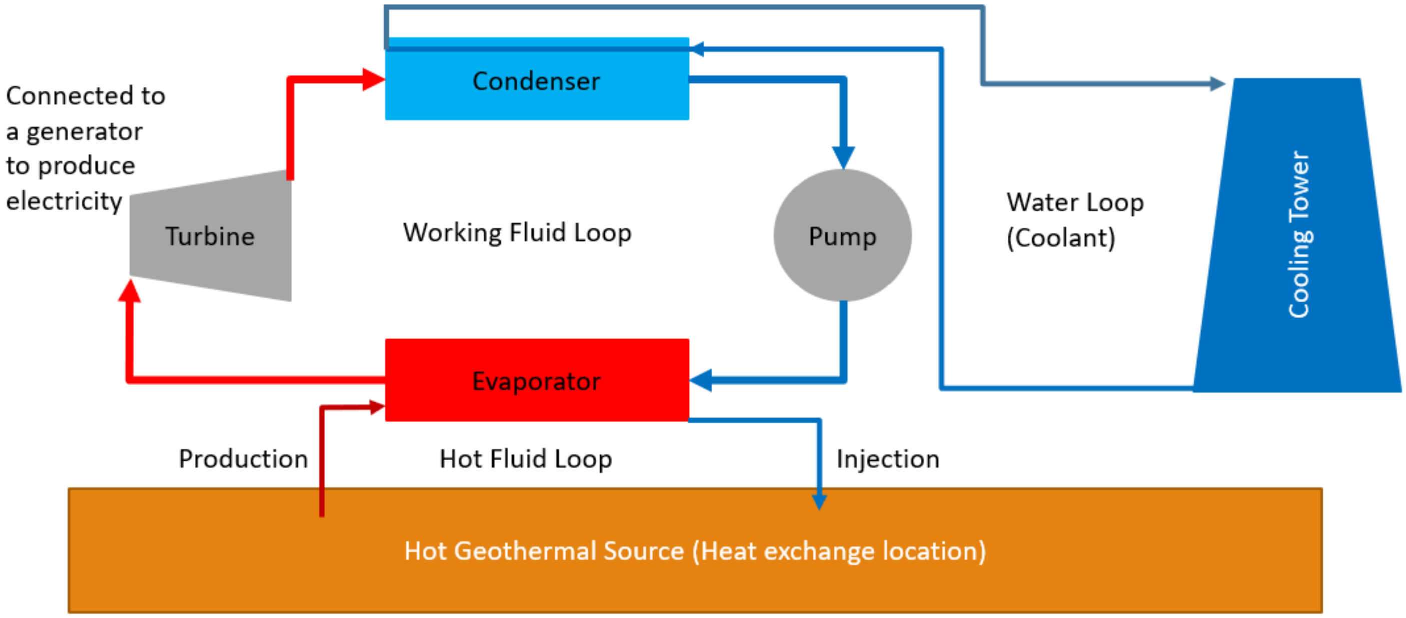


Figure 2.6: Binary geothermal power plant

Figure 2.7 presents the principle of a thermos syphon heat pipe for extracting thermal energy from the geothermal reservoir which could be used for generating power. Two working fluids are used: methanol in the heat pipe and $CO_2$ as a working fluid for the power cycle. The efficiency of the system can be improved by increasing any of the flow rates of the working fluids (methanol or $CO_2$).

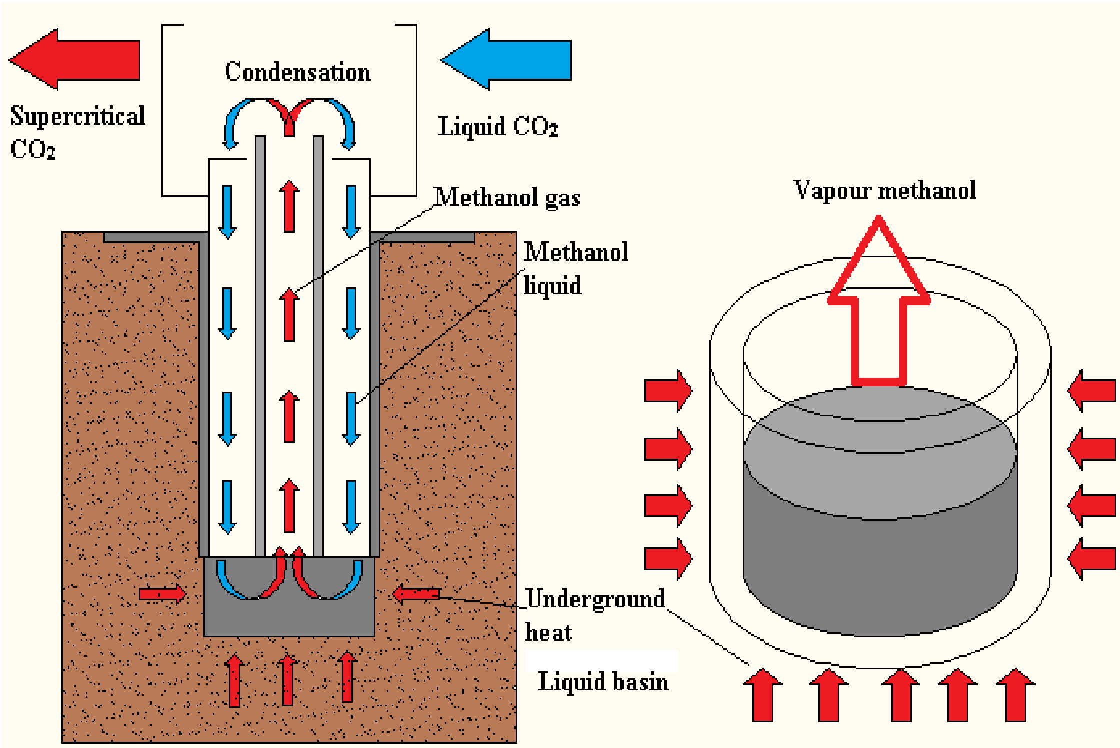


(a) (b)

Figure 2.7: (a) Low-temperature geothermal heat pipe and (b) detail view of a bottom basin, reproduced from [33]

Kujawa *et al.* [34] presented the difference between two types of deep GE systems (one hole and two holes); these can operate as one or two-layer systems. The study was done while varying the depth between 1600 and 2044 m, and the injected temperature between 5 and 30ºC. The authors reported that using two-layer and two-hole system is the most advantageous way of operation. This was deduced while studying the effects of flow rate and heat exchange conditions to provide the needed amount of heat extraction. Figure 2.8 shows the difference between one and two-layer systems.

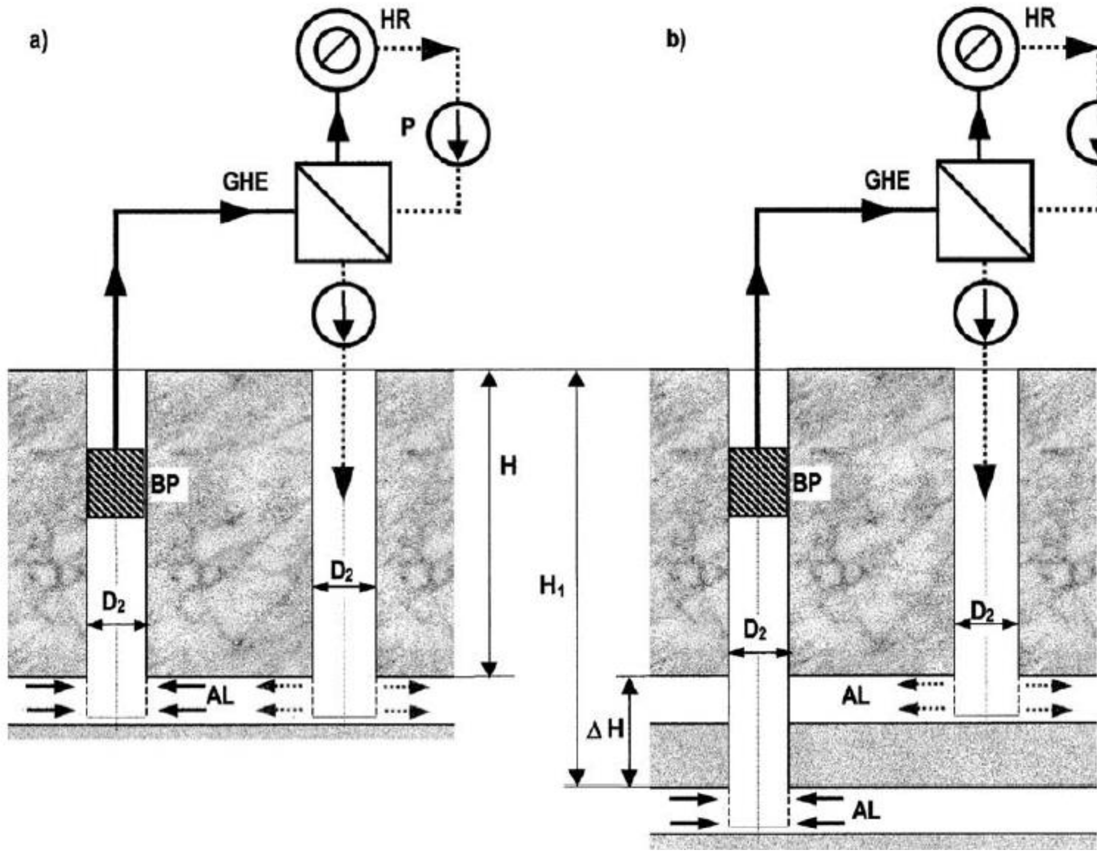


Figure 2.8: Closed two-hole system for extracting geothermal water: (a) one layer, (b) two layer; aquifer layer (AL), geothermal heat exchanger (GHE), pump (P), borehole pump (BP), and heat reservoir (HR) [34]

As like the closed two-hole system, another concept could be introduced to the deep GE installations which is the well system that is presented in Figure 2.9. The difference between this system and the hole system is that the production well is always connected to all paths.

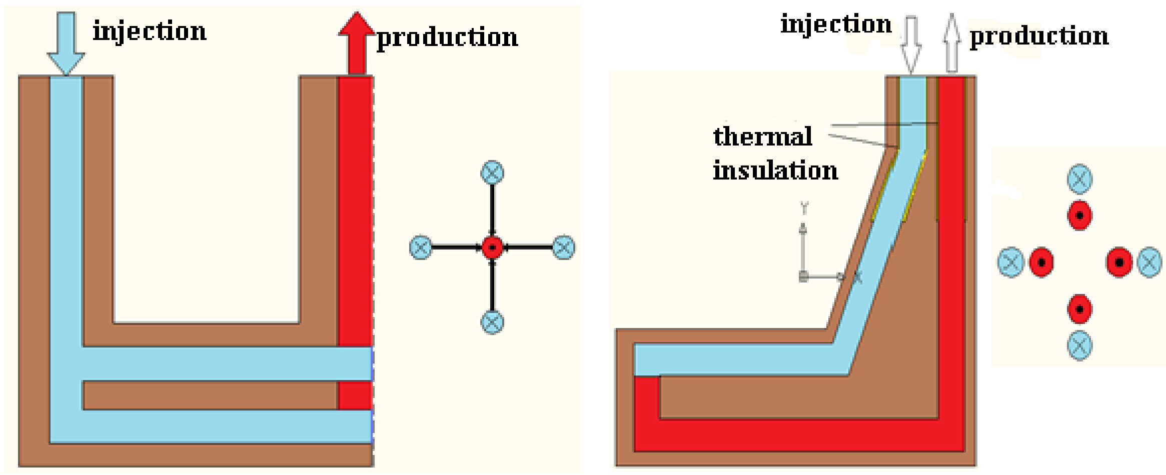


(a) (b)

Figure 2.9: (a) Multi-horizontal-well system and (b) annular-well system, reproduced from [35]

### 2.1.3 Hydrogen production

Geothermal-driven hydrogen production systems mainly utilize proton exchange membrane (PEM) electrolyzers to decompose water into hydrogen and oxygen. The temperature of water at which the electrolysis is taking place is one of the most important parameters affecting hydrogen production, required power, and operating cost. Yilmaz *et al.* [36] investigated the effect of temperature on the electrolysis process in a geothermal-driven hydrogen production system based on an artificial neural network. It was observed that when temperature increases from 25°C to 70°C the power required for hydrogen production will decrease from 43.51 kW/kg to 42.2 kW/kg, which corresponds to a reduction of approximately 3%. Typically, a preheater is placed to increase the water's temperature entering the electrolyzer [37]. In GPP-hydrogen production systems, the geothermal fluid has two roles: generating electricity via power plant and preheating water. First, the hot geothermal fluid drawn from the production well passes through the GPP and secondly, the residual heat will be used for water preheating. The air preheater is responsible for extracting the heat remaining in the geothermal fluid before it is reinjected back into the ground. In Cao *et al.* [38], the geothermal fluid temperature change was also investigated in a combined cooling and power system used for ice-making and hydrogen production. The system was formed of four subsystems, namely, geothermal flash cycle, Kalina cycle, ammonia-water absorption refrigeration cycle, and the electrolyzer. The results showed that when the geothermal fluid temperature was 150°C, 160°C, and 170°C the exergy efficiency was calculated as 23.59%, 25.06%, and 26.25%, respectively.

The geothermal fluid's mass flow rate is also an important factor that greatly influences the system's performance. This is related to the heat transfer rate and grade of GE utilized since it represents the working fluid in case of flash cycle and heat transfer fluid in the binary cycle. This means that the geothermal fluid's flow rate can control the hydrogen production rate. Yilmaz *et al.* [39] studied the importance of this parameter and deduced that a 0.253 g of hydrogen is produced for each kilogram of geothermal water. This was calculated at geothermal resource temperature and flow rate of 160°C and 100 kg/s, respectively, such that the rate of hydrogen production was 0.0253 kg/s. The authors also investigated another study based on a geothermal resource temperature of 200°C with the same flow rate [40]. The proposed system was driven by a flash binary GPP as shown in Figure 2.10. The power plant consists of two subsystems: topping and bottoming cycles. The geothermal fluid passes through a flash separator which separates steam and water. Steam is used as a working fluid in the flash cycle such that it enters the steam turbine to generate electricity while the heat carried by the hot water exiting the separator will be extracted via heat exchanger. This heat is transferred to the organic fluid which is responsible for generating additional amount of electricity by means of an ORC turbine. In comparison with the first system studied by the authors, the latter was able to produce more amount of hydrogen such that it was increased up to 0.0498 kg/s. However, this was accompanied by an increase in hydrogen production cost from \$2.366/kg to \$3.14/kg $H_2$.

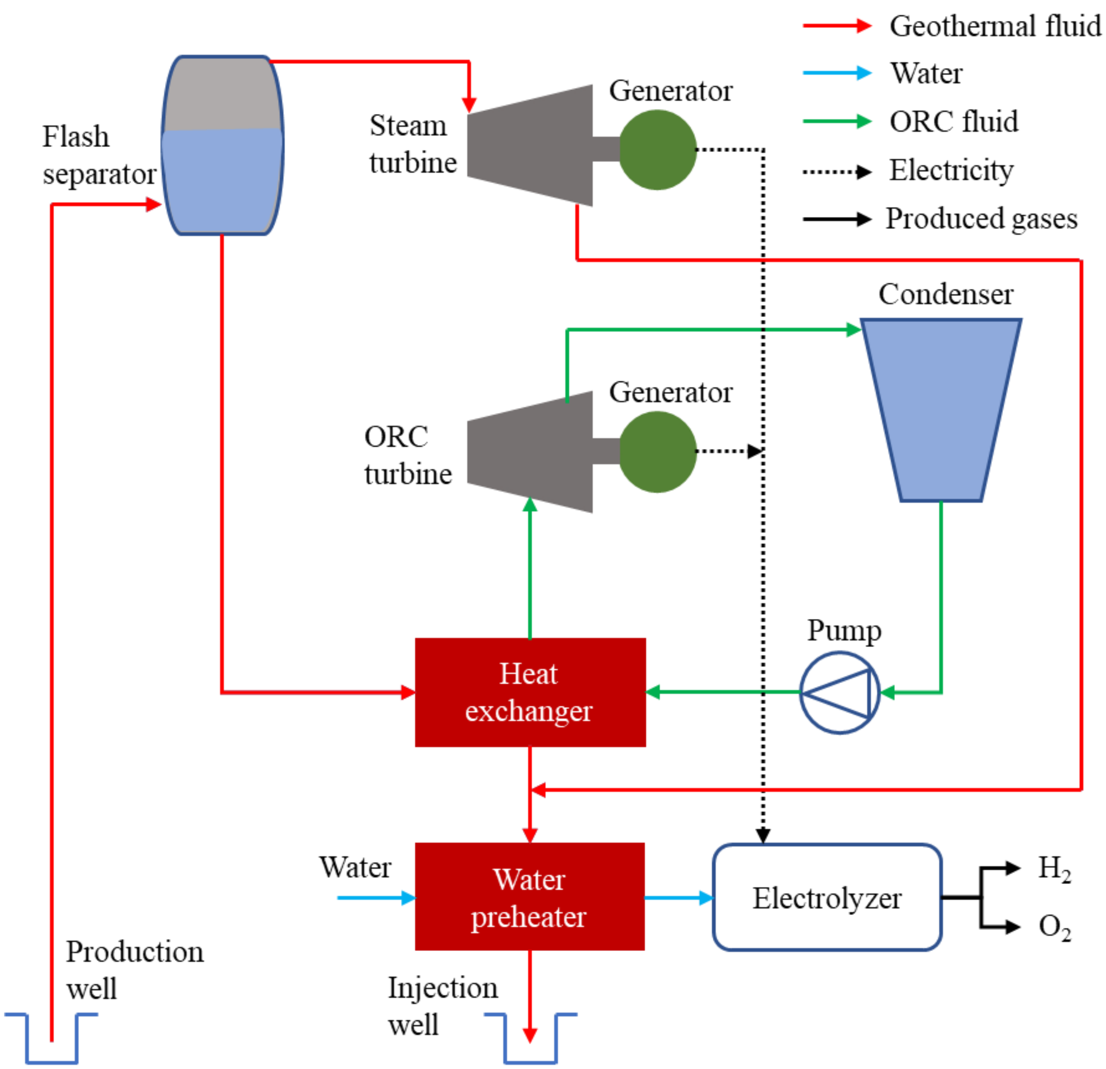


Figure 2.10: Hydrogen production using flash-binary geothermal power plant

The cycle's operating conditions are essential parameters that need to be chosen precisely to achieve the optimal operation. Therefore, it is necessary to perform parametric studies to determine the optimal cycle's conditions since they can be controlled easier than the geothermal fluid's temperature. For example, the turbine inlet pressure and the pinch point temperature are two of the most important parameters affecting the output power and production rates [41]. Thus, producing hydrogen from geothermal systems is not only dependent on the available geothermal conditions even though the ground is the main energy source. There are other critical components in these hydrogen production systems such as the cooling system which usually corresponds to the highest exergy destruction. Liquefied natural gas (LNG) has been recently considered as an improvement to the cooling system (condenser) which has a good heat sink potential. It also provides additional amount of power due to the presence of secondary power generator which is the LNG-turbine [42]. With this focus on the exergetic performance and destruction, it is a must to perform thermo-economic optimization to reduce the unit cost of products, which can be applied by using the genetic algorithm method [43]. This analysis usually considers the effect of all the system's components on the exergetic performance and product cost. Several parameters are involved in the exergo-economic performance analysis: fuel exergy and cost, product exergy and cost, exergy destruction and cost, exergetic unit cost of electricity, and exergetic cost of hydrogen production.

In GPPs, the extracted geothermal fluid is usually formed of steam and non-condensable gases (NCG). These gases are harmful to the environment when released, such as hydrogen sulphide ($H_2S$) which is emitted in large amounts in GPPs. Thus, modern technologies have been focused on managing treatments for the NCG, such as the AMIS unit (AMIS® - acronym for "abatement of mercury and hydrogen sulphide" in the Italian language) which is displayed in Figure 2.11. This unit mainly contributes to mitigate the effects of mercury and hydrogen sulphide. However, modern types of AMIS have been updated to produce hydrogen by sending the hydrogen sulphide to an electrolyzer. The AMIS unit captures the NCG and separates them to be treated with the help of other mechanisms (ex: hydrogen sulphide electrolyzer). Such techniques can enhance geothermal-driven hydrogen production systems in terms of environment and economic viability due to the reduction in pollution and increase in productivity. The hydrogen sulphide electrolyzer is responsible for decomposing hydrogen and sulphur, which is activated via electric power similarly as that of the water PEM electrolyzer [44]. The electrical power required for activating the hydrogen sulphide electrolyzer depends mainly on the inlet temperature. As calculated in Karapekmez and Dincer [45], the required electric power drops from 73.7 kW to 58 kW if the hydrogen sulphide temperature rises from 300 K to 800 K. The corresponding exergy efficiency was also increased due to the change in temperature from 54.4% to 68.9%. Another important parameter in the AMIS unit is the mass flow rate of hydrogen sulphide that has presented an inverse proportional relation with respect to the required input power. The authors achieved a hydrogen production rate of 9.7 g/s that was obtained at superheated steam and $H_2S$ mass flow rates of 1500 g/s and 165 g/s, respectively.

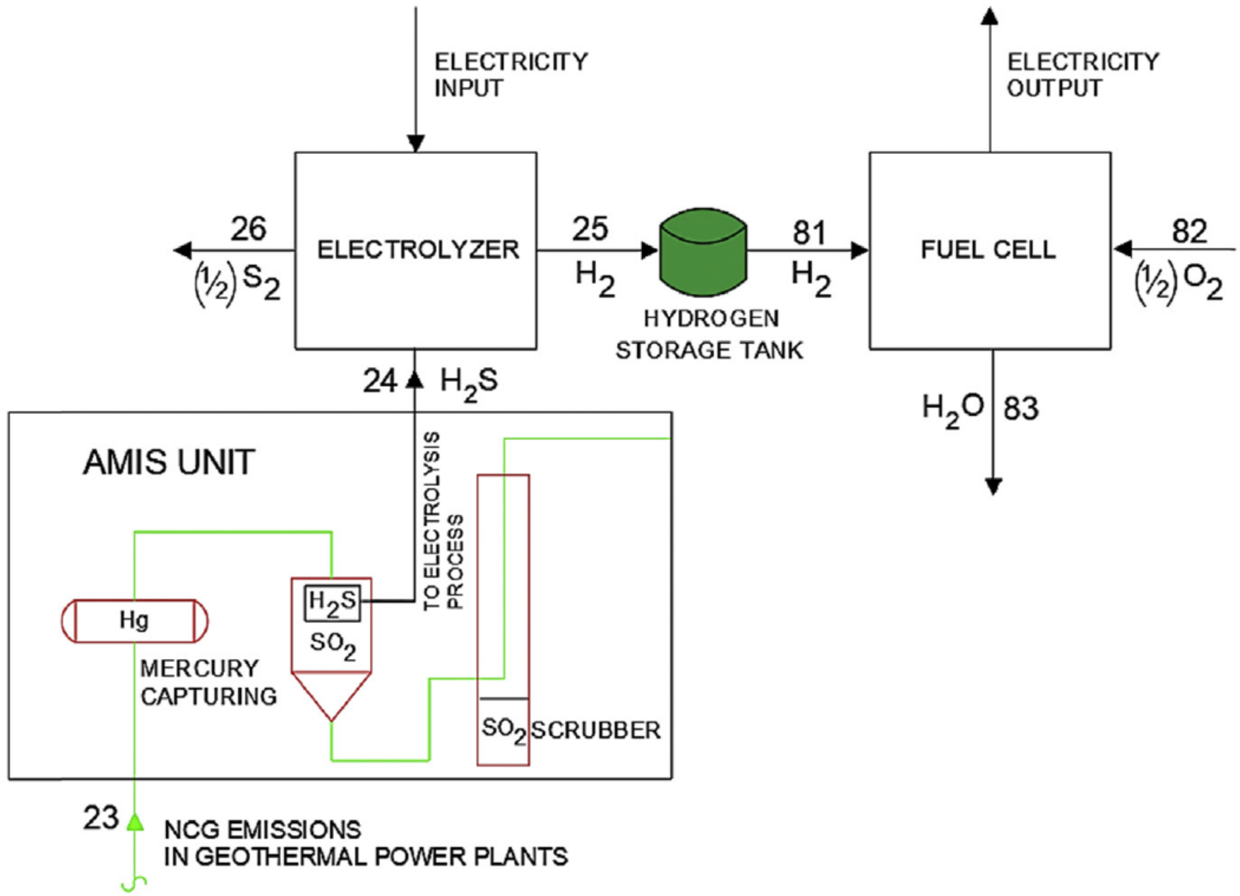


Figure 2.11: AMIS technology used for hydrogen production [44]

As presented previously, producing different types of outputs is a key factor used to enhance the system's overall efficiency. Conventional electrolyzers usually produce only one type of output, such as the PEM, which produces hydrogen only. However, in the case of using a chlor-alkali cell, two more substances could be produced in addition to the hydrogen, namely, chlorine and sodium hydroxide as shown in Figure 2.12. Karakilcik *et al.* [46] investigated a chlor-alkali cell based on a geothermal powered system to produce hydrogen. The authors deduced that if the geothermal fluid temperature rises from 140°C to 155°C, the amount of hydrogen produced and electricity generated will increase from 10.5 kg/hr to 21.1 kg/hr and 2.5 MW to 3.9 MW, respectively. The corresponding energetic and exergetic efficiencies were also calculated as 6.2% and 22.4%.

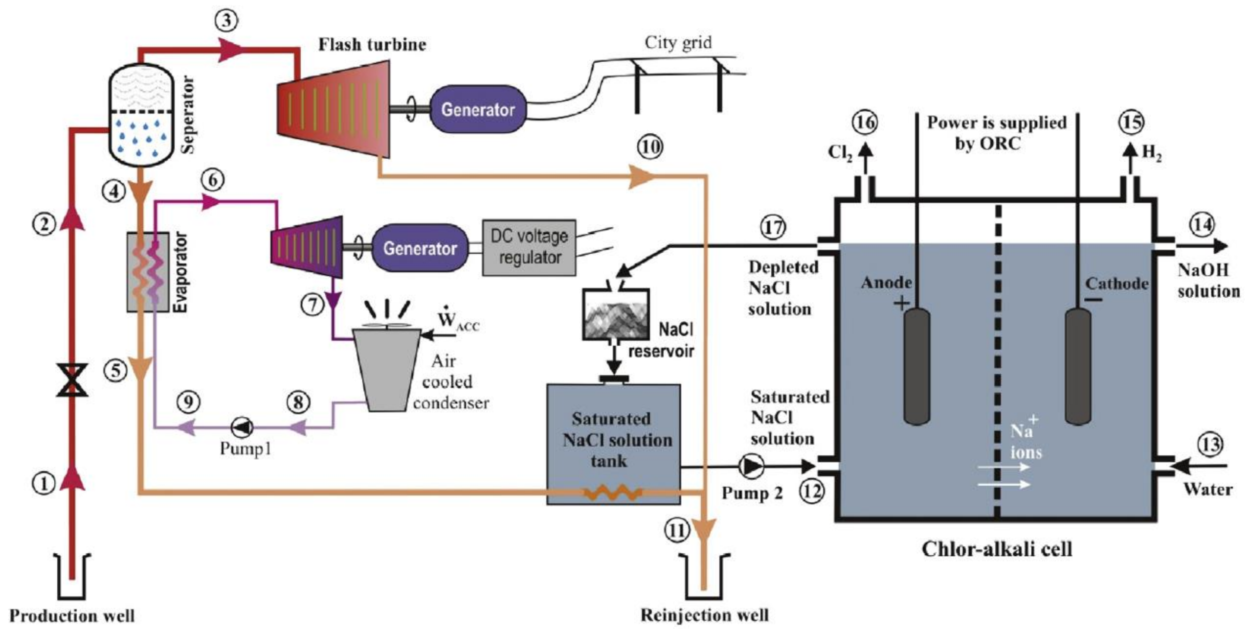


Figure 2.12: Chlor-alkali cell integrated into a geothermal power plant [46]

### 2.1.4 Cooling power cycles

The heat sink temperature is one of the most crucial factors affecting the efficiency of a power cycle. This is also more effective in low temperature power generation systems. Thus, several solutions have been previously proposed to decrease the heat sink temperatures. One of these solutions could be the utilization of water-cooled condenser instead of air-cooled condenser. However, there are many regions where this cannot be applicable due to the lack of water. Another approach could be the use of ground as a cooling source since it is more stable and can provide cooling when the ambient air temperature is relatively high. On the other hand, there are only few reports that have investigated this approach which represents a notable gap in research as will be discussed in section 2.7 [47, 48]. Vidhi *et al.* [49] employed the EAHE as a cooling device for low to medium temperature power generation systems. The power cycle under investigation was the supercritical organic Rankine cycle in which six organic fluids were compared that are R32, R125, R134a, R143a, R170, and R218. The highest efficiency was achieved when using R134a as a working fluid. It was observed that the soil temperature surrounding the GHE pipes increase with the penetration depth. The results obtained showed that the incorporation of EAHE helps increasing the power cycle by approximately 1% as well as reducing the daily power output fluctuations.

### 2.2 Borehole Heat Exchanger

The installation is the main concern in shallow geothermal energy systems which is represented by the borehole heat exchanger (BHE). Boreholes are made up of underground buried pipes, fluid refrigerant, and backfill material (see Figure 2.13). There are several factors that are found to have significant effects on the BHE [50] such as thermal conductivity, ground temperature, depth, transmissivity, hydraulic gradient, porosity, permeability [51], ground water flow [52], U-tube length [53] and friction heat gain [54]. It is also necessary to mention that the temperature distribution around the BHE depends mainly on the geothermal gradient and properties of stratigraphic layers.

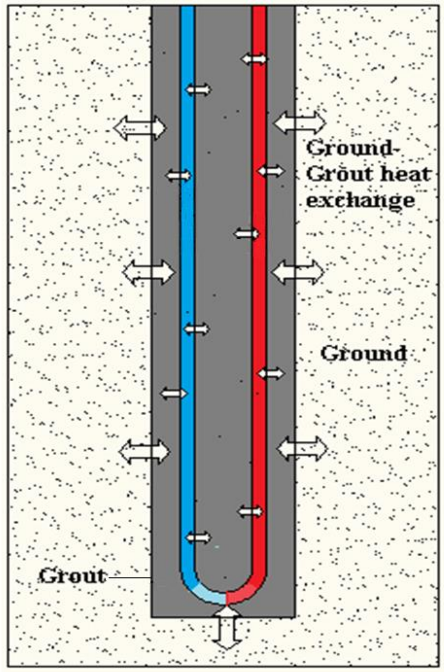


Figure 2.13: Geothermal borehole heat exchanger

The thermal resistance of the borehole depends on the characteristics of pipe, grout, and soil. Thermal response test (TRT) is one of the most used tests that helps determining the thermal ground properties. TRT could be used to ascertain the average thermal conductivity of the ground. The line source model is the most appropriate analytical tool used to investigate the thermal response. The efficiency of the borehole is highly affected by the heat exchange between the pipes and grout material followed by that from the latter to the soil (see Figure 2.14). The line source model could be used to determine the thermal conductivity of grout mix. The grout mix is found to be very crucial when the underground water is not rich to achieve the required ground thermal conductivity [55]. This is due to the low thermal conductivity of soil in the absence of water. As a matter of fact, the borehole thermal resistance and the grout's thermal conductivity are inversely proportional.

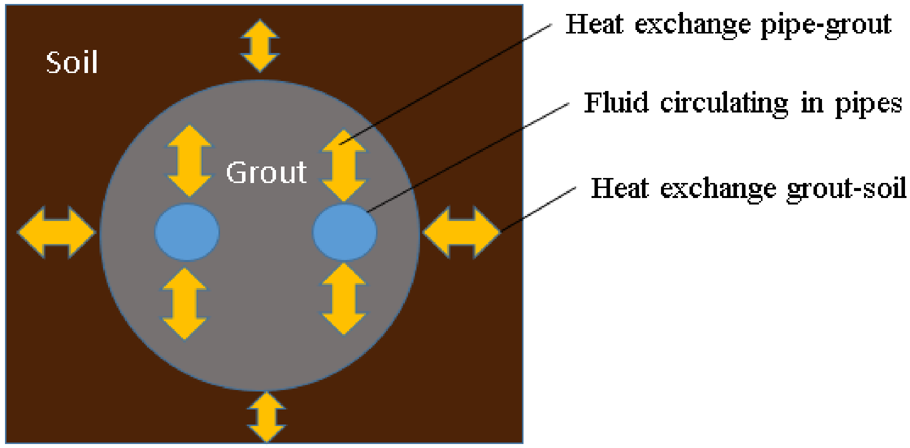


Figure 2.14: Heat transfer inside the ground heat exchanger

High-density polyethylene (HDPE) is the predominant material used for the GHE's pipes. In Borinaga-Treviño *et al.* [56], the authors deduced that the best results could be produced by using galvanized steel instead of polyethylene for the outside coaxial tube. However, polyethylene has a longer life span. A 35% reduction was achieved in the borehole thermal resistance. These characteristics in terms of performance are attributed to low material thermal resistance. The mixture of drilling rests was used as grout material to achieve a 34% reduction in the borehole resistance. Mixing sand with cement and bentonite also gave similar results. The application of thermally enhanced grouts did not contribute significantly to the performance compared to the addition of sand to the standard mixture. Figure 2.15 presents the main parameters that affect the thermal resistance of the BHE.

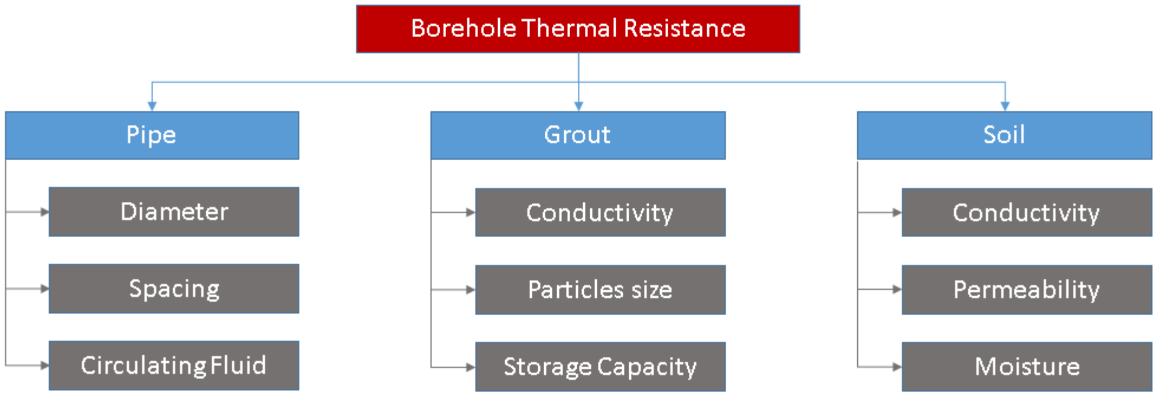


Figure 2.15: Factors that affect the borehole thermal resistance

Latent heat investigation is very important in geothermal energy systems. In some cases, it is considered beneficial while in others it is a liability. Freezing around the borehole can cause complex effects. Soil expansion may damage the pipes and a serious destruction may happen to the foundation of the building. On the other hand, the soil freezing can delay the soil temperature drop. Figure 2.16 presents the position of freezing with respect to the operating time. Soil freezing is a very critical underground issue which can affect the thermal resistance and capacity [57]. This change of phase is almost accompanied by the increase of heat transfer capacity and underground temperature uniformity.

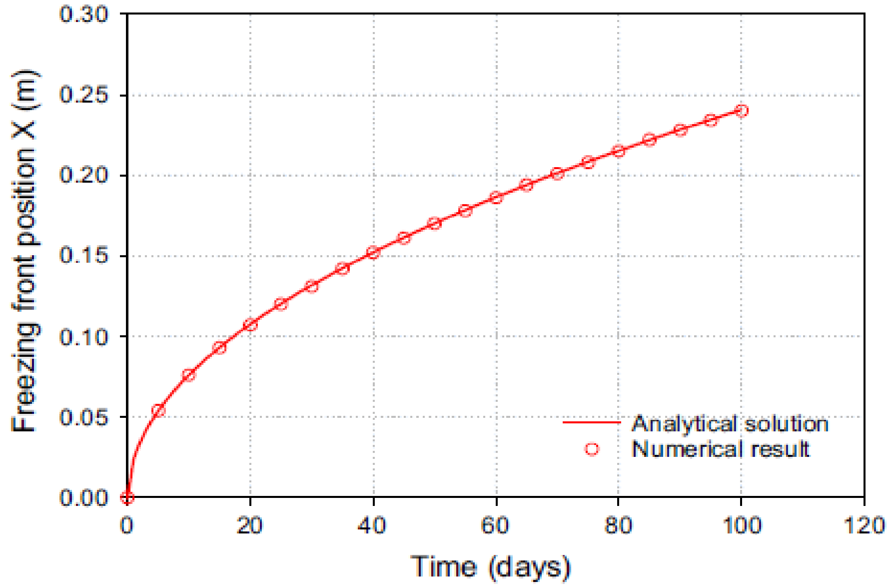


Figure 2.16: The propagation of freezing over time [58]

### 2.3 Grout Materials

Grout material has several important roles in GE systems such as enhancing the thermal conductance, preventing the contamination of ground water during operation, providing stability of boreholes and pipes, acting as a hydraulic barrier, and optimizing the heat transfer rate [59]. Enhancing the heat exchange between the ground and working fluid is a pragmatic approach that can be adopted by increasing the efficiency of the BHE. Grout material must provide the appropriate medium for heat transfer because it has a great influence on the shallow GE system's efficiency. The two major crucial characteristics of grout are the thermal conductivity and heat capacity [60]. The heat transfer coefficient of the grout material has approximately a constant effect on the BHE regardless of the type of GHE installed. In Sliwa and Rosen [61], three types of GHEs were compared: single U-tube, double U-tube, and co-axial. The effect of grout's heat transfer showed the same rate of variation in the effective heat transfer coefficient of the BHE in all cases. Bentonite and cement are the conventional used types of grouts. Many recent studies have investigated mixtures and new types of grout materials and compared them to the conventional ones. Figure 2.17 presents all types of grout materials that could be used in BHEs.

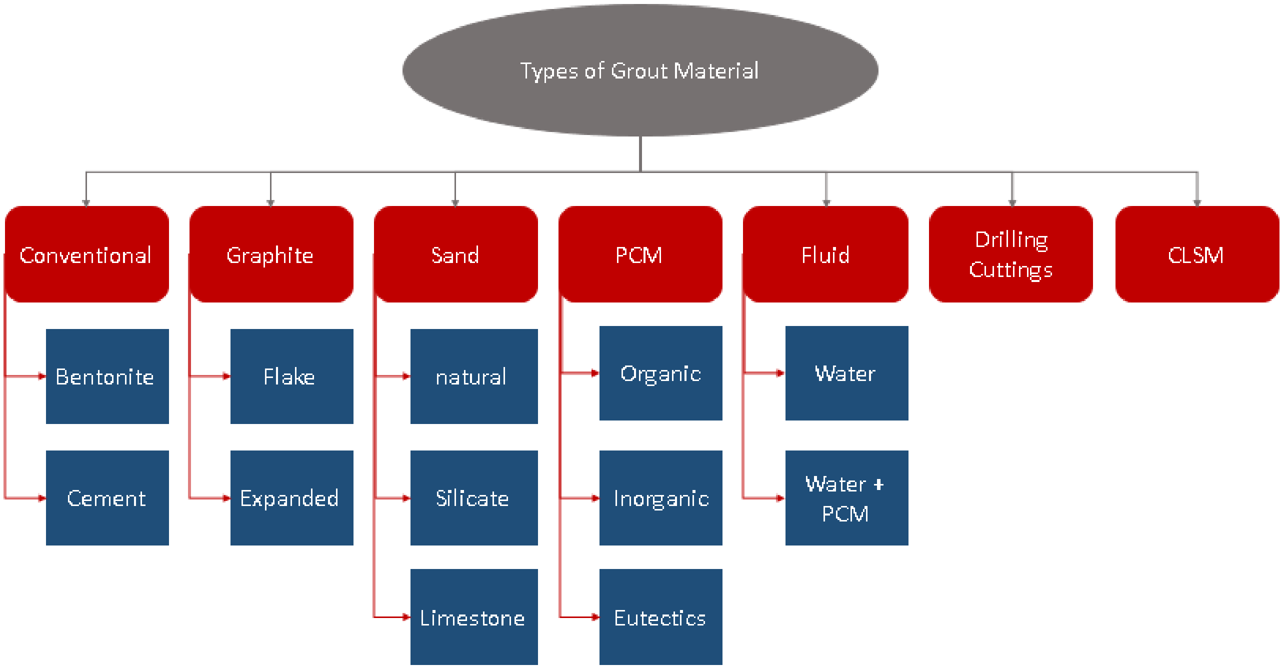


Figure 2.17: The types of grout materials that could be used in a borehole heat exchanger

During the installation of GHE, a gap is created between the pipes and ground. Thus, a backfilled material is inserted to fill the space inside the BHE. The objective of this material is not only to fill the gaps; while it is also used to provide a convenient medium for heat transfer and avoid pipes' damaging. It is usually recommended to use particles having small sizes to increase the heat capacity of the grout. However, it is essential to avoid affecting the thermal conductivity of the selected material. Clay, silt and coarse are the commonly used grout sizes. Selecting the suitable size is important to reduce the need for constructing long boreholes because the length of BHE depends on the choice of grout material. For example, as the thermal conductivity of the grout increases, the required length of borehole length decreases. There are several factors that need to be taken into consideration before selecting the grout material (see Figure 2.18).

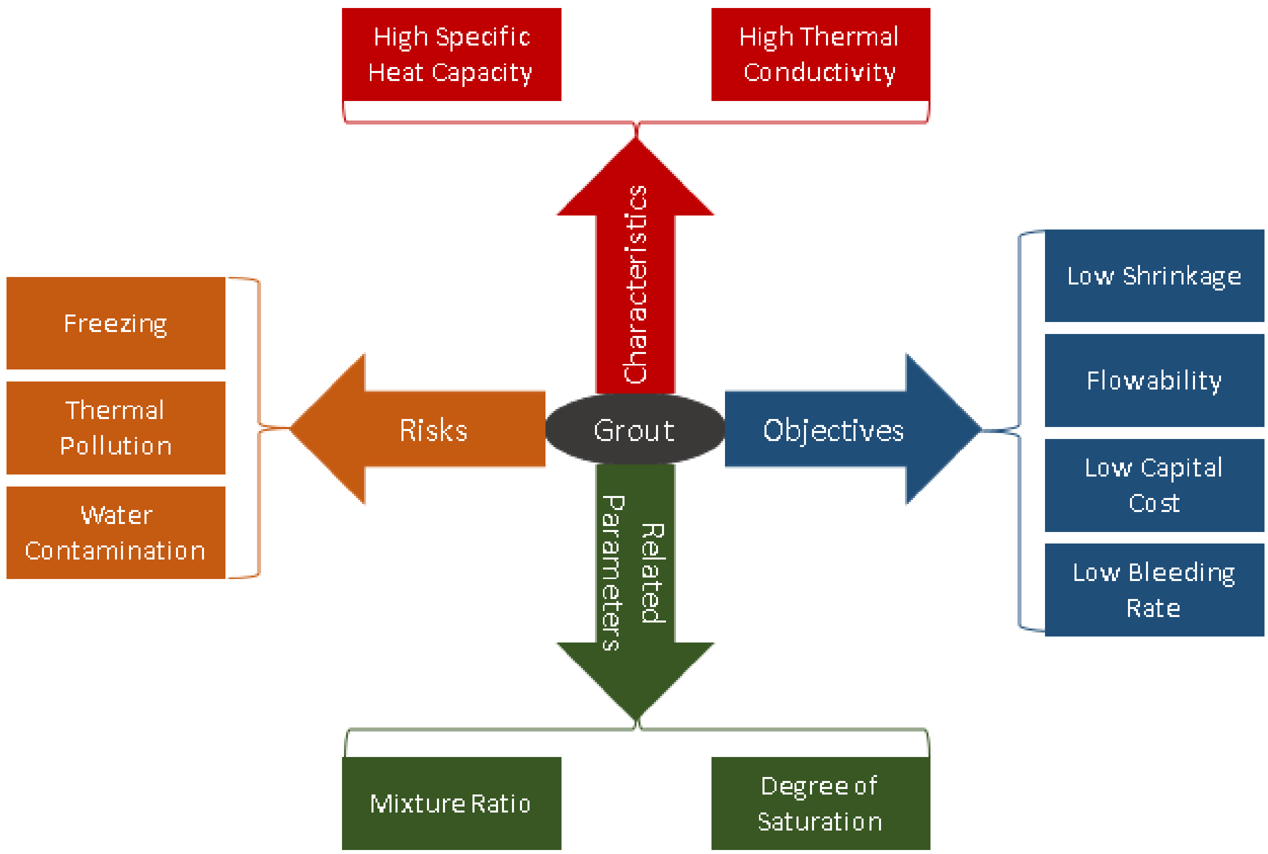


Figure 2.18: Grout material specifications

### 2.3.1 Conventional grout materials

Bentonite and cement are conventional types of grout materials used in BHEs. Table 2.1 presents a comparison between these materials in terms of thermal conductivity and thermal resistance. It can also be seen that these parameters are affected by the load, spacers, and grout's thickness. The flexibility of bentonite makes it a good sealant to be used in GE and water well systems. Common types of bentonites used are sodium, calcium, and potassium. It is considered as one of the best fluid barriers due to its low permeability preventing fluids from passing easily. In many cases, bentonite is mixed with other materials forming a grout mix aiming to enhance its thermal conductivity. Cement, water, sand, and graphite are the commonly used bentonite additives. Pahud and Matthey [62] compared different types of grout mixtures to conclude that sand and quartz mixture has the lowest thermal resistance amongst the grouts studied. The grout-based materials compared were bentonite, cement, and quartz. The study was performed by applying TRTs on six different boreholes in which the double U-pipe was used as GHE. Bentonite-based grouts were also compared by Lee *et al.* [63] to ascertain the effect of viscosity and salinity on the thermal performance of the grout materials. After applying experimental testing, the authors deduced that the interaction between bentonite and salinity can cause significant volume reductions. This was considered a crucial factor leading to an incomplete borehole filling, which can negatively affect the GHE's performance. Apart from that, there are also some other parameters that can inhibit the complete backfilling of BHEs such as density and viscosity differences.

The second type of conventional grout materials used in GE systems is cement. It could be found in several types; however, the commonly used cement-based grout is the Portland cement. It was compared with gravel by Choi and Ooka [64] such that the first grout was formed of cement and 20% of silica sand while the second was formed of gravel with a grain size of 8-15 mm. The results showed that the borehole thermal resistance was higher in the case of cement and needed more time to be backfilled compared to that of gravel. The rate of heat injection was also considered as an important parameter in which it was varying between 45 W/m and 90 W/m. The authors reported that the heat injection rate has a more significant effect than the type of grout on the BHE's thermal performance. This change in heat injection improved the thermal performance in case of cement and gravel by 8.7% and 9.8%, respectively. Borinaga-Treviño *et al.* [65] compared the different types of cement-based grout materials and aggregates to investigate the corresponding thermal conductivities, water content and mechanical properties. Silica sand showed the highest thermal conductivity compared to pure cement and other tested aggregate materials such as limestone sand, electric arc furnace slag, construction waste and demolition waste. The authors also studied the differences between natural and recycled materials considering the replacement of bentonite by cement as a grout-based material in the BHE. Different types of mortars and aggregates were compared in which water, cement and plasticizer were used as mortars while the aggregates were formed of construction/demolishing waste, electric arc furnace slag, silica, and limestone.

Table 2.1: Comparison between the conventional grout materials; bentonite and cement

| **Reference** | **Borehole heat exchanger** | **Effective thermal conductivity (W/m.K)** | **Calculated thermal resistance (m.K/W)** |
|---|---|---|---|
| Pahud and Matthey [62] | 13 cm bentonite without spacers | 0.7 | 0.240 |
| | 13 cm bentonite with spacers | 0.7 | 0.142 |
| | 12 cm bentonite without spacers | 0.7 | 0.150 |
| | 12 cm bentonite with spacers | 0.7 | 0.223 |
| Choi and Ooka [64] | Cement (2 kW heater TRT) | 1.962 | 0.159 |
| | Cement (4 kW heater TRT) | 2.076 | 0.155 |

### 2.3.2 Additives

The thermal resistance of the BHE relies on the characteristics of its components: pipes, grout material, and soil. The components' performances depend significantly on each other such that any change in one of them may affect the other two. For example, if the ground is poor in terms of moisture, it is necessary to choose a grout with high thermal conductivity to enhance the heat transfer rate between soil and GHE. However, conventional grouts cannot offer such high thermal conductivities, making it essential to introduce grout mixtures. Usually, as the grout thermal conductivity increases, the borehole thermal resistance decreases, resulting in a better thermal performance. Endeavours have focused on investigating several types of grout mixtures and compared them to conventional materials as shown in Table 2.2. Aluminium shavings and sulpha-aluminate cement were studied by Blazquez *et al.* [59] to improve the thermal conductivity of sand-based grout. The results showed that these materials can be used as additives since they have good thermal conductivity and mechanical properties. It was deduced that saturated sand-aluminium shavings and aluminium cement-sand have the highest thermal conductivities. Among the compared materials, the grout mixture that corresponded to the lowest thermal conductivity was formed of bentonite and superplasticizer. Material shavings are usually characterized by their small sizes in which this helps achieving almost uniform distribution.

Graphite is one of the most used additives that have been integrated into conventional grout materials to improve the thermal performance due to its stability regarding carbon content. The contribution of graphite to the thermo-physical properties of grouts was studied by Erol and François [66]. Graphite was better introduced as an additive and not as grout-based material because when pure graphite was used alone the performance of the BHE decreased. Additionally, the flowability and strength were negatively affected in the presence of large amounts of graphite. Thus, the authors found that a 5% of graphite would be the best percentage resulting in the highest grout enhancement. The graphite content was further studied by Delaleux *et al.* [67] to enhance the grout material's thermal conductivity. The study aimed to use a percentage of compressed natural graphite less than 10%. The results showed that the overall heat transfer could be enhanced by 1.5 times while using 5% of graphite in the mixture. This was obtained considering other important factors such as the particle’s size and amount of moisture in the grout. Graphite is usually found in two different forms: flake and expanded. Both are formed of high percentages of natural graphite in which the former and latter correspond to values above 94% and 99%, respectively [68]. Expanded graphite is more used as grout additive than the flake-type due to its high surface area and sealing properties. The expanded type is manufactured by passing through an oxidation reaction and expansion process reaching a ratio of 200-300. Additionally, the important factor that makes graphite a good additive is the insolubility in water. Thus, when it is used as a grout material, there is no risk of contamination even if it interacts with water.

Another commonly used additive is sand, which has been frequently utilized to enhance conventional-based grout materials' performances. Blázquez *et al.* [59] investigated the effect of aluminium shavings' amount on sand-based grout's thermal conductivity. Below 2.5% of aluminium, the grout's thermal conductivity was proportional to the amount of shavings, while the relationship was inverted at higher percentages. The authors deduced that when using high amounts of aluminium shavings, the number of holes will increase, resulting in an increase in the grout's thermal resistance. It was also expected that these results would change at different amounts of moisture. Kim and Oh [69] compared two types of cement-based grouts to ascertain the effect of additives on the thermal conductivity in which water and sand were used as grout additives. The addition of water showed a better performance compared to that of sand, while the change in sand content percentage was more significant. The comparison was carried out taking into consideration different saturation levels (see Table 2.2).

Table 2.2: The effect of introducing additives into grout materials

| **Reference** | **Grout** | **Additive** | **Additive percentage/ratio** | **Thermal conductivity (W/m.K)** |
|---|---|---|---|---|
| Blazquez *et al.* [59] | Sand | Aluminium shavings | 0.5% | 3.270 |
| | | | 2% | 3.752 |
| | | | 3.5% | 3.620 |
| Erol and François [66] | Homemade admixture | Graphite | 0% | 1.5 |
| | | Natural graphite | 5% | 2.3 |
| | | Synthetic graphite 150 μm | 5% | 2.5 |
| Delaleux *et al.* [67] | Bentonite | Graphite | - | 1.5 |
| | | | 5% | 5 |
| Kim and Oh [69] (Water/Cement ratio = 0.3) | Cement | Sand | S/C = 0 | Saturated: 1.06<br>Air-dried: 0.79 |
| | | | S/C = 0.5 | Saturated: 1.62<br>Air-dried: 1.28 |
| | | | S/C = 1 | Saturated: 1.87<br>Air-dried: 1.58 |

### 2.3.3 Controlled low-strength material

Controlled low-strength material (CLSM) is a concrete mix suitable for backfilling applications such as BHEs in which it is characterized by low strength, good flowability, low shrinkage and high thermal conductivity [70]. Natural sand and marine dredged soil mixture were integrated into CLSM-based grout by Do *et al* [71]. The aim was to reduce the grout material's bleeding rate to decrease the geothermal system's capital cost. The studied mixture's thermal conductivity was suitable for BHEs such that it was varying between 1.4 W/m.K and 1.82 W/m.K. The commonly used CLSM types are composed of fine aggregates, cement, fly ash, and water. Usually, sand and coal are used as fine aggregates. The heat exchange rate in the BHE was investigated by Do *et al.* [72] while comparing different CLSM mixtures with conventional grout materials. The composition ratio of CLSM was also varied to select the optimal material and study its effect on the total cost. The results showed that the incorporation of all CLSM types can enhance the GE system's performance regarding thermal properties and economical aspect. Two types of GHEs were involved in the mentioned study that are the U-type and spiral-type. The geothermal system's total construction cost was reduced by 20.8% in a study performed by Kim *et al.* [73] while using a by-product-based CLSM with bentonite-sand mixture. Quartz-based mine tailings and pond ash were used as fillers and aggregates, respectively. Pond ash was introduced as an alternative to natural sand. The aim was to enhance the mechanical strength of CLSM. Quartz-based mine tailings and pond ash are usually formed of $SiO_2$, $AL_2O_3$, $Fe_2O_3$, CaO, MgO, MnO, $Na_2O$, $K_2O$, $TiO_2$ and $P_2O_5$. The difference between the two materials (quartz and pond ash) is the ratio of each chemical substance. The addition of such materials into CLSMs must be based on compromising between the mechanical and thermal properties because this addition may be accompanied by a decrease in grout's thermal conductivity. The thermal conductivity of CLSMs can be further enhanced by decreasing the fineness modulus as reported by Do *et al.* [74]. This was deduced while comparing the excavated soil and pond ash in CLSM mixtures.

### 2.3.4 Dolomite

Calcium magnesium carbonate rock is known as dolomite and can be used as a backfill material in boreholes to reduce the GE system's installation capital cost. Dolomite drilling cuttings were investigated by Luo *et al.* [75] and compared with bentonite and cement mixtures. The application was based on a GSHP in which a TRT was carried out to study the system's heat transfer performance and economic feasibility. The reduction in cost using dolomite drilling cuttings was significant compared to that of concrete and bentonite-quartz. The corresponding reductions were 14.87% and 17.16%, respectively. The geological profile of the BHE studied was formed of several layers of dolomite drilling cuttings with a total depth of 100 m. The thickness of each layer depends on the characteristics of ground and grout. The shallower layer was backfilled with 2.5 m of gravel and clay while the deeper layers were backfilled with dolomite. As for bentonite-based grout, the optimal mixture ratio of dolomite to bentonite was 2 to 8 and the thermal conductivity of this mixture was 1.96 W/m.K. The thermal conductivity was higher in case of using cement mixture in which the value was 2.19 W/m.K considering an optimal dolomite to cement mixture ratio of 3 to 7.

### 2.3.5 Phase change materials

Having said that, GE is one of the most stable renewable energy sources, phase change materials (PCM) could be introduced to avoid thermal depletion or heat accumulation in the presence of high loads [76]. This incorporation can stabilize the geothermal system's performance while decreasing its operating cost. Thermal energy storage (TES) is generally divided into two categories: sensible and latent. The former stores energy by changing the temperature of the storage material while the latter relies on storing heat at nearly constant temperature by the help of PCM. There are three main types of PCM; organic, inorganic and eutectics (see Figure 2.19). PCM are highly used in applications that are based on waste heat recovery systems [77] or solar energy [78]. Most recent investigations utilize composite PCM to enhance their thermal performance such as foam-based [79], nano-enhanced [80, 81], and shape-stabilized [82]. TES can be incorporated with shallow GE to avoid thermal pollution. Thus, PCM is favourable in geothermal systems to provide thermal balance and ensure stability. It could be used as grout material around the GHE, or underground TES as presented in Figure 2.20.

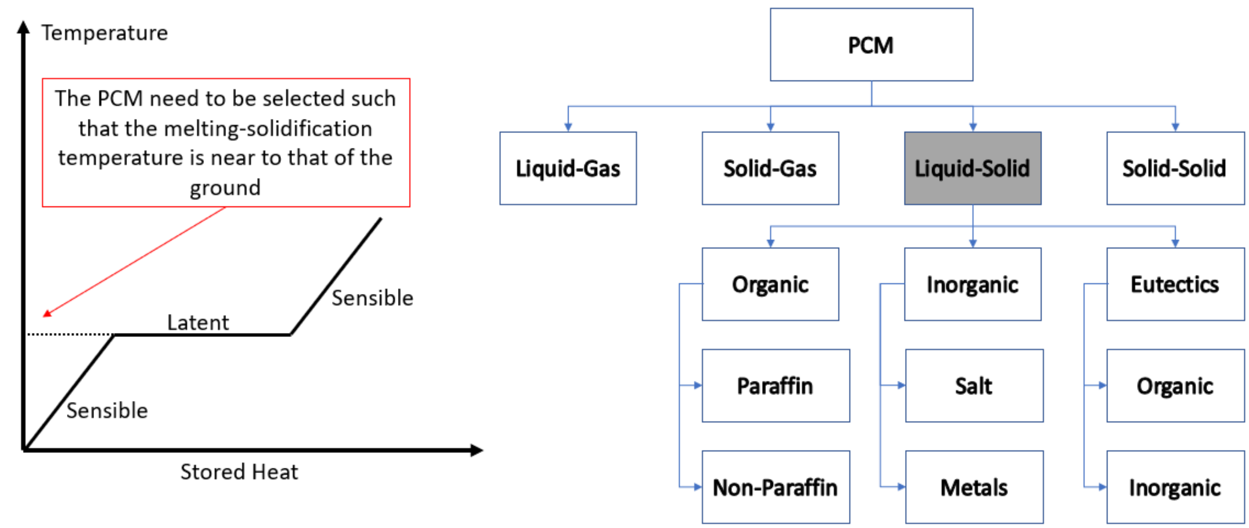


(a) (b)

Figure 2.19: Phase change materials; (a) the commonly used type in geothermal energy and (b) different types

One of the most barriers that faces GE systems is the capital cost and especially when using the vertical GHE or deep GE systems. For this reason, PCM is introduced to the horizontal shallow GHE usually to make it more feasible to compete the vertical type [83]. It can increase the performance of horizontal GHE to avoid thermal depletion and heat accumulation. In addition, it contributes to reducing the GHE's length and consequently the total borehole size. In Bernier and Eslami-nejad [84], research was conducted to study the single U-tube borehole with a ring made up of thermally PCM mixed with sand. The PCM sand ring was used to harness its high energy content which resulted in a 7.3% borehole length reduction. On the other hand, the energy consumption was increased by 2%. The melting did not exceed the ring's radius while increasing the thickness of the ring by 4.1 cm at peak conditions which was also accompanied by a decrease in the borehole length by 9.3%. This phenomenon caused a 2.7% increase in the pump energy usage. Some PCM have low thermal conductivities leading to a decrease in the geothermal system's performance. However, they still provide stability to the GSHP when compared to the conventional grout materials. According to Chen *et al.* [85], PCM with high thermal conductivity is recommended in cases where the underground water is poor. Chen *et al.* [86] confirmed that PCM is preferred when the thermal demand is less persistent. In this case, it ensures ground restoration and especially if the load is not alternating uniformly between heating and cooling. Under the investigated conditions, the best phase transition temperature was 20.4°C. There is also another important factor to be studied which is the cycle ratio that represents the operating hours to that of non-operating ones. If the cycle ratio decreases, the efficiency of the GSHP and the PCM restoration performance will both increase. In Kong *et al.* [87], the microencapsulated PCM (MPCM) was investigated to improve the GSHP performance such that the COP was between 3.2 and 4. This type of grout material significantly enhances the heat transfer inside the borehole. It was also deduced that the cavity pump is better than the centrifugal one in case of MPCM such that it can increase the life span to 10.5 years. Pu *et al.* [88] studied the effect of MPCM volume fraction. As the volume fraction varied from 7% to 15%, the heat transfer coefficient increased from 8.2% to 11.1% while the pressure loss decreased from 39.6% to 21.1%. One of the most important advantages of using PCM as grout material is its small thermal effect radius. This helps reducing the pipe spacing leading to a decrease in the GHE's construction area. On the other hand, it is crucial to keep in mind that the liquid fraction of PCM is affected by the initial ground temperature and pipe spacing. In each case, according to the load, if the pipe spacing exceeds a certain distance, the liquid fraction will be independent [89]. In Yang *et al.* [90], the soil thermal interference radius was reduced by 13% when using PCM instead of soil backfill. The authors concluded that the best PCM type to be used depends on the season. A mixture of decyl acid and lauric acid was used in summer while oleic acid in winter. This shows that it is very important to mix between the different types of PCM or investigate new composites to balance between the performances of heating and cooling seasons.

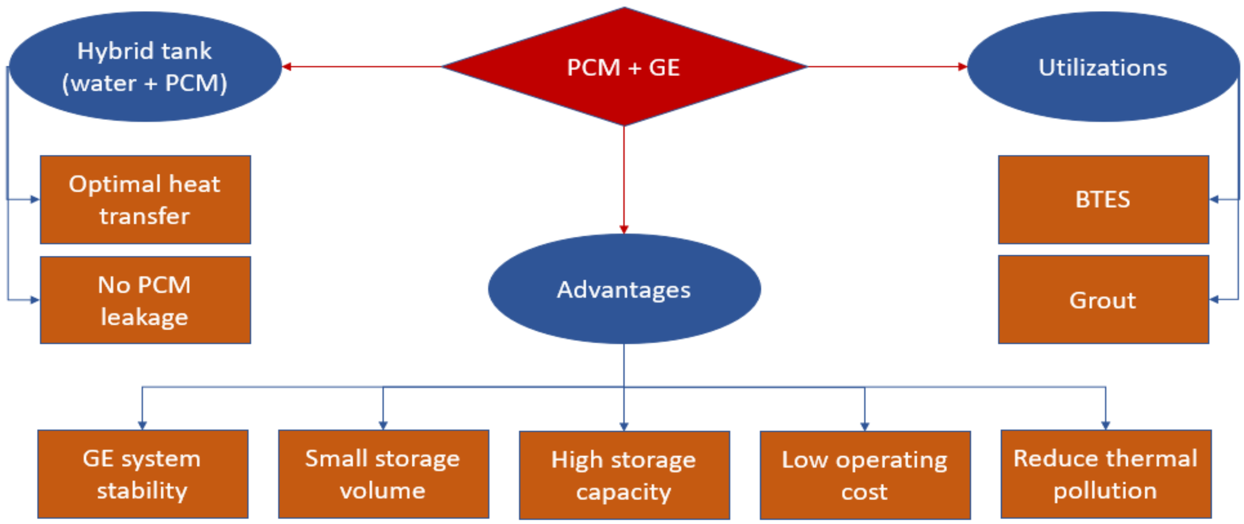


Figure 2.20: The characteristics of phase change materials and geothermal energy combination

Zhu *et al.* [91] compared the usage of PCM for cooling storage and cooling tower in a GSHP application. It was deduced that PCM can decrease the annual cost by 34.2% if the cooling storage ratio is 40%. Moreover, the increase in the storage ratio provides more stability to the ground such that it can reduce the maximum soil temperature considerably. PCM encapsulation geometry helps achieving complete melting and solidification. It could be immersed in a water tank to form a hybrid storage tank to decrease the storage volume. A 65% reduction in the storage volume could be achieved if 50% PCM is used compared to water alone [92]. This hybridization allows the PCM to have a better release and capture heat ability due to the convenient heat transfer conditions of water [93]. In addition, the PCM leakage will be almost eliminated because there will be no moving solid particles compared to the direct contact with soil.

## 2.4 Ground Heat Exchangers

There are three main types of ground heat exchangers (GHEs): vertical [94], horizontal [95] and slinky or spiral [96, 97]. Figure 2.21 presents the three different GHEs, however, there are still some remaining sub-types that will be presented in the below sections of each GHE.

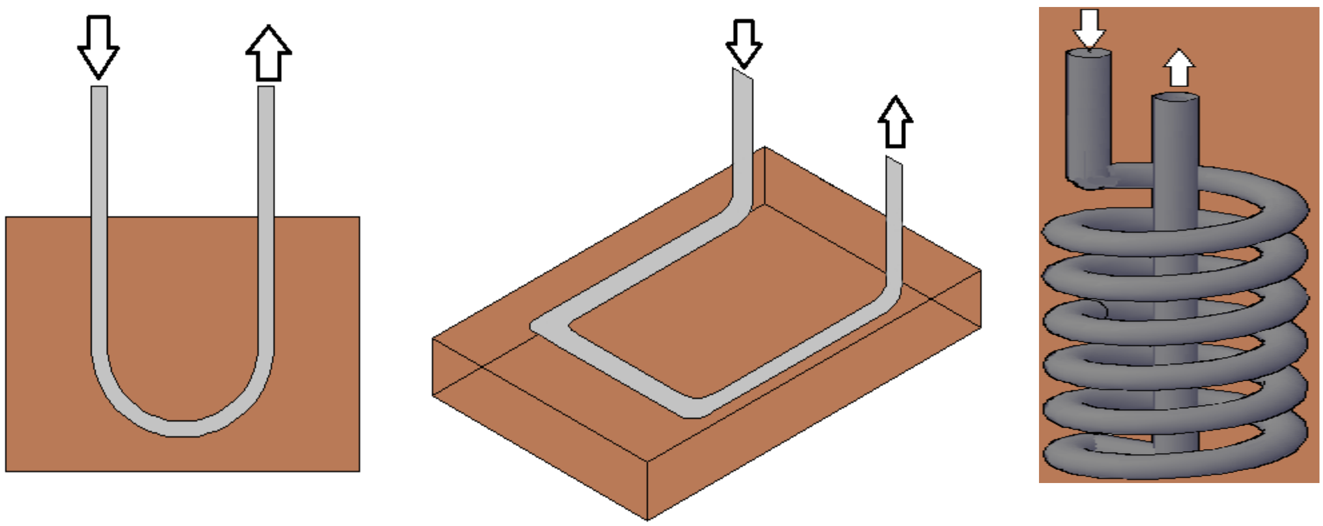

(a) (b) (c)

Figure 2.21: Ground heat exchanger configurations; (a) vertical, (b) horizontal and (c) spiral

### 2.4.1 Vertical ground heat exchanger

The vertical GHE has the highest performance and stability because it is less affected by the external conditions. This can be obviously recognized because it is a deep underground system, which means that it is much less affected by all atmospheric conditions compared to the other GHEs. GSHPs are mostly used for heating due to the huge amount of heat embedded underground which is usually extracted by using vertical GHEs. In some cases when the existing heating load is very high, specific types should be used such as the deep geothermal (DG) system in which depths vary between 1000-5000 m [98]. Besides the single vertical GHE presented in Figure 2.21, there is another type which is frequently used. This type is known as double pipe vertical heat exchanger which is depicted in Figure 2.22.

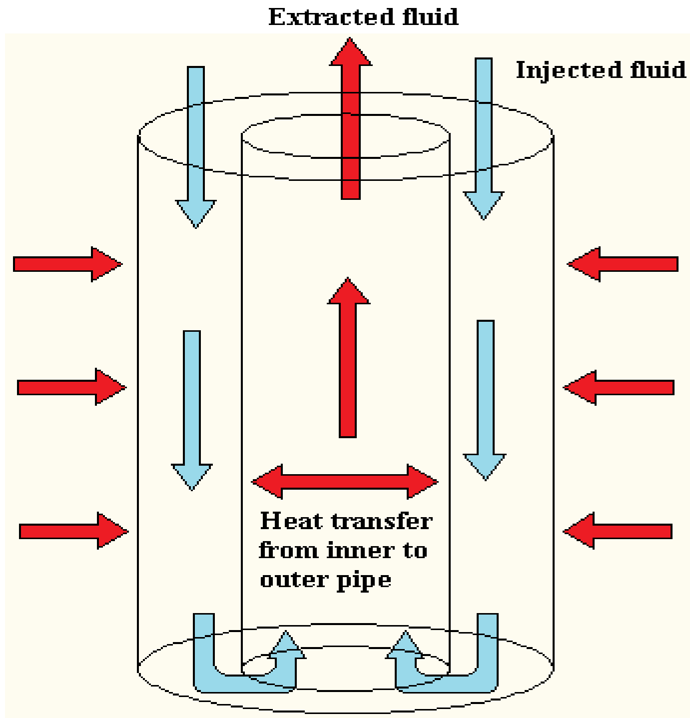


Figure 2.22: Heat transfer through a closed loop double pipe heat exchanger, reproduced from [99]

### 2.4.2 Horizontal ground heat exchanger

The conventional horizontal GHE was presented in Figure 2.21. In the presence of several paths, different configurations could be offered such as parallel and series (see Figure 2.23). A comparative study should always be carried out to select the optimal configuration which must be based on the heat transfer conditions and the total area of heat exchange.

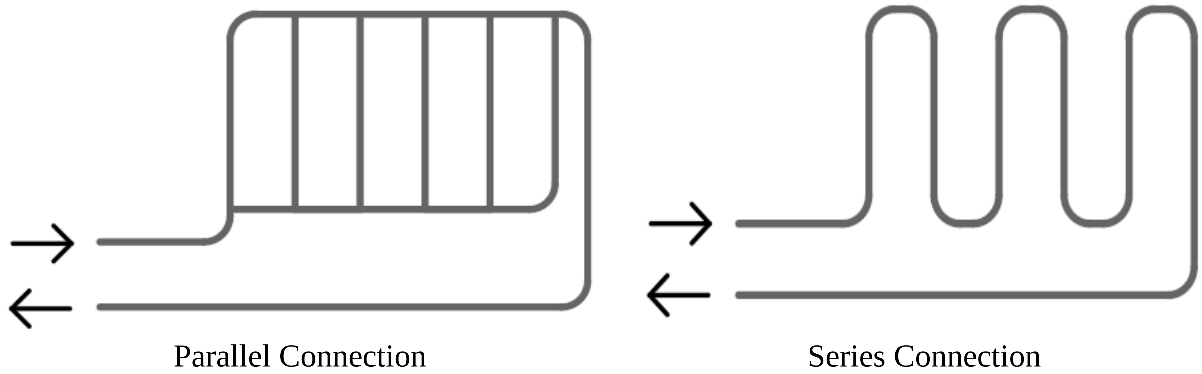


Figure 2.23: Horizontal ground heat exchanger configurations

### 2.4.3 Coiled ground heat exchanger

This type is highly favourable when the GHE is surrounded by water which is the case in the sea or lake. This is mainly due to the low effect of distance between pipes in the presence of water. This GHE has two different shapes: spiral/helical and slinky. The one presented in Figure 2.21 is the spiral/helical. However, the slinky could be found in two other forms; vertical slinky and horizontal slinky (see Figure 2.24). The installation itself could also be either vertical or horizontal based on the principle shown in Figure 2.21. The ground coiled heat exchanger is always preferred among the conventional GHEs due to its small volume. However, this may be accompanied by thermal depletion or heat accumulation. Thus, the GHE's installation mainly depends on the amount of load and the operating conditions.

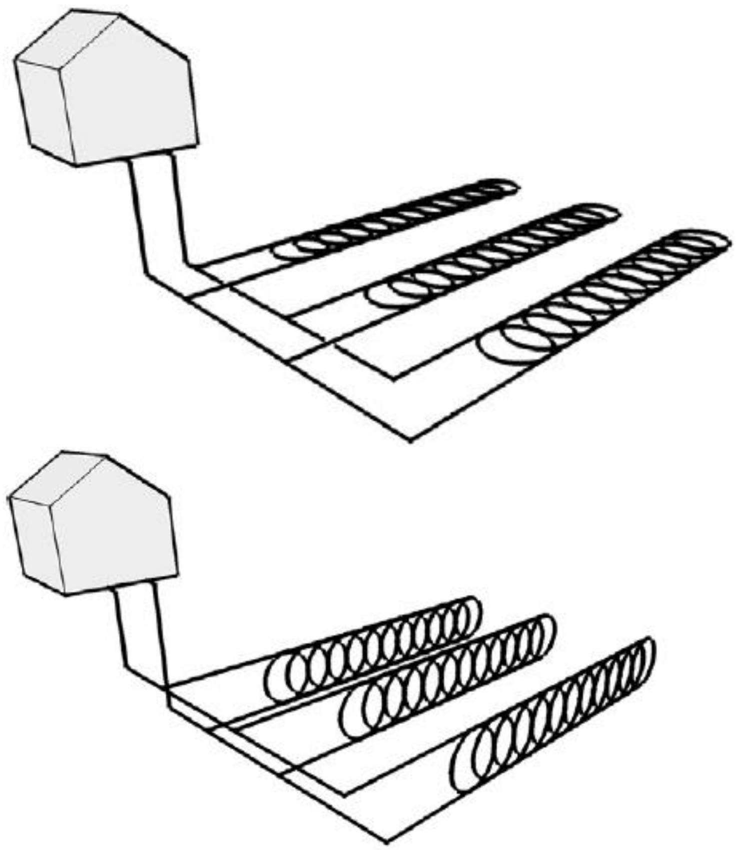

(a)

(b)

Figure 2.24: Schematics of (a) horizontal and (b) vertical slinky ground heat exchangers [100]

### 2.5 Hybrid Geothermal Energy Systems

One of the most frequent issues faced in shallow GE systems is the thermal imbalance and heat accumulation. A practical solution is to adopt hybrid system that combines geothermal energy with other energy sources [101]. There has been significant interest recently on hybrid systems that integrate geothermal and other forms of energy sources to increase the overall output and efficiency. Hybrid geothermal systems (HGSs) used for heating and cooling applications are commonly encountered in the form of a hybrid ground source heat pump (HGSHP) or a hybrid ground coupled heat pump (HGCHP) [102]. Figure 2.25 shows the difference between the conventional GSHP and HGSHP designs.

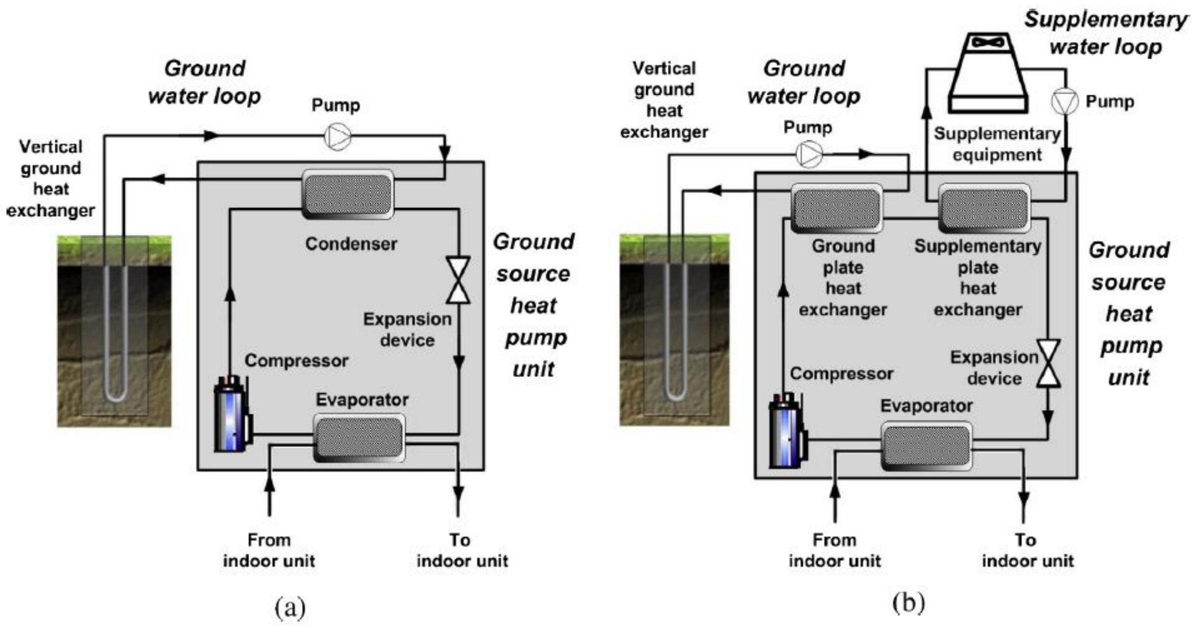


Figure 2.25: Difference between (a) ground source heat pump and (b) hybrid ground source heat pump [103]

Alavy *et al.* [104] investigated the use of a HGSHP for district heating and cooling through a common water loop distribution. The system showed high potential that depends mainly on building size and type as well as weather conditions and location. One of the most important parameters to be studied in these hybrid systems is the ratio between the heating and cooling loads to design the optimum ground regeneration cycle. Regenerating the ground potential can be achieved by adding a secondary energy source as mentioned above, or through a traditional heating, ventilating, and air conditioning (HVAC) system based on an ASHP. On the other hand, it is possible to achieve the required regeneration using a dry cooler. The cooler can be used to inject ambient heat into the cold bore field in winter and extract it from the warm bore field in summer. This would require the use of a dual bore field as recommended by Allaerts *et al.* [105]. Choosing the best hybrid system is not straight forward because each HGS must be considered from a different perspective such as initial or operating cost.

GE can be coupled with various energy sources depending mainly on sources' availability and effect on system's performance. Several possible integrations that involve geothermal energy systems will be discussed below. Based on previous investigations, it has been found that it is obviously better to use geothermal energy in hybrid systems regardless of other affecting parameters. The combination of GE with other sources provides various advantages especially associated with cost of energy. Table 2.3 highlights the advantages and disadvantages of geothermal hybrids as compared to conventional GE systems.

Table 2.3: Advantages and disadvantages of geothermal hybrids

| **Advantages** | **Disadvantages** |
|---|---|
| Low energy consumption | Complexity |
| Low cost of electricity | Control problems |
| Support higher peak loads | Connection troubles |
| Low capital cost | |
| Low operating cost | |
| No ground fouling | |
| Smaller bore field area required | |

There has been increasing interest in research related to the hybridization of geothermal energy systems. Figure 2.26 presents the trend of publications in the literature related to hybrid geothermal systems (reported by Olabi *et al.* [101] in 2019). Interest in such systems has increased tremendously during the past five to six years.

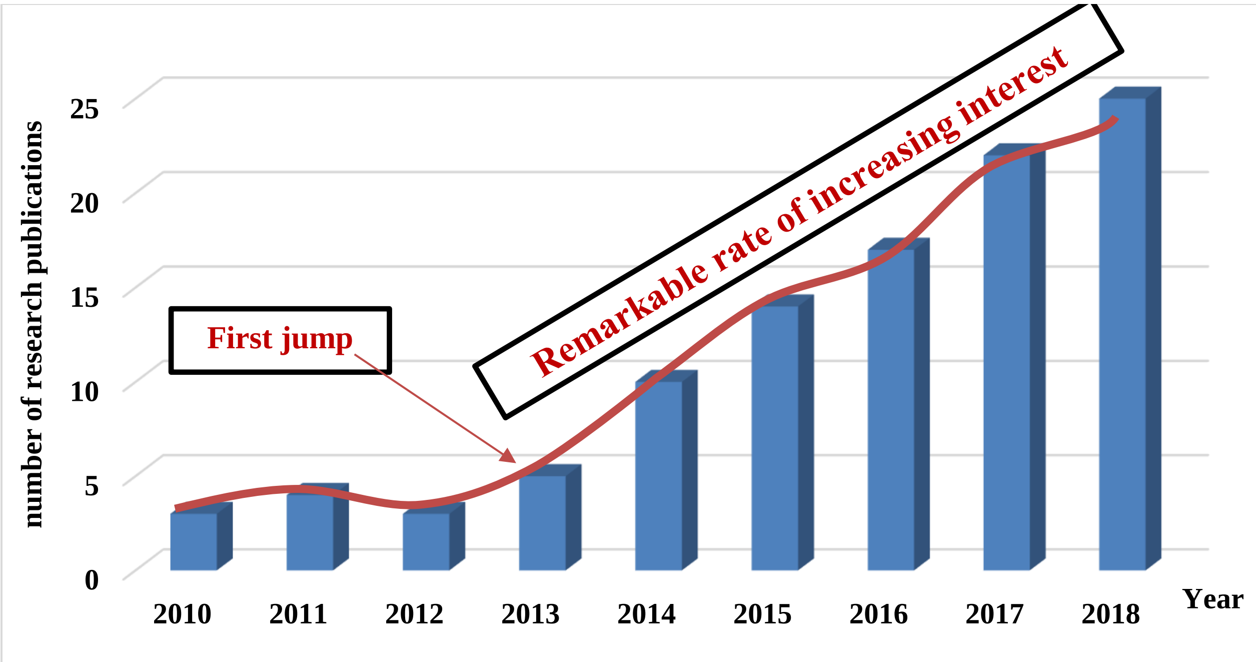


Figure 2.26: Evolution of research in hybrid geothermal systems [101]

Hybrid systems involving GE can provide different forms of energy. The chart in Figure 2.27 shows that HGSs are utilized mostly in the form of heat pumps with approximately equal share (44% each) for heating and cooling applications. The remaining 12% of hybrids reported in the literature are utilized for generation of electricity. The tendency to use these systems for thermal applications (heating and cooling) is directly related to the thermal nature of the energy source and available geothermal conditions.

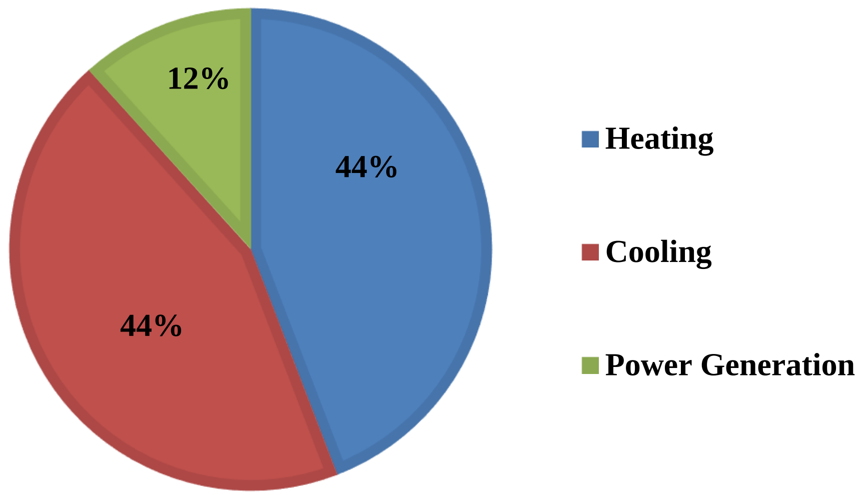


Figure 2.27: Different applications of geothermal hybrids; research conducted at the end of 2019 [101]

Hybridizations depend on many factors including resource availability, environmental effects, desired performance, energy price target, capital costs, operational costs, etc. The chart in Figure 2.28 shows the prevalence of the different types of systems integrated with geothermal installations as reported in the literature. The most common combination is geothermal-solar (about 45% of reported systems) followed by geothermal with a cooling tower (about 30%).

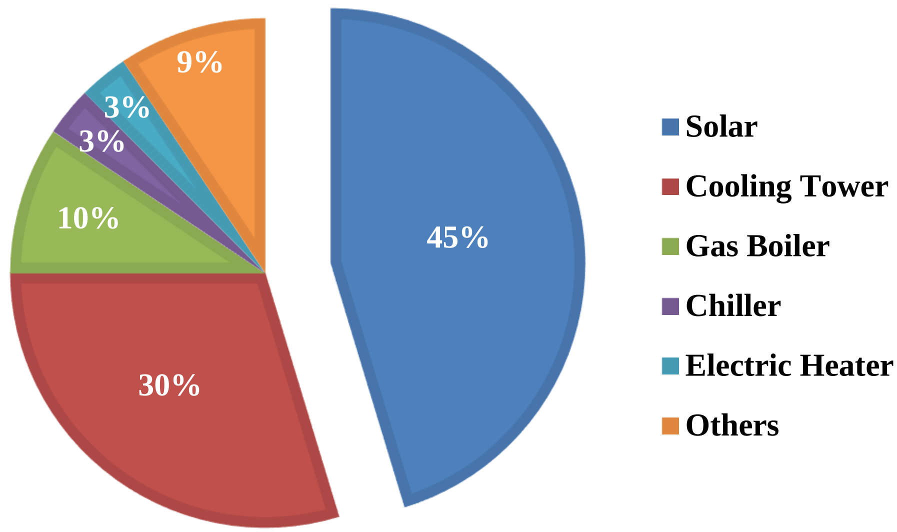


Figure 2.28: Types of systems integrated into geothermal hybrids; research conducted at the end of 2019 [101]

There are several factors that could affect the geothermal hybrid system's efficiency and economic feasibility (see Figure 2.29). This depends highly on the compatibility between the ground and the other source used in both cases, power plant and heat pump. Thus, it is very important to apply an accurate pre-study to check the viability of combining the two proposed sources to check if they could fit into one system from a thermodynamic point of view while examining the energy that could be generated with respect to time. This will highlight the expected problems that could mainly be solved by the help of energy storage systems. The capital and operating costs vary significantly from one country to the other based on the availability and abundance of energy resources and equipment.

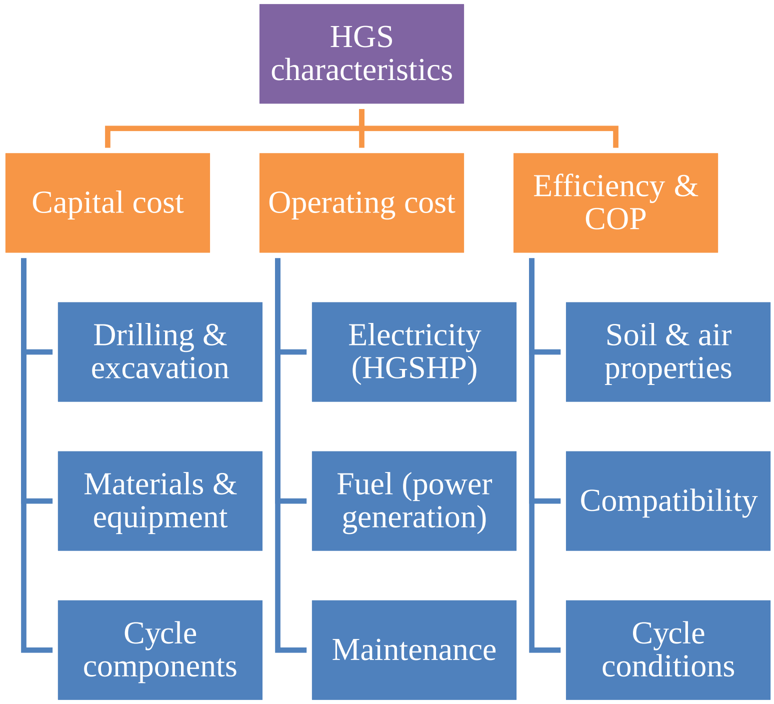


Figure 2.29: Factors affecting hybrid geothermal energy systems characteristics

Based on the literature, it is recommended first to determine the dominant load (cooling, heating, or power) to specify the preferable supplementary source in addition to the geothermal. In this regard, geothermal energy is prioritized over the other energy sources while avoiding thermal imbalance and heat accumulation (in case of shallow GE). Moreover, the supporting source must be highly abundant and have low impact on the environment. Therefore, increasing renewable energy and waste heat recovery utilizations is the most favourable method to encourage people toward adopting eco-friendly systems.

### 2.5.1 Integration of geothermal and solar energy systems

There are several ways that solar and geothermal energies can be integrated to form a hybrid energy system. For example, thermal solar collectors can be used to generate additional heat energy to shore-up any deficit from the geothermal system. A common hybrid solar-geothermal combination is the solar assisted ground source heat pump (SAGSHP). While there may be different implementations, the main objective of this combination is the reduction of annual operating costs and $CO_2$ emissions. Usually, hybrid power plants are much better than individual systems especially when the available sources are of low-grade natures which is almost the case of shallow GE. Geothermal and solar thermal storage combination is recently being a very important hybrid system that is employed to increase the seasonal coefficient of performance and decrease the ground loop size. One of the most important reasons for coupling the geothermal and solar thermal plants is to decrease the electricity required for operating the system. This system has four different operation modes: solar thermal ground storage, solar direct heating, direct heat exchange and geothermal heat pump. Boreholes can be used as energy storage systems by storing the excess of solar energy. This energy storage could face several barriers such as the geological conditions, unclear heat transfer mechanism and distributing underground environment. In addition to that, hybrid systems can solve the problem of inadequate drilling area in large commercial buildings while operating with a minimum cost compared to other individual systems. Therefore, hybridization of geothermal systems is very crucial because it improves the system's efficiency and prevents thermal imbalance which otherwise may lead to the system's failure. SAGSHP optimization studies are usually performed by the help of a seasonal regeneration system with a focus on the BHE thermal behaviour, system operation and seasonal effects of solar regeneration.

Solar thermal collectors can also be used for ground heat recovery and stabilizing the geothermal system [106]. Conversely, a geothermal heat exchanger can be used as a second heat source to support the solar thermal power plant [107, 108]. This combination can increase the overall efficiency by 3.6% compared to the combined individual systems as reported by Ghasemi *et al.* [109]. Another motivation for integrating geothermal and solar thermal systems might be the need to increase the steam flow in the geothermal cycle [110]. Researchers have been able to reduce the initial costs associated with a geothermal system by using a SAGSHP to reduce the required borehole heat exchanger field size. It is also possible to use a supercritical ORC based on a geothermal system integrated with a concentrated solar power system to increase peak loads for demand-side management [111]. While most hybrid systems are designed for heating applications, it is also possible to integrate a GHE with a solar cooling system to improve its performance [112].

Solar thermal systems suffer from seasonal deterioration in energy output depending on the sun's position and ambient air temperatures. One way to improve the seasonal coefficient of performance is to use the geothermal system as a seasonal energy storage. The system is mainly composed of solar collectors, short-term thermal storage devices, heat pump, and borehole heat exchanger for long-term storage. A staged series of GHEs can be used to reduce temperature differences and maintain the effectiveness of the storage system for an elongated period [113]. Ground water flow may be the main limiting factor against the use of such an integration [114]. Ground water flow levels at the site must be low enough to ensure that the induced thermal plume is not dissipated. Based on the previous mentioned investigations, several researchers have reported that seasonal heat storage is not reliable for solving the thermal imbalance if ground water seepage velocity is large.

As can be seen from the above examples, integrating solar thermal system with geothermal plant can either assist in producing additional power, or reducing the consumed geothermal energy. An essential factor to consider in the design of hybrid solar-geothermal systems is the state of the available ground fluid. If the available fluid is in the steam-liquid state, then a flash cycle (see Figure 2.30 and Figure 2.31) would be the preferred design [115, 116]. Incorporating the solar system contributes to superheating and evaporating the geothermal fluid and therefore boosting the generated power [109].

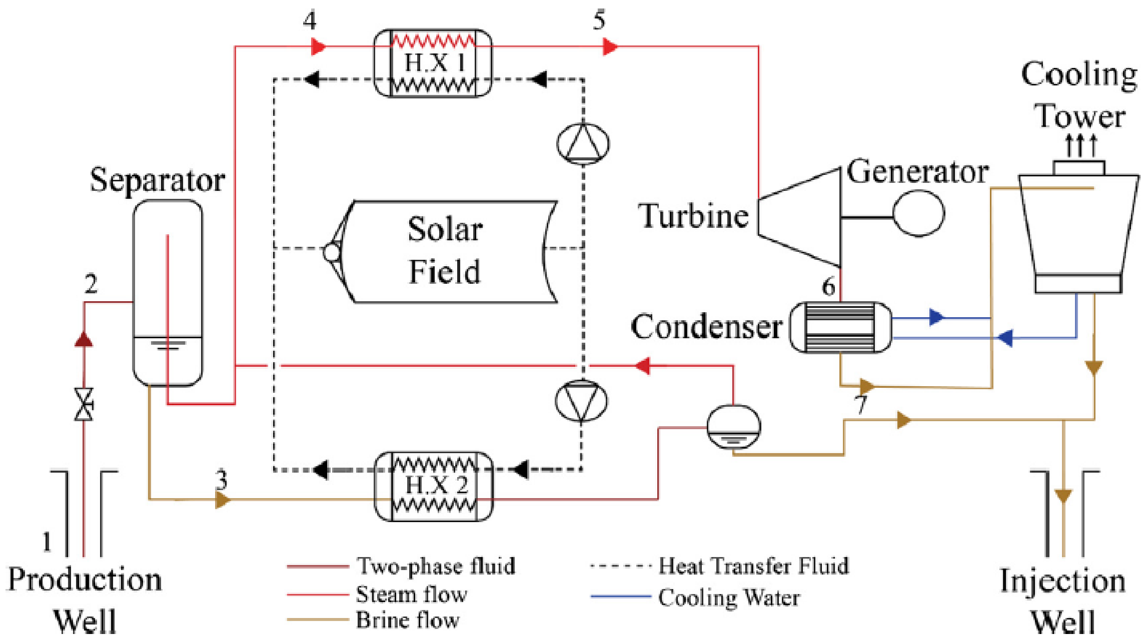


Figure 2.30: Single-flash hybrid power plant [115]

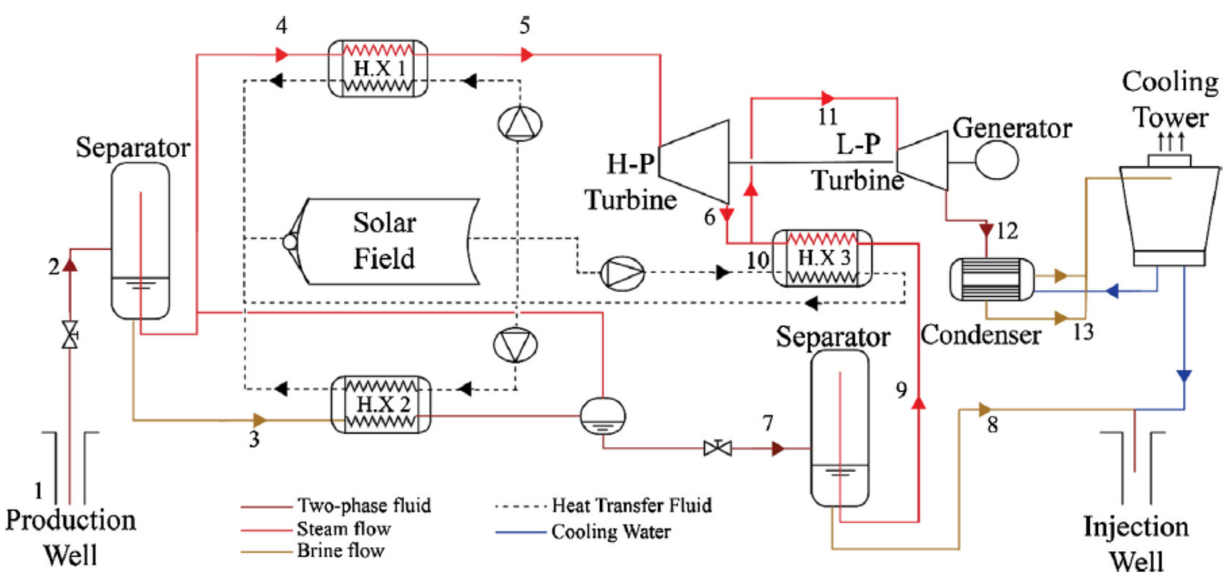


Figure 2.31: Double-flash hybrid power plant [115]

A photovoltaic thermal hybrid system (PVT) can be integrated with a GSHP to produce different forms of energy at the same time (as shown in Figure 2.32). While the GSHP system works on extracting thermal energy from the ground, the PVT system produces electrical energy from the incident sun light and at the same time extracts additional thermal energy from the sun's heat. Careful consideration for the working fluid is necessary to ensure best results from these systems. Most designs have concentrated on using organic fluids. However, it is also possible to use a refrigerant fluid like $CO_2$ in which the cycle would require some modifications such as the incorporation of a reverse transcritical cycle [117, 118]. Other studies have also investigated the use of hybrid systems for water distillation in addition to power generation [119]. Recently, poly-generation and tri-generation systems are becoming more common. The system presented in Siddiqui *et al.* [120] shows a solar-geothermal system being used for generating electricity, cooling, and hydrogen production. The energy and exergy efficiencies were found to be 19.6% and 19.1%, respectively.

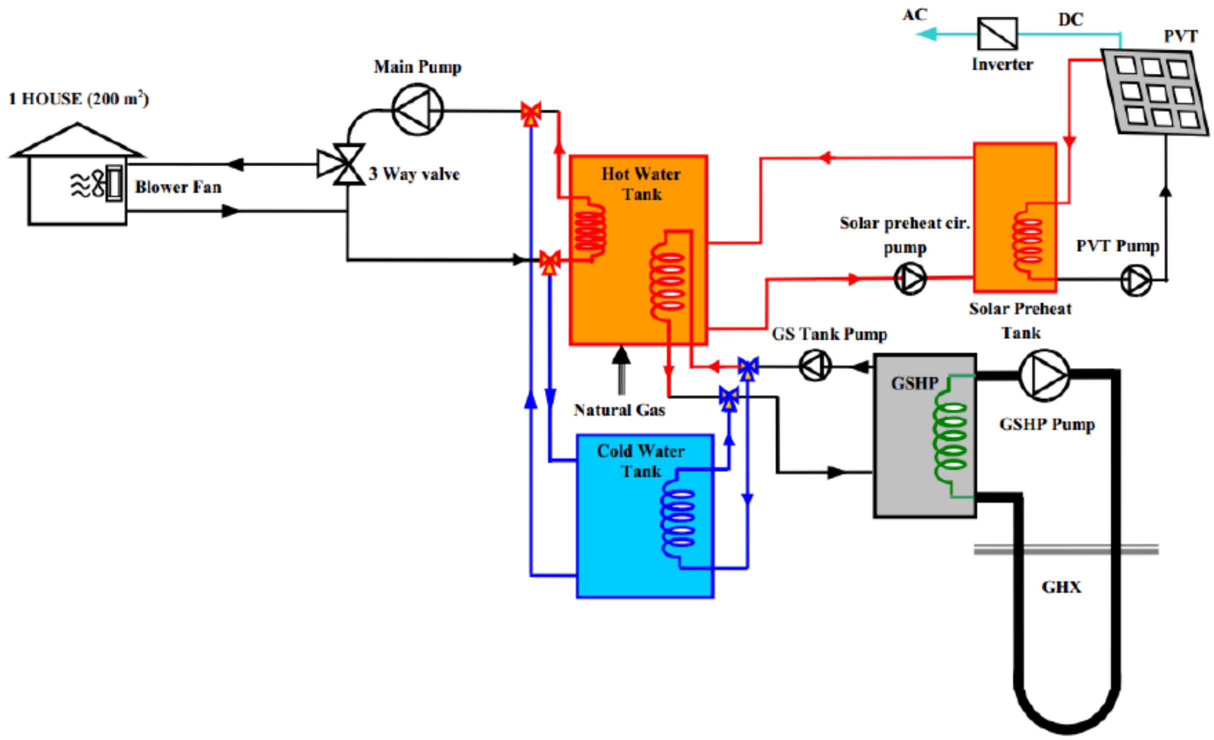


Figure 2.32: Photovoltaic thermal integrated with ground source heat pump [121]

Because of inherent uncertainties and nonlinearities, all the mentioned hybrid systems suffer from issues related to control. This has motivated researchers to find new control methods such as fuzzy logic (FL) controllers [121] and model predictive control (MPC) [122].

Trillat-Berdal *et al.* [123] presented a combination between GSHP and solar collectors (see Figure 2.33). The roles of the solar collectors are domestic water pre-heating, dwelling heating, and soil thermal recharging (if excess). This coupling helps reducing the borehole length and hence decreasing the capital cost of the system. It was found that if there are several BHEs in the same field, a thermal ground recovery is needed, which is directly related to the operating duration.

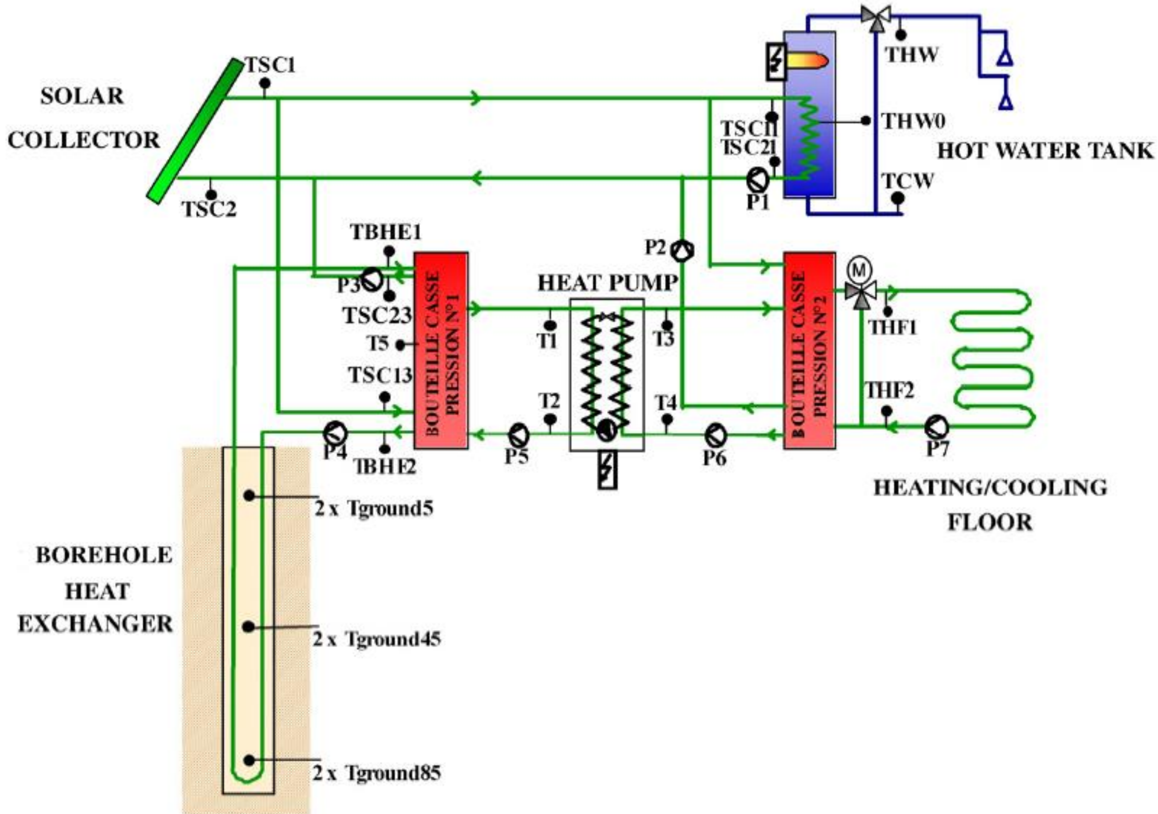


Figure 2.33: Diagram of GEOSOL process proposed by Trillat-Berdal *et al.* [123]

### 2.5.2 Integration of cooling tower into geothermal systems

It has been shown that it is advantageous to incorporate a cooling tower with the ground source heat pump (see Figure 2.34) to improve the cooling efficiency [103]. This hybrid system can maintain soil thermal balance such that the annual overall COP of the GSHP can be around 3.96 (3.93 for cooling and 4.09 for heating) [124]. The capacity of the cooling tower needs to be chosen taking into consideration the difference between peak and average load values or the cooling load percentages. Simulation studies have shown that the cooling tower needs to be activated two years after initial heat pump operation. An optimal auxiliary cooling ratio (ACR) needs to be chosen based on the system's configuration (see Figure 2.35) [125].

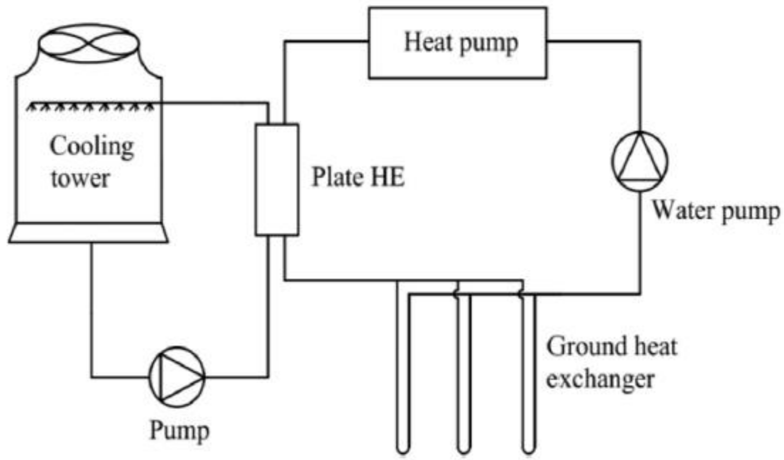


Figure 2.34: Ground source heat pump coupled with a cooling tower [126]

It has been recommended in the literature that the cooling tower needs to be integrated in a serial configuration as depicted in Figure 2.35 to avoid heat accumulation [127]. In addition, it is necessary to keep the temperature of the circulating water in the cooling tower as low as possible to increase the coefficient of performance (COP). If the cooling load is very high for a standard cooling tower, then a traditional HVAC system can be added to meet the cooling demand [128]. It is also possible to incorporate a second cooling tower having the same capacity as the ground heat exchanger to serve as an alternator or accumulator [129].

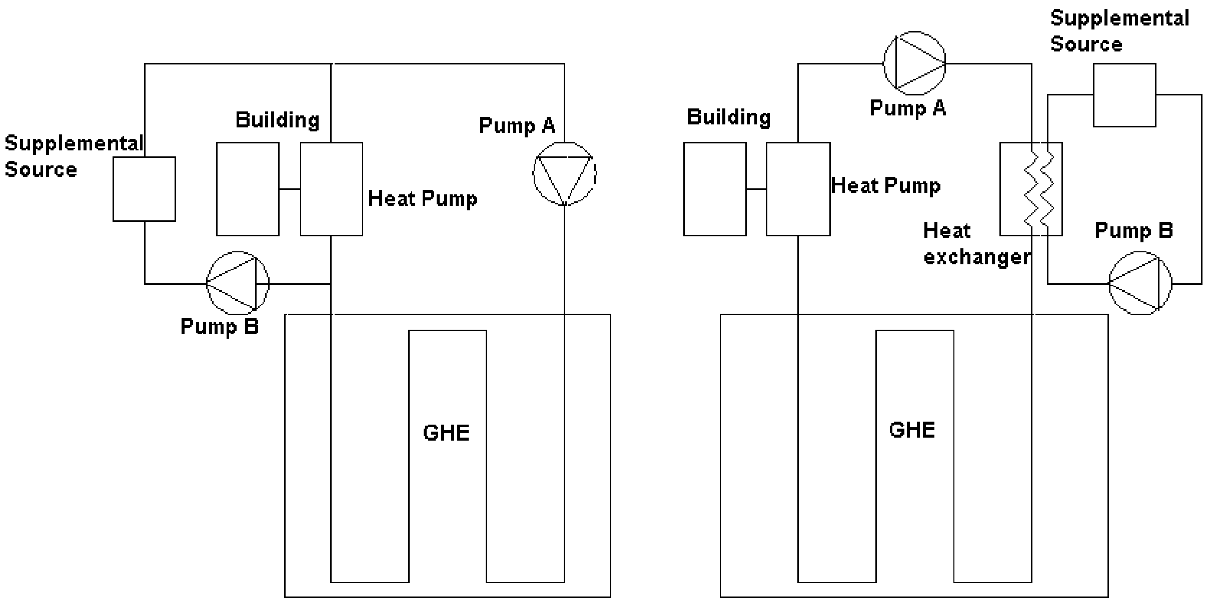


(a) (b)

Figure 2.35: Parallel (a) vs. serial (b) hybrid ground source heat pump configurations

After studying the different strategies for controlling the geothermal-CT system, researchers have reported that the most optimal strategy is the wet bulb temperature control method. This method is based on the difference between outlet fluid temperature and the temperature of wet bulb [124]. The aim of investigating this method is to make full use of heat exchange between air and soil. It concentrates on deriving the most benefit from ambient capacity by prioritizing the use of ambient air as the cooling source. Artificial neural network (ANN) models were developed to predict the temperature of the water exiting the GHE in comparison with that of the cooling tower. The ANN showed an absolute error of about 0.2°C according to the study carried out by Gang and Wang [130].

Another control method that has been suggested for hybrid geothermal-CT systems is the extremum seeking control (ESC) [126]. This feedback-based method (depicted in Figure 2.36) is based on the comparison between the total power consumption, flow rate entering the CT, and pump speed. ESC has been shown to provide 9.3% energy savings as compared to other methods. This method is very helpful in applications where the system consists of multiple borehole heat exchangers. In such systems, it would be advisable to normally operate some of the BHEs only and limit the operation of all BHEs together to peak load periods [131].

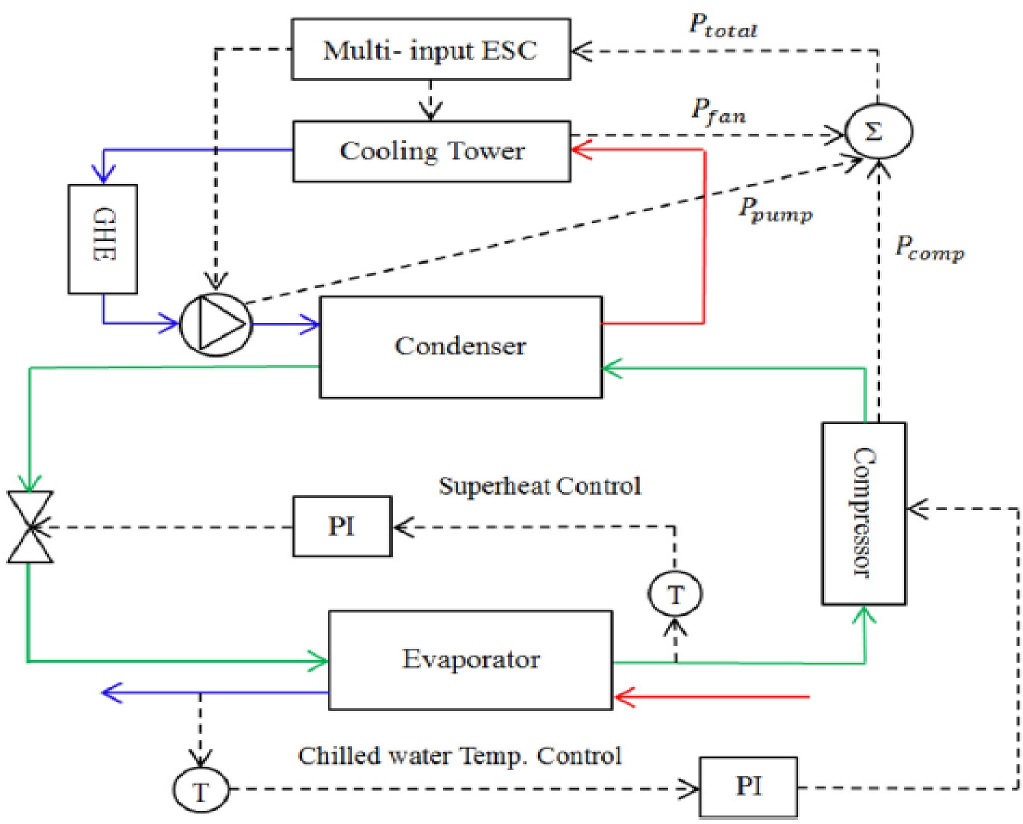


Figure 2.36: Extremum seeking control for optimizing efficiency of hybrid ground source heat pump [126]

### 2.5.3 Less-commonly used hybrid geothermal systems

There are some less common hybridization techniques that can integrate GE with other sources of energy. For example, it is possible to integrate geothermal with waste heat recovery (another source of low-grade energy) in a power generation system. Another example would be the injection of industrial waste heat into geothermal boreholes. This integration exploits the thermal storage characteristics of the boreholes and allows the extraction of waste energy exhausted by industrial processes.

A geothermal installation can be integrated into an existing coal fired power plant to improve efficiency and lower the cost. The geothermal system can be used to preheat the boiler's feed water and can also be used as a carbon capture storage. Researchers have determined that a serial configuration for geothermal preheating is better at temperatures below 140°C [132]. A detailed analysis of available conditions with regards to coal sufficiency and availability of geothermal hot water are needed before such a system can be contemplated. Another integration can be based on utilizing the coal plant for electricity generation and the geothermal system for providing additional capacity to meet high heating demands [133, 134].

GE can be used to preheat the organic fluid in a dual-fluid biomass system to achieve the highest possible output power (see Figure 2.37) [135]. Researchers have reported that it is advisable to integrate a pre-heater and evaporator into the geothermal system to achieve the combined heat and power system improvements [136].

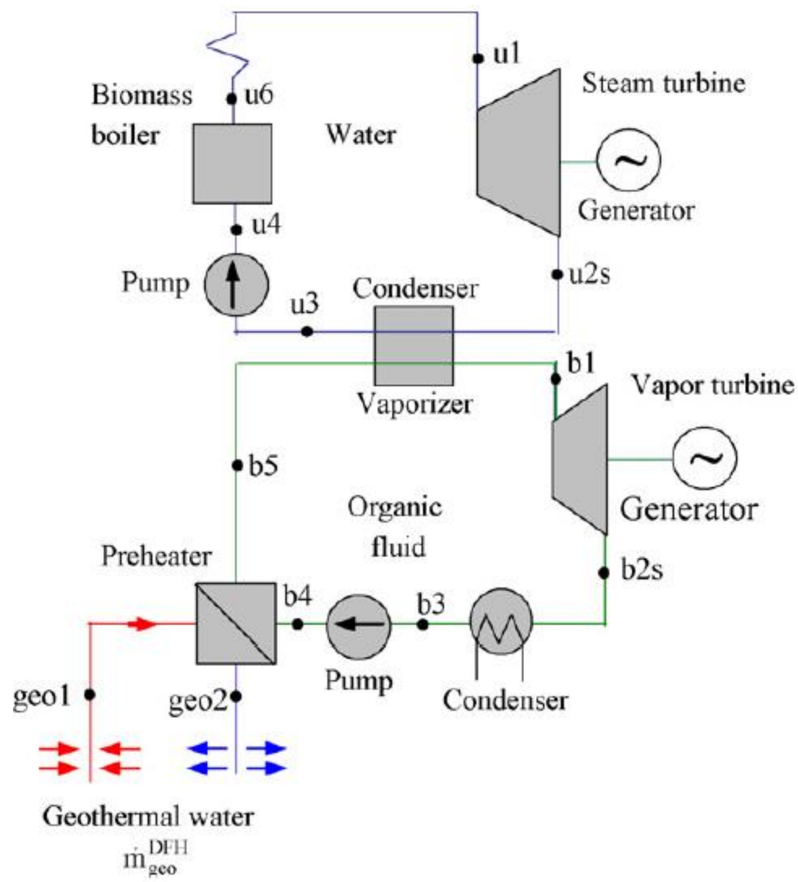


Figure 2.37: Dual fluid hybrid geothermal-biomass power plant [135]

One of the main issues affecting GSHPs is the thermal imbalance. It has been shown that increasing the size of the heat exchanger can alleviate this issue. However, this may not be always feasible if the available space is limited. If the load is cooling dominated, then a chiller can be integrated into the geothermal system to improve the system's performance [137]. Adequate consideration should be given to factors affecting the chiller's design such as required cooling, compressor efficiency, and climate conditions. A geothermal system can be integrated with a floor cooling system to provide a secondary cooling source [138]. The geothermal system can provide elimination of the floor condensation due to excessive heat that would be generated if the floor radiator is used alone.

Several studies have shown that hybrid systems integrating geothermal energy into existing energy systems can provide improvements in efficiency as well as economics. Cui *et al.* [139] have shown that coupling a geothermal source with an electric heater could produce 3.4% savings in energy used for heating and provision of domestic hot water.

Various studies have been performed to compare the performance of traditional geothermal systems with hybrids. It was shown that it is more beneficial to control the temperature of the fluid entering the system when a geothermal system is integrated with a gas boiler and electric air-conditioning system [140]. In Liu *et al.* [133], a COP of 2.79 was achieved while combining the gas boiler with the GSHP to provide heating. On the other hand, it would be more beneficial to vary the temperature of the fluid exiting the system when a geothermal system is integrated with a cooling tower and a boiler [141].

GE can also be used to retrofit other existing plants such as preheating the boiler feed water of a coal fired facility to capture efficiency improvements. Several studies were performed to maximize the utilization of renewable energy and waste heat recovery by designing a borehole thermal energy storage (BTES) system [142, 143]. BTES can provide a convenient medium to store the excess of energy supplied by the main source feeding the system.

## 2.6 Ecological Impact

Among the two types of geothermal energy, it is considerably clear that deep GE has more impact on the environment compared to shallow GE. Water contamination is one of the major drawbacks of deep systems since geothermal fluids contain harmful substances such as sulphur, salts, and minerals. Another disadvantage is the large consumption of water of open loop GE systems. The extraction of geothermal fluids for generating power can cause severe air pollution since they usually contain hydrogen sulphide, carbon dioxide, ammonia, and methane. These gases are very harmful to human life and have huge effect on climate changing [144, 145]. On the other hand, shallow GE systems have much less ecological impacts. Regulations are more considered for open loop shallow systems where there is consumption of water and high probability of water contamination. However, in case of closed loops, there must be no water contamination unless it is improperly designed where leakage may occur [146]. The major adverse environmental impact of shallow GE closed loop systems is the thermal imbalance of soil which is usually due to the inappropriate design conditions and overloading [147]. Consequently, this imbalance may cause soil volume changing which may negatively affect nearby foundations. This effect depends significantly on the properties of soil and grout material as previously discussed in this chapter. Fujimitsu *et al.* [148] investigated the subsurface environmental changes caused by the use of GSHP over 20 years of operation. The authors deduced that the amplitude and phase of annular temperature are almost the same for 20 and 2 years of operation. Figure 2.38 presents the results corresponding to the 2-year operation for a depth of 35 m.

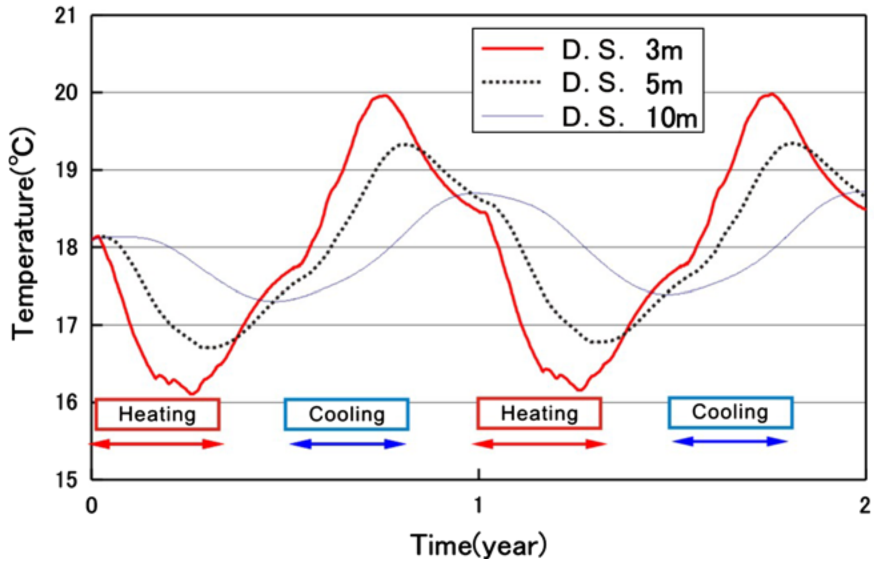


Figure 2.38: Subsurface temperature changes during 2 years at the downstream side (D.S.) of the heat exchanging well at a depth of 35 m [148]

## 2.7 Research Gap

The literature presented in this chapter shows that GE has been immensely developed in the recent years. Figure 2.39 presents a summary of the commonly known geothermal energy-related systems reviewed in the current chapter including applications, installations, advantages, and disadvantages. It is obvious that there are no direct reports on the use of shallow GHEs for cooling power cycles. However, there are several investigations that examined the usage of GE for heating and power generation applications. Thus, this research highlights the research gap in this domain and focuses on using shallow GE as a cooling system for enhancing power cycles.

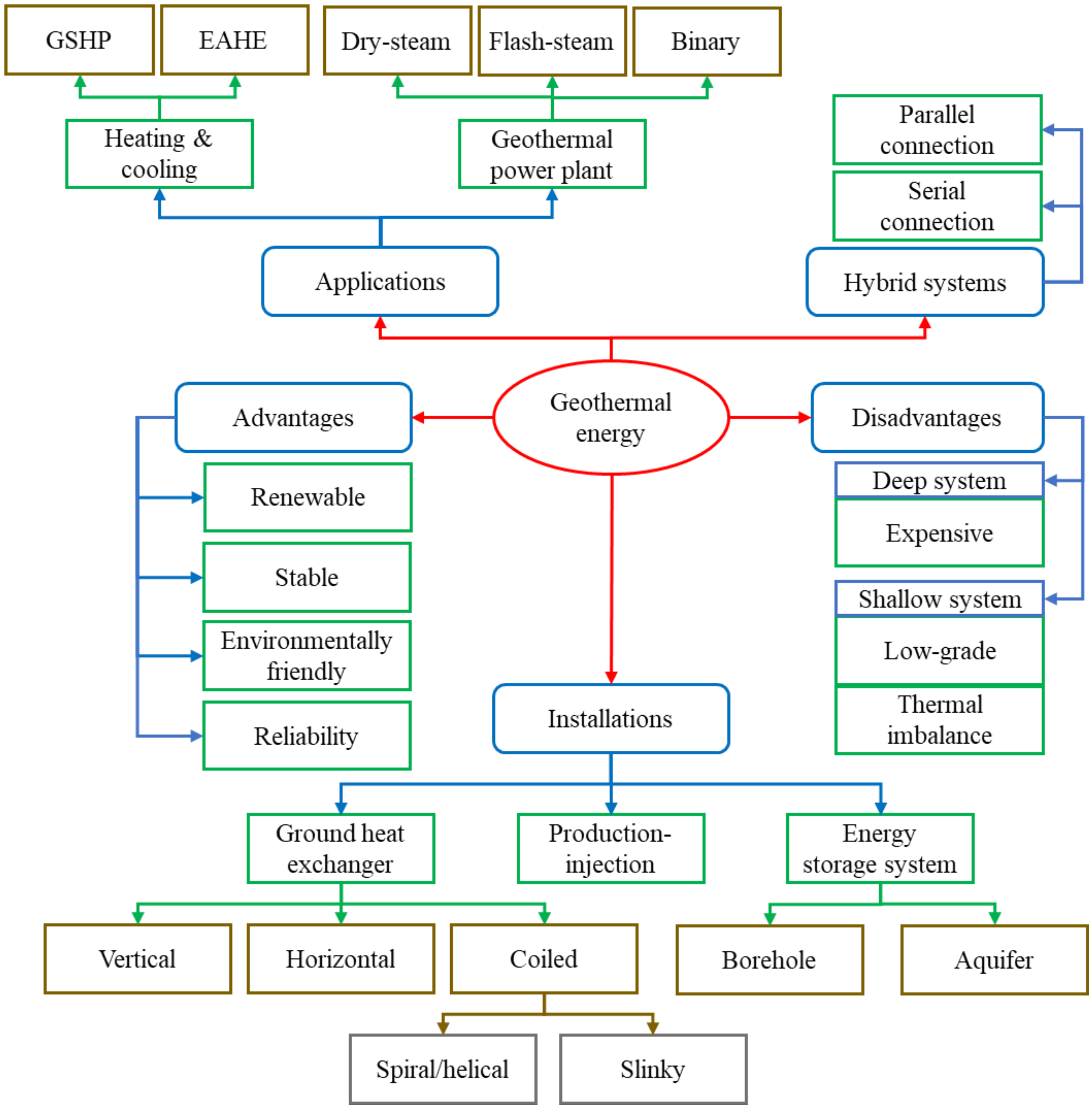


Figure 2.39: The characteristics of geothermal energy-related systems

# Chapter 3. Ground-Cooled Condenser Investigation using EES

In this chapter, $CO_2$-based transcritical Rankine cycle (CTRC) will be used to generate electricity from different heat source conditions while using the underground water as a condenser [149]. Usually, all previous studies that investigated geothermal energy in power generation have used the ground as a source of heat. These systems could be found in four different forms: dry steam, binary, single and double flash cycle depending on the geothermal conditions. These have also passed through several enhancements to improve the cycle's performance such as the combined flash-binary [150, 151] and regenerative cycle [152, 153]. However, the innovative aspect in this study is to use the ground as a heat sink (condenser). This will provide a lower cooling medium temperature, so that the condenser's pressure could be decreased accordingly. Thus, the net output power will be maximized which depends mainly on the pressure difference between the gas heater and condenser. The different conditions of the cycle are discussed in this chapter such as pressures, temperatures, and flow rate to optimize the cycle's performance and heat exchangers' sizes. Figure 3.1 shows the temperature-entropy diagram of CTRC displaying the enhancement in the cycle's net output power.

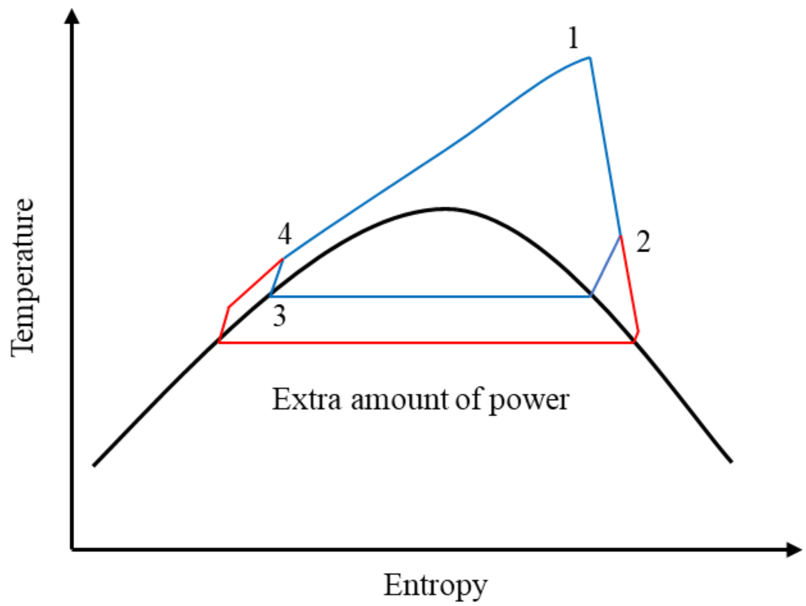


Figure 3.1: Adjusted temperature-entropy diagram of a transcritical Rankine cycle enhanced with a ground cooling system

## 3.1 Initial Concept

The aim of this study is to investigate a new system using CTRC with a ground-cooled condenser. It is proposed to generate electricity especially in summer because the ground temperature under a certain depth is approximately independent of the ambient conditions. Therefore, the ground heat exchanger is a better choice compared to the air heat exchanger when the ambient temperature is high during summer. To provide the suitable heat transfer conditions, the geothermal condenser is embedded in a well to facilitate the process of heat exchange by the help of underground water. Figure 3.2 presents the proposed CTRC showing all its components knowing that the source of heat considered in this study is a heat wasted from an engine exhaust (see section 3.4).

In this chapter, the underground water temperature is assumed to be constant which means that it is not affected by the amount of heat rejected from the cycle to the ground. This assumption can be considered only in two cases, either when the well's volume is relatively very large, or the ground-cooled condenser is functioning as a secondary condenser. The latter is highly recommended to ensure stability since the primary condenser (air/water-cooled) can reduce the amount of heat rejected to the ground and compensate the coolth energy during off-periods. This will be more illustrated in Chapter 4 and Chapter 5 showing the detailed operational strategy in addition to the different operating modes. This will explain how the ground temperature surrounding the GHE could be maintained constant by managing the operation of the cooling system and using a coolth recovery approach. In this case, the ground/underground water can be used as a cooling storage medium and especially because the proposed system is mainly designed to be convenient for waste heat recovery applications knowing that such applications usually do not operate 24 hours/day.

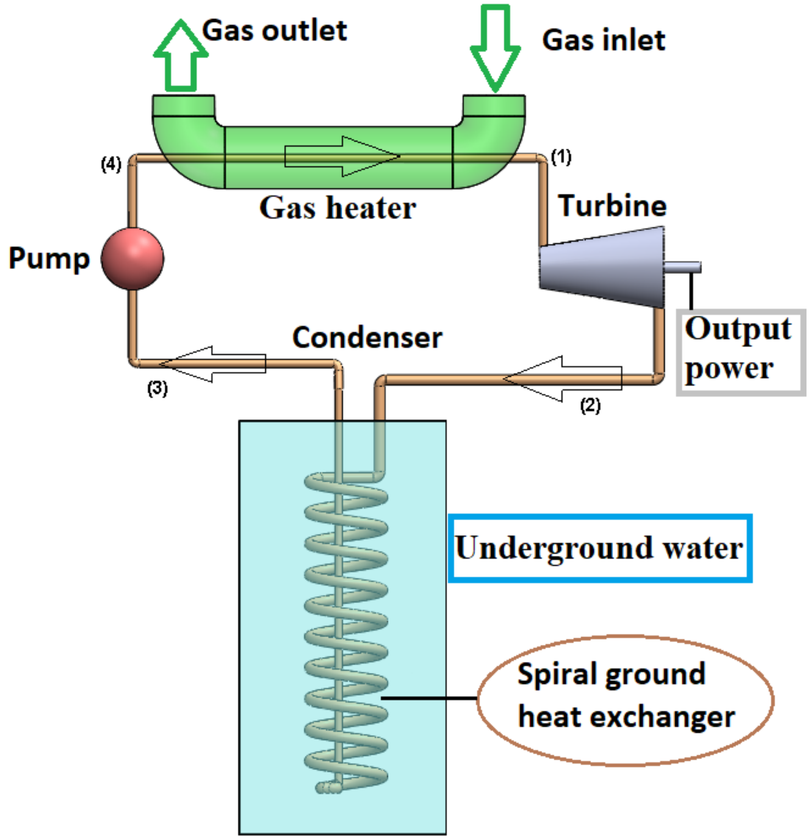


Figure 3.2: $CO_2$-based transcritical Rankine cycle combined with an underground water condenser

As shown in Figure 3.2, the condenser is selected as a helical GHE to minimize the total volume of the GHE. The heat recovery system is chosen as a counter flow heat exchanger also to obtain the minimum possible size. This study covers several variable conditions of gas, cycle, and underground water to find out the optimal conditions for the cycle and minimal size of heat exchangers.

### 3.2 Theory of Modelling

The model presented in this section shows the equations used for calculating the cycle's performance and heat exchangers' lengths that were developed in Engineering Equation

Solver (EES) as shown in Appendix A.1. EES is very compatible with such models since it includes all required thermodynamic properties and has a very simple programming language. The thermodynamic performance of the power plant depends on the amount of heat extracted from the gas, choice of pressures and temperatures of the cycle and the efficiencies of turbine, pump, and generator. The net output power can be calculated by:

$$\dot{W}_{net} = \dot{W}_t . \eta_g - \dot{W}_p \tag{3.1}$$

where $\dot{W}_t$ is the turbine power, $\eta_g$ is the generator efficiency and $\dot{W}_p$ is the pump power. $\dot{W}_t$ and $\dot{W}_p$ mainly depend on the mass flow rate of $CO_2$ and the enthalpy variation as shown in equations (3.2) and (3.3).

$$\dot{W}_t = \dot{m}_f (h_1 - h_2) \tag{3.2}$$

$$\dot{W}_p = \dot{m}_f (h_4 - h_3) \tag{3.3}$$

After calculating the net output power, the efficiency can be evaluated as follows:

$$\eta = \frac{\dot{W}_{net}}{\dot{Q}_{in}} \tag{3.4}$$

$$\dot{Q}_{in} = \dot{m}_g c_{pg} \left(T_{gi} - T_{go}\right) = \dot{m}_f (h_1 - h_4) \tag{3.5}$$

where $\dot{Q}_{in}$ is the heat extracted from the gas and added to the cycle gas heater. The value of heat added is based on the specific heat ($c_{pg}$), flow rate ($\dot{m}_g$) and temperature difference of hot gas ($T_{gi}$ and $T_{go}$). Then, it is necessary to check the area of heat exchangers involved in the proposed system shown in Figure 3.2 (gas heater and condenser). The lengths of gas heater and condenser are mainly affected by the amount of heat added and extracted to/from the cycle, respectively. The area of each heat exchanger is based on the energy balance equation (between $CO_2$ and heat source/sink) which is represented by:

$$\dot{Q} = U.A.\Delta T_{lm} \tag{3.6}$$

where $\dot{Q}$ is the heat added or extracted to/from the system, $U$ is the overall heat transfer coefficient that depends on the convection heat transfer coefficient of both fluids and the thermal conductivity of the pipe, $A$ is the heat exchanger's area and $\Delta T_{lm}$ is the logarithmic mean temperature difference. Equation (3.7) represents the relation between the overall heat transfer coefficient ($U$) and the equivalent thermal resistance ($R_{eq}$) of the heat exchanger.

$$U.A = \frac{1}{R_{eq}} \tag{3.7}$$

As shown in Figure 3.3, the three thermal resistances represent a serial connection. Thus, the following equations (3.8 and 3.9) can be used to calculate the equivalent thermal resistance.

$$R_{eq} = R_{conv-1} + R_{cond} + R_{conv-2} \tag{3.8}$$

$$R_{eq} = \frac{1}{h_i \pi d_i L} + \frac{ln\left(^{r_0}/_{r_i}\right)}{2\pi k L} + \frac{1}{h_o \pi d_o L} \tag{3.9}$$

where $h_i$ and $h_o$ are the convective heat transfer coefficients of the internal and external fluids and $k$ is the thermal conductivity of the pipe. $r_i$, $d_i$, $r_o$ and $d_o$ corresponds to the internal and external radii and diameters, respectively.

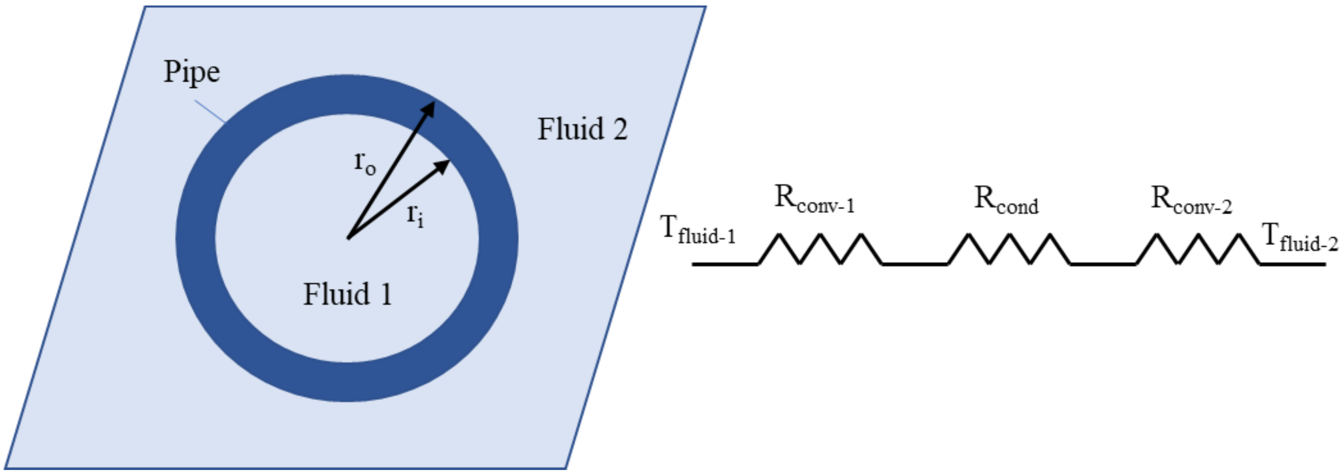


Figure 3.3: Schematic representation for the thermal resistances inside the heat exchanger

The logarithmic mean temperature difference used in equation (3.6) depends on the temperature difference between inlet and outlet of hot and cold fluids in the heat exchanger as shown in Figure 3.4. The following equation presents the relation between these temperatures and $\Delta T_{lm}$:

$$\Delta T_{lm} = \frac{\Delta T_1 - \Delta T_2}{ln\left({}^{\Delta T_1}/_{\Delta T_2}\right)} \tag{3.10}$$

where $\Delta T_1$ and $\Delta T_2$ are the temperature difference between the hot and cold fluids entering and exiting the heat exchanger.

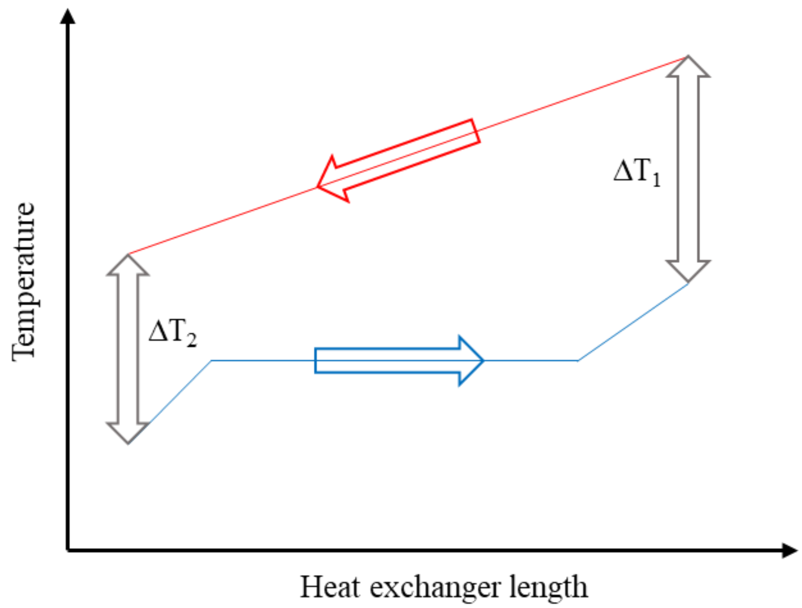


Figure 3.4: The variation of hot and cold fluid temperatures inside a counter flow heat exchanger

The convection heat transfer coefficient of all fluids involved (hot gas, underground water, and $CO_2$ is given by:

$$h = \frac{Nu.k}{L_r} \tag{3.11}$$

where *Nu* is the Nusselt number, *k* is the thermal conductivity and $L_r$ is the characteristic length. In the case of turbulent internal flow forced convection, the hydraulic diameter is considered as the characteristic length and the following equation could be used to calculate the Nusselt number of hot gas and working fluid [154]:

$$Nu = 0.023.Re^{0.8}.Pr^{n} \tag{3.12}$$

where *Re* and *Pr* are the Reynolds and Prandtl numbers, respectively. *n* is equal to 0.3 in case of cooling and 0.4 for heating. When the velocity of the fluid is equal to zero, free convection will take place which is the case of underground water. According to Izadpanah *et al.* [155], the following Nusselt number correlation could be used for coiled heat exchanger natural convection applications:

$$Nu = Ra^{0.3071} \left(\frac{H}{D}\right)^{-0.1097} \tag{3.13}$$

where *Ra* is the Rayleigh number, *H* is the height of the coil and *D* is the coil diameter. This correlation is only considered when the characteristic length is taken as the coil length ($L_c$) which is presented in equation (3.14) [155].

$$L_c = n_c({p_c}^2 + \pi^2 D^2)^{0.5} \tag{3.14}$$

where $n_c$ is the number of turns and $p_c$ is the pitch (distance between two consecutive turns).

### 3.3 Methodology

The methodology that was followed in this chapter to develop the presented model is as follows:

- Entering the heat source characteristics: composition, specific heat, thermal conductivity, viscosity, and Prandtl number.
- Choosing the condensation and evaporating temperatures based on the ground and heat source temperatures, respectively.
- Evaluating the enthalpy of working fluid at all states.
- Calculating the working fluid’s mass flow rate as presented in equation (3.5).
- Calculating the cycle’s net output power and efficiency as shown in equations (3.1) and (3.4), respectively.

- Dividing the heat exchangers (evaporator and condenser) into two parts to separate the change of phase and temperature investigations.
- Determining the working fluid's characteristics based on the average temperature in the two parts of heat exchangers: Reynolds number, Nusselt number, Prandtl number, viscosity, thermal conductivity, and convection heat transfer coefficient.
- Calculating the heat transfer coefficient of heating and cooling sources using equations (3.12) and (3.13), respectively.
- Calculating the overall heat transfer coefficient (*U*) to evaluate the required size for both heat exchangers.

### 3.4 Model Validation

The proposed model was validated by comparing the net output power with the $CO_2$-RC studied by Shu *et al.* [156] based on the conditions presented in Table 3.1. The cycle was used as a heat recovery system at the exhaust of an engine. The exhaust gas is formed of 19.84% $CO_2$, 8.26% $H_2O$ and 71.49% $N_2$. The presented model was inserted into the Engineering Equation Solver (EES) to carry out the simulations of this study.

Table 3.1: The parameters considered for the model validation [156]

| Parameters (Units) | Values |
|---|---|
| Gas inlet temperature (°C) | 777 |
| Gas outlet temperature (°C) | 120 |
| Gas flow rate (kg/hr) | 202.6 |
| $CO_2$ condensation temperature (°C) | 25 |
| Pump isentropic efficiency | 0.8 |
| Turbine isentropic efficiency | 0.7 |
| Generator efficiency | 0.9 |

Figure 3.5 presents the validation of the proposed model by displaying the variation of net output power as a function of the temperature entering the turbine (100-700°C) such that (a) and (b) are the results obtained from Shu *et al.* [156] and (c) is the result of the CTRC used in the current research.

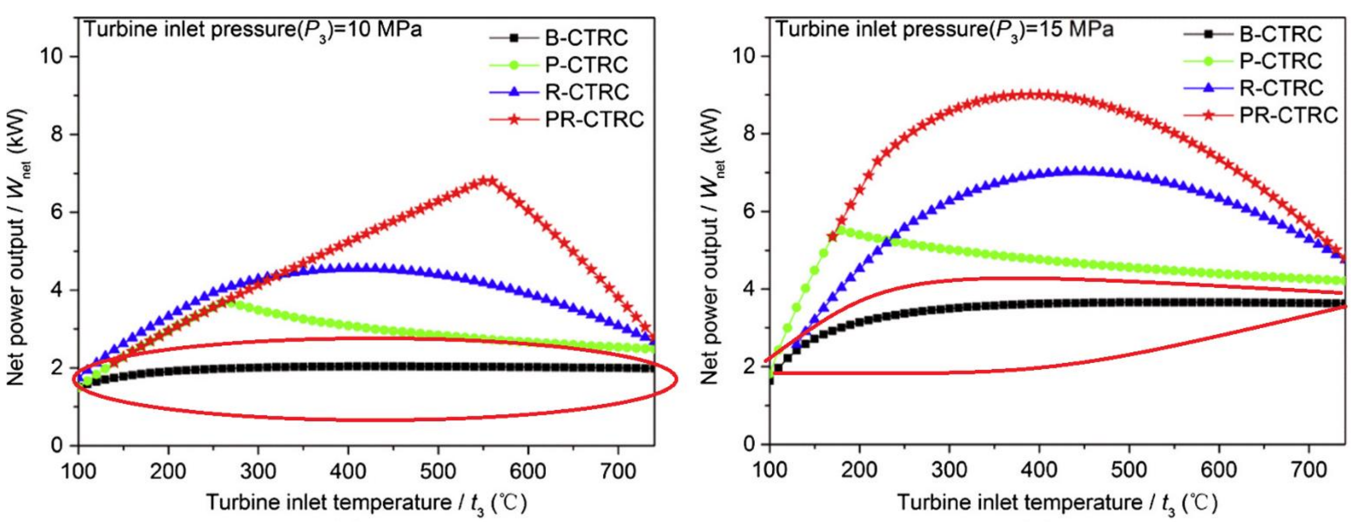

(a) (b)

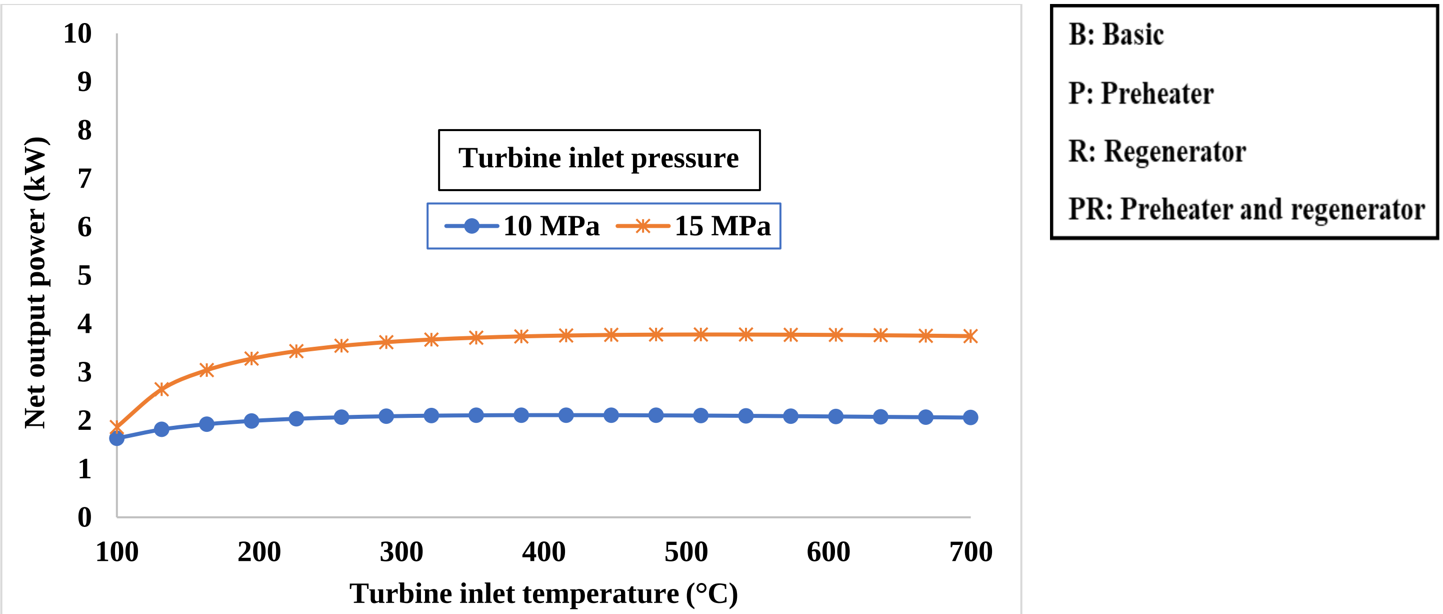


(c)

Figure 3.5: The variation of net output power as a function of turbine inlet temperature; (a) and (b) are obtained from Shu *et al.* [156] at 10 MPa and 15 MPa respectively while (c) refers to the proposed model

According to Figure 3.5, the proposed model behaves as expected due to the similarity in the net output power generated at the two different operating pressures (10 MPa and 15 MPa) compared to the results obtained by Shu *et al.* [156]. As the turbine inlet temperature increases from 100°C to 700°C, the power generated increases approximately from 1.8 kW to 2 kW and from 2 kW to 3.9 kW at $p_1$ = 10 MPa and $p_1$ = 15 MPa, respectively.

### 3.5 Design conditions

Table 3.1 and Table 3.2 present all cycle's conditions such that these values are considered as a reference for the upcoming investigations. However, some of them may vary aiming to study a specific relation which will be clearly presented within the discussion and analysis of each result. The gas components are still the same as mentioned in section 3.4, even though they refer to an engine waste, but this study could fit any other heat source application because a range of gas flow rate and temperature are examined. The main difference that may vary from one application to the other is the heat transfer coefficient of gas since it is directly affected by the gas composition.

Table 3.2: Parameters considered for the proposed model

| **Parameters (Units)** | **Values** |
|---|---|
| Gas heater diameter (mm) | 40 |
| CTRC diameter (mm) | 20 [157] |
| Turbine inlet pressure (MPa) | 15 |
| Underground water temperature (°C) | 15 |
| Turbine inlet temperature (°C) | 350 |
| Coil diameter (m) | 0.5 |
| Coil pitch (mm) | 2 |

## 3.6 Results and Discussion

In this section, some parameters are always fixed while the others could either be constants or variables. This will be clearly presented in each subsection such that when a parameter is not mentioned as a variable then it is assumed to be constant if not varying as an output. The different parameters to be studied are the turbine/gas inlet temperatures, turbine inlet pressure, underground water temperature, mass flow rate of $CO_2$/gas, cycle's performance, and heat exchangers' sizes.

### 3.6.1 Performance assessment

The performance of the cycle depends on three main parameters: working fluid's mass flow rate, net output power and thermal efficiency. It is very crucial to study the thermodynamic behaviour of the cycle to find out the conditions required to generate the maximum amount of power. The aim of this section is to study the effect of operating conditions (turbine inlet pressure and temperature, mass flow rate, and gas inlet temperature) on the mass flow rate of working fluid, output power and cycle's efficiency.

Figure 3.6 shows that the mass flow rate of the working fluid ($CO_2$) and turbine inlet temperature ($T_1$) are inversely proportional. At low $T_1$ (below 200°C), there is a slight difference between the mass flow rate of $CO_2$ at the different presented turbine inlet pressures, while it starts do decrease gradually to be nil after that. This is mainly due to the dependency of $CO_2$ enthalpy on the pressure at low temperatures. However, at high temperatures, the enthalpy of $CO_2$ entering the turbine is slightly affected by the change in pressure. On the other hand, the variation in turbine inlet pressure at high temperatures only changes the enthalpy of $CO_2$ exiting the turbine and hence affects the fluid's expansion in the turbine and output power. Therefore, the mass flow rate of the working fluid is affected considerably by the turbine inlet temperature while insignificantly by the pressure. In this simulation study, the amount of heat extracted form gas is assumed to be constant as shown in Table 3.1 since the gas flow rate and temperatures are fixed. This means that the enthalpy at state one and the working fluid's mass flow rate vary oppositely based on the energy balance between the gas and $CO_2$ in the gas heater. Besides, the temperature and enthalpy are directly proportional showing the reason for the decrease in mass flow rate (see Figure 3.6). According to equation (3.1), it is expected that the output power varies similarly as the mass flow rate of the working fluid. Conversely, Figure 3.5-c and Figure 3.6 have showed a different relation between the power generated and mass flow rate. This is due to that the net output power is highly affected by the enthalpy difference between inlet and outlet states of the turbine.

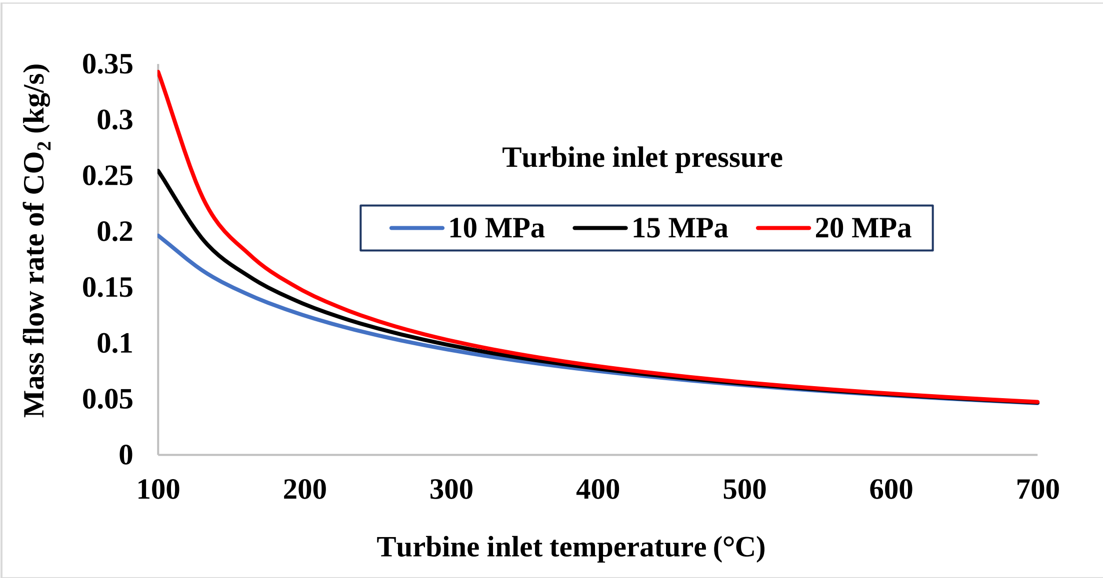


Figure 3.6: The effect of turbine inlet temperature ($T_1$) on the mass flow rate of $CO_2$ at different Pressures ($p_1$)

The efficiency of the cycle is highly affected by the change of turbine inlet pressure ($p_1$) as shown in Figure 3.7. The cycle's efficiency is independent from the mass flow rate of the working fluid in contrast with the output power (see equations 3.1 and 3.4). Almost when the turbine inlet temperature is higher than 150°C, the increase in $p_1$ could lead to an increase in the efficiency such that the highest efficiency is achieved at turbine inlet pressure of 20 MPa which is around 11%. However, the efficiency usually increases with the turbine inlet temperature ($T_1$). This relation is also more effective at high pressures which is the case of 20 MPa since the efficiency raised remarkably from 1% to 11% while

$T_1$ varied from 100°C to 300°C. On the other hand, at 10 MPa, the efficiency did not show any remarkable jump under the same range of temperature. This does not mean that the efficiency is not affected by the turbine inlet temperature at low pressures, however, this depends on the range of temperature studied. The reason is that the efficiency is almost constant after exceeding a specific temperature in which the latter is proportional to the turbine inlet pressure. Thus, it is expected that the sudden rise in the cycle's efficiency at 10 MPa had already occurred below 100°C. At low temperatures, the efficiency referring to the highest turbine inlet pressure becomes the lowest. At these conditions, the cycle cannot be considered as transcritical cycle yet. Thus, it is very necessary to use high temperatures to ensure that the $CO_2$ is totally superheated otherwise a significant drop in the efficiency and power may occur. This may also be accompanied by a damage in the turbine since the nature of fluid entering it is not only vapor.

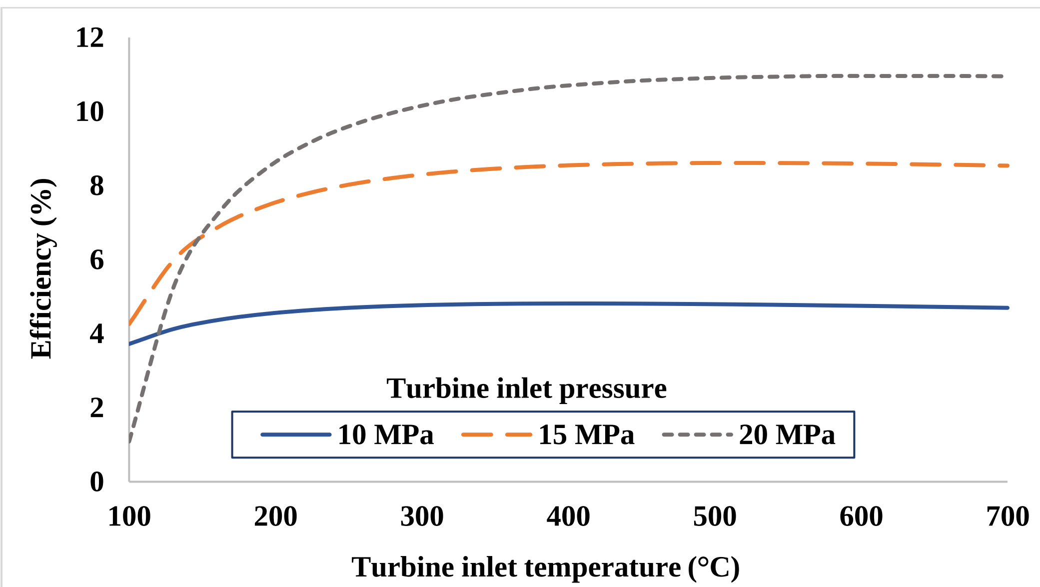


Figure 3.7: The effect of turbine inlet temperature ($T_1$) on the cycle's efficiency at different pressures ($p_1$)

The surface plot presented in Figure 3.8 shows the influence of gas temperature and its mass flow rate on the cycle's net output power. The proportional relation is very noticeable with an equality of influence, which means that both have approximately the same effect. This could also be verified since the vertex of the plot is at the highest gas temperature (1500°C) and mass flow rate (350 kg/hr), and that the surface plot has the same rate of increase with respect to the two axes. It is also essential to compare the opposite sides of the surface plot to study the effect of both variables on each other. In other words, the increasing rate of output power with respect to gas inlet temperature is higher at 350 kg/hr than that at 100 kg/hr such that it changes approximately from 3.8 kW to 14.5 kW and 1 kW to 6 kW, respectively. Similarly, the output power increases with a higher rate with respect to the mass flow rate at 1500˚C compared to that at 500˚C.

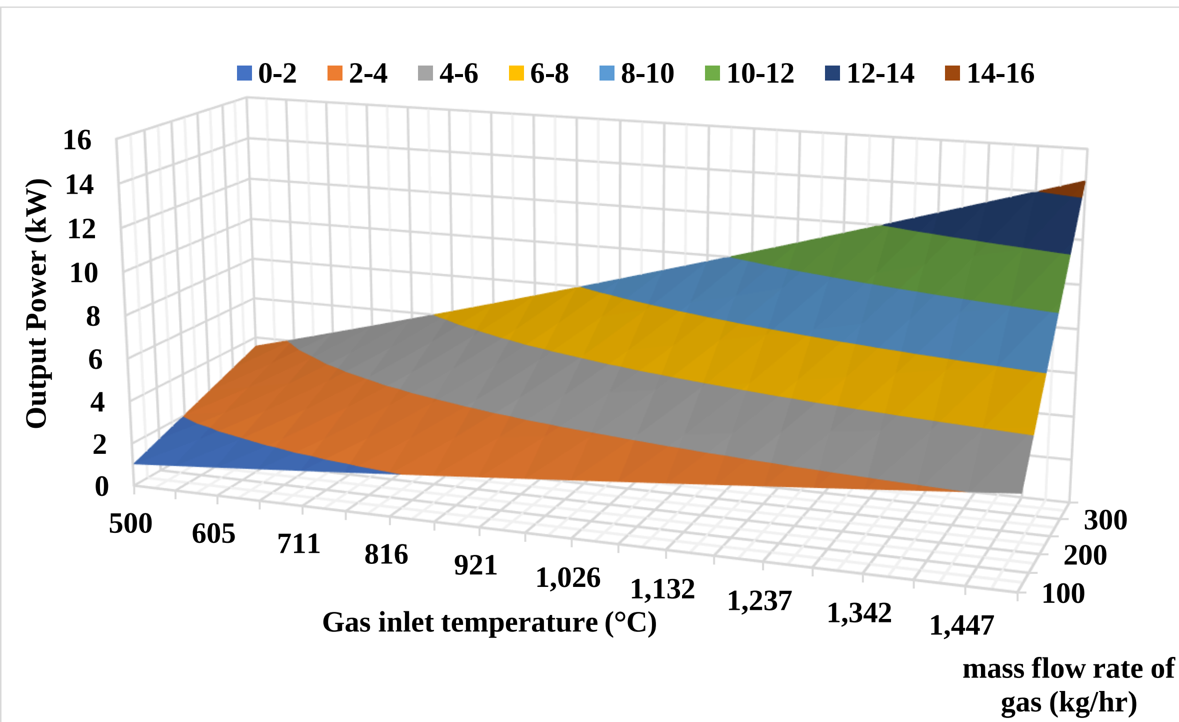


Figure 3.8: The variation of net output power as function of the gas temperature ($T_{gi}$) and its mass flow rate ($\dot{m}_g$)

The underground water temperature is one of the most important uncontrollable parameters, thus, it is necessary to study its effect before installation to determine the expected feasibility in terms of performance. Figure 3.9 shows the effect of underground water temperature on the cycle’s efficiency and net output power. Both are inversely proportional to the water temperature. The same relation was obtained when varying the pinch temperature which is the minimum temperature difference between the working fluid and the underground water (cooling source). These results verify the direct effect of condenser’s pressure on the cycle’s performance. Therefore, as the pressure of the condenser increases, the output power decreases due to the reduction in enthalpy difference between the inlet and outlet turbine states. This shows the importance of using a ground-cooled condenser in summer which is the main reason of the current investigation. For example, if the underground water temperature is less than that of the ambient by 10˚C, then the ground-cooled condenser will be able to increase the output power by 1 kW approximately compared to that of air-cooled condenser. This can be deduced from Figure 3.9 such that for each 1˚C decrease in the coolant temperature, a 0.1 kW additional power could be produced.

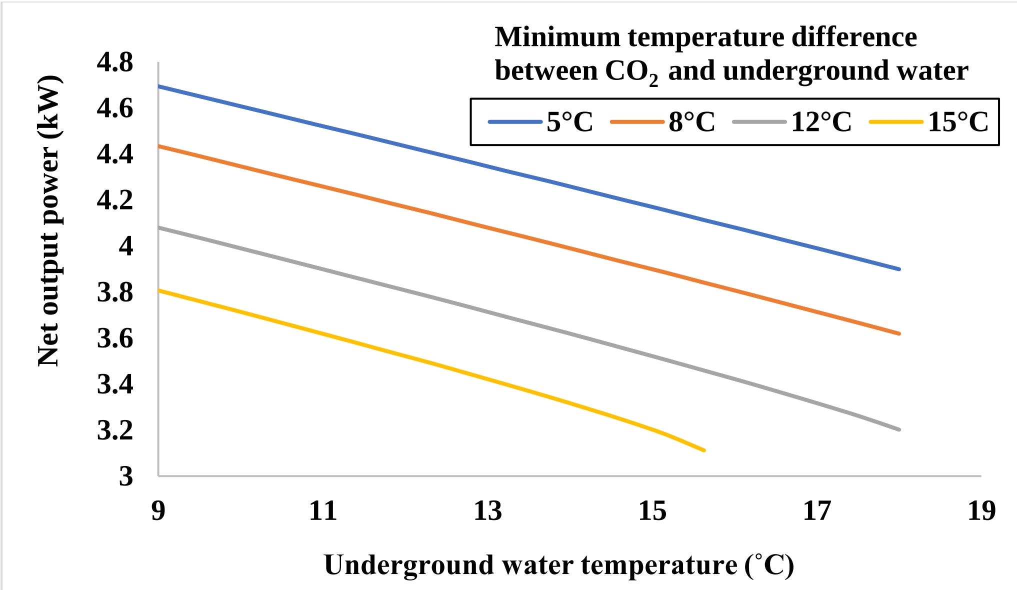


(a)

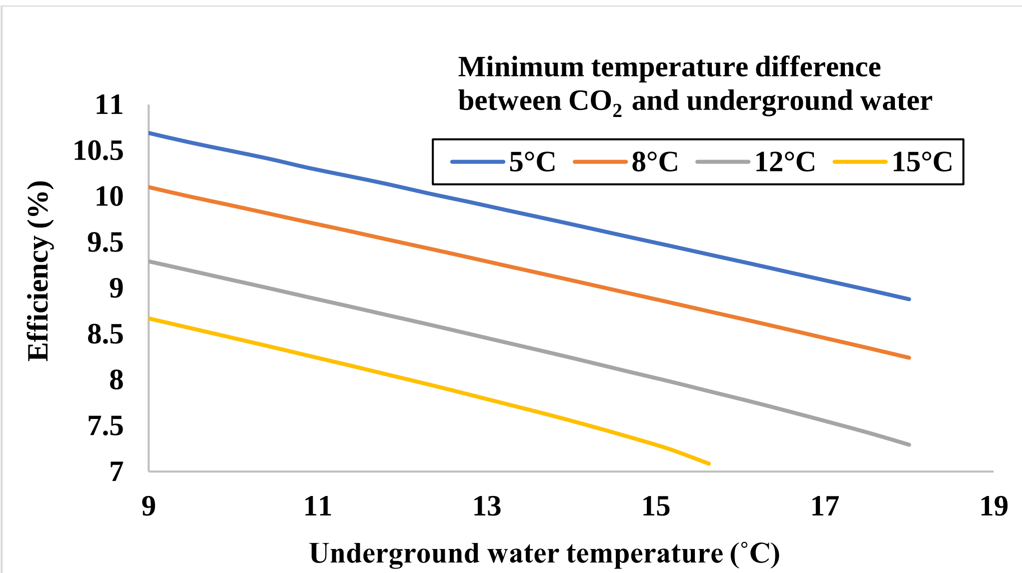


(b)

Figure 3.9: The effect of underground water temperature on the cycle's performance with respect to the minimum temperature difference in the condenser

### 3.6.2 Size of the gas heater

The gas heater is usually considered as the most critical component because it is the heat exchanger responsible for extracting the maximum possible amount of heat. This objective must be achieved considering the smallest acceptable heat exchanger's size to save money and space.

According to Figure 3.10, as the pipe diameter of the CTRC increases, the length of the gas heater decreases in contrast to the effect of gas heater diameter. In addition, the influence of gas heater diameter on the gas heater's length appears more significantly at low CTRC pipe diameter. This impact is not only due to the variation in heat exchanger surface area and hydraulic diameter, but it also depends on the convective heat transfer coefficient which is directly affected by the flow velocity inside the pipe. Even though it is better to use small gas heater diameters to decrease the total size of the gas heater, it is also necessary to study the effect of hydraulic diameter on the gas flow. This depends on other specifications that need to be taken into consideration in further studies to make sure that the gas is smoothly flowing without any negative effect on the systems' components and cycle's performance. Under these conditions, the *UA* value of the gas heater was calculated as 0.2135 kW/K and remained constant with the variation of gas heater diameter and CTRC diameter.

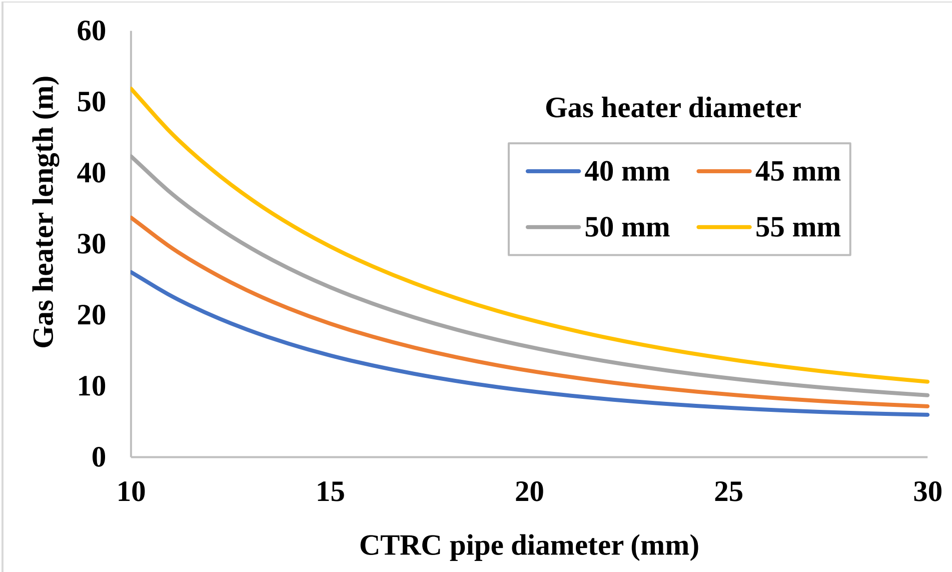


Figure 3.10: The relation between gas heater's length and the diameter of both pipes; gas heater and CTRC

As the gas inlet temperature rises from 500° to 1500°C, the length of the gas heater is reduced in all cases (see Figure 3.11), while this relation is inverted when varying the mass flow rate of gas. Although both parameters have the same influence on the heat added to the cycle, but they are also involved in the length's calculation from another side in which the overall heat transfer coefficient and logarithmic mean temperature difference are affected by the mass flow rate and temperature, respectively. The major parameter that affects the heat transfer coefficient in forced convection is the velocity which is a function of the mass flow rate. Moreover, the logarithmic mean temperature difference is one of most crucial factors that can change the size of the heat exchanger which represents the temperature difference between the working fluids. Thus, it can be deduced that the effect of gas temperature on the heat exchange area is higher than that on heat addition which is opposite to that of mass flow rate. The *UA* values of the gas heater are presented in Figure 3.12 as a function of inlet temperature and mass flow rate of gas.

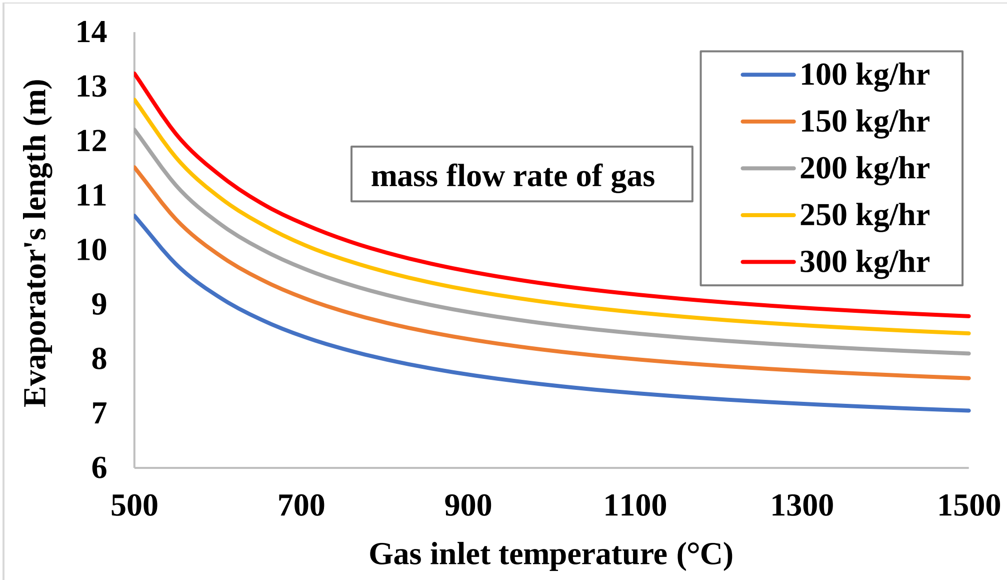


Figure 3.11: The effect of gas conditions (flow rate and temperature) on the gas heater's length

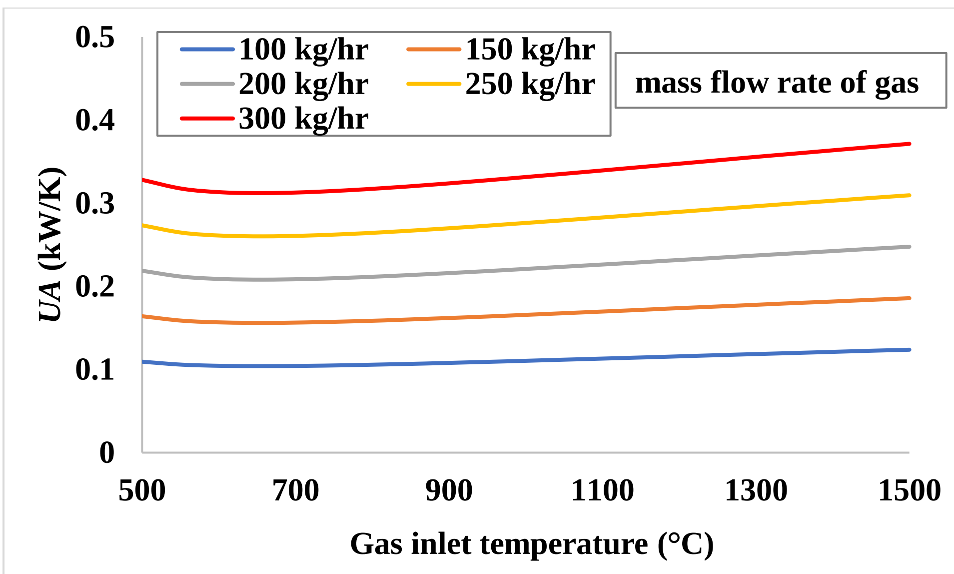


Figure 3.12: The effect of gas conditions (flow rate and temperature) on the *UA* value of the gas heater

### 3.6.3 Size of the condenser

The area of the condenser is a crucial part to be studied very precisely in to make sure that the underground water can extract the required amount of heat from the cycle. This is very important due to the high complexity of maintenance since it is installed under the ground.

Figure 3.13 presents a linear relation between the gas inlet temperature and condenser's length, however, the ratio of proportionality is controlled by the mass flow rate of gas (diverging). The slope of condenser's length function is proportional to the mass flow rate with respect to the gas inlet temperature. For example, the condenser's length increases from 18 m to 32 m and 27 m to 65 m at 100 kg/hr and 300 kg/hr, respectively. These relations verify the change in the mass flow rate of $CO_2$ which directly modifies the amount of heat rejected and thus, the condenser's length. In addition to that, it is necessary to keep in mind that they also have an influence on the convection heat transfer coefficient of the $CO_2$ within the condenser due to the change in the $CO_2$ mass flow rate. As presented in Figure 3.14, it can be noticed that the effect of heat source conditions on the *UA* value of the condenser is same as that on the length.

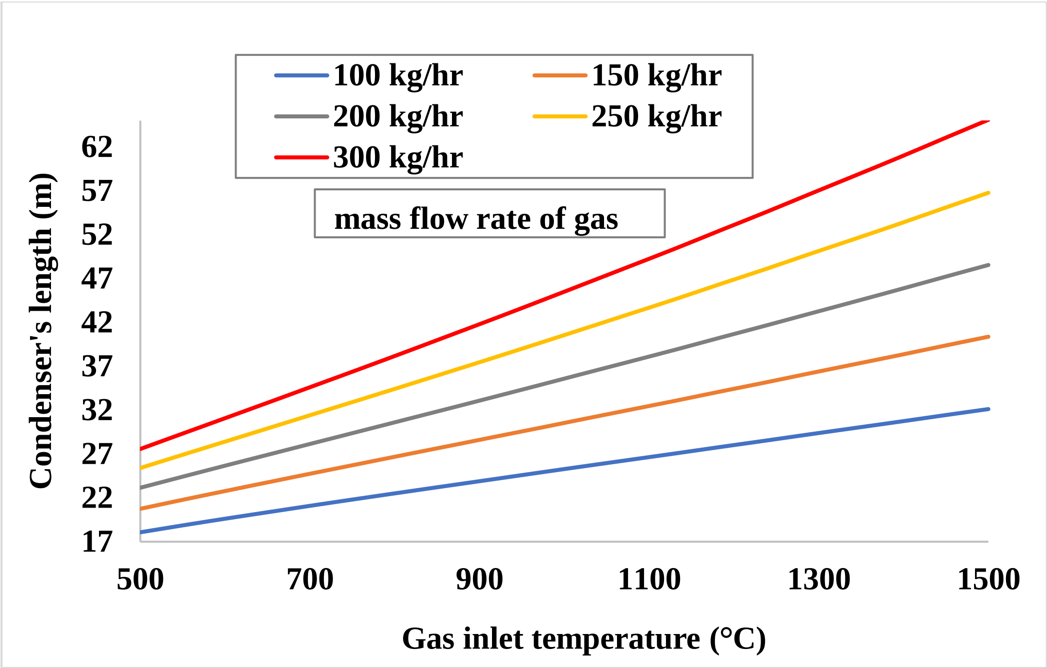


Figure 3.13: The effect of gas conditions (flow rate and temperature) on the condenser's length

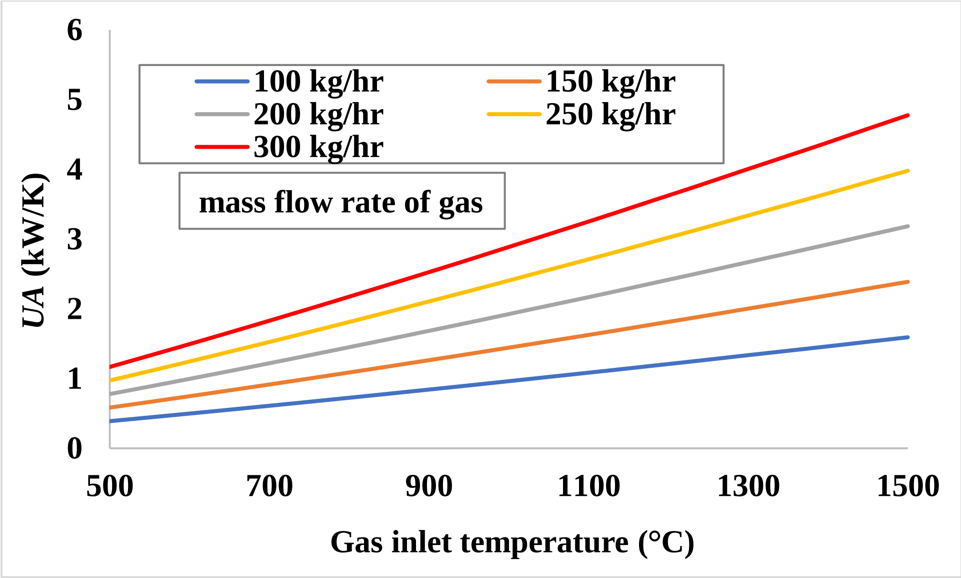


Figure 3.14: The effect of gas conditions (flow rate and temperature) on the *UA* value of the condenser

Figure 3.15 shows that the underground water has a great influence on the length of the condenser which can be obviously recognized from the significant empty space between the two curves corresponding to 15°C and 18°C water temperatures. These results are obtained at a constant condensation temperature of 25°C. All curves are taking the shape of wide parabola which means that for every specific underground water temperature there is a specific CTRC pipe diameter that corresponds to the minimum condenser length. The value of this diameter is approximately around 15 mm. However, this must not be the only criterion for selecting the optimal diameter. This is due to the diameter's effect on pressure drop which may affect other parameters in the cycle such as the net output power. This means that in some cases, choosing the smallest diameter would not be the best solution even though it clearly reduces the length of the condenser. Thus, it is very necessary to balance between the heat exchangers' sizes and overall cycle's performance. Under this investigation, the *UA* value of the condenser was found to be dependent on the underground water temperature only such that it increased from 0.9743 to 1.899 kW/K as the mentioned temperature increased from 9°C to 18°C.

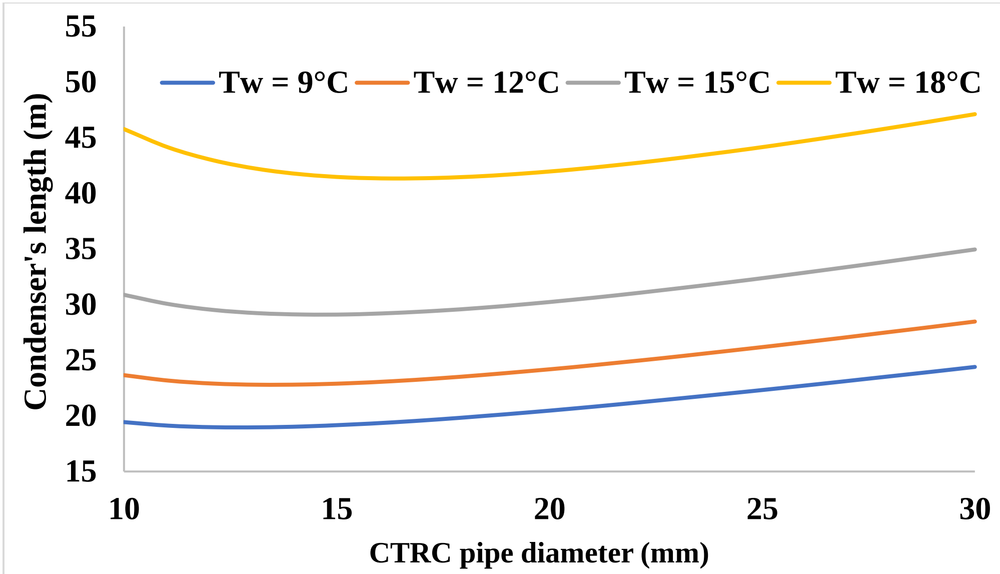


Figure 3.15: The variation of condenser's length as a function of cycle's pipe diameter at several underground water temperatures ($T_w$)

The result shown in Figure 3.16 is based on varying the condensation temperature similarly as the underground water temperature such as the difference between them is the minimum temperature difference between $CO_2$ and water. This pinch temperature has a greater effect on the condenser's length than that of the underground water temperature. This is due to the inversely proportional relation between the logarithmic mean temperature difference and the heat exchanger's area as shown in equation (3.6). In addition, the rate of decrease in the length is more sensitive at high pinch temperature difference. Figure 3.15 and Figure 3.16 seem to be presenting opposing results, however, the difference is that the condensation temperature in Figure 3.15 is kept constant at 25˚C which means that the net output power is also fixed. However, for a specific curve in Figure 3.16, as the underground water temperature increase the condensation temperature of $CO_2$ will increase similarly. This will consequently lead to a drop in the net output power due to the change in condenser's pressure. Figure 3.16 shows that it is a good option to fix the minimum temperature difference between the two fluids to minimize the condenser's length and hence to reduce the capital cost of installation. On the other hand, this reduction must be balanced with the decrease in output power as shown in Figure 3.9 which is related directly to the operating cost. By comparing Figure 3.16 and Figure 3.17, it can be seen that the effects of underground water temperature and minimum temperature difference are almost the same on that of condenser's length and *UA* value.

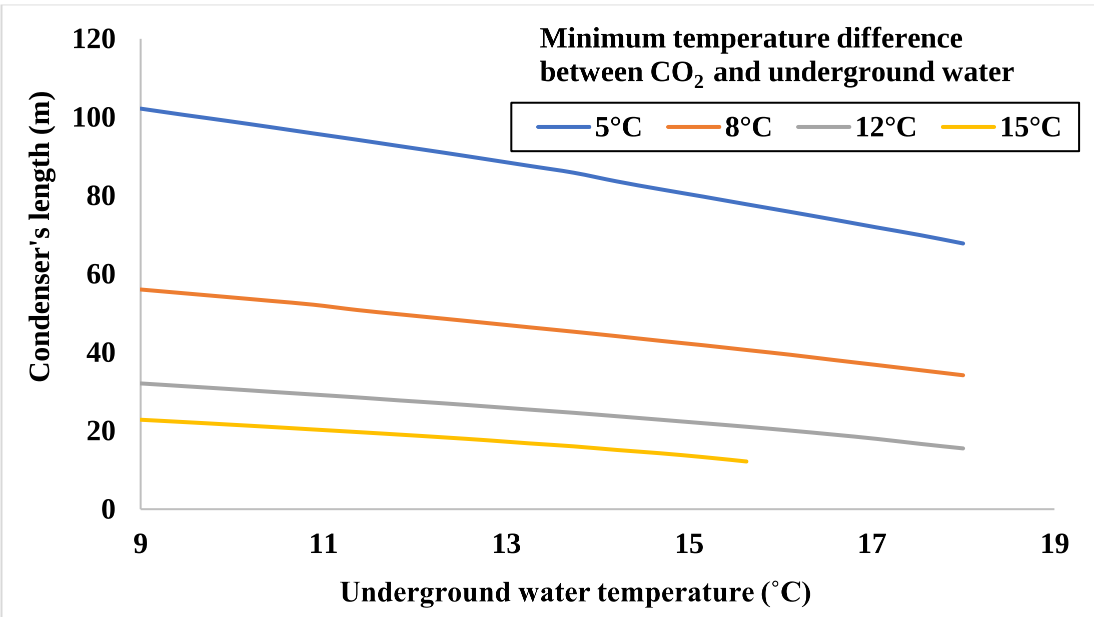


Figure 3.16: The effect of underground water temperature under different minimum temperature differences on the condenser's length

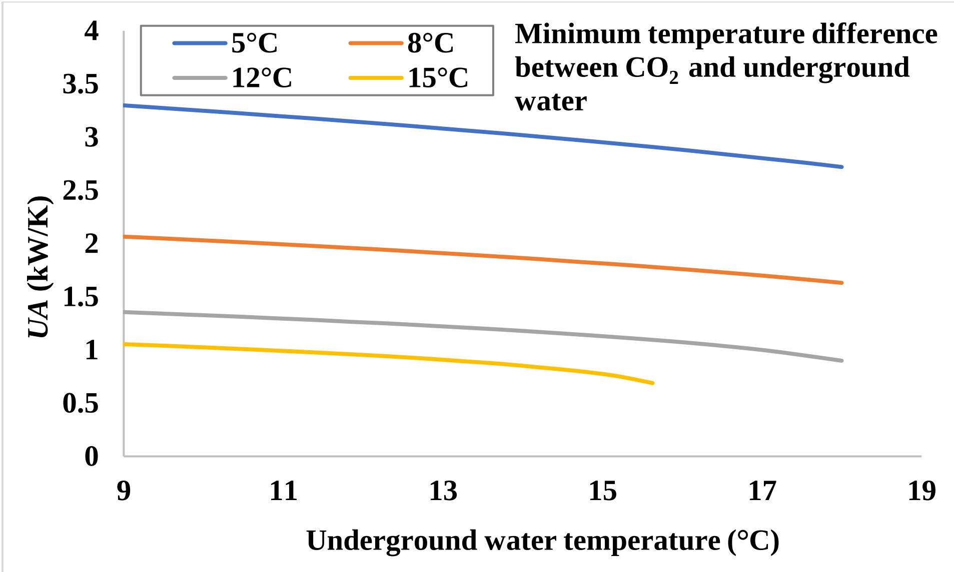


Figure 3.17: The effect of underground water temperature under different minimum temperature differences on the condenser's *UA* value

Figure 3.18 presents the major dimensions' parameters of the condenser. The relation between coil height, coil diameter and pipe diameter must be studied to choose the suitable volume. The curves are diverging when the pipe diameter is increasing. This shows that the variation in coil diameter is more effective on the condenser's length at large pipe diameters. The relation between pipe diameter and coil height is similar to that with total condenser's length presented in Figure 3.15 because at a specific coil diameter, the variation of coil height represents the same variation of length. Indeed, it is favourable to choose the lowest pipe diameter to minimize the coil height and consequently achieving the smallest volume of GHE. However, there are some other parameters that need to be taken into consideration and investigated in future studies such as thermal pollution/imbalance and pressure drop. Under these conditions, the *UA* value of the condenser is found to be constant at 1.415 kW/K.

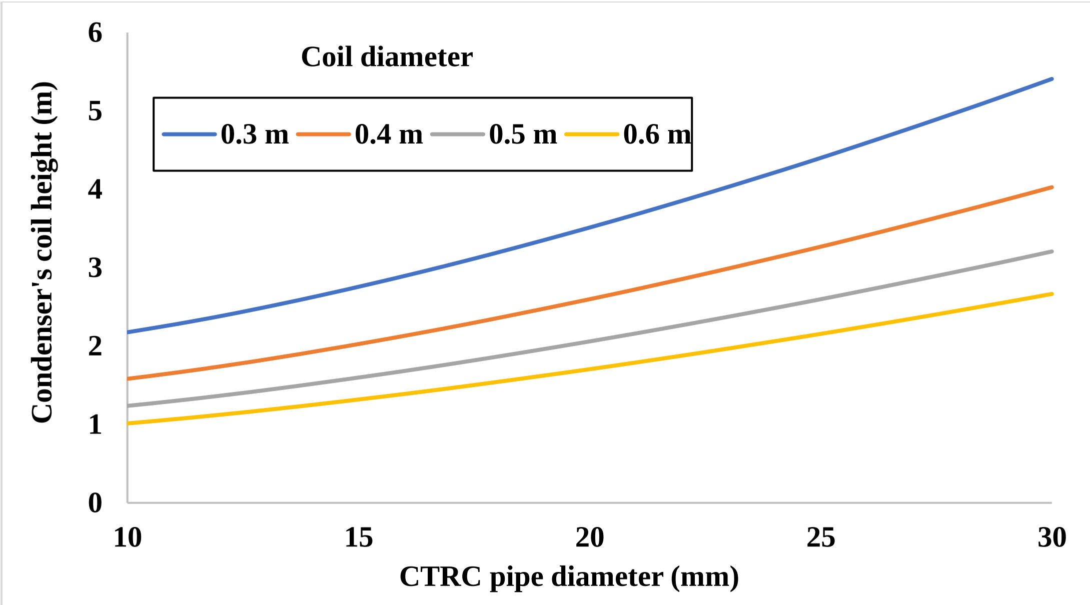


Figure 3.18: The variation of condenser's coil height with respect to the pipe and coil diameters

### 3.6.4 Gas heater vs. condenser

This section will present a comparison between the heat exchangers in the proposed CTRC (gas heater and condenser) to balance between the two sizes. This will contribute to choosing the best optimum conditions to select the heat exchangers' sizes accordingly.

The turbine inlet temperature has more influence on the condenser's length compared to that of the gas heater (see Figure 3.19). From this point of view, it could be very beneficial to choose a high turbine inlet temperature so that both heat exchangers are of moderate lengths which is around 650°C (both lengths were approximately 23 m). The amount of heat added to the cycle is constant since it is only a function of gas flow rate and temperatures. Thus, the turbine inlet temperature will vary oppositely to the mass flow rate of $CO_2$ based on the energy balance between the two fluids. As the mass flow rate of working fluid decreases the heat rejected from CTRC will decrease too leading to a drop in the condenser's length. On the other hand, the turbine inlet pressure has no significant influence on the heat exchangers' lengths such that condenser's and gas heater's length remain around 30 m and 9 m, respectively. Figure 3.20 shows the comparison between heat exchangers' *UA* values as a function of turbine inlet temperature and pressure. The results are similar to that of lengths presented in Figure 3.19.

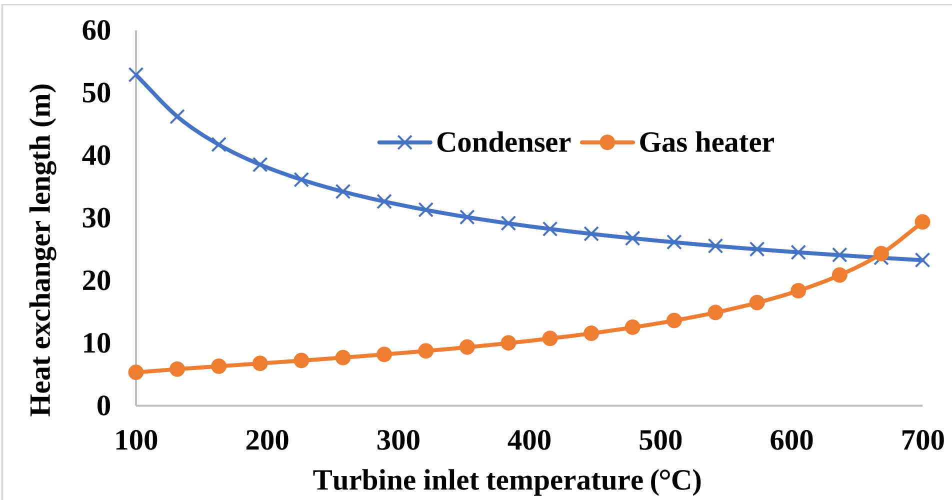


(a)

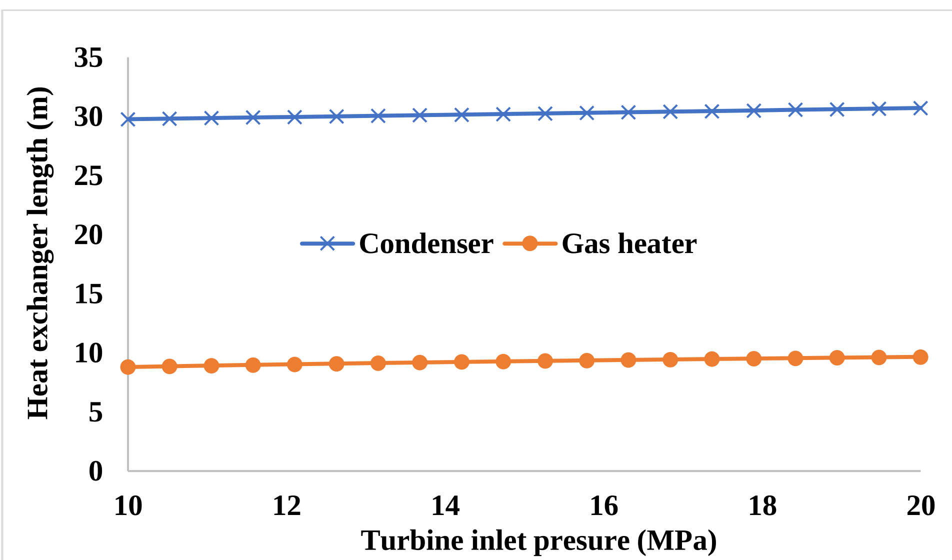


(b)

Figure 3.19: The difference between heat exchangers' lengths (gas heater and condenser) with respect to the (a) turbine inlet temperature ($T_1$) and (b) pressure ($p_1$)

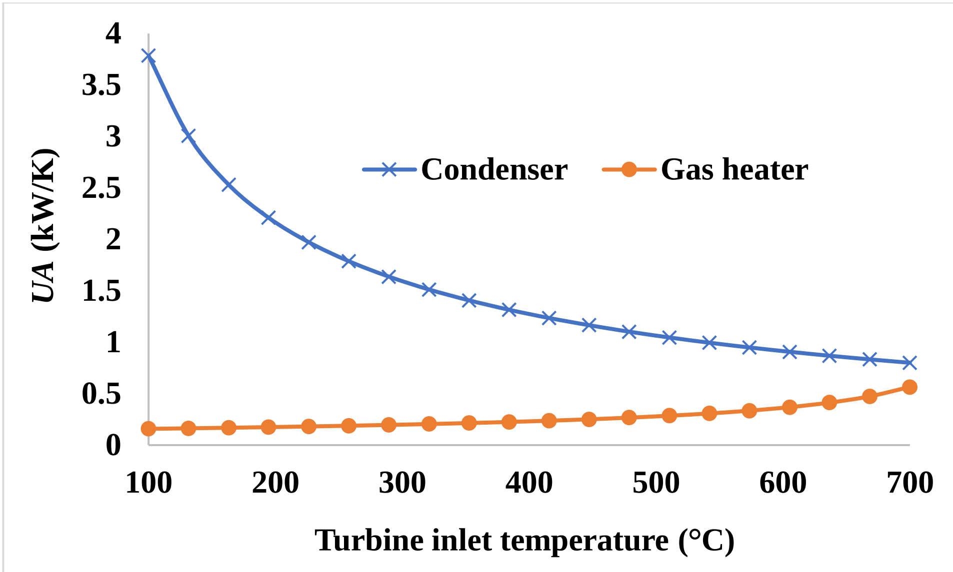


(a)

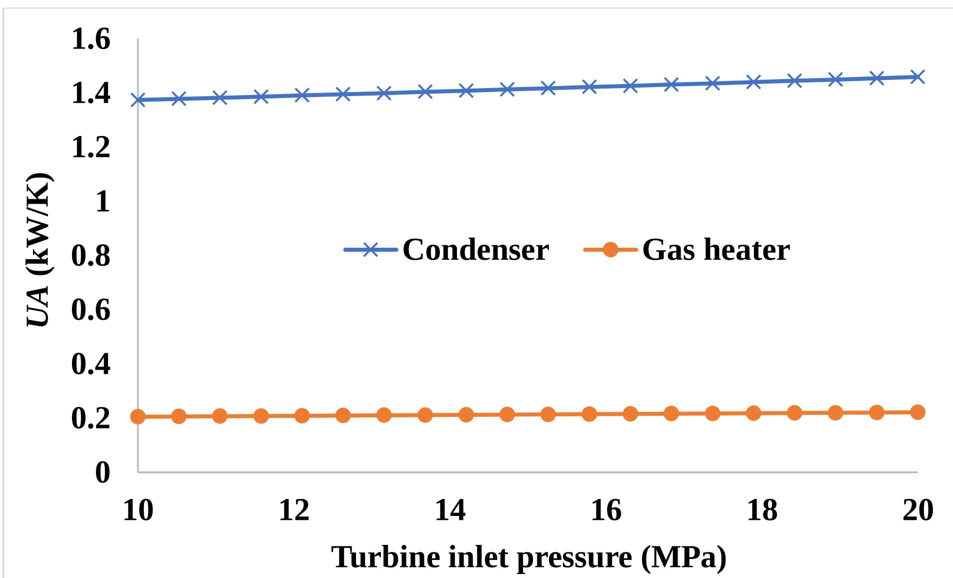


(b)

Figure 3.20: The difference between heat exchangers' *UA* values (gas heater and condenser) with respect to the (a) turbine inlet temperature ($T_1$) and (b) pressure ($p_1$)

After studying the influence of the highest temperature in the cycle ($T_1$), it is also important to study the lowest one which corresponds to the condensation ($T_3$). As shown in Figure 3.21 and Figure 3.22, it will not affect the gas heater's length and *UA* value, while it remarkably changes that of the condenser and the net output power. The condenser's length and net output power vary from 80 m to 13 m and 4.2 kW to 3.2 kW respectively for condensation temperature range of 20-30°C. The drop in power is due to the decrease in expansion while that of condenser's size because of variation in the amount of heat extracted and the logarithmic mean temperature difference. As the condensation temperature rises, the difference between fluid and underground temperature will increase too which improves the conditions of heat transfer and hence, a smaller heat exchanger will be required. Thus, it is very necessary to balance between the heat exchangers' lengths and the net output power to make sure that both meet the desired requirements. In addition, if the cycle is going to be designed considering a high condensation temperature, then it will not be feasible to use a ground-cooled condenser. The most important specification in this system is the ability to operate at low condensation temperatures in summer compared to the ambient temperature to increase the net output power of the cycle.

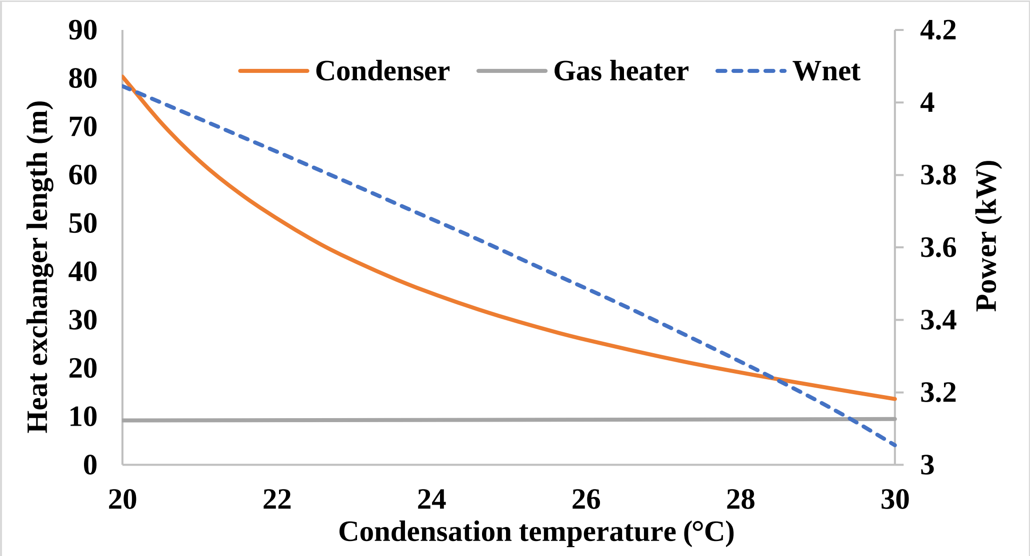


Figure 3.21: The variation of heat exchangers' lengths (gas heater and condenser) and net output power as a function of condensation temperature ($T_3$)

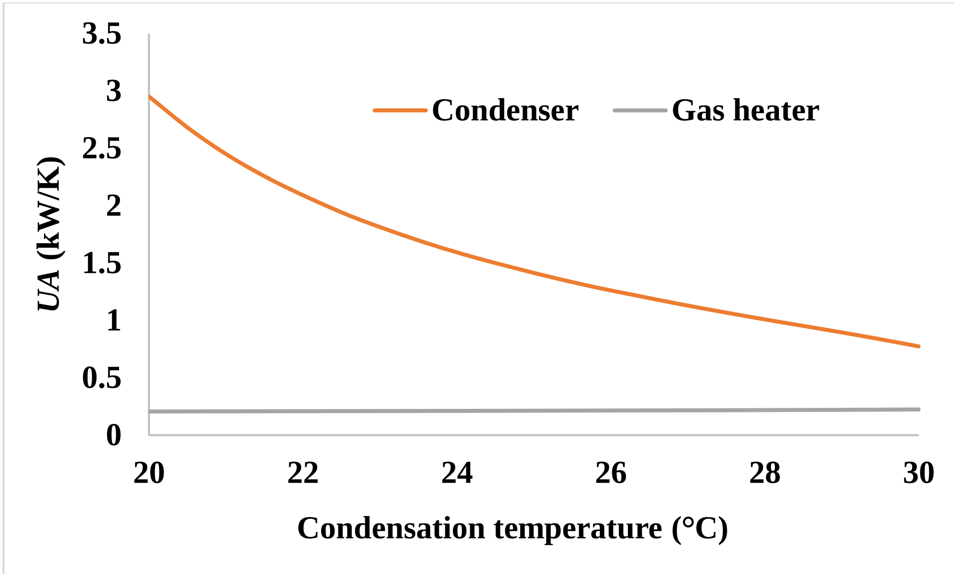


Figure 3.22: The variation of heat exchangers' *UA* values (gas heater and condenser) and net output power as a function of condensation temperature ($T_3$)

### 3.7 Conclusion

The proposed CTRC coupled with ground-cooled condenser can generate electricity from several heat sources such that it can produce a perfect amount of power that depends on the cycle's conditions and gas specifications. The parametric analysis contributes to extract the maximum amount of energy while preserving small heat exchangers. A positive linear relation was noticed between the net output power and the available heat. The use of ground-cooled condenser generated approximately 30% more power compared to the conventional Rankine cycle. This enhancement is mainly affected by the ground's temperature since it controls indirectly the working fluid's expansion. The turbine inlet temperature was found to be an effective variable such that it does not affect the net output power significantly while providing acceptable heat exchanger's lengths. The second crucial parameter to be controlled is the cycle's pipe diameter since it can be used to balance between the lengths of heat exchangers.

The current study focuses on small scale power cycles which can be noticed from the low net output power presented in this chapter. This makes it necessary to replace the turbo expander with a scroll expander which better fits such applications [158]. This is crucial to avoid inefficient expansions in small turbines that operate at very high rotational speeds. In such cases (below 10 kW), the scroll expander efficiency is almost always considered as ~70%. Thus, the mentioned assumption will be considered for the upcoming chapters of this research.

# Chapter 4. Experimental Study for Ground Temperature Measurement

One of the objectives of this research is to study the potential of shallow geothermal energy in Lebanon [159]. The ground temperature has been monitored in Bekaa-Lebanon and compared with the highest and lowest ambient temperatures. The sensors of temperatures are placed at depths of 0.3 m, 0.6 m, 1 m, 1.3 m, 1.6 m, and 2 m underground. This chapter presents the experimental study and analysis in terms of temperatures and operating durations.

## 4.1 Experimental Setup

The setup used to measure the ground temperature is presented in Figure 4.1 including digital meter and thermocouple. The digital meter used has an accuracy of 0.5% as mentioned by the manufacturer and can measure a range of temperature between -9°C and 99°C, making it suitable for this experiment. It was a new device, and the calibration was done according to the manufacturer instructions. Six thermocouples of type HT15T are inserted under the ground as shown in Figure 4.1b. The measuring device has a fast response speed of 4.5 s with a low power consumption which is less than 3 VA. It could be easily used as depicted in Figure 4.1c and Figure 4.1d. It was also mentioned in the operation instructions of the digital panel meter that the best applicable temperature range is 0-50°C. This also makes this device more accurate in the experiment since the ground temperature in Bekaa-Lebanon is usually within this range as will be presented in the next section. However, this accuracy is only valid for temperature measurements when the humidity is below 85%. Thus, it is decided to undertake the experiment in a place where the soil is dry all over the year, so not to compromise the accuracy of the results, especially for shallower ground temperatures. For this reason, the results obtained at a maximum depth of 2 m correspond to the most reliable collected data. To check further the reliability of the obtained results, the temperature variation was monitored precisely and especially during the winter season when raining. Accordingly, there was no significant variations in the corresponding values.

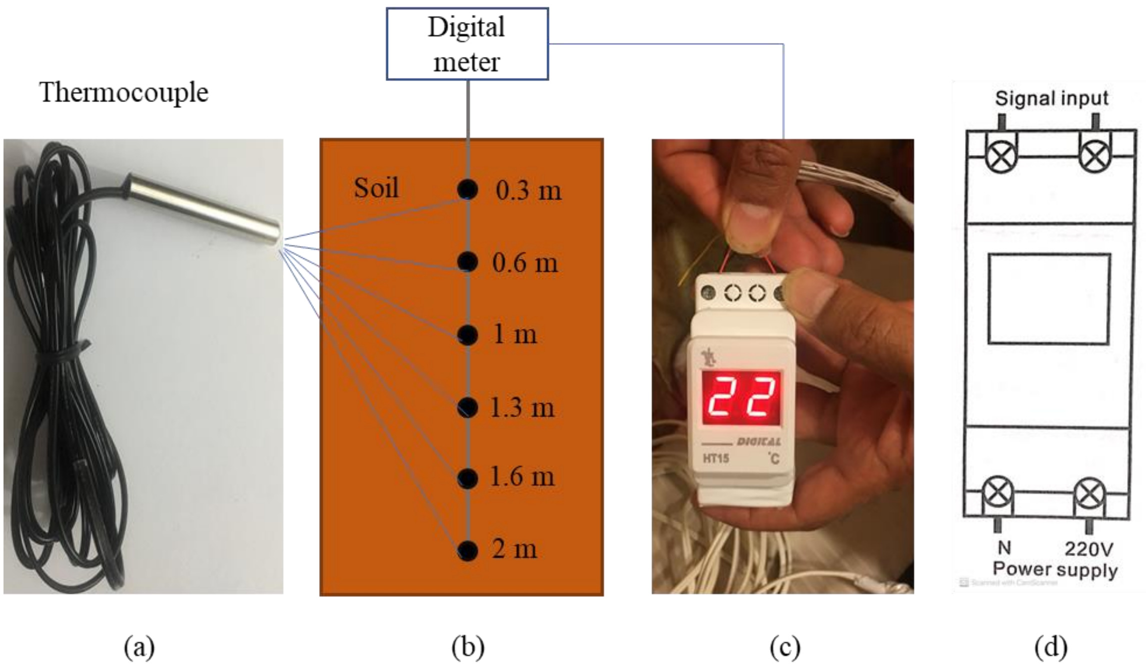


Figure 4.1: Temperature measuring setup; (a) thermocouple, (b) depths of measurement, (c) digital meter and (d) schematic of digital meter

### 4.2 Ground Temperature Measurement Results

Figure 4.2 shows the recorded ambient and ground temperatures during 2020. It can be seen that the ambient temperatures fluctuate significantly while the ground temperatures are considerably stable. As the depth increases the stability increases in which the curve corresponding to the depth of 2 m represents the least temperature fluctuations. During

2020, the maximum temperature difference at 2 m was 7°C since the temperature varied between 12°C and 19°C. This shows the great potential of using ground-cooled condenser in this location and mainly because the ground temperature is nearer to the lowest ambient temperature. Due to the stability recorded at 2 m, this depth will be considered as a reference for the ground temperature in the upcoming analyses.

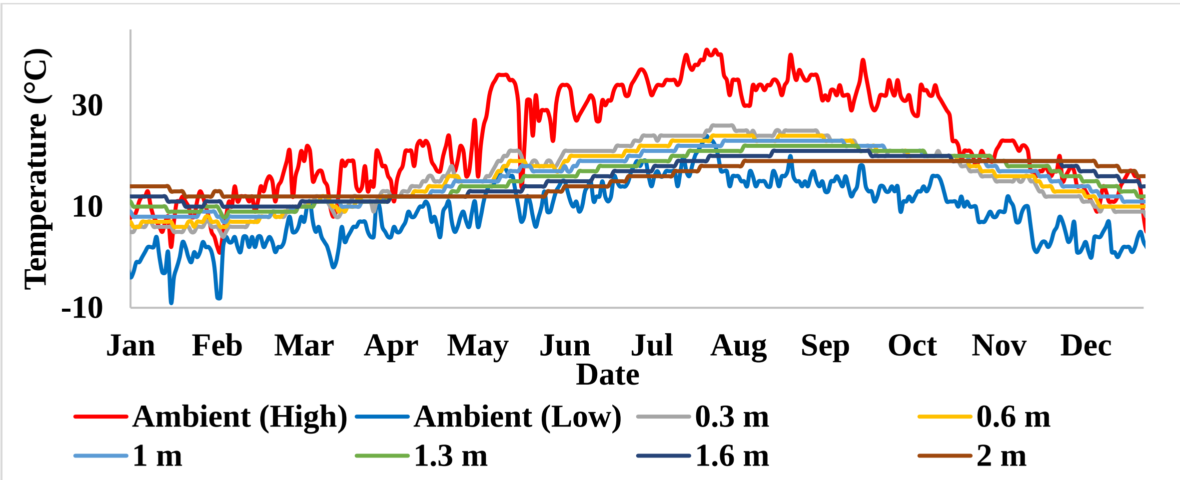


Figure 4.2: Ambient and ground temperature measurement in Bekaa-Lebanon during 2020

The ground temperatures in Bekaa are almost constant when compared to the ambient temperature due to the high fluctuations and temperature differences between ambient highest and lowest values during the day. This makes the use of shallow GE very important to stabilize energy related systems because even at very shallow depths the ground temperature is more stable than that of ambient as shown in Table 4.1. The results show that the annual average values of all ground temperatures are approximately equal to 15.5°C. This makes the results reliable revealing the effect of ground layers on each other which can be noticed from different temperature variation all over the year and equal average temperatures.

Table 4.1: The difference between ambient and ground temperatures; average, highest, lowest and temperature difference in Bekaa-Lebanon during 2020

| **Temperature** | **Average** | **Highest (°C)** | **Lowest (°C)** | **Difference (°C)** |
|---|---|---|---|---|
| Ambient high | 22.83 | 41 | 1 | 40 |
| Ambient low | 8.87 | 24 | -9 | 33 |
| Ground (0.3 m) | 15.74 | 26 | 4 | 22 |
| Ground (0.6 m) | 15.62 | 24 | 6 | 18 |
| Ground (1 m) | 15.72 | 23 | 7 | 16 |
| Ground (1.3 m) | 15.67 | 22 | 8 | 14 |
| Ground (1.6 m) | 15.57 | 21 | 10 | 11 |
| Ground (2 m) | 15.51 | 19 | 12 | 7 |

The highest, lowest, and average daily ambient temperatures highly fluctuate compared to that of the ground at 2 m depth as shown in Figure 4.3, while the annual ground and ambient average temperatures are almost the same (15.5-16°C). However, it is essential to consider that this comparison is missing a crucial part which is that peak loads are usually reported during the daytime when the ambient temperature is relatively high. This makes the use of ground-cooled condenser very efficient for two main reasons that are stability and low temperature compared to that of ambient during operating hours. It is also expected that the ground temperature can be decreased using a cooling recovery strategy as will be presented in section 5.2 to enhance the performance of ground-cooled condenser during operation. Additionally, the peak load is not only the main reason for comparing the ground temperature with that of daytime ambient average temperature, but in many applications the system does not operate at night. This will be discussed in detail in section 5.3 showing the significance of choosing the operational duration of the proposed power cycle which is assumed to be from 06:00 to 24:00. However, the actual system's operating duration is 8 hours/day but randomly distributed during 06:00-24:00. Therefore, the upcoming sections in this chapter will be based on these assumption as if the system's maximum possible operating duration is 18 hours/days.

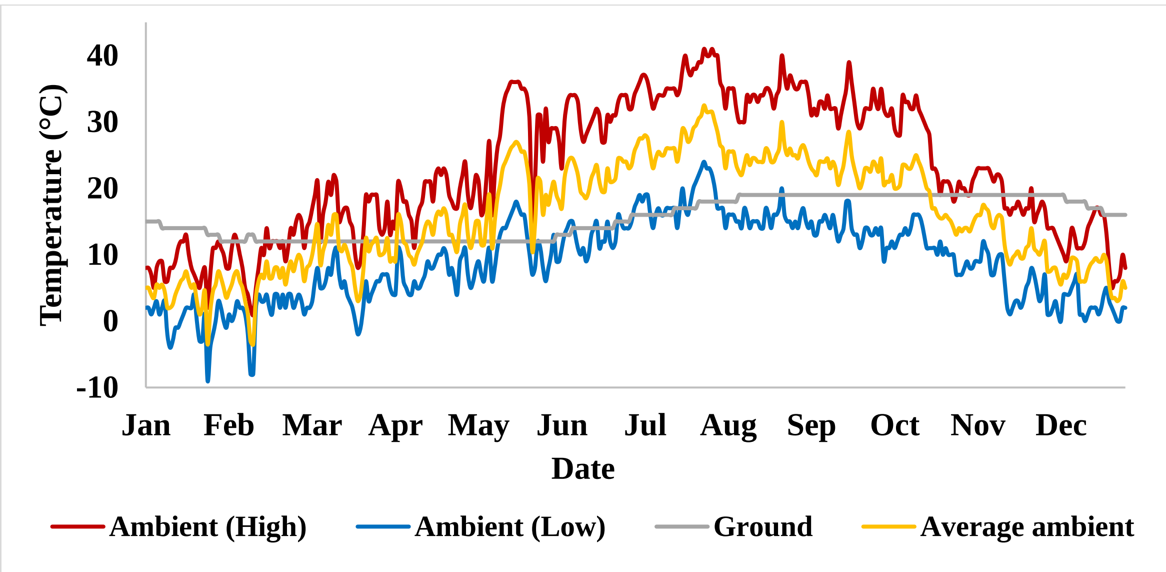


Figure 4.3: The variation of ambient highest, lowest, and average temperatures in comparison with the ground temperature at 2 m depth in Bekaa-Lebanon during 2020

### 4.3 Ground Temperature Results Analysis

The aim of this section is to manage the operation of each condenser according to the lowest available temperature. This is essential because the aim of this research is to decrease the condensation temperature in the ORC knowing that this parameter is directly proportional to the cooling source temperature. As will be discussed in section 5.2, a hybrid-cooled condenser is used and composed of GHE and air/water-cooled heat rejector such that they utilize the ground and ambient air as cooling sources, respectively. This makes it necessary to control the operation of each cooling source by comparing the ground and ambient air temperature at each instant during the day. This means that when the ground temperature is lower than that of ambient, the GHE will be operating, otherwise the primary heat rejector will be the only functioning heat exchanger. In this section, the ambient air temperature is assumed to be varying linearly during the day such that the lowest and highest ambient temperatures are at 06:00 and 13:00, respectively. The equations and algorithm were coded into Visual Basic within Excel and used to carry out the simulation to estimate the value of daily effective cooling source temperature (Appendix B).

### 4.3.1 Ground cooling system operating cases

- *Case 1: Ground temperature is less than the lowest ambient temperature*

This case occurs in summer when the ambient temperature is greater than that of ground during the entire day. Figure 4.4 presents a representation of case 1 such that the ground temperature horizontal line is always lower than that of ambient. In this case, the effective cooling source temperature during this day will be equal to that of the ground. This means that the GHE has the potential to operate from 06:00 to 24:00. However, this does not mean that the other heat rejector is not operating (see section 5.2). The primary heat rejector can remain functioning to reduce the heat rejected to the ground avoiding heat accumulation. In addition, the air/water cooled heat exchanger has an important role in such days in which it will be running at night to ensure providing coolth compensation.

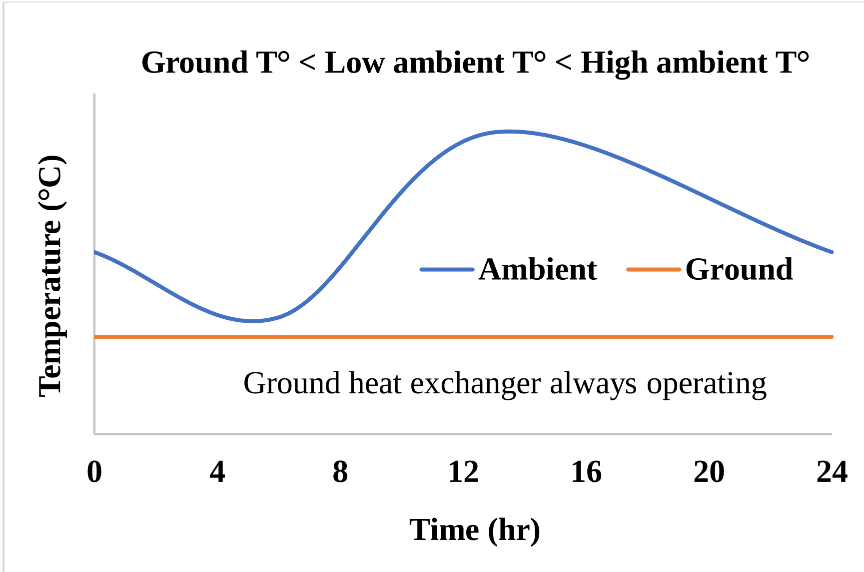


Figure 4.4: Ground cooling system operating the entire day (case 1)

- *Case 2: Ground temperature is higher than the highest ambient temperature*

During winter, the ground temperature can be totally higher than that of ambient in some days as shown in Figure 4.2 and Figure 4.3 (mainly in January, February, and December). In such cases, it is needless to use the ground as a secondary cooling source since it is incapable of rejecting heat from water after passing through the primary heat rejector. Case 2 is depicted in Figure 4.5 in which the ground temperature at a depth of 2 m is greater than the highest ambient temperature. In this case, the condenser will be only depending on the air/water cooled heat exchanger since it is providing the lowest temperature during the entire operating duration. For this reason, the effective cooling source temperature in case 2 is equal to the average ambient temperature during operating hours. It is essential to mention that the possibility of having this case can be reduced after adopting the optimized system (see section 5.2). Therefore, it is expected that this case will be mainly representing the days where there is a sudden drop in the ambient air temperature.

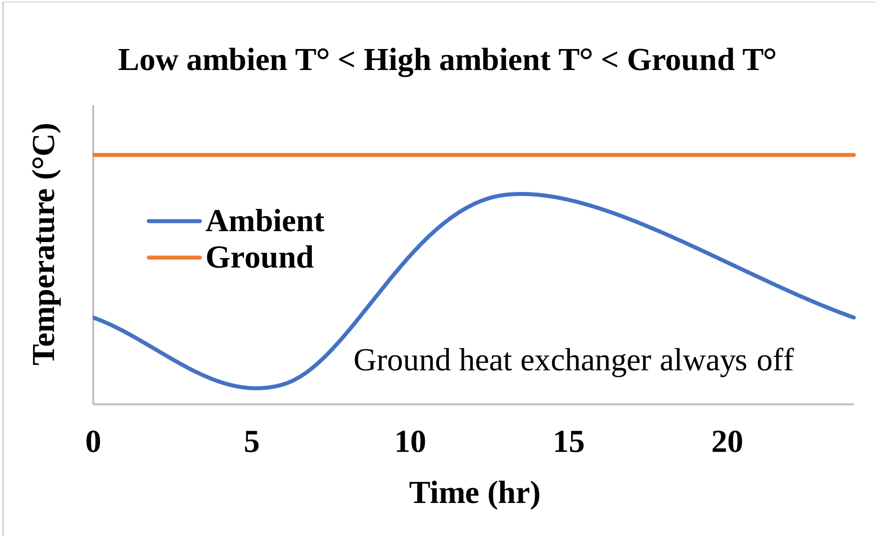


Figure 4.5: Ground cooling system not operating (case 2)

- *Case 3: The ambient temperature fluctuates around the ground temperature*

This is the most complex case in which the ground temperature is lower than the highest ambient temperature while it is higher than that of lowest ambient. Figure 4.6 presents case 3 showing that the maximum and minimum ambient temperatures are recorded at 06:00 and 13:00. As shown in Figure 4.2, this is the most frequently occurring case in the year 2020. Assuming that the ambient temperature is varying linearly during the day, the equation of a straight line is used to represent the temperature as shown in equation (4.1). The temperature function can be divided into two parts such that it is increasing during 06:00-13:00 and decreasing during 13:00-24:00. Thus, it is necessary to find the equations of these lines in terms of maximum and minimum ambient, and ground temperatures to calculate the daily effective cooling source temperature based on the ground cooling system (GCS) operating duration.

$$T = at + b \tag{4.1}$$

where *T*, *a*, *t*, and *b* are the temperature, slope, time, and y-intercept.

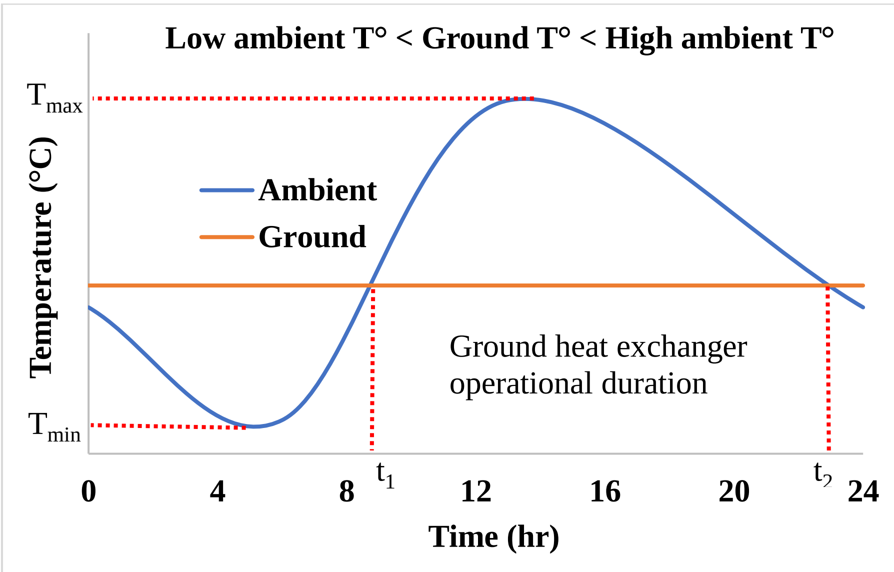


Figure 4.6: Ground cooling system partially operating (case 3)

As for the duration between 06:00 and 13:00, the following equations are used to find the intersection between ground and ambient temperatures:

$$a_1 = \frac{T_{max} - T_{min}}{13 - 6} \tag{4.2}$$

$$b_1 = T_{min} - \frac{6(T_{max} - T_{min})}{7} \tag{4.3}$$

where $T_{max}$ and $T_{min}$ are the maximum and minimum ambient temperatures during the day at 13:00 and 06:00, respectively. After substituting equations (4.2) and (4.3) in equation (4.1), the following is obtained to represent the temperature variation during the first phase:

$$T_1 = \frac{T_{max} - T_{min}}{7}(t - 6) + T_{min} \tag{4.4}$$

Equation (4.5) shows the first intersection point between the ground and ambient temperatures which is obtained by taking a particular case ($T_1 = T_g$) and substituting it in equation (4.4):

$$t_1 = \frac{7\left(T_g - T_{min}\right)}{T_{max} - T_{min}} + 6 \tag{4.5}$$

where $t_1$ and $T_g$ are the starting operation time of GCS and ground temperature at 2 m depth, respectively. (Note: the value of $t_1$ must be between 06:00 and 13:00)

As for the duration between 13:00 and 24:00, first it is required to calculate the approximate temperature at 24:00. Assuming that the temperature is decreasing linearly from 13:00 to the next day at 06:00, then the slope of the second phase can be estimated as follows:

$$a_2 = \frac{T_{min} - T_{max}}{17} \tag{4.6}$$

where the number 17 refers to the duration between 13:00 and next day at 06:00. Therefore, if the temperature is decreasing at this rate, then the temperature at 24:00 can be calculated as shown in equation (4.7).

$$T@24{:}00 = \frac{6(T_{max} - T_{min})}{17} + T_{min} \tag{4.7}$$

Equations (4.8) and (4.9) shows the method used for evaluating the y-intercept and temperature function during the second phase. The latter is derived by substituting equations (4.8) and (4.6) in the general temperature function which is equation (4.1).

$$b_2 = T_{max} + \frac{13(T_{max} - T_{min})}{17} \tag{4.8}$$

$$T_2 = T_{max} - \frac{T_{max} - T_{min}}{17}(t - 13) \tag{4.9}$$

Equation (4.10) shows the second intersection point between the ground and ambient temperatures which is obtained by taking a particular case ($T_2 = T_g$) and substituting it in equation (4.9):

$$t_2 = \frac{17\left(T_{max} - T_g\right)}{T_{max} - T_{min}} + 13 \tag{4.10}$$

where $t_2$ corresponds to the second point of intersection between the ground and ambient temperature which is the time when the GCS is turned off. (Note: the value of $t_2$ must be between 13:00 and 24:00)

Figure 4.7 presents the effective cooling source temperature based on the model used for case 3 in which it shows that the GHE limits the increase in ambient temperature during the daytime. Equation 4.11 is used to calculate the average effective cooling source temperature during the days of case 3. For this reason, the area under the curve of Figure 4.7 is divided into three areas to easily apply the integration shown in equation (4.11). The area is divided into two trapezoids and one rectangle. Thus, equation (4.12) can be considered as a representation of the final approximate average temperature. (Note: this temperature must always be between the ground and lowest ambient temperatures)

$$T_{avg.eff} = \frac{\int_{t=6}^{t=24} T dt}{18} \tag{4.11}$$

$$T_{avg.eff} = \frac{(T_g + T_{min})(t_1 - 6) + 2T_g(t_2 - t_1) + (T_g + T@24{:}00)(24 - t_2)}{36} \quad (4.12)$$

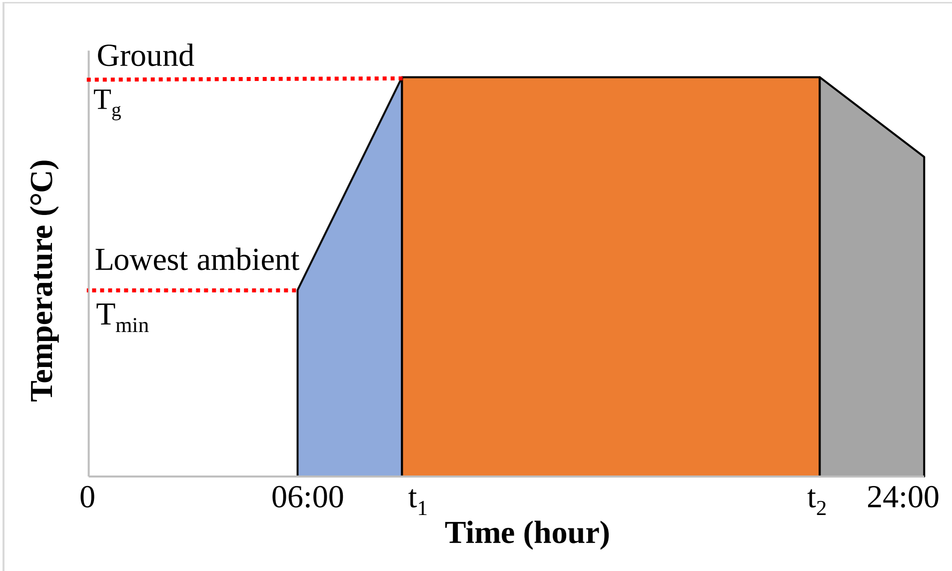


Figure 4.7: The effective cooling source temperature during a day representing case 3

### 4.3.2 Ambient vs. effective average temperatures

It is very important to calculate the daily average cooling source temperature since it directly affects the condensation temperature of working fluid. These temperatures have the same fluctuations during the year which is due to that they have a constant temperature difference (condenser's pinch temperature difference). Figure 4.8 shows the difference between average ambient and effective cooling source temperatures during 2020. The average ambient temperature is calculated considering only the operating hours (06:00-24:00) while that of effective is based on the cases presented in section 4.3.1. The results show that there is a significant difference between the two average temperatures and especially during summer. This confirms the contribution of ground cooling source to decreasing the condensation temperature of the cycle. In some days of the year, the curves coincide representing case 2 where the ground temperature is always higher than that of ambient. In addition, the difference between the two curves almost represents the operating duration of the GCS.

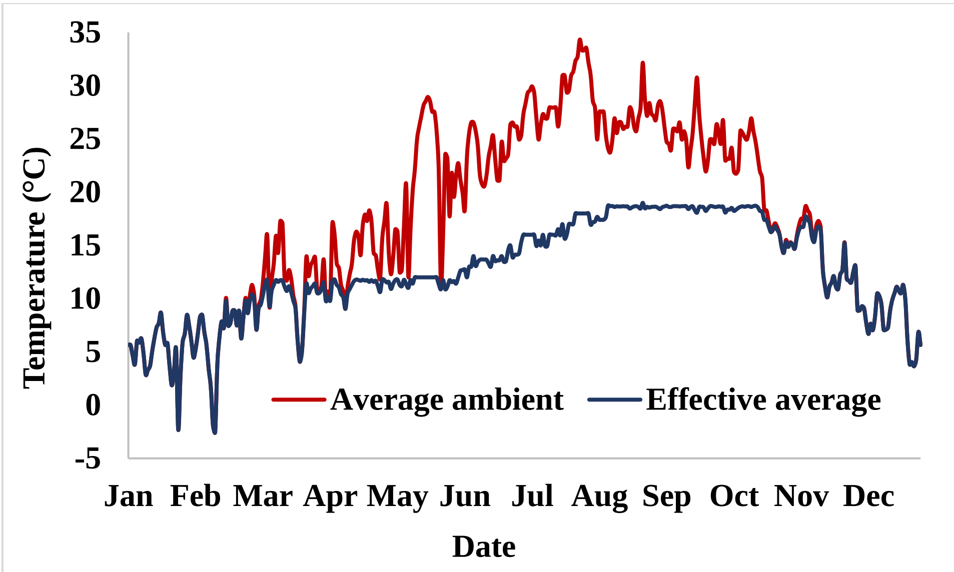


Figure 4.8: The variation of average ambient and effective cooling source temperatures in Bekaa-Lebanon during 2020

### 4.3.3 Operation assessment

This section aims to present the daily and annual GCS operating durations. The maximum possible operating duration per day is assumed to be 18 hours (06:00 to 24:00). Thus, when the GCS can operate 18 hours, then it will be reported as full operation (100%/day). Figure 4.9 shows the variation in the daily operating potential of GHE during 2020. It presents a great potential since the average operating duration is approximately 10 hours which represents 55.56% of the total operating time.

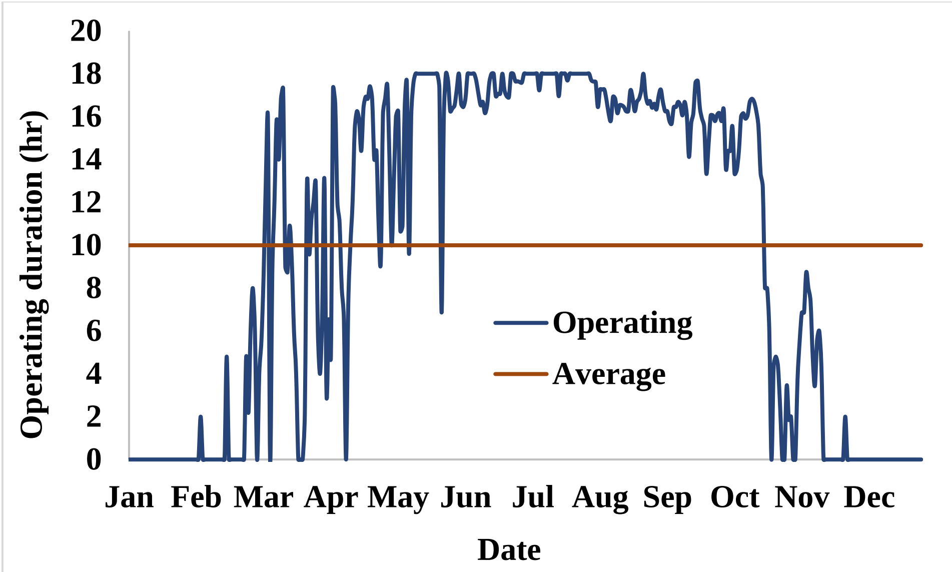


Figure 4.9: The estimated annual operating hours of ground cooling system

The results presented above have shown that the ground source can immensely decrease the condensation temperature of the power cycle. This is not only noticeable from the difference between the temperatures, but also because the GCS can operate for long durations with large portions of the total time of operation. Table 4.2 presents a detailed comparison between the ground and ambient sources regarding their differences in terms of temperatures and operations.

Table 4.2: The difference between the effect of ground and ambient cooling sources on the proposed system; operations and temperatures

| **Parameters (ground)** | **Value** | **Unit** |
| --- | --- | --- |
| Maximum operating duration | 18 (100) | hours/day (%) |
| Average operating duration | ~10 (55.56) | hours/day (%) |
| Full operation (18 hours/day) | 51 (13.97) | days/year (%) |
| Total operation (0-18 hours/day) | 258 (70.68%) | days/year (%) |
| Maximum difference with highest ambient temperature | 24 | °C |
| Maximum difference with lowest ambient temperature | 22 | °C |
| Average difference with highest ambient temperature | 7.33 | °C |
| Average difference with lowest ambient temperature | 6.64 | °C |

According to the mentioned operating cases in section 4.3.1, the GCS can be fully operating, partially operating, or turned off during the day. These possible operations refer to the cases 1, 2 and 3, respectively. Figure 4.10 shows the number of days for each case such that the GCS can be operating 258 days/year. However, 51 days of them correspond to full operations (18 hours/day). It is expected that the GCS can be turned off for 107 days/year, but it is essential to mention that the operating days can be more than 258 after adopting the optimized system (see section 5.2). Even though, the GCS is not operating during these 107 days, it is very important to take advantage of the cold ambient air in winter to recover the ground's coolth energy. This allows the ground source cooling system to operate more than 258 days/year considering the decrease in its temperature due to the additional heat rejection provided by the primary heat exchanger.

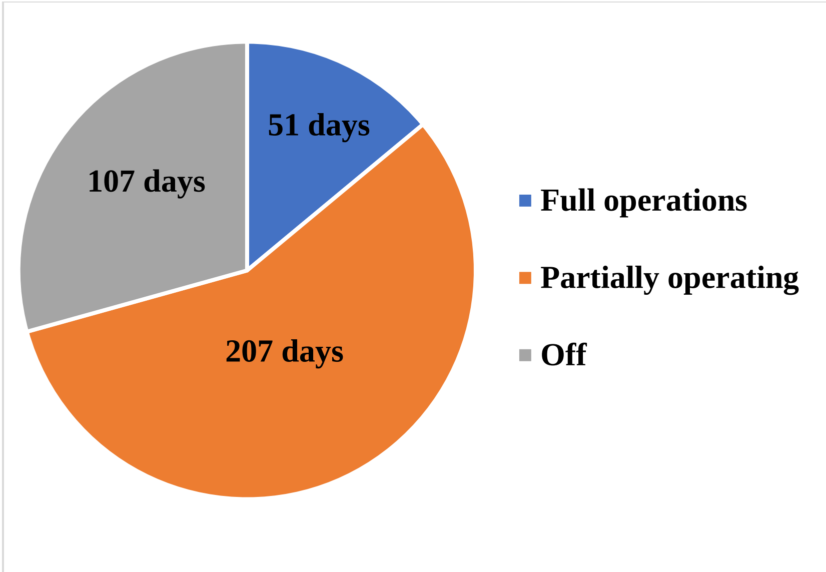


Figure 4.10: Summary of the potential of using a ground cooling system in Bekaa-Lebanon

### 4.4 Conclusion

The ground and ambient temperatures were measured in Bekaa-Lebanon during 2020 and a detailed comparison was provided. The thermocouples were inserted at depths of 0.3, 0.6, 1, 1.3, 1.6 and 2 m. The maximum differences between highest and lowest temperatures during 2020 were 40°C, 33°C and 7°C for ambient high, ambient low and ground temperature at 2 m, respectively. The corresponding average values were 22.83°C, 8.87°C and 15.51°C. All ground temperatures were more stable than that of ambient such that as the depth increased the stability increased. These results show that shallow geothermal energy has a great potential for cooling a power cycle in Bekaa-Lebanon.

# Chapter 5. Parametric Study for System Optimization

This chapter presents the methodology that was followed to optimize the power generation system incorporating a ground-cooled condenser, proposed in Chapter 3. However, in this chapter, the ground heat exchanger is placed in soil considering the absence of shallow underground water in many regions (ex: Bekaa-Lebanon). System optimization also aims to mitigate the negative effects of critical parameters such as pressure drop, low mass flow rate and large ground loops. This requires the investigation of different configurations and working fluids to ascertain their effects on the performance of the system. The purpose of system optimization is to help increase the net output power whilst reducing the capital cost of installation, such optimizations capturing the importance of both thermodynamic and economic aspects. Figure 5.1 presents the flow chart diagram for the current chapter including both parametric and optimization approaches. The first part of this chapter aims to compare two different possible ground cooling system's configurations based on the pressure drop inside the ground loop. After that, a parametric study is applied on the optimized system intending to select the suitable working fluid [160].

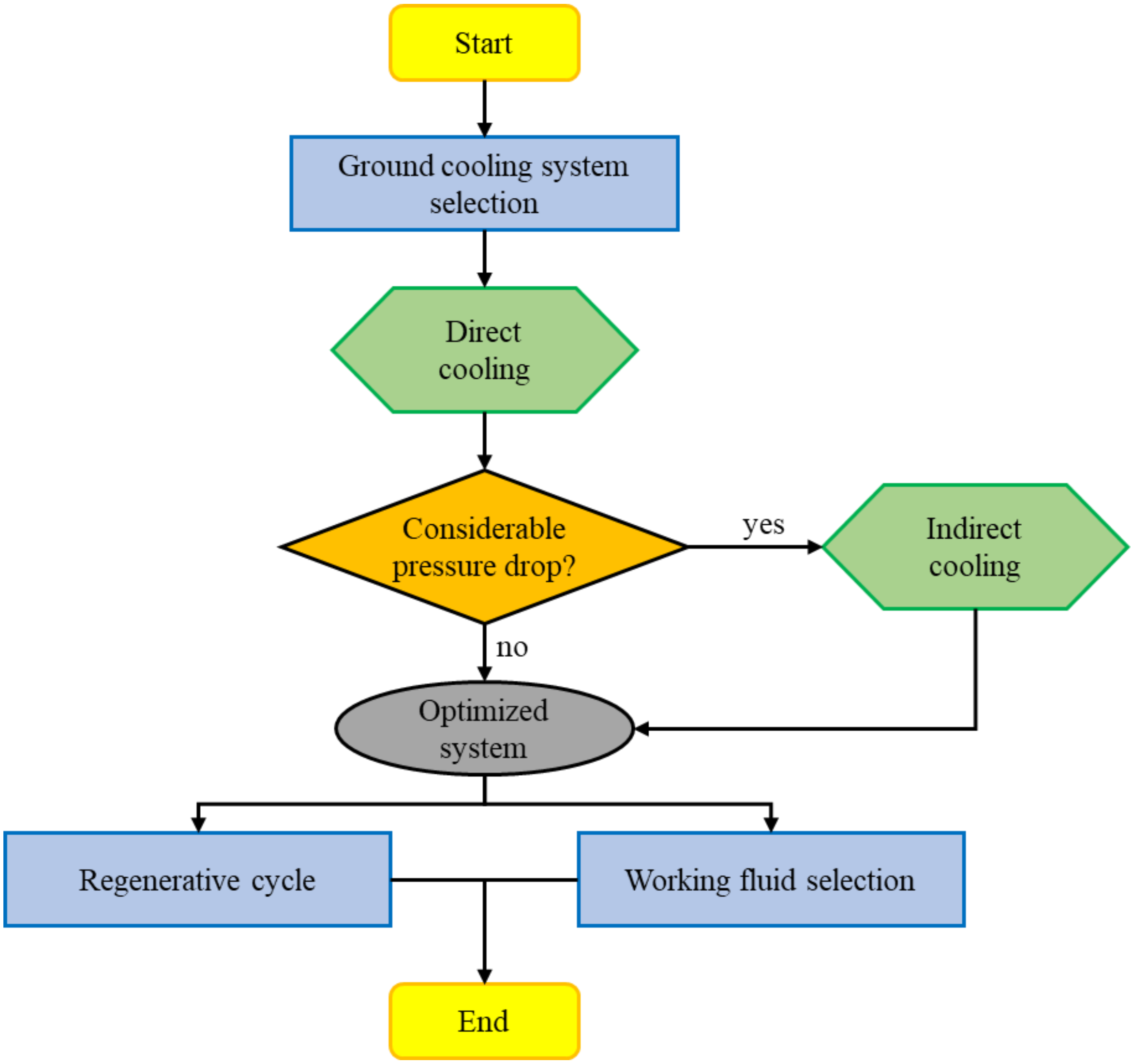


Figure 5.1: A flow chart diagram representing the methodology used in this chapter

### 5.1 Direct Cooling vs. Indirect Cooling

The system depicted in Figure 3.2 shows the ground-cooled condenser concept exhibiting a direct cooling method. This means that a direct contact between the cooling source and power cycle is available. This method is usually used to produce the highest amount of power since no intermediate loops are involved (minimum pinch temperature can be assumed). However, this may be accompanied by severe pressure drops in the condenser and hence negatively affecting the overall system's performance. This is also more considerable in the absence of underground water when large ground loop is required. In most cases, the ground loop is installed in the soil as shown in Figure 5.2. The main concepts of using shallow horizontal ground-cooled condenser as direct and indirect cooling systems are presented in Figure 5.2a and Figure 5.2b, respectively.

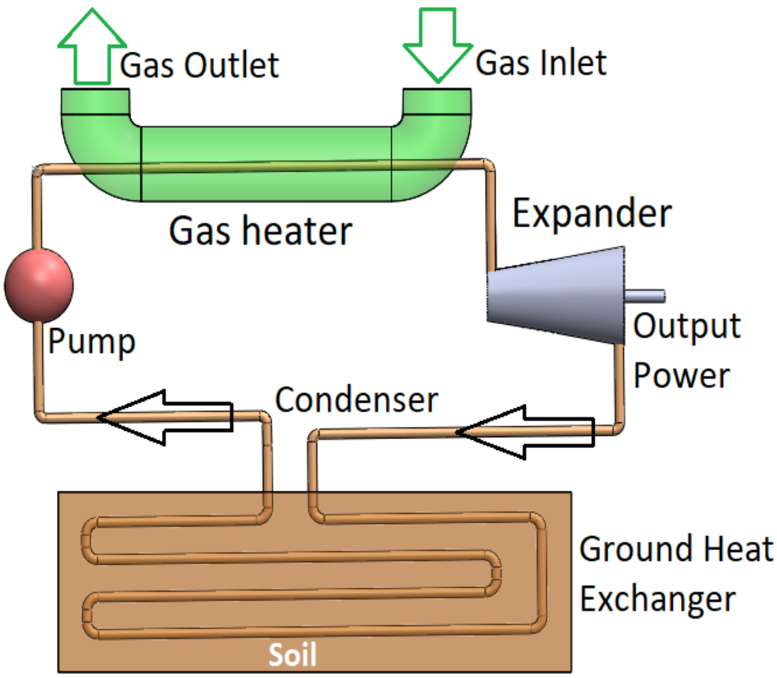


(a)

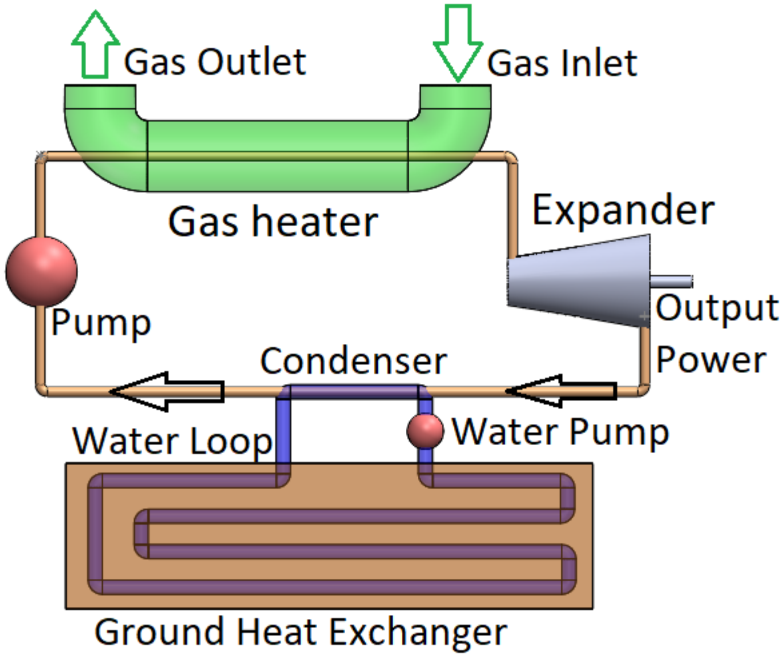


(b)

Figure 5.2: (a) Direct and (b) indirect ground cooling systems

### 5.1.1 Effect of pressure drop

This section aims to investigate the effect of pressure drop in the direct ground cooling system (see Figure 5.2a) to check if it is feasible to use such a strategy or is better to add an intermediate loop to make the system more controllable and avoid negative impacts. The same model presented in section 3.2 is used to calculate the system's performance (Appendix A.2), whilst equations (5.1) and (5.2) show the method used to ascertain the pressure drop effect [161].

$$f = \frac{0.316}{Re^{0.25}} \tag{5.1}$$

$$\Delta P = \frac{\rho . f . L . v^2}{2D} \tag{5.2}$$

where $f$, $Re$, $\Delta P$, $\rho$, $L$, $v$ and $D$ are friction coefficient, Reynold's number, pressure drop, density, length, velocity, and diameter, respectively. The working fluid's velocity is calculated as shown in equation (5.3).

$$v = \frac{4\dot{m}}{\rho . \pi D^2} \tag{5.3}$$

Table 5.1 presents a summary of the conditions used for investigating the effect of pressure drop. These parameters are either fixed at the values mentioned in the table or will be varied and reported later during the simulation. According to a study carried out by Fujii *et al.* [162], it is recommended to keep the horizontal installed pipes 2 m apart to avoid thermal interference between them. This means that the effect of each pipe could reach 1 m. For this reason, in this section, the soil thermal interference is assumed to be 1 m. In other words, the ground temperature is assumed to be constant at 1 m far from the GHE.

Table 5.1: Parameters considered for investigating the effect of pressure drop

| **Parameters (Units)** | **Values** |
|---|---|
| Gas heater diameter (mm) | 40 |
| Gas mass flow rate (kg/hr) | 300 |
| Gas inlet temperature (°C) | 777 [156] |
| Gas outlet temperature (°C) | 120 [156] |
| Expander inlet pressure (MPa) | 15 |
| Expander inlet temperature (°C) | 500 |
| Ground temperature (°C) | 15 |
| Condensation temperature (°C) | 25 |
| Cycle pipe diameter (mm) | 10 |
| Expander isentropic efficiency | 0.7 |
| Pump isentropic efficiency | 0.8 |
| Generator efficiency | 0.9 |

### 5.1.2 Results and discussion

In this section, the simulations are carried out to compare three models with minor differences; ideal direct ground cooling (I-DGC), considering pressure drop in the condenser (C-DGC) and considering pressure drop in both heat exchangers (DGC). The effect of pressure drop can be represented by the difference in net output power between the mentioned cases.

Figure 5.3 shows that the net output power is significantly affected by the cycle's pipe diameter. This is especially noticed at small pipe diameters (below 15 mm). However, the minimum value of diameter can also change depending on the grade of energy since it was increased from ~13 to ~16 mm when the mas flow rate of gas increased from 200 to 300 kg/hr. From this point of view, it can be reported that the negative effect of pressure drop can be avoided, but this depends on the available gas conditions and equipment cost that may be changed when large diameters are required.

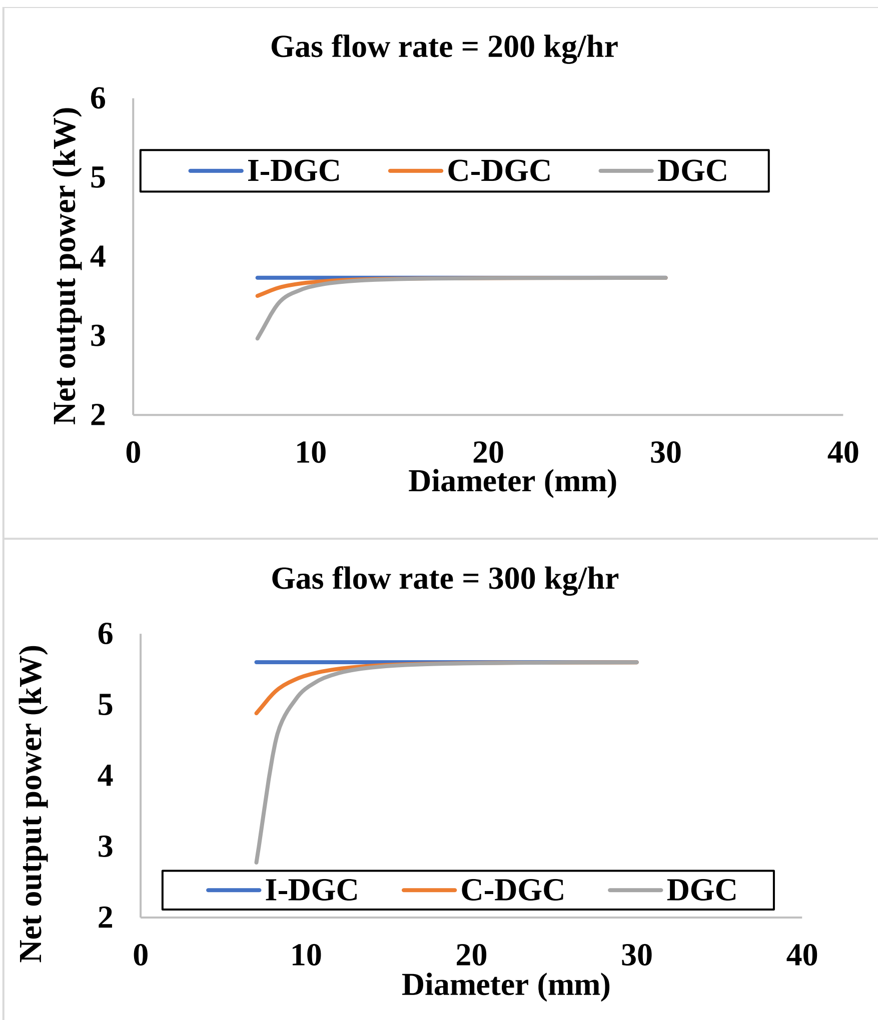


(a)

(b)

Figure 5.3: The effect of cycle's pipe diameter on the pressure loss at gas mass flow rates of (a) 200 kg/hr and (b) 300 kg/hr

To study further the effect of energy grade source on the pressure drop consideration, the gas temperature and mass flow rate were varied from 700 to 1500°C and 100 to 300 kg/hr, respectively as shown in Figure 5.4. It can be noticed that the curves corresponding to the ideal case are diverging, while those of DGC are converging. This confirms that the pressure drop is relatively more considerable for higher grade energy sources. This shows that the pressure loss is increasingly affected by the amount of heat added to the cycle. The pressure drops in both heat exchangers is almost the same which can be determined from the rate of change between the three presented models. The main reason causing the pressure loss effect to increase with the grade of energy is the increase of working fluid mass flow rate. As shown in equation (5.2), the pressure drop is highly affected by the fluid's velocity knowing that the latter and mass flow rate and directly proportional at a given cross-sectional area.

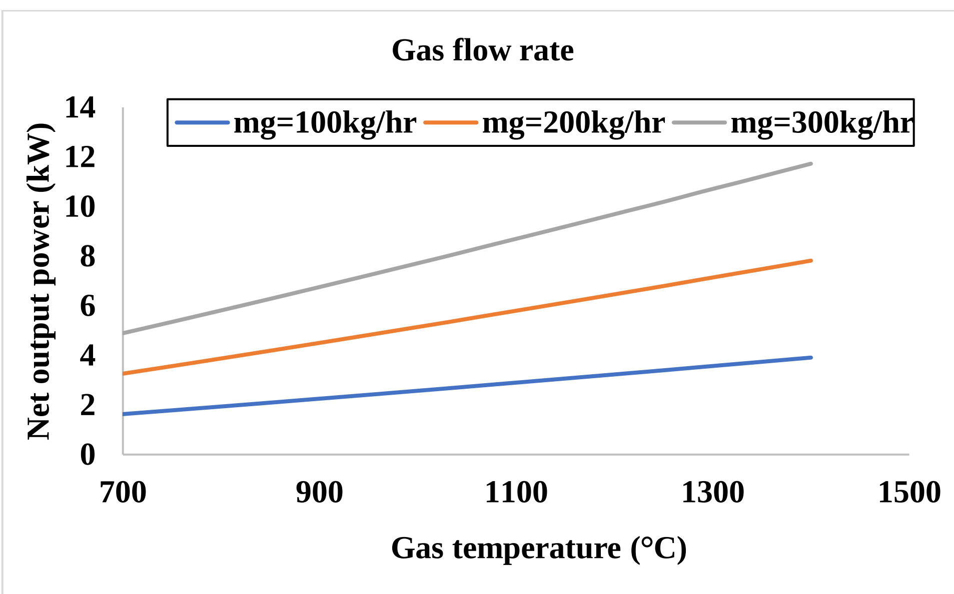


(a)

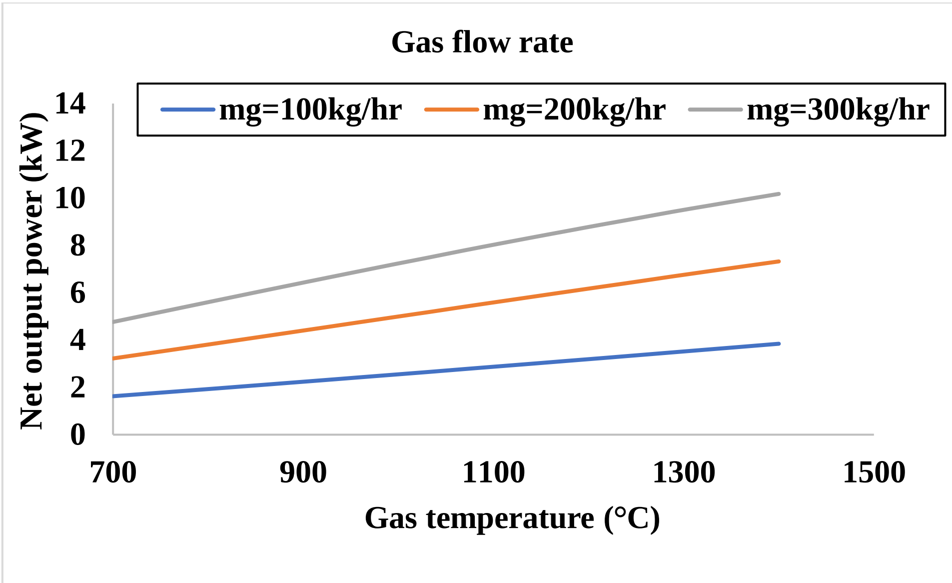


(b)

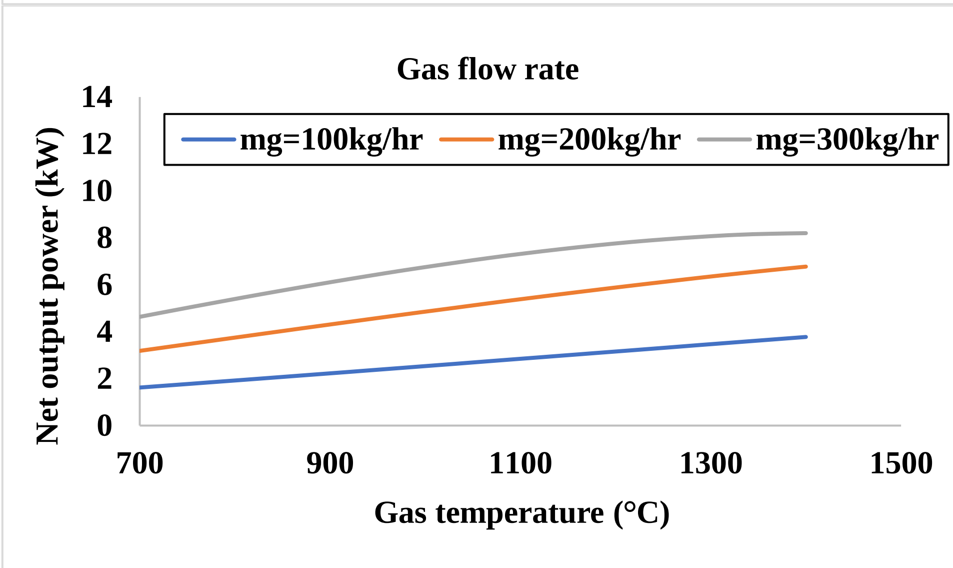


(c)

Figure 5.4: Effect of energy grade source on the net output power of (a) I-DGC, (b) C-DGC and (c) DGC

It may appear good in some cases to change the conditions for the cycle to optimize the system and achieve the best operating conditions. However, this is an ineffective method for avoiding the negative impacts accompanied by pressure drop. This can be noticed from the results presented in Figure 5.5 since the change in expander inlet temperature and pressure did not significantly affect the discrepancy between the studied models. Even though the net output power difference between the three considerations was decreased at high temperatures and pressures, this requires a considerable change in the conditions which is usually unacceptable.

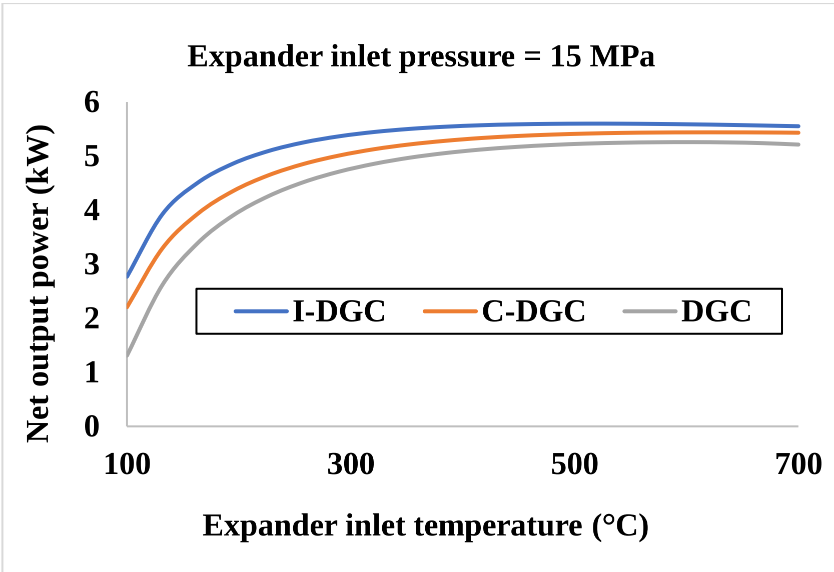


(a)

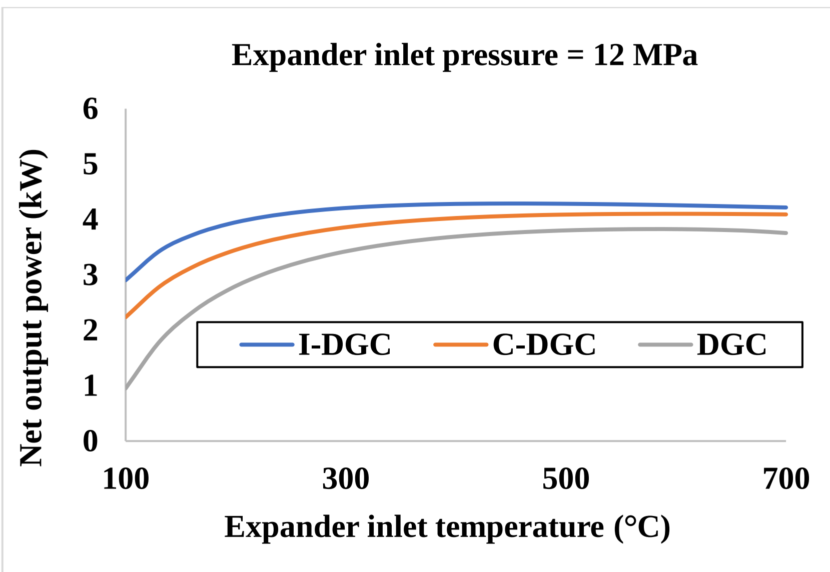


(b)

Figure 5.5: The influence of expander inlet conditions on the effect of pressure drops at (a) 15 MPa and (b) 12 MPa

The results presented in this section show that the effect of pressure drop cannot be neglected and will indeed cause significant drawbacks and changing of cycle's conditions.

Thus, it would be recommended to introduce an intermediate water loop between the cycle and ground to ensure stability, make the system more controllable and avoid critical issues resulting from pressure losses. This encourages using the indirect cooling strategy presented in Figure 5.2b. However, this system needs to be further modified to avoid a large ground loop installation. It is also important to mention that an antifreeze liquid must be mixed with water to avoid freezing since the cooling source temperature can decrease below 0°C as presented in Chapter 4.

### 5.2 Optimized System

The heat rejected from a power cycle can be relatively massive with respect to the shallow GHE capacity, otherwise a large installation would be required. This causes additional expense making this system inappropriate for such utilizations. For this reason, it is better to integrate another cooling source into the hybrid power cycle such as an air-cooled or water-cooled heat exchanger to operate as a primary heat rejector. Another advantage of this integration is to provide coolth compensation to the GHE in which this can immensely enhance its performance during operating hours. This recovery system can operate during the night whilst the ORC is off such that only the water loop will be running to transfer heat from the ground to the ambient air. However, it is recommended to introduce an underground storage medium that has high thermal conductivity and storage capacity, such as composite phase change materials, to allow the surrounding around the GHE to store coolth energy. This contributes to compensating the cooling ability of the ground source as well as improving the overall heat transfer coefficient to increase the heat transfer rate between the ground and circulating coolant.

The optimized system is presented in Figure 5.6 in which the two types of heat exchangers are connected in series. A bypass line is connected in parallel with the GHE to avoid exchanging heat with the ground when the ambient temperature is lower than that of the ground. On the other hand, the primary heat rejector will always be operating to reduce the amount of heat rejected from the cycle to the ground preventing heat accumulation and the need for large GHE installations. Therefore, a directional control valve (DCV) is used at the exit of primary heat rejector (state 6) to control the flow path of water; either passing through the GHE or overtaking it to directly enter the circulating pump. Another DCV is placed at state 8 to allow bypassing the cycle’s condenser at night when the system is operating under recovery cooling mode. Thus, the two bypass lines help the ground to recover its coolth energy by decreasing its temperature when the power cycle is off (mainly at night) by extracting heat from the ground to the ambient air. It is also necessary to use a DCV at the inlet of primary heat rejector which helps overtaking this heat exchanger when the water exiting the condenser is below that of ambient (state 5). A particular case with detailed input will be shown in Chapter 7 presenting the conditions of all states.

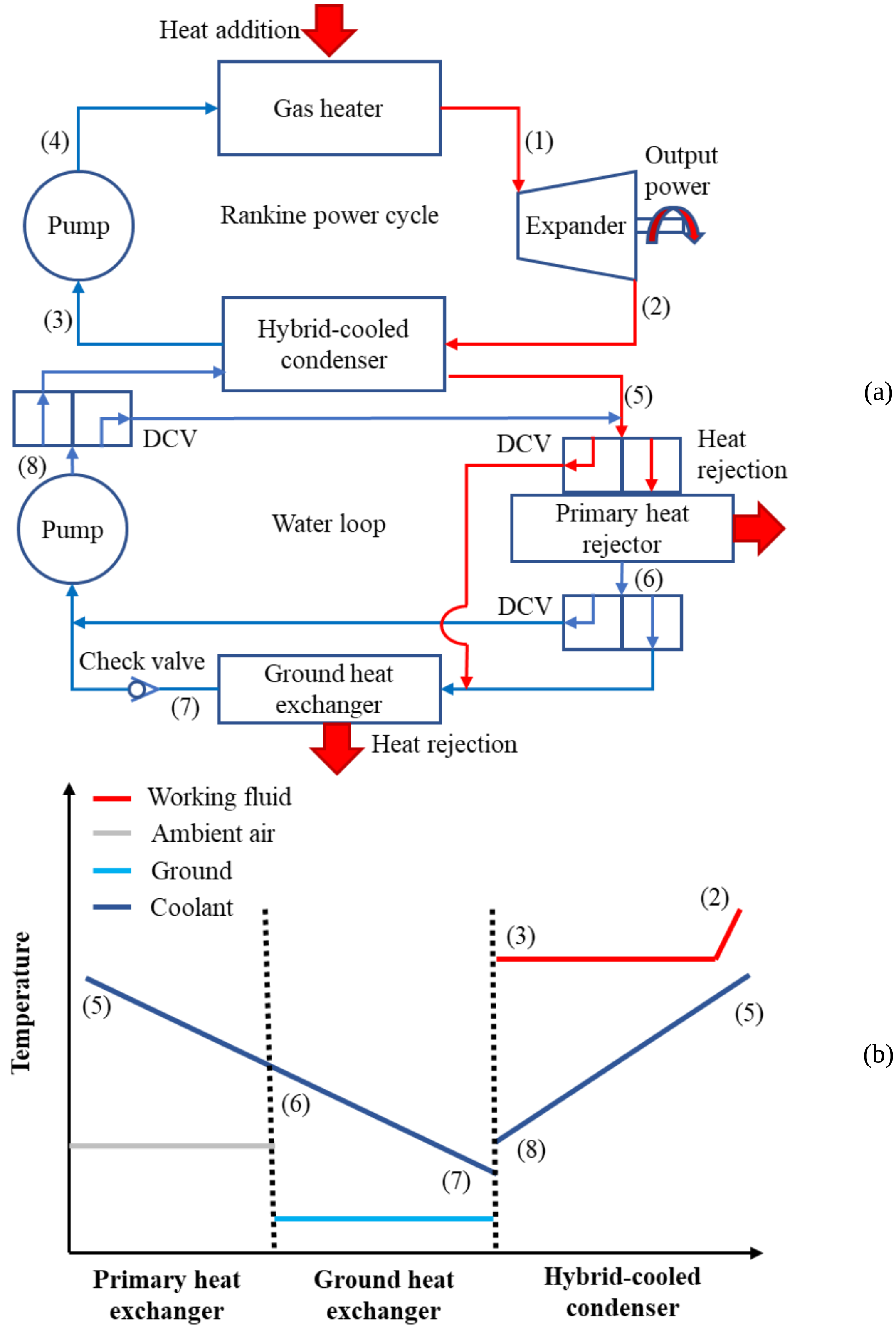


Figure 5.6: (a) Schematic diagram of the optimized system and (b) temperature variation in the cooling system; directional control valve (DCV)

The optimized system can be further enhanced by utilizing the heat rejected from the cycle between states 5 and 6 to increase the overall system's efficiency. This can maximize the output of the system by providing two types of outputs: electricity from the ORC and heat from the water loop. A large portion of heat is rejected from the water loop by the air/water-cooled heat exchanger, and this can be used to heat domestic water or utilized as an input to a heating system during winter months. Another possible utilization is the preheating of water prior to entering an electrolyzer. This can be helpful in producing hydrogen knowing that this type of combination suits the proposed system well since the electrolysis process requires both available forms of energy, electrical and thermal. It is also possible to use a regenerator which is a heat exchanger used to transfer the heat remaining in the working fluid when exiting the expander to that entering the gas heater. This can also reduce the required heat input for producing the same amount of power or increase the net output power while maintaining constant heat addition.

## 5.3 Operating Modes

This section aims to manage the operation of the optimized system presented in Figure 5.6. The DCVs placed at states 5, 6 and 8 are responsible for controlling the flow paths of the intermediate water loop, while the water pump helps regulating the amount of heat rejected from the cycle. Another advantage of the latter regulation is to facilitate the ground's coolth recovery at night. Concerning the operating modes, the ORC is either turned on or off, while the water loop has four operating modes with different flowing paths.

### 5.3.1 Normal operation (mode 1)

This mode corresponds to the case when the ground temperature is below that of the ambient air. For this reason, the coolant exiting the primary heat rejector (state 6) passes through the GHE to further decrease its temperature as shown in Figure 5.7. Then, cold water (state 7) is supplied to the condenser (state 8) via a circulating pump. In this mode, there is no need to use any of the bypass lines since both heat rejectors are activated. This operation is usually required during the daytime when there is electricity demand, and the power cycle is turned on. However, it is essential to ensure that the ambient temperature during this mode is higher than that of the ground, otherwise the coolant entering the GHE will gain heat instead of rejecting it. The portions of heat rejected to the ground and ambient air will be calculated and compared in the next chapter to investigate the feasibility of normal mode operation.

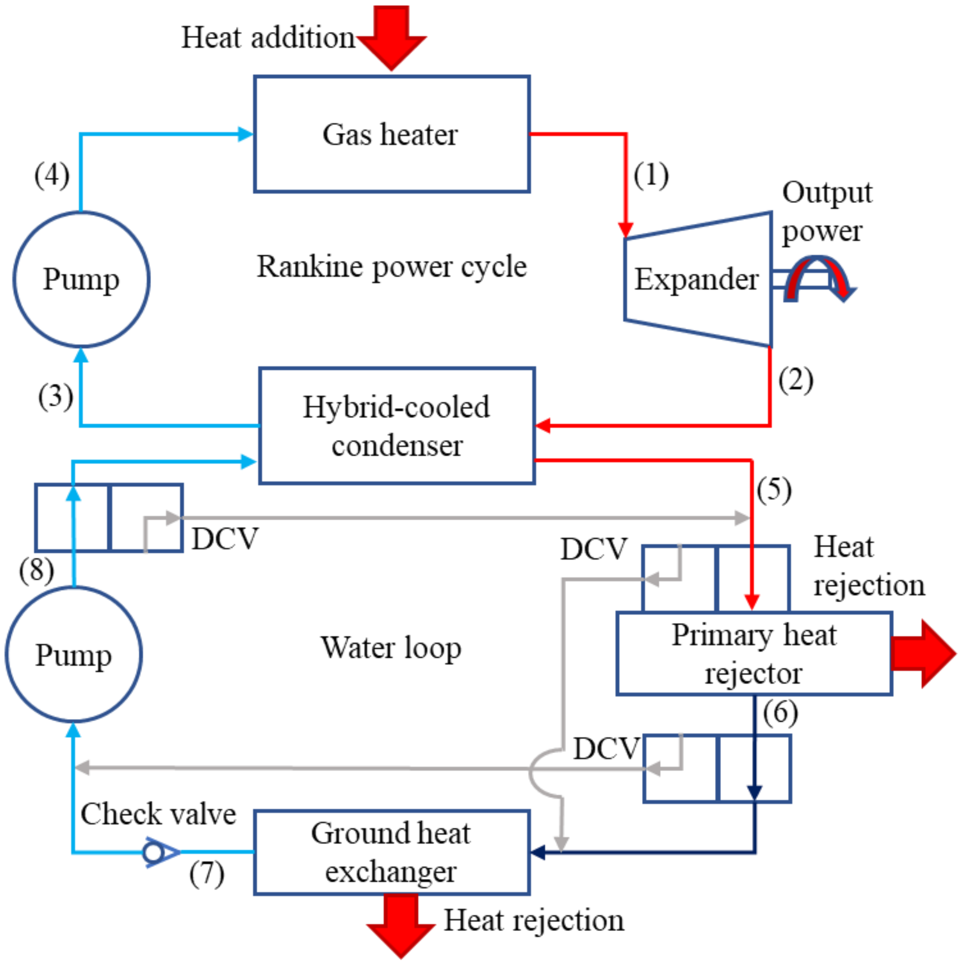


Figure 5.7: Schematic diagram of the normal mode operation

### 5.3.2 Ground cooling system turned off (mode 2)

The mode presented in Figure 5.8 shows the second possible mode of operation which represents the case when the ground temperature is higher than that of the ambient air. This is also needed only when the power cycle is turned on, otherwise mode 4 will operate. The ground's temperature can be relatively high mainly in two cases, either in winter or due to high loads leading to heat accumulation. Thus, it is necessary to connect thermal sensors to allow regulatory control of the operating modes. The thermocouples must be placed very near to the GHE to detect the increase in effective ground's temperature and compare it with that of ambient. This regulation can significantly affect the cycle's performance since it helps to select the suitable operating mode (1 or 2).

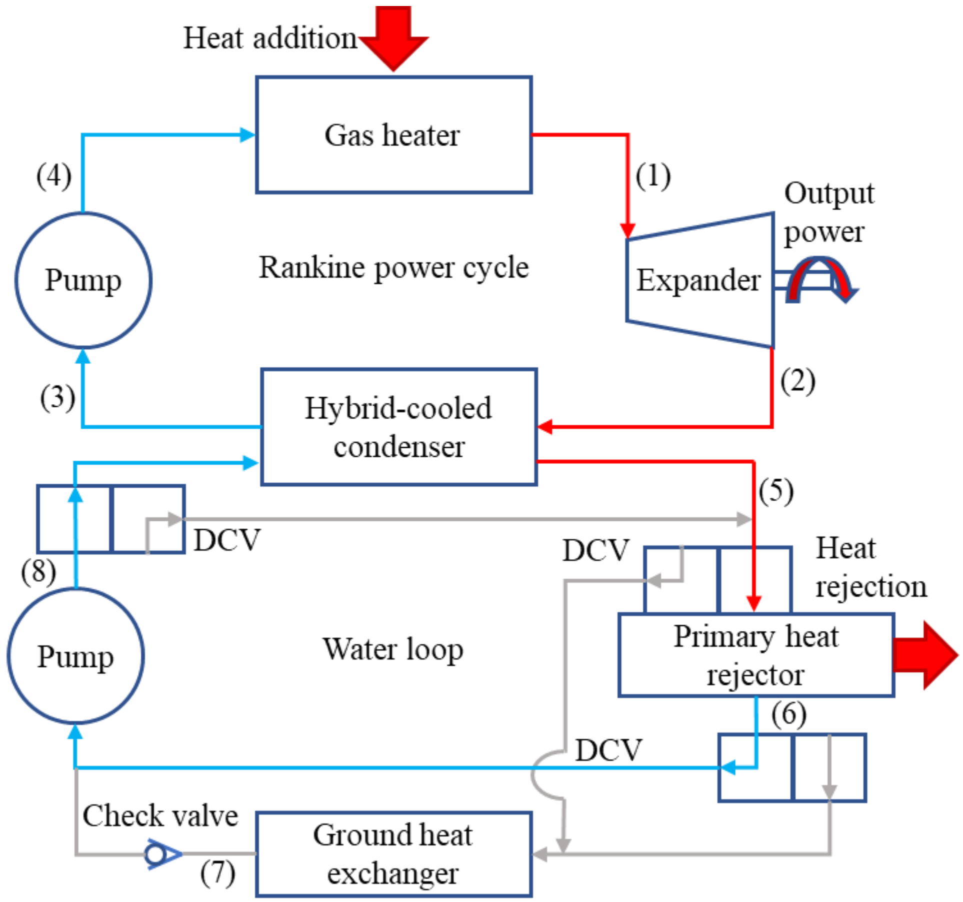


Figure 5.8: Schematic diagram representing mode 2; only primary heat rejector is operating

### 5.3.3 Primary heat rejector turned off (mode 3)

In some summer days, the ambient air cannot be used to extract any heat from the water loop due to the low water temperature exiting the condenser compared to that of ambient. In this case, it is better to bypass the primary heat rejector as shown in Figure 5.9. Hot water directly enters the ground loop to decrease its temperature. In this mode, the ground cooling system (GCS) is operating at full load and the ground is receiving the highest amount of heat compared to other operating modes. In these periods, mode 4 is very essential during night hours to ensure coolth compensation because the condenser is only depending on the GCS during the daytime.

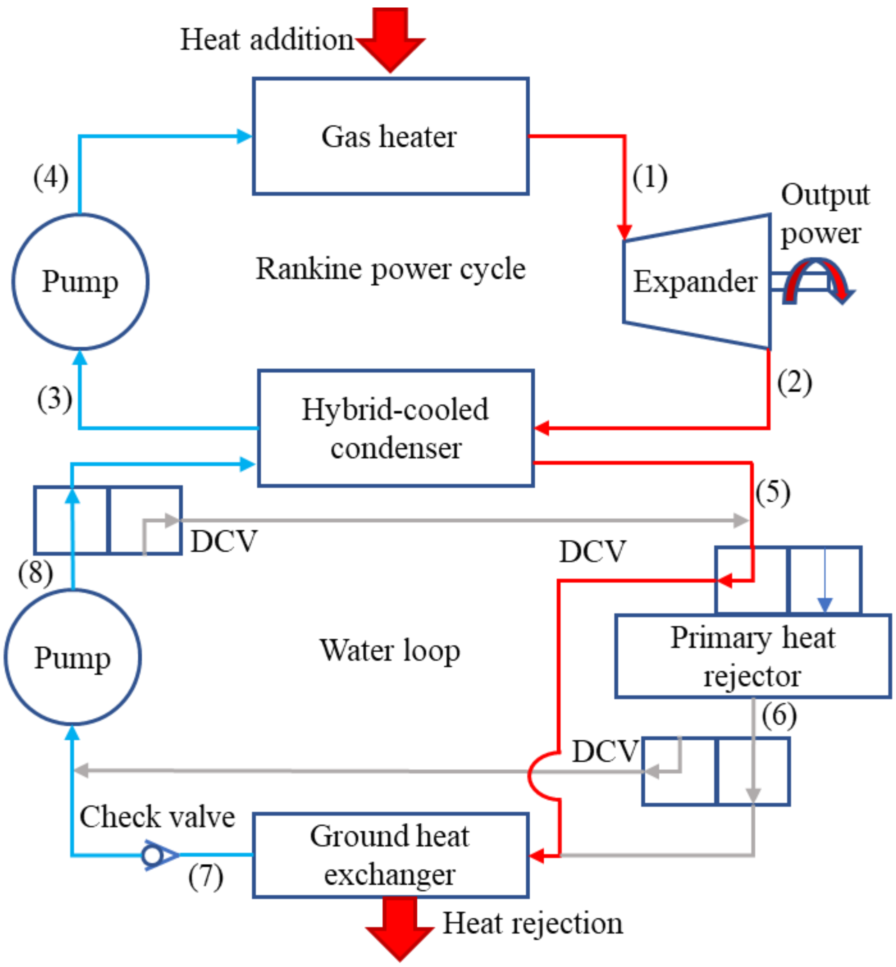


Figure 5.9: Schematic diagram representing mode 3; primary heat rejector is turned off

### 5.3.4 Coolth recovery (mode 4)

In this mode, the power cycle is turned off while water is only circulating in the primary heat rejector and GHE as shown in Figure 5.10. This operation contributes to decreasing the ground's temperature by recovering its coolth energy. It helps to maintain low condensation temperatures and avoid ground heat accumulation. This mode is mainly used at night when the ground temperature is higher than that of ambient. However, it can also be used during off-periods in some days of winter as presented in section 4.3.1. This operational mode shows the importance of integrating ground thermal energy storage technologies into the proposed optimized system. This means that introducing storage material in the form of grout can store coolth energy during night hours to increase the heat rejection capacity of the ground cooling system. This decreases the effective cooling source temperature during operation.

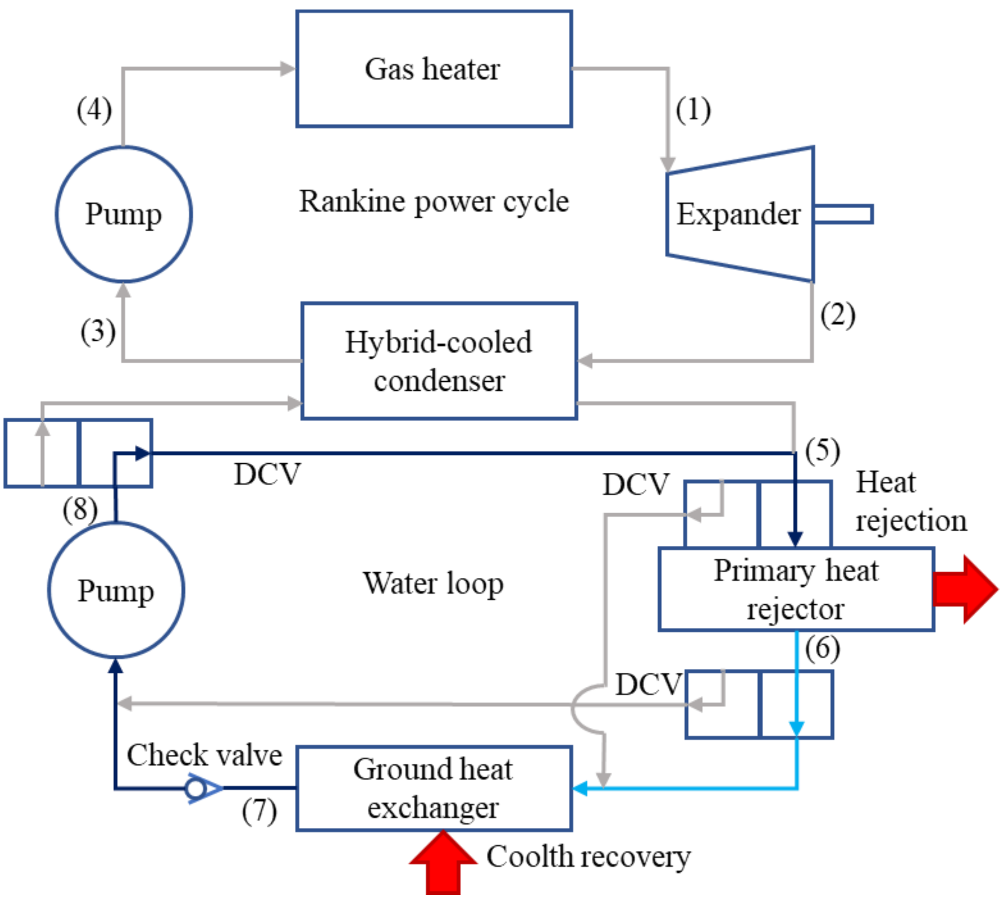


Figure 5.10: Schematic diagram of the recovery operating mode

## 5.4 Working Fluid Selection

The $CO_2$-based transcritical Rankine cycle presented in Chapter 3 was used only as a reference system to investigate the potential of ground-cooled condenser. This section describes the analysis in which the most suitable working fluid was selected for the optimized system (see Figure 5.6). Low to medium-grade sources of energy are considered in this study representing the source used in the real application presented in Chapter 7 (Appendix A.3.1). Such sources require adoption of ORC instead of the conventional steam Rankine cycle and this is mainly due to the low flow rate of water resulting in inefficient expansion and requirement for high turbine rotational speeds [163].

### 5.4.1 Methodology

Firstly, to select the best working fluid, it is necessary to carry out parametric studies to compare the different usable working fluids. Choosing the fluid corresponding to the highest net output power and efficiency is not always the optimal method since it is essential to be aware of critical drawbacks and negative effects. These may include toxicity, flammability, and global warming potential. There are some other issues that are related to the fluid's nature like requiring high pressures to operate optimally or low flow rate. 1,1,2-Trichloro-1,2,2-trifluoroethane (R113) presents a good example of organic fluids that can produce high amount of power, while it is unfavourable due to its negative effect on public health and ozone layer. For these reasons and according to previous investigations, three compatible refrigerants will be compared in terms of performance that are 2,2-Dichloro-1,1,1-trifluoroethane (R123), 1-Chloro-1,2,2,2-tetrafluoroethane (R124) and 1,1,1,3,3-Pentafluoropropane (R245fa). However, $CO_2$ is also included in this comparison only to represent the results related to the reference system presented in Chapter 3. After stating the negative effects of unsuitable working fluids, it is also important to mention the factors that encourage using the convenient fluids. The most important factors are mainly the availability, cost, and performance. These are the main reasons for choosing the mentioned refrigerants in this parametric study. The methodology used to choose the best working fluid can be represented by the following points:

- Proposing different working fluids based on their availability and cost.
- Studying the negative effects of the proposed working fluids.
- Eliminating the unacceptable fluids based on their environmental impacts.
- Investigating the best point temperature of each working fluid.
- Investigating the relation between best point temperature and cycle's conditions.
- Comparing the working fluid's performance regarding net output power.
- Examining the flow rate of the best working fluid to check if it is feasible for an expander.

Table 5.2 presents the IUPAC names of the investigated working fluids in addition to their critical temperatures and pressures.

Table 5.2: The critical temperatures and pressures of the working fluids investigated

| **Working fluid** | **IUPAC name** | **Critical temperature (°C)** | **Critical pressure (kPa)** |
|---|---|---|---|
| $CO_2$ | Carbon dioxide | 30.98 | 7377 |
| R123 | 2,2-Dichloro-1,1,1-trifluoroethane | 183.7 | 3668 |
| R124 | 1-Chloro-1,2,2,2-tetrafluoroethane | 122.3 | 3624 |
| R245fa | 1,1,1,3,3-Pentafluoropropane | 154 | 3651 |

### 5.4.2 Results and discussion

Each working fluid has optimal operating conditions in which these depend mainly on the available grade source of energy (flow rate and temperature). This section aims to figure out the best operating conditions for the investigated working fluids in the basic ORC.

**Effect of energy grade source**

In this section, the mass flow rate of gas, expander inlet pressure and condensation temperature are kept constant at 200 kg/hr, 10 MPa and 25°C, respectively. Figure 5.11 shows the variation of net output power resulting from the compared working fluids as function of expander inlet temperature at gas temperatures of 300°C and 600°C. The gap presented in Figure 5.11a corresponds to the unsuitability of refrigerants at these conditions such that the lowest temperature of operation depends directly on the expander inlet pressure. Thus, it would be better to decrease the pressure to ensure the superheating of working fluid at low temperatures. It is essential to ensure that the fluid exiting the expander is in vapor state otherwise it will not be possible to operate properly, and the expander blades will be damaged with time. This is also better considering lower pressures inside the pipes and hence minimizing the required thickness and preventing leakage. This is the first reason that makes the refrigerants preferable with respect to $CO_2$. Another advantage is the high extracted power compared to $CO_2$ in which all investigated refrigerants show better performances with noticeable differences (see Figure 5.11). Among the studied working fluids, R123 presented the highest net output power at the different gas and expander inlet temperatures. In the next sections, $CO_2$ will be removed from the comparative study due the observed significant difference compared to other working fluids.

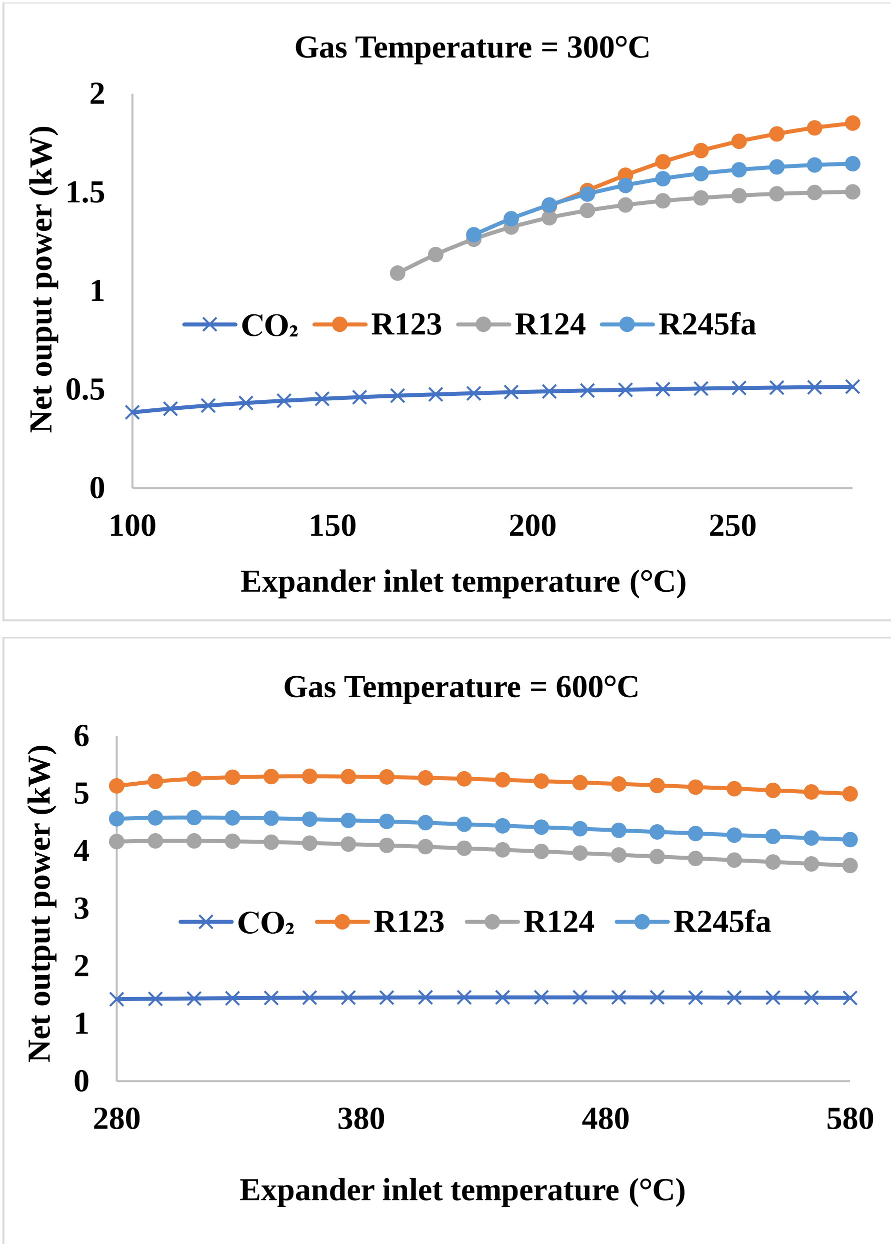


(a)

(b)

Figure 5.11: Effect of gas and expander inlet temperatures on the performance of working fluids

**Optimal operating temperature**

After eliminating $CO_2$ from the possible working fluid choices, it is better to decrease cycle's high pressure. This is mainly because the chosen refrigerants can operate properly at low pressures and especially at low grade sources of energy. The gas flow rate, gas temperature and condensation temperature are maintained at 200 kg/hr, 600°C and 25°C respectively in this section. The optimal operating temperatures of the refrigerants are presented in Figure 5.12 in which it can be noticed that the best point temperature can vary with the change in the expander inlet pressure. This temperature is more noticeable at 3 MPa such that it is recorded as 131.6°C, 163.2°C and 184.2°C for R124, R245fa and R123, respectively. This shows that the refrigerant that has higher critical temperature requires higher operating temperature to achieve its optimal performance (see Table 5.2). Figure 5.12 shows that when the expander inlet pressure increases from 3 to 6 MPa, the curves become smoother which means that the variation in expander inlet temperature is more effective at low pressures. This makes the choice of operating temperature more critical at low grade sources of energy because it will not be possible to increase the expander inlet pressure as presented in section 5.4.2. According to this comparison, R123 still corresponds to the highest performance at low expander inlet pressures achieving net output power of 4.57 kW at 3 MPa and 5.046 kW at 6 MPa. This is another reason for making R123 suitable for low grade applications since there is no significant difference between the net output power at the different studied pressures.

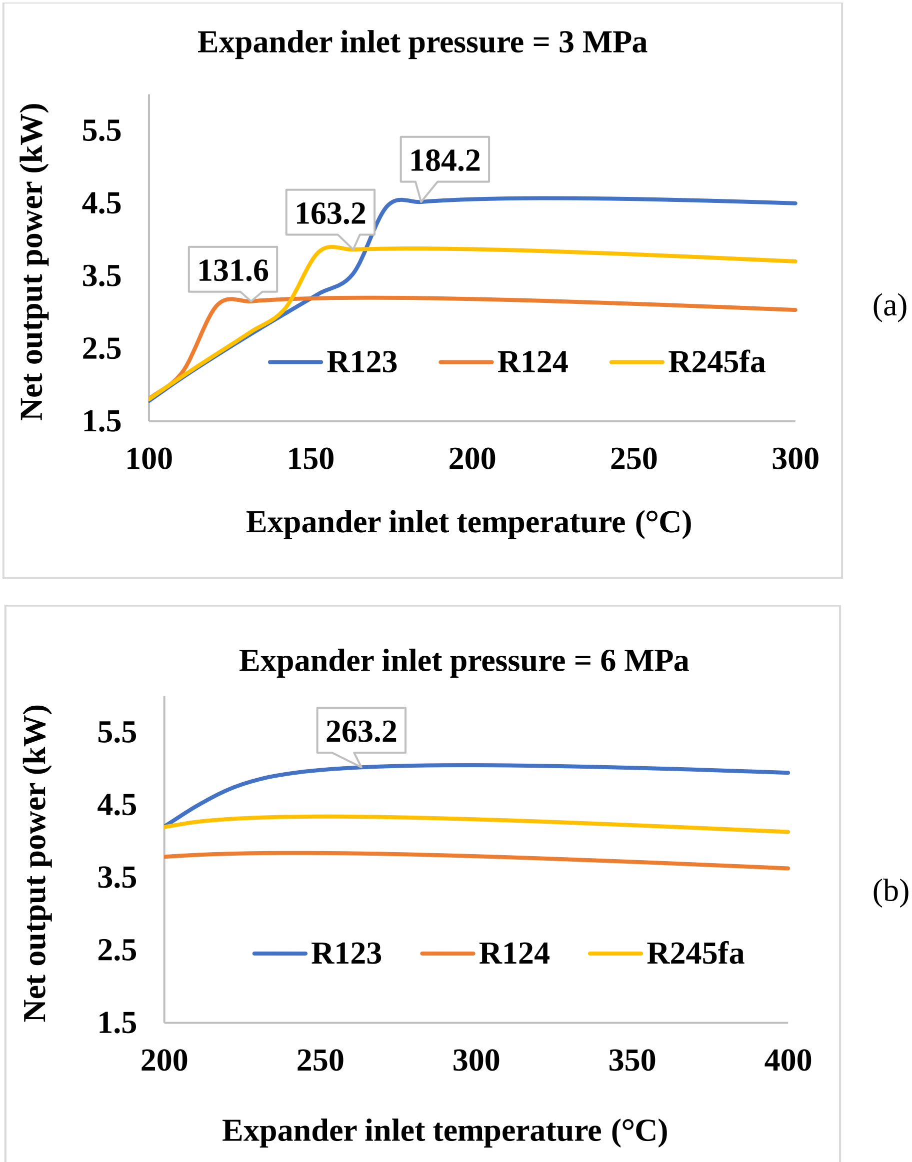


Figure 5.12: Effect of expander inlet pressure on the best point temperature

**Effect of condensation temperature**

The aim of investigating the ground-cooled condenser presented in Chapter 3 was to decrease the condensation temperature to increase the difference between the low and high cycle's pressures. Consequently, this has helped improving the system's efficiency and net output power due to the increase in working fluid's expansion in the expander. To study the effect of using ground-cooled condenser (decreasing the condensation temperature), the values considered in the previous section are kept the same whilst only changing the condensation temperature from 25°C to 15°C. The results are presented in Figure 5.13 in which R123 generates the highest net output power with highest values of 5.367 kW at 3 MPa and 5.615 kW at 6 MPa. In comparison with the results presented in Figure 5.12, the corresponding enhancements are 7.35% and 6.36%. This shows that the importance of using ground-cooled condenser is more noticeable at low grade sources of energy.

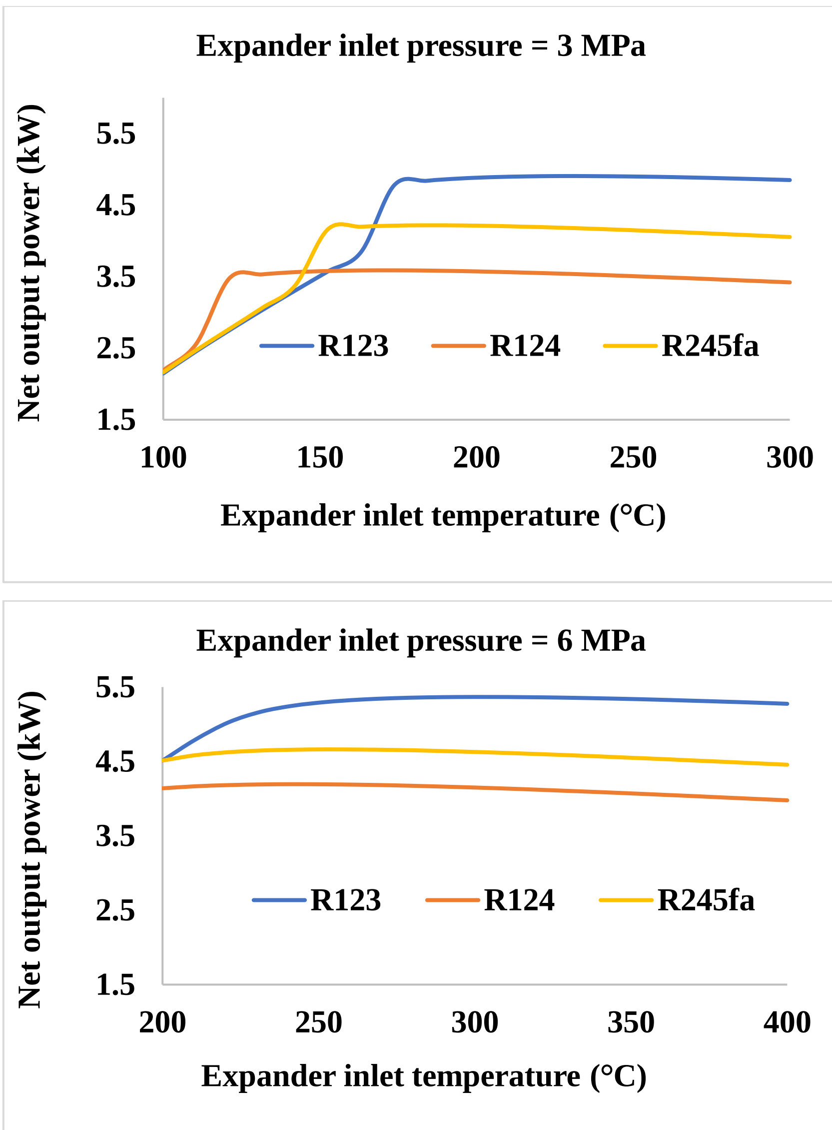


(a)

(b)

Figure 5.13: The effect of using ground-cooled condenser on the performance of working fluids

Table 5.3 shows the performance enhancements of all working fluids in terms of net output power. The highest enhancements are recorded by the refrigerant that has the lowest critical temperature which R124. However, the refrigerants with high critical temperatures that are R123 and R245fa still generate higher amounts of power at the investigated conditions. The highest enhancement recorded by R124 is also obtained at the low pressure (3 MPa) with a value of 12.13% representing the increase in net output power from 3.2 kW to 3.588 kW.

Table 5.3: The enhancement of net output power when using ground-cooled condenser

| **Working fluid** | **Net output power enhancement (%)** | |
|---|---|---|
| | Expander inlet pressure: 3 MPa | Expander inlet pressure: 6 MPa |
| R123 | 7.35 | 6.36 |
| R124 | 12.13 | 9.28 |
| R245fa | 8.77 | 7.37 |

## 5.5 Regenerative Cycle

Adding a regenerator to the optimized system presented in Figure 5.6 would be an attractive method to enhance the thermodynamic performance of the cycle and specially when there is a huge difference between the temperatures of states (2) and (4). The regenerative cycle is depicted in Figure 5.14 which aims to take advantage of the energy remaining in the working fluid exiting the expander [164] (Appendix A.3.2). On the other hand, it is necessary to check out if there are any negative consequences associated with this integration such as the amount of heat rejected to the ground. In this section, the inlet and outlet heat source temperatures are maintained at 500°C and 120°C, respectively.

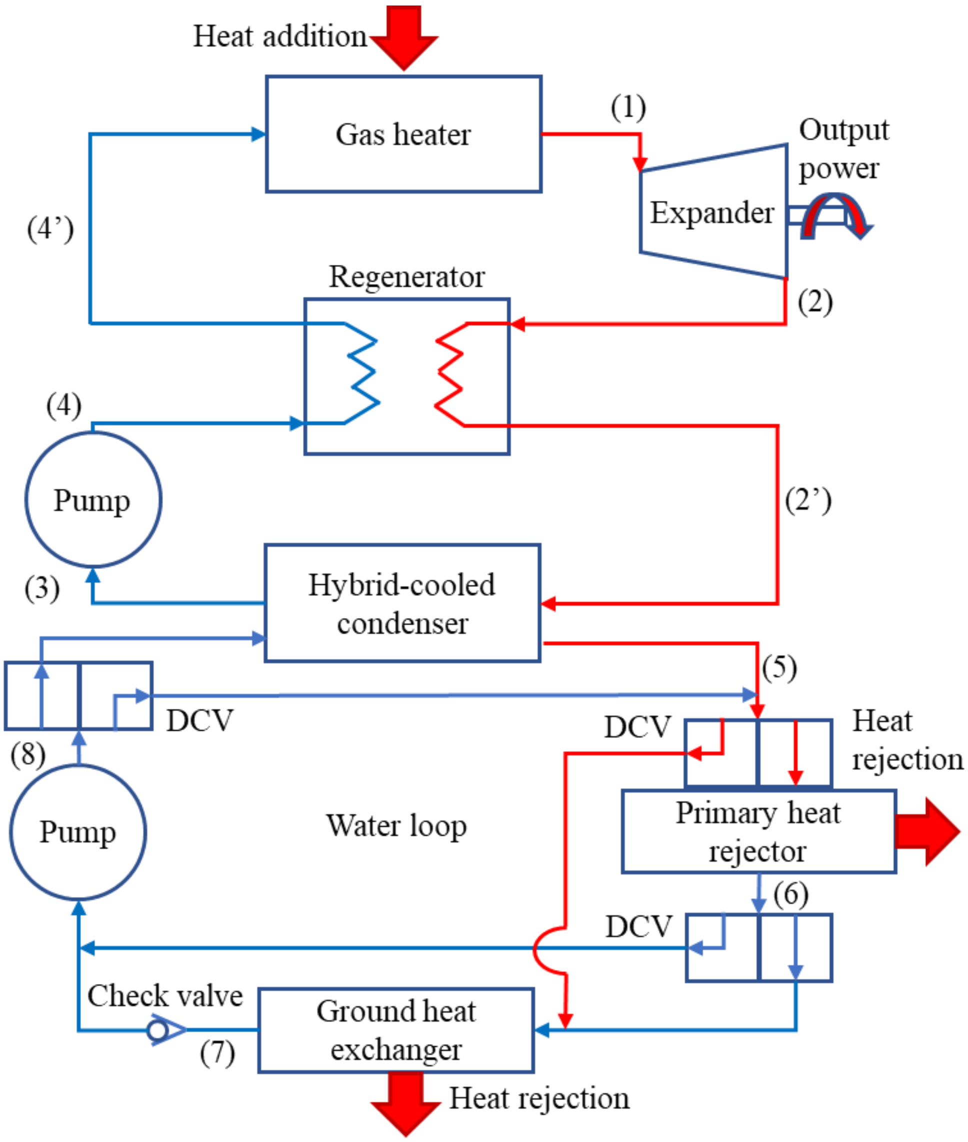


Figure 5.14: Schematic diagram of the regenerative cycle

### 5.5.1 Methodology

Figure 5.15 presents the temperature-entropy diagram of the regenerative cycle showing the states of the organic Rankine cycle. It is essential to compare the temperatures entering and exiting the regenerator in all cases to ensure that the regeneration is applicable. This means that $T_{4'}$ must be always greater than $T_4$ as well as $T_{2'}$ must be greater than $T_4$ and $T_3$. For this reason, in the upcoming sections, some points have been eliminated from the figures representing the results. This mainly depends on the thermodynamic properties of the investigated working fluids. The temperature difference between the working fluid entering the gas heater and that exiting the expander is assumed to be 30°C to avoid the installation of large heat exchanger (regenerator).

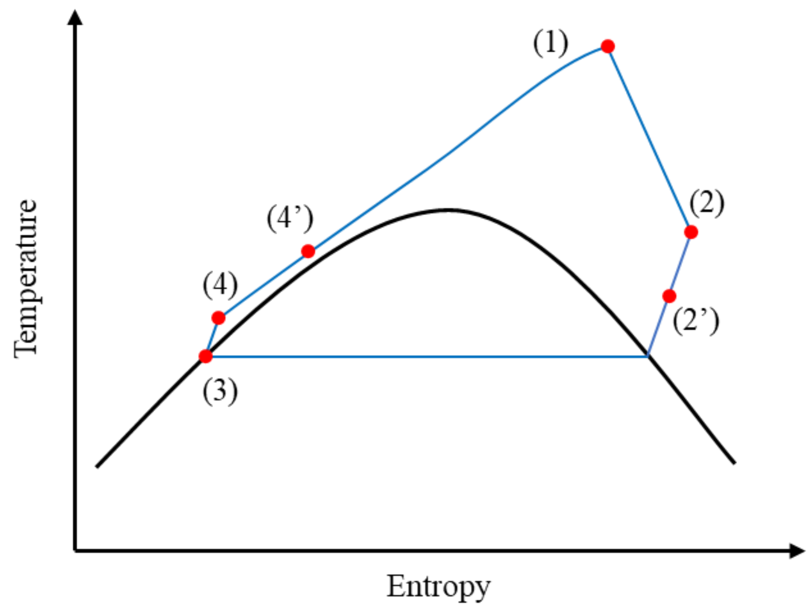


Figure 5.15: Temperature-entropy diagram of the regenerative transcritical organic Rankine cycle

Equation (5.4) presents a relation between the enthalpies of working fluid entering and exiting the regenerator. The effectiveness of regenerator ($\varepsilon_r$) is assumed to be 80%.

$$\varepsilon_r = \frac{h_2 - h_{2'}}{h_{4'} - h_4} \tag{5.4}$$

where $h_2$, $h_{2'}$, $h_4$ and $h_{4'}$ are the working fluid's enthalpies exiting the expander, entering the condenser, exiting the pump, and entering the gas heater, respectively. This equation aims to calculate the enthalpy at state (2') and hence to evaluate $T_{2'}$ considering a negligible pressure drop inside the regenerator.

### 5.5.2 Results and discussion

The upcoming subsections aim to compare the basic and regenerative ORC in terms of net output power, working fluid's mass flow rate and heat rejection. This will be carried out whilst varying the expander inlet temperature and pressure, condensation temperature, and heating source flow rate.

**Expander inlet temperature**

The temperature of working fluid entering the expander ($T_1$) has a significant effect on the net output power of the regenerative cycle as shown in Figure 5.16. The expander inlet pressure, condensation temperature and gas flow rate are maintained at 10 MPa, 25°C and 200 kg/hr, respectively. The net output power of the basic ORC is almost around 3.5 kW for all working fluids, however, that of the regenerative cycle has a sharp increase while increasing the expander inlet temperature from 200°C to 400°C. The effect of adding a regenerator is more considerable for R124 than R245fa and R123 at each specific temperature which can be noticed from the difference between the slopes. On the other hand, the unsuitability of regeneration occurs earlier for R124 and R245fa allowing R123 to reach the highest net output power of 8.6 kW at 380°C. The corresponding values for R124 and R245fa are 7.27 kW and 8.07 kW at 312°C and 344°C, respectively.

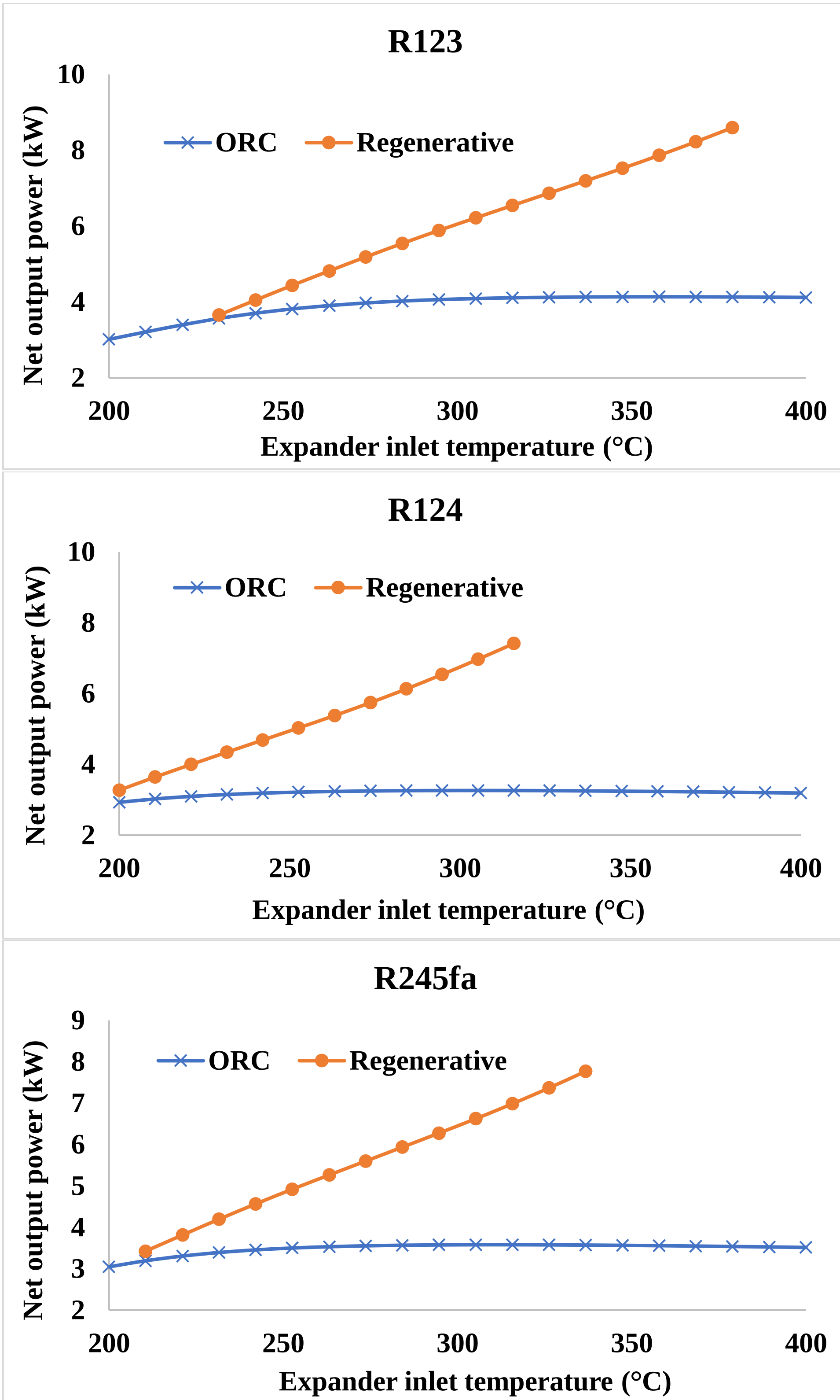


(a)

(b)

(c)

Figure 5.16: Effect of expander inlet temperature on the net output power of basic and regenerative organic Rankine cycles for (a) R123, (b) R124 and (c) R245fa

The highest net output power of the basic ORC and regenerative cycles for the three working fluids is recorded and tabulated (see Table 5.4). The corresponding expander inlet temperatures vary between ORC and regenerative cycle as well as between the working fluids. For the regenerative cycle, the highest power is always achieved at the maximum allowable temperature.

Table 5.4: The enhancement in net output power using a regenerative organic Rankine cycle

| **Working fluid** | **Net output power (kW)** | |
|---|---|---|
| | **Organic Rankine cycle** | **Regenerative cycle** |
| **R123** | 4.14 @ 358°C | 8.86 @ 386°C |
| **R124** | 3.26 @ 305°C | 7.27 @ 312°C |
| **R245fa** | 3.58 @ 310°C | 8.07 @ 344°C |

**Expander inlet pressure**

To investigate the impact of expander inlet pressure on the cycle's performance, the expander inlet temperature, condensation temperature and gas flow rate are kept constant at 300°C, 25°C and 200 kg/hr, respectively. It can be noticed from Figure 5.17 that as the expander inlet pressure increases the net output power of basic ORC increases while that of regenerative cycle decreases for all working fluids. The highest performances are recoded as 6.83 kW for R123, 7.2 kW for R124 and 7.26 kW for R245fa. Even though, R245fa corresponds to the highest net output power, but R123 is still the preferable working fluid. This is due to that R123 can operate at wide range of temperatures and pressures as shown in Figure 5.16a and Figure 5.17a. Another reason is that the results presented in Figure 5.16 is obtained at an expander inlet temperature of 300°C which is near to the best point temperature of R124 and R245fa (see Table 5.4). Thus, it would be possible to enhance the net output power of R123 by increasing the temperature ($T_1$). Additionally, R123 can operate at lower pressures than that of R124 and R245fa in case of regenerative cycle at the same expander inlet temperature. This makes R123 the favourable working fluid and specially because the net output power is still highly acceptable compared to R124 and R245fa when operating far from its optimal temperature at lower pressures. For R123, it can operate normally between 5 MPa and 10 MPa at an expander inlet temperature of 300°C. However, for R124 and R245fa, the regenerative cycle is unsuitable for pressures lower than 9.1 MPa and 6.8 MPa, respectively.

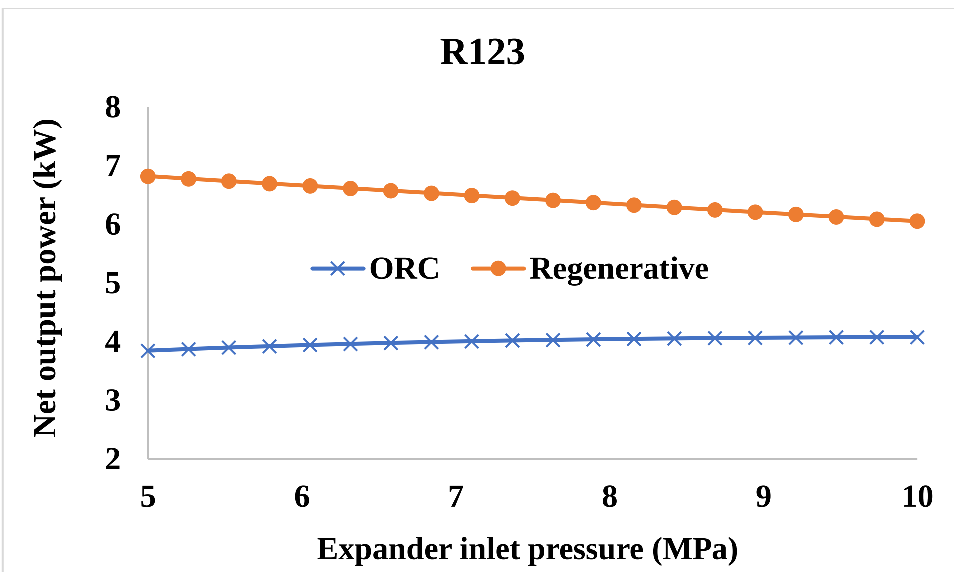


(a)

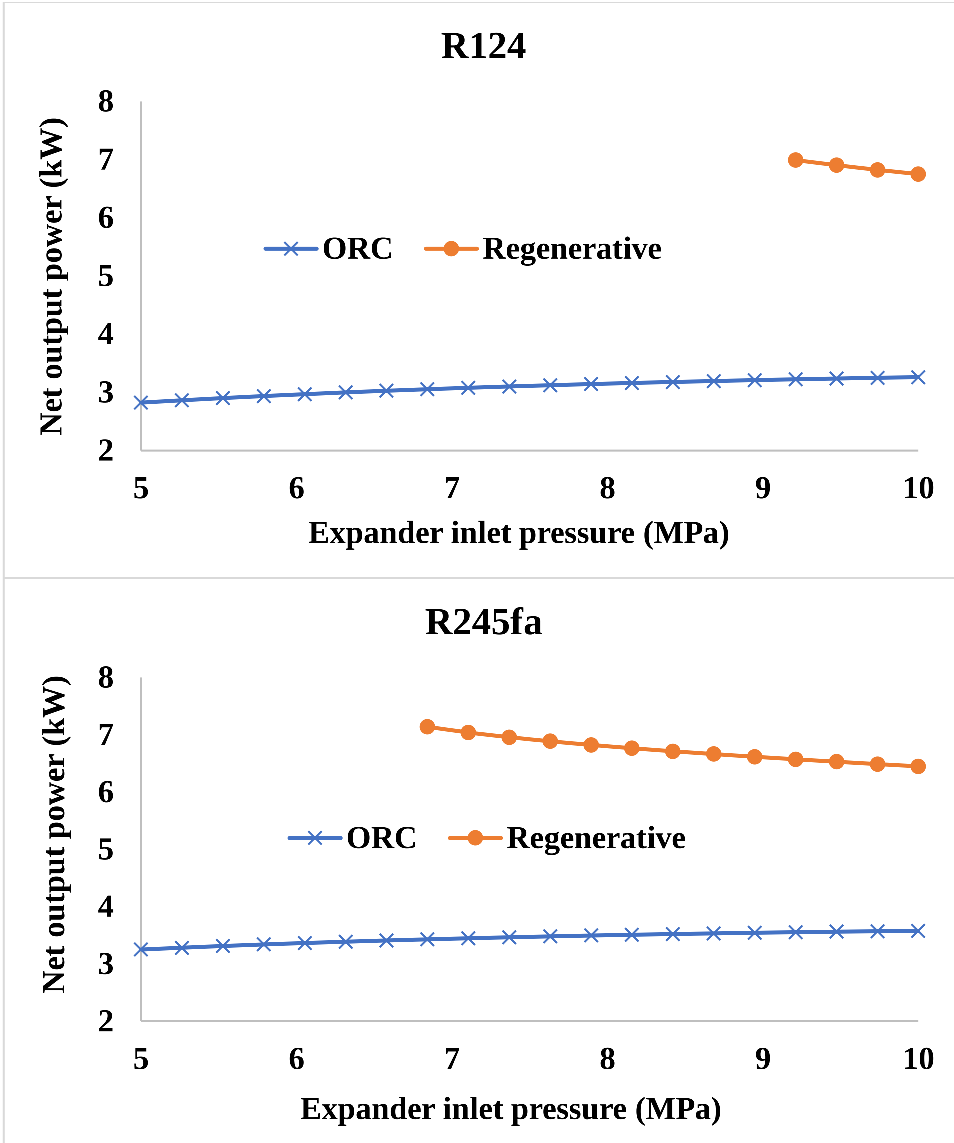


(b)

(c)

Figure 5.17: Effect of expander inlet pressure on the net output power of basic and regenerative organic Rankine cycles for (a) R123, (b) R124 and (c) R245fa

**Condensation temperature**

The variation of condensation temperature ($T_3$) affects the basic ORC and regenerative cycle almost in the same manner for all working fluids. Figure 5.18 shows that as the condensation temperature increases from 15°C to 25°C the net output power of the cycles decreases by an amount of ~0.3 kW. The decrease in condensation temperature corresponds to the use of ground cooling system since the ground is responsible for heat removal. Thus, if this system is activated, and considering a condensation temperature drop from 25°C to 15°C, the enhancement of net output power for regenerative R123, R124 and R245fa can be estimated as 5.4%, 4.8% and 5.4%, respectively. This shows that the ground cooling system is more effective for R123 and R245fa than that of R124 regenerative ORCs.

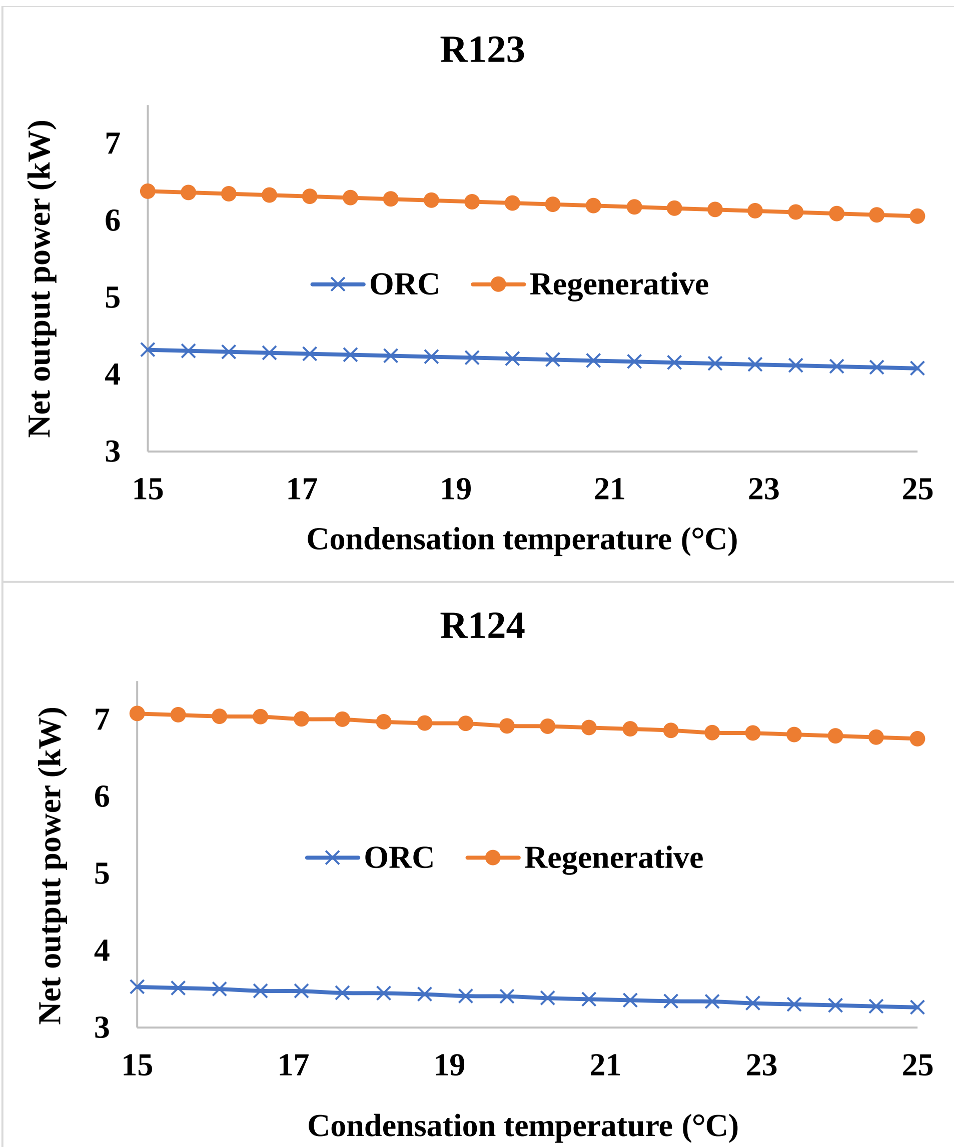


(a)

(b)

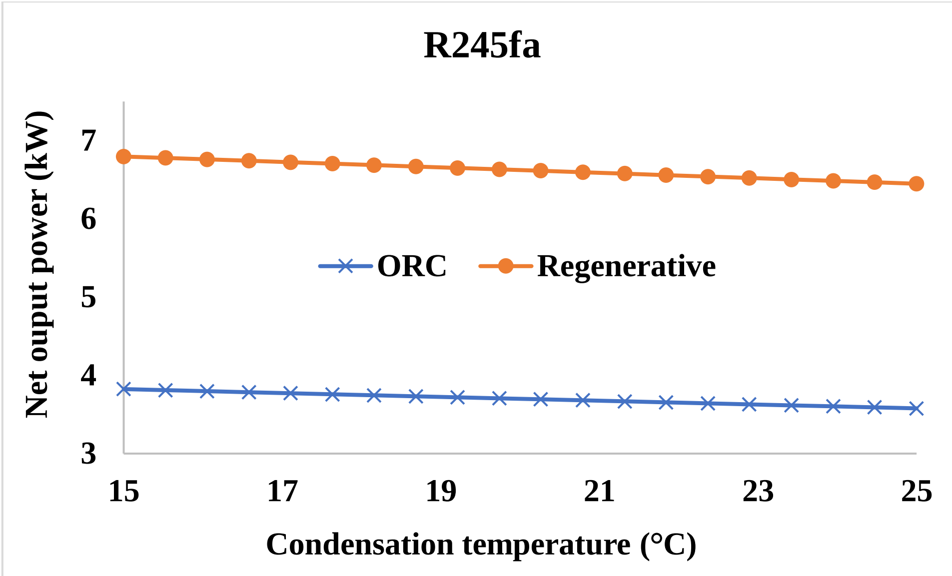


(c)

Figure 5.18: Effect of condensation temperature on the net output power of basic and regenerative organic Rankine cycles for (a) R123, (b) R124 and (c) R245fa

**Flow rate of heat source**

According to the energy balance inside the gas heater, the following equation can be used to represent the relation between heat source gas and ORC's working fluid in case of a regenerative cycle:

$$\dot{m}_g . c_{pg} \left( T_{gi} - T_{go} \right) = \dot{m}_f \left( h_1 - h_{4'} \right) \tag{5.5}$$

where $\dot{m}_g$, $c_{pg}$, $T_{gi}$, $T_{go}$, $\dot{m}_f$, $h_1$ and $h_{4'}$ are the gas flow rate, gas specific heat, gas inlet temperature, gas outlet temperature, working fluid's mass flow rate, enthalpy at state (1) and enthalpy at state (4'), respectively. It is obvious that the flow rates of heat source and working fluid are directly proportional. This relation can be observed in Figure 5.19 such that both flow rates vary similarly in ORC and regenerative cycle for all working fluids. However, the slope of curve corresponding to the regenerative cycle is greater than that of basic ORC showing that the regeneration approach is more attractive at high heat source flow rates. The mass flow rate of working fluid in the regenerative cycle is always higher than that of ORC revealing the results presented in Figure 5.16, Figure 5.17 and Figure 5.18. Therefore, the increase in net output power is mainly due to the increase in the working fluid's mass flow rate that is affected by the enthalpy change at the gas heater's inlet. Based on equation (5.5), if the enthalpy of the working fluid entering the gas heater increases, the mass flow rate will also increase. So, by comparing the basic ORC and regenerative cycle, the enthalpy has increased from state (4) to (4') resulting in an increase in the working fluid's mass flow rate.

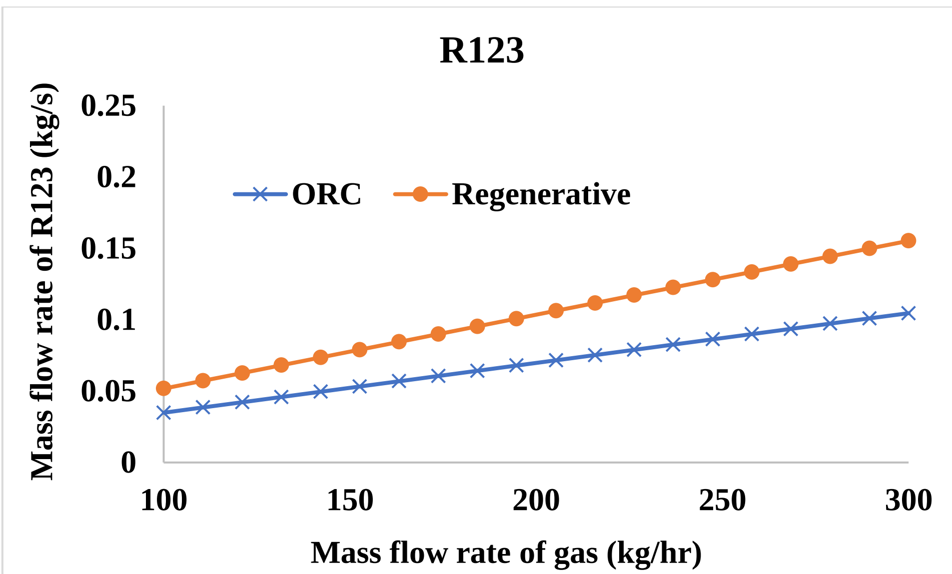


(a)

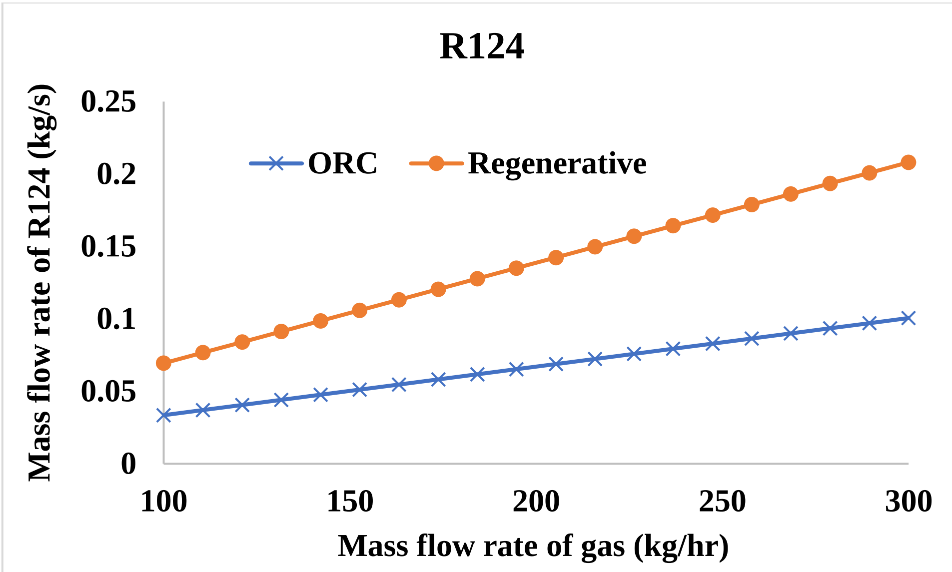


(b)

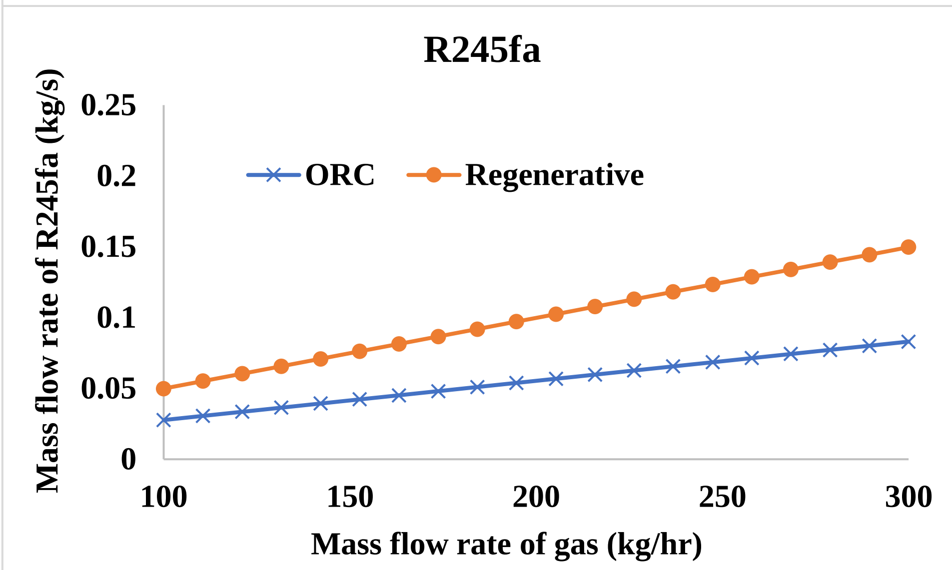


(c)

Figure 5.19: The relation between mass flow rate of heat source and working fluids in basic and regenerative organic Rankine cycles for (a) R123, (b) R124 and (c) R245fa

**Heat rejection**

From the previous sections, the increase in working fluid's mass flow rate has been considered as an advantage to enhance the overall cycle's thermodynamic performance. On the other hand, this may cause negative impact on the ground loop resulting in a larger ground heat exchanger which mainly depends on the amount of heat rejected from the cycle. Equation (5.6) is used to estimate the heat transferred from the regenerative ORC to the ground.

$$\dot{Q}_{rej} = \dot{m}_f(h_{2'} - h_3) \tag{5.6}$$

The amount of heat rejected from the cycle is presented in Figure 5.20 for the three investigated working fluids as a function of the expander inlet temperature. It can be noticed that the effect of adding a regenerator on the amount of heat rejected from the cycle is more considerable for R124 and R245fa than that for R123. This is clearly presented from the gap between the curves corresponding to ORC and regenerative cycle. The heat rejected in case of R124 and R245fa increases slightly from 20.98 to 21.94 kW and 20.66 to 21.18 kW, respectively while that of R123 decreases from 20.16 to 19.72 kW. This makes R123 also more attractive and especially because the highest net output power is achieved at high expander inlet temperatures (see Figure 5.16) while the heat rejected is less than that of other fluids by approximately 2 kW.

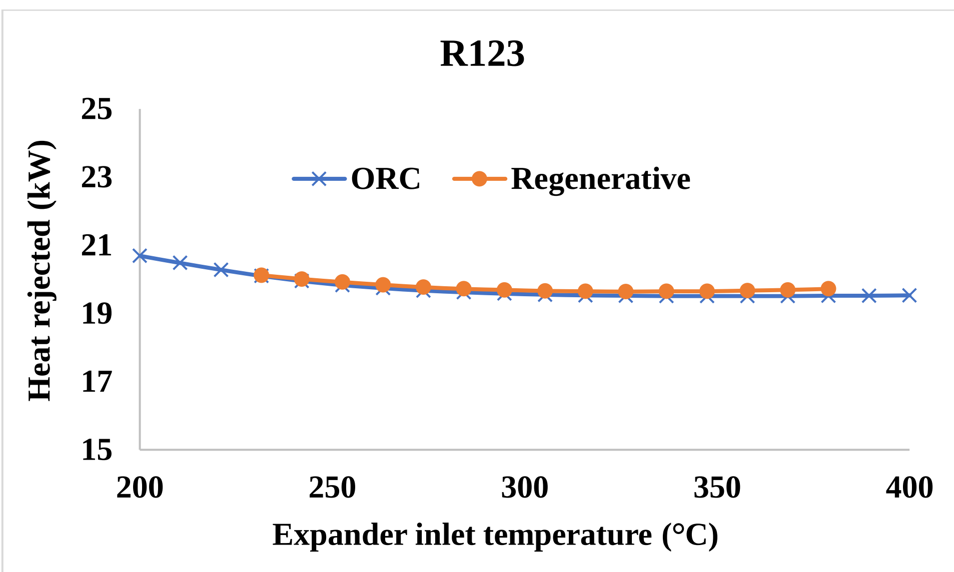


(a)

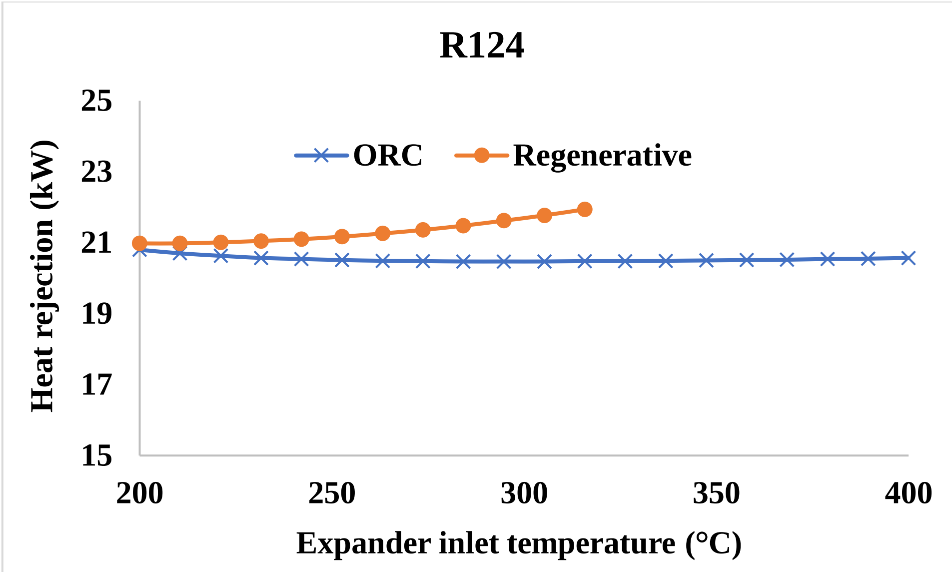


(b)

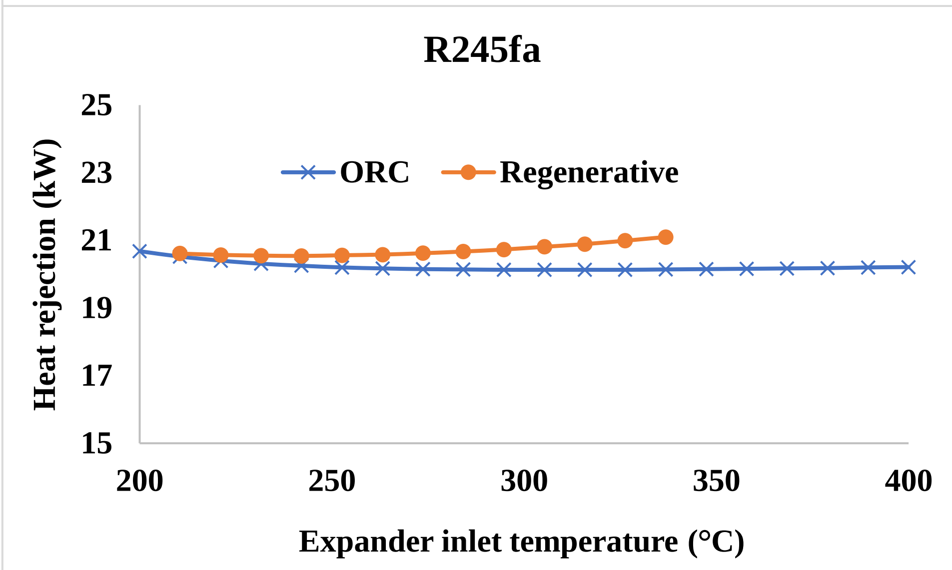


(c)

Figure 5.20: The influence of regenerator on the heat rejected to the ground for (a) R123, (b) R124 and (c) R245fa

### 5.6 Conclusion

After performing the parametric and comparative studies, it is seen that R123 is the best suitable working fluid under the investigated conditions. This has been recorded for the basic ORC and regenerative cycle. R123 is not only preferable due to the corresponding thermodynamic performance, but it also resulted in the lowest amount of heat rejected to the ground as well as it can operate at wide range of pressures and temperatures. The latter reason makes the cycle more flexible while using R123 as a working fluid allowing it to operate normally at different heat source conditions. Thus, R123 will be considered as working fluid in Chapter 7 to investigate a real application to check the feasibility of the system in terms of performance and cost.

# Chapter 6. Simulation of Ground Thermal Distribution

This chapter aims to investigate the soil thermal interference radius in the ground heat exchanger (GHE) to ensure that there will be no heat accumulation during the operation. The study is simulated using ANSYS and EES software to examine the thermal distribution in the soil for the period of 8 hours which is the maximum operating duration per day (see Appendix C). The ground temperature measured in Chapter 4 is considered as an input to the system simulated on ANSYS. This investigation compares the thermal distribution in two cases: with and without phase change materials (PCM) [165]. The latter is used to provide stability during operation and maintain the boundaries of the GHE pipes at low temperatures to enhance the heat transfer [166]. However, the incorporation of PCM must only be considered if there is a significant change in the ground thermal distribution during the operating hours. This is essential to avoid high capital cost of installation when there is no remarkable enhancement in the GHE performance. After performing these simulations and estimating the soil thermal interference radius, the size of ground loop will be evaluated (section 6.4).

## 6.1 Design Conditions

As presented in Chapter 4, there are three operating cases based on the ground and ambient temperatures. In this study, the first case is chosen to ascertain the design conditions since the ground cooling system is operating 8 hours/day. This corresponds to the maximum amount of heat injected to the ground in a day compared to the other two cases. The highest temperature reported at 2 m depth was 19°C which can be considered as the initial temperature of the soil in the current simulations. Taking a minimum temperature difference between the cooling source and working fluid of 8°C, the condensation temperature can be assumed as 27°C. Thus, the water circulating through the ground heat exchanger must have a temperature varying between 19°C and 27°C. According to the theory of modelling presented in section 3.2, the convection heat transfer coefficient depends significantly on the mass flow rate of the circulating fluid (see equations 3.11 and 3.12). The following equation can be used to evaluate the mass flow rate of water:

$$\dot{Q}_{rej} = \dot{m}_w c_{pw} \Delta T_w \tag{6.1}$$

where $\dot{m}_w$ is the mass flow rate of water, $c_{pw}$ is the specific heat and $\Delta T_w$ is the temperature difference of water which is assumed to be 4°C. Table 6.1 summarizes the design conditions needed for the numerical simulations.

Table 6.1: The design conditions for ANSYS simulations

| **Parameters** | **Values** | **Units** |
|---|---|---|
| Initial ground temperature | 19 | °C |
| Water inlet temperature | 25 | °C |
| Water outlet temperature | 21 | °C |
| Water mass flow rate | 0.85 | kg/s |
| Specific heat of water | 4.18 | kJ/kg.K |

## 6.2 Material Properties

The properties of soil, pipe and phase change material are presented in Table 6.2. The values related to the soil are taken as average values since there are different types of soil.

The inner and outer radii represent the thickness of each material such that the pipe and PCM have a thickness of 2.3 mm. However, the soil has two values for its inner radius considering the two investigated cases, with and without PCM. Rubitherm (RT 21HC) is used as the latent storage material since its melting/solidification temperature is between the highest and lowest temperatures of the fluid circulating through the pipes. It has a latent heat of 190 kJ/kg and densities of 770 and 880 kg/m$^3$ for the liquid and solid phases. The specific heat of both phases is approximated as 2 kJ/m.°C, however, during the change of phase it varies significantly. This rise in its specific heat represents the latent heat of fusion in ANSYS software. RT 21HC has also an advantage in the sensible storage since its specific heat in both phases is higher than that of soil and high-density polyethylene. The corresponding values of the latter materials are 0.8 and 1.865 kJ/m.°C.

Table 6.2: The properties of the materials considered for the current simulations

| **Materials** | **Soil** | **High-density polyethylene pipe** | **Phase change material (RT 21HC)** |
|---|---|---|---|
| **Thermal conductivity (W/m.K)** | 2 | 0.5 | 0.2 |
| **Density (kg/m$^3$)** | 1500 | 953 | 770-880 |
| **Specific heat (kJ/m.°C)** | 0.8 | 1.865 | 2 |
| **Latent heat (kJ/kg)** | - | - | 190 |
| **Inner radius (mm)** | 34.3-36.6 | 32 | 34.3 |
| **Outer radius (mm)** | 600 | 34.3 | 36.6 |

## 6.3 ANSYS Simulation

The simulations were carried out using ANSYS software to investigate the thermal distribution. This software has been selected since it is simple, robust, available, and cheap. The study covers a circular area with a radius of 0.6 m since it is expected that the thermal interference will not exceed this radius as well as the results will be more precise and reliable. The areas created in ANSYS have different colours such that each area represents a specific material, where three areas are created in case of using phase change materials, soil, pipe, and RT 21HC. However, only two areas are created in the other case when the phase change material is not added. The inner and outer radius of each area are taken as presented in Table 6.2.

### 6.3.1 Meshing

The materials used in this study were created using the Solid (Quad 4node 55) as the thermal element type. These were all modelled as areas in which they were glued allowing the user to use different types of material properties. The created meshes are almost the same in both cases (with and without PCM) due to the large relative radius of area under study compared to that of PCM and HDPE (see Figure 6.1). The size of elements was kept as default since it is found to be suitable for the accuracy of thermal distribution (small elements near the centre). The size of elements created at the peripheries is not a constraint because the soil thermal interference radius will not spread to reach these elements.

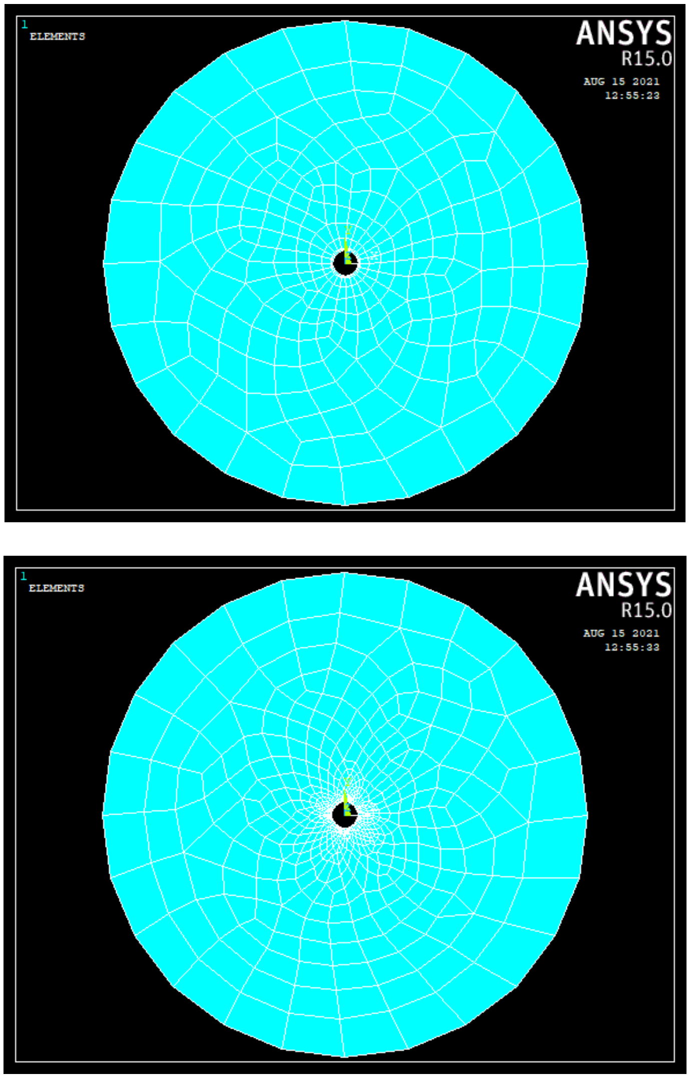


(a)

(b)

Figure 6.1: The meshing of areas in ANSYS (a) with and (b) without phase change materials

### 6.3.2 Sensitivity analysis

As mentioned previously (section 6.3.1), the size of element edge was set by the software automatically (default size). On the other hand, similar results could be obtained if the size is added manually by the user. Thus, a sensitivity analysis based on the size of meshing was done to determine the maximum acceptable element edge length and avoid high computational durations (see Figure 6.2). The results shown correspond to the nodal thermal distribution after 8 hours of operation. It can be noticed that the results are not acceptable for the first two cases where the element edge sizes are 150 and 100 mm since the soil thermal interference radius is not steady. In the third case (75 mm), the soil thermal interference radius is almost clear and agree well with the simulation results of 50 mm and those of section 6.3.3. However, it does not provide detailed results regarding the thermal distribution in the HDPE pipe where the inner edge of the pipe is presented as a square. Thus, the size of the element edge must not exceed 50 mm where the results are steady and provide detailed and clear image for the thermal distribution and soil thermal interference radius.

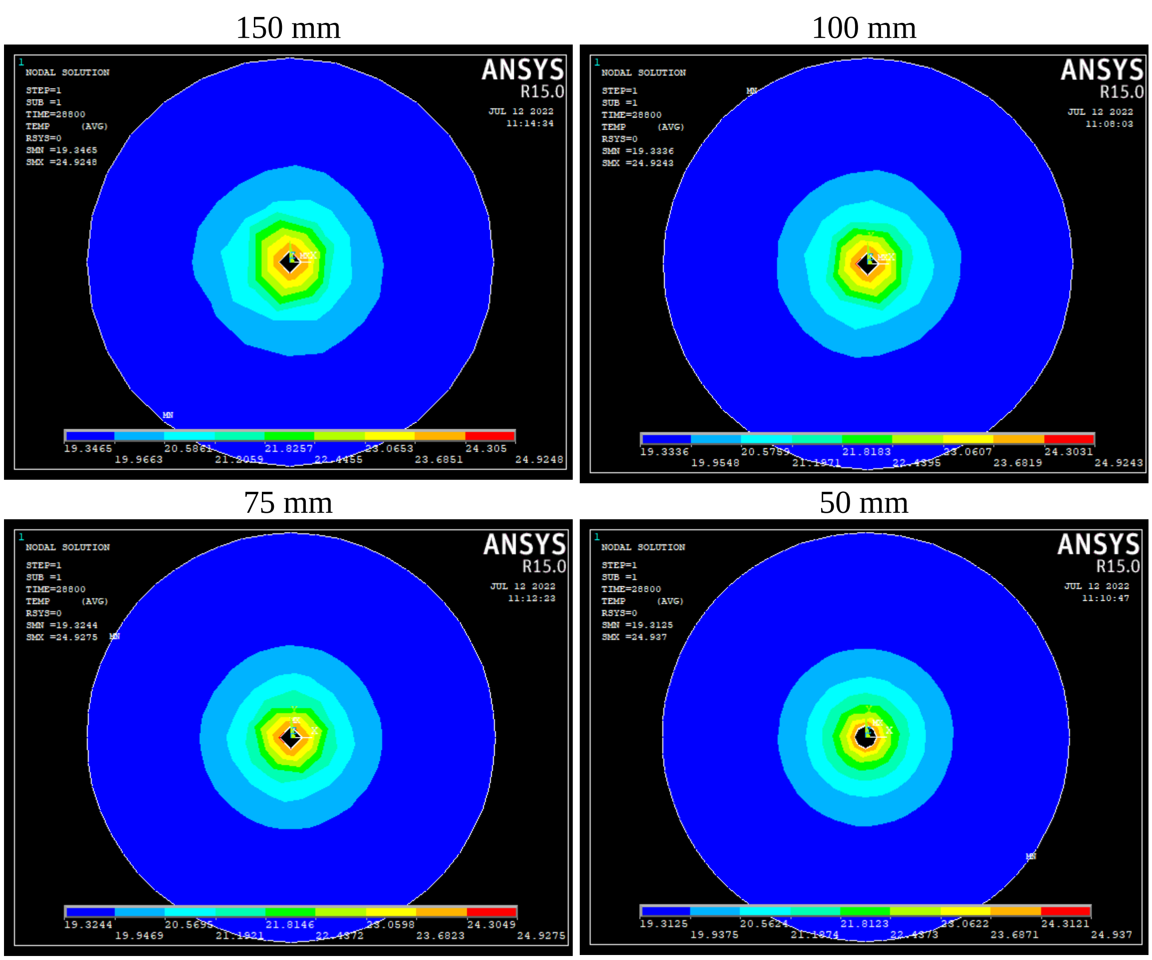


Figure 6.2: Sensitivity analysis based on the element edge size

### 6.3.3 Simulation results

The first run of simulations was carried out in the absence of latent storage material. Based on the nodal thermal distribution analysis, the temperature at the boundaries of the pipe immediately increased to reach approximately the same temperature of the circulating fluid (25°C) after one hour (see Figure 6.3). However, the soil thermal interference radius increases slowly with time reaching a value of ~0.32 m after 8 hours which is the maximum operating duration. This means that the distance between the horizontal pipes must be equal or greater than 0.64 m to avoid heat accumulation.

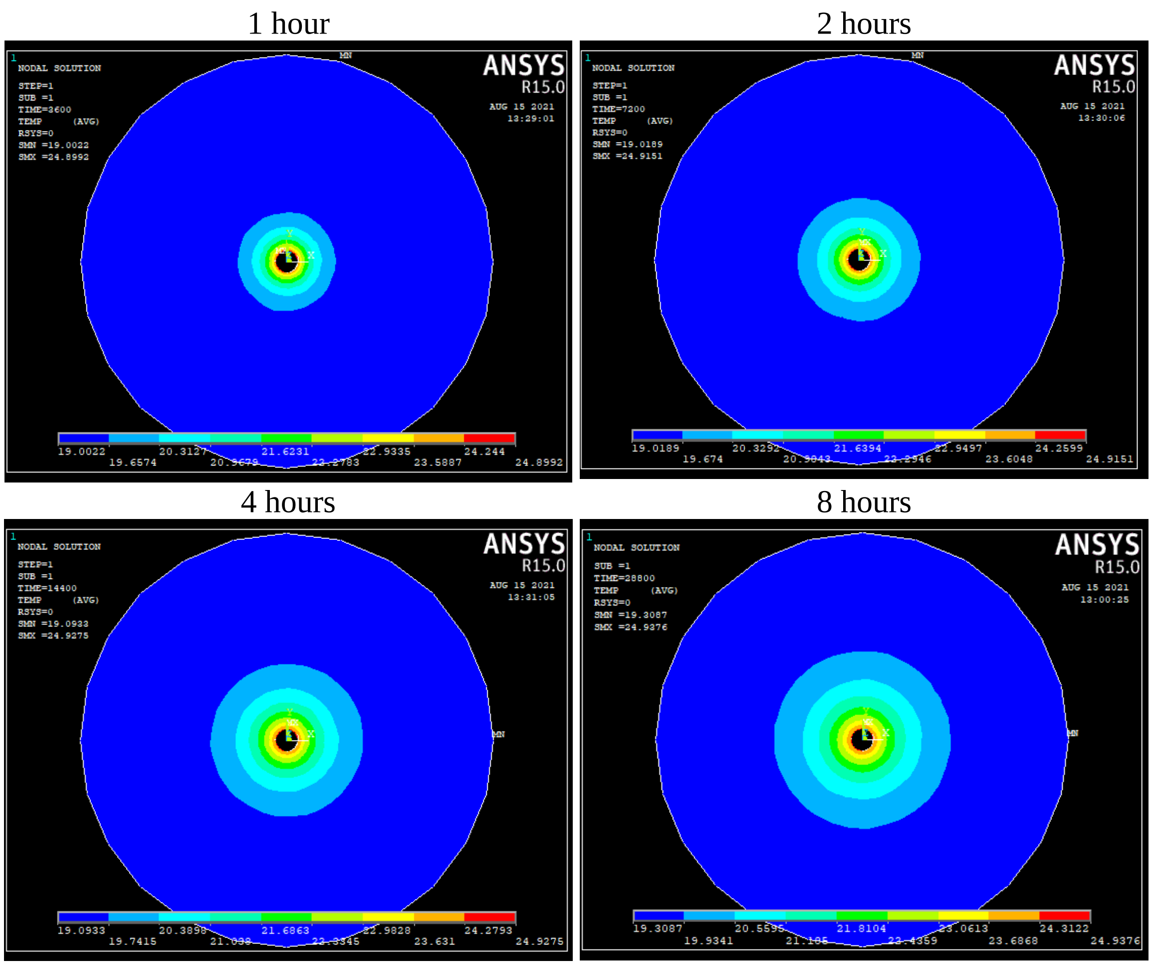


Figure 6.3: The nodal thermal distribution in soil without using phase change materials during 8 hours of operation

The second run of simulations was carried out considering the insertion of RT 21HC as a PCM around the HDPE pipe. Based on the contour plot of temperature distribution, it can be noticed that the soil thermal interference radius (~0.32 m) is insignificantly affected by the incorporation of PCM (see Figure 6.4). However, high temperatures were more bounded to the centre in this case. Additionally, the temperature near to the pipe is lower than that without PCM at all instants revealing the effect of PCM's melting during the charging process.

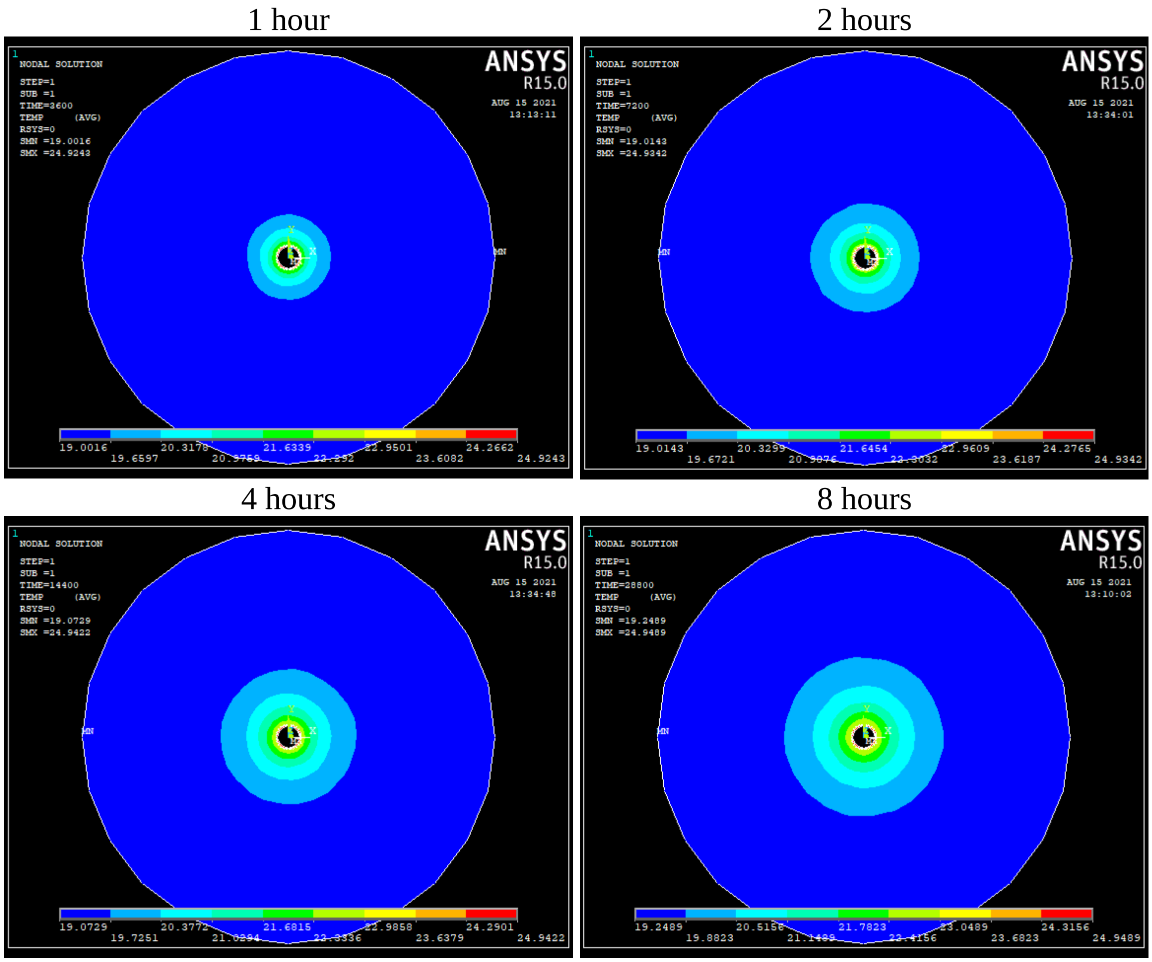


Figure 6.4: The nodal thermal distribution in soil using RT 21HC as a phase change material

## 6.4 Ground Loop Sizing using EES

Considering the same design conditions presented in Table 6.1, the size of the ground loop will be evaluated based on the same theory of modelling using EES shown in section 3.2 (Appendix A.4).

### 6.4.1 Methodology

The length of the ground heat exchanger will be calculated for the case where no PCM is used. This is mainly due to the insignificant effect of PCM on the soil thermal interference radius and the high capital cost of the PCM incorporation. Thus, three resistances are considered that correspond to the convection between the coolant and pipe, conduction of HDPE and conduction of soil. The temperature of the ground is taken as 19°C at 0.32 m far from the centre of pipe which is the estimated soil thermal interference radius (see section 6.3.3). The following equation can be used to calculate the size of the ground loop based on the value of heat rejected computed using equation (6.1):

$$\dot{Q}_{rej} = \frac{\Delta T_{lm}}{R_{eq}} \tag{6.2}$$

where $\dot{Q}_{rej}$ is the heat rejected from the coolant, $\Delta T_{lm}$ is the log mean temperature difference and $R_{eq}$ is the equivalent resistance of the three materials considered.

### 6.4.2 EES results

To estimate the length of the ground heat exchanger, the exhaust gas of a diesel generator is taken as the source of energy which will be presented completely in the next chapter. The flue gas has constant mass flow rate and temperature of 150 kg/hr and 500°C, respectively. The selected working fluid is R123 based on the analysis presented in Chapter

5 and the heat added to the cycle is evaluated as 17.72 kW when the expander inlet temperature is fixed at 300°C. At these values, the heat rejected from the cycle varies between 14.13 and 14.58 kW depending on the cooling source temperature with an average value of 14.45 kW. Based on equation (6.2), the length of ground heat exchanger can be calculated as 1423 m for the basic ORC and the regenerative cycle considering the same expander inlet temperature. However, if this temperature increases to 450°C, the length will also increase but insignificantly to 1480 m. This is the case of the regenerative cycle when running at its highest performance. The increase of size is mainly due to the rise in the amount of heat rejected from the cycle which will increase from 14.45 to 15.72 kW. Table 6.3 summarizes the results obtained from this chapter.

Table 6.3: Summary of the results obtained from ANSYS simulations and analytical calculations for ground loop sizing

| **Parameters** | **Values** |
|---|---|
| Maximum operating duration | 8 hours |
| Soil thermal interference radius | ~0.32 m |
| Heat rejected from the cycle | 14.45 – 15.72 kW |
| Ground loop length | 1480 m |

## 6.5 Conclusion

The soil thermal interference radius is one of the most crucial parameters in the ground heat exchanger. It depends mainly on the amount of heat rejected to the ground, mass flow rate, operating duration, fluid temperature, and initial ground temperature. In the proposed system, the heat rejected to the ground was evaluated as 14.45-15.72 kW. Under the investigated conditions, the soil thermal interference radius was found to be approximately 0.32 m considering a maximum operating duration of 8 hours/day.

# Chapter 7. Waste Heat Recovery: Application

This chapter aims to present a real application on the use of the proposed technology (hybrid cooling system). This will be based on the results and analyses of previous chapters that are ground temperature variation (Chapter 4), working fluid (Chapter 5), and ground loop size (Chapter 6). In Lebanon, electricity outage is a common problem that occurs daily. For this reason, the private sector managed to overcome this problem by providing electricity via diesel engine generators. The capacities of these generators are usually very small avoiding high capital costs. Here comes another problem which is the low efficiency of old generators that are mostly used. The proposed system presented in the previous chapters suits well such application which can be used as a waste heat recovery system to provide additional amount of power. This can be easily adopted in rural areas such as Bekaa where there are enough spaces for installing horizontal GHEs. In Bekaa, the maximum operating duration of diesel generators is 8 hours/day, but randomly distributed between 06:00 and 24:00. The upcoming sections will present the contribution of GCS to reducing fuel consumption and increasing the net output power.

## 7.1 Design Conditions

The diesel generator's exhaust gas conditions presented in this chapter are estimates and taken as average values due to the high fluctuations in the supply and demand. To avoid the effect of such significant variations, a diesel generator of 30 kW capacity is investigated with a diesel consumption of ~11 L/hr. This choice makes it easy to compare and compromise between the information provided by the manufacturer and the details reported by the generator's owner. The exhaust mass flow rate of gas can be estimated as 150 kg/hr assuming an air to fuel ratio of 15. The specifications and design conditions of diesel generator and ORC are presented in Table 7.1.

Table 7.1: The design conditions of organic Rankine cycle and exhaust gas of diesel generator

| **Parameters** | **Values** | **Units** |
|---|---|---|
| Gas mass flow rate | 150 | kg/hr |
| Gas inlet temperature | 500 | °C |
| Gas exit temperature | 100 | °C |
| Diesel generator capacity | 30 | kW |
| ORC working fluid | R123 | - |
| Expander inlet pressure | 5 | MPa |
| Expander isentropic efficiency | 70 | % |
| Pump isentropic efficiency | 90 | % |
| ORC generator efficiency | 90 | % |

### 7.2 Stress Analysis

One of the most important studies that need to be considered is the assessment of heat exchanger's mechanical design. As shown in Table 7.1, the highest pressure in the cycle is 5 MPa which is the pressure inside the gas heater. It is recommended to use copper pipes for the ORC since it has very high thermal conductivity. The maximum allowable tensile stress of copper is 90 MPa. Based on the American Society of Mechanical Engineers

(ASME), the minimum required thickness of the pipe can be calculated using the following equation [167]:

$$thickness = \frac{pr}{\sigma} \tag{7.1}$$

where $p$ is the internal pressure, $r$ is the inner radius, and $\sigma$ is the maximum allowable tensile stress. Based on the previous chapters, the inner radius varied between 0.005 and 0.01 m. Thus, according to equation (7.1), the minimum required thickness can be calculated as 0.278 and 0.556 mm, respectively. These correspond to outer diameters of 10.56 and 21.11 mm.

### 7.3 Optimal Operation

As mentioned in sections 5.4 and 5.5, each working fluid has an optimal expander inlet temperature at a given pressure. Thus, it is essential first to find this temperature before installation to achieve the highest possible performance. Figure 7.1 shows the variation of net output power for R123 while varying the expander inlet temperature. This result is obtained at an expander inlet pressure of 5 MPa and condensation temperature of 18°C. It can be noticed that the maximum net output power is approximately 3.8 kW which was achieved at an expander inlet temperature of ~300°C. For this reason, the expander inlet conditions will be fixed in the upcoming sections. However, the other cycle’s conditions will vary based on the cooling source temperature which is assumed to be fluctuating daily.

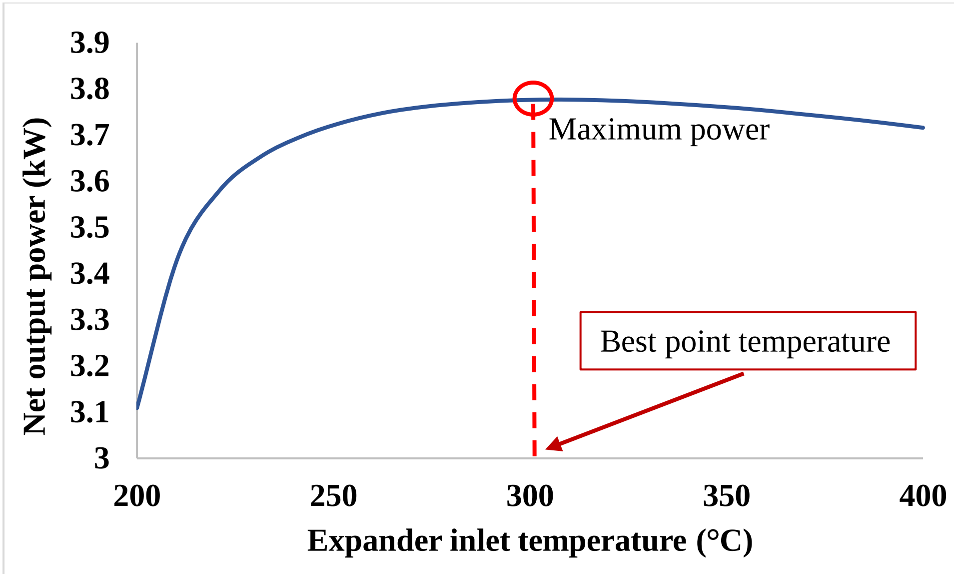


Figure 7.1: The variation of net output power as function of expander inlet temperature for R123 at 5 MPa

On the other hand, if the regenerative cycle is to be adopted, the best point temperature will change since the net output power of the cycle will be directly proportional to the expander inlet temperature (see Figure 5.16). However, to make a good comparison between the basic and regenerative ORC, two cases will be considered for the regenerative cycle. The first case will be based on the same conditions of the basic ORC with an expander inlet temperature of 300°C. Then, to increase the net output power, the expander inlet temperature will be increased to 450°C in the second case keeping an acceptable temperature difference with the diesel engine generator's flue gas that is 500°C (see Table 7.1).

### 7.4 Thermodynamic Performance

The equation used (3.1) for the calculation of net output power in Chapter 3 and Chapter 5 has been adjusted in this section to include the effect of ground heat exchanger's length and water pump (Appendix A.5). Equation (7.2) shows the adjusted form for the calculation of net output power.

$$\dot{W}_{net} = \dot{W}_t . \eta_g - \dot{W}_{po} - \dot{W}_{pw} \quad (7.2)$$

where $\dot{W}_{net}$ is the net output power, $\dot{W}_{po}$ is the power consumed by the ORC pump, and $\dot{W}_{pw}$ is the power consumed by the water pump. The latter depends mainly on the length of the ground heat exchanger and mass flow rate of circulating water. The following equation can be used to evaluate the amount of power consumed by the water pump:

$$\dot{W}_{pw} = \Delta P . Q \quad (7.3)$$

where $\Delta P$ is the pressure drop (see section 5.1.1) and $Q$ is the volumetric flow rate of water. According to calculations and simulations carried out in the previous chapters, the mass flow rate of water can be approximated as 0.85 kg/s and the length of the ground heat exchanger can vary between 1423 and 1480 m. Thus, the amount of power consumed by the water pump could be estimated as 0.55 kW for the basic and regenerative ORC at an expander inlet temperature of 300°C. However, if this temperature increases to 450°C, the pumping power will also increase to 0.65 kW.

### 7.4.1 Basic organic Rankine cycle

The daily average effective cooling source temperature varies based on the ambient air and ground temperatures as shown in Chapter 4. Assuming a constant temperature difference (8°C) between the cooling source and condensation temperatures, both should vary similarly. According to this variation, the daily ORC net output power has been calculated and presented in Figure 7.2.

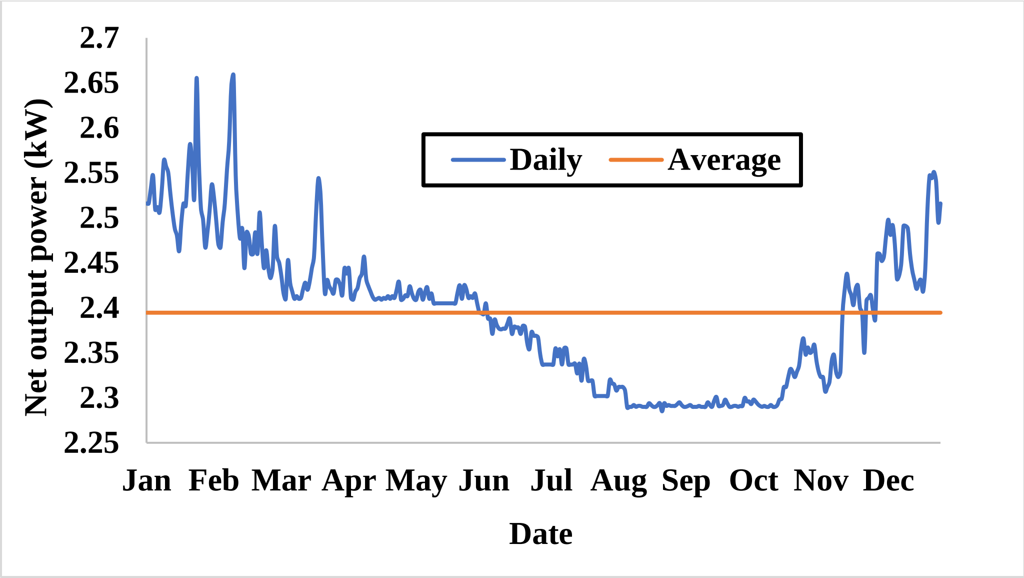


Figure 7.2: The annual energy generated by the organic Rankine cycle

The average power generated by the ORC is 2.395 kW which corresponds to an enhancement of 7.98%. This means that the owner can increase the supply capacity from 30 kW to 32.395 kW. The second method that could be used is to fix the generator's capacity at 30 kW and reduce the diesel consumption. However, the first method would be better considering the difference between levelized cost of electricity and fuel consumption cost per unit of energy. The overall system's efficiency varies between 12.89% and 15% with an average value of 13.52% (see Table 7.2). The total energy generated per year from the ORC is approximated as 7,011 kWh.

Table 7.2: The performance of organic Rankine cycle; power and efficiency

| Performance | Minimum | Maximum | Average |
|---|---|---|---|
| Net output power (kW) | 2.285 | 2.658 | 2.395 |
| Efficiency (%) | 12.89 | 15 | 13.52 |

### 7.4.2 Regenerative ORC

Based on the same model used in the previous section, the net output power for the regenerative cycle can be evaluated at two different expander inlet temperatures (see Figure 7.3). A considerable extra amount of power can be generated at 450°C compared to that of 300°C with an average difference of 5 kW. However, this may be accompanied by a significant increase in the capital cost which will be discussed in the next section.

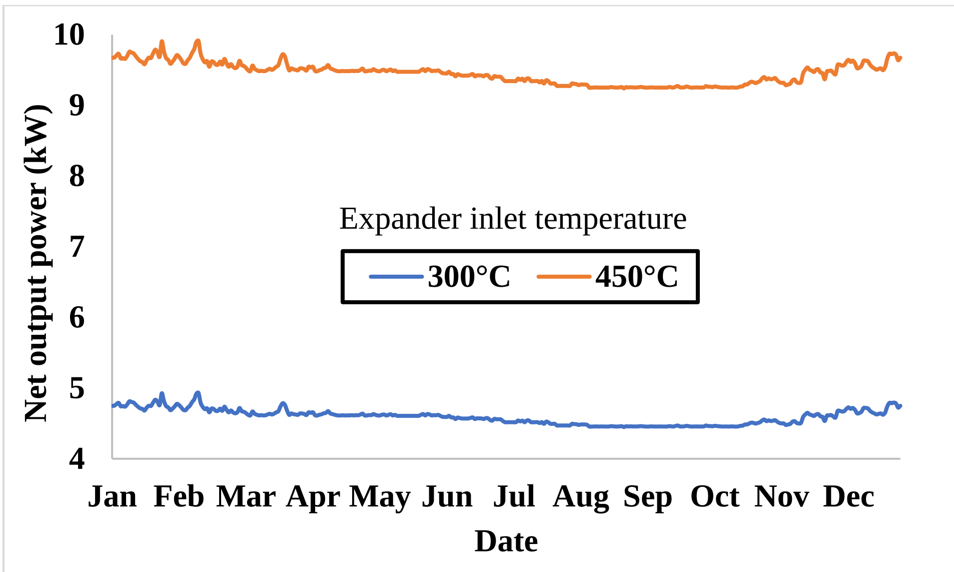


Figure 7.3: The annual energy generated by the regenerative organic Rankine cycle

The average power of both regenerative cycles is significantly higher than that of the basic ORC with an enhancement of 15.31% and 31.5% compared to the original power supplied by the diesel engine generator (30 kW). These values correspond to the regenerative cycles running at expander inlet temperatures of 300°C and 450°C, respectively. Table 7.3 summarizes the regenerative cycles' performances with respect to their net output power and power enhancement compared to the basic power generated by the diesel generator (30 kW). If the system operates 8 hours/day, the annual energy generated by the regenerative ORC could be estimated as 13,447 and 27,670 kWh at expander inlet temperatures of 300°C and 450°C, respectively.

Table 7.3: The performance of the regenerative organic Rankine cycle at two expander inlet temperatures; 300°C and 450°C

| **Performance** | **Minimum** | **Maximum** | **Average** |
|---|---|---|---|
| Regenerative ORC at 300°C | | | |
| Net output power (kW) | 4.449 | 4.932 | 4.592 |
| Power enhancement (%) | 14.83 | 16.44 | 15.31 |
| Regenerative ORC at 450°C | | | |
| Net output power (kW) | 9.239 | 9.912 | 9.45 |
| Power enhancement (%) | 30.8 | 33.04 | 31.5 |

### 7.5 Cost Analysis

The levelized cost of electricity supplied by the private sector (£0.35/kWh) is approximately twice that of the government. This makes the use of waste heat recovery system highly attractive since it is expected to have an acceptable payback period. The operating cost of diesel generator is calculated as £0.188/kWh since the cost of diesel in Lebanon is £0.5/L and the fuel consumption per unit of energy is 0.37 L/kWh. Concerning the capital cost, it can be divided into three main parts that are the ORC, groundwork and GHE pipes. The groundwork has been presented as a range based on the shallow geothermal conditions, however the cost of ground loop depends on the diameter, thickness and material used. High density polyethylene is selected in this case with a 32 mm diameter for several reasons: corrosion resistance, durability, resistance to pressure, easy mounting, and low friction. Table 7.4 presents all details required for estimating the capital and operating costs.

Table 7.4: The average cost of system's components and operation

| Component/operation | Cost |
| --- | --- |
| **Organic Rankine cycle (£/kW)** [168] | 2,250-3,000 |
| **Diesel consumption (L/kWh)** | 0.37 |
| **Levelized cost of electricity (£/kWh)** | 0.35 |
| **Diesel cost (£/L)** | 0.50 |
| **Operating cost (£/kWh)** | 0.188 |
| **High density polyethylene - 32 mm inner diameter (£/m)** | 1.25 |
| **Groundwork (£/m)** | 2.07-5.18 |

According to the same levelized cost of electricity (£0.35/kWh), the entire plant becomes more profitable when the operating cost decreases from £0.188/kWh to £0.173/kWh while using the proposed system. This is due to the extra amount of power produced for the same diesel consumption per hour. However, the diesel consumption per unit of energy is also reduced from 0.37 to 0.34 L/kWh. The detailed cost assessment of the proposed system is presented in Table 7.5 in which the capital and operating costs are £11,945-18,770 and £0.173/kWh, respectively. As mentioned previously, the proposed system is expected to work 8 hours/day at a rated average power of 2.395 kW. This means that the total gain can be estimated as £2,419/year considering the levelized cost of electricity as £0.35/kWh. Thus, the payback period of the system is expected to be between 4.9 and 7.8 years depending on three main factors that are the operating hours, diesel generator load operation and shallow geothermal conditions.

Table 7.5: Final estimates for the basic organic Rankine cycle's capital and operating cost

| **Parameter** | **Value** |
|---|---|
| **Organic Rankine cycle (£)** | 7,218-9,624 |
| **High density polyethylene (£)** | 1,782 |
| **Groundwork (£)** | 2,945-7,364 |
| **Total capital cost (£)** | 11,945-18,770 |
| **Operating cost (£/kWh)** | 0.173 |
| **Diesel consumption (L/kWh)** | 0.34 |
| **Net profit (£/year)** | 2,419 |
| **Payback period (years)** | 4.9-7.8 |

Considering the adoption of the regenerative cycle running at an expander inlet temperature of 300°C, it can be noticed that the capital cost of the system is approximately 1.4 times greater than that of the basic ORC (see Table 7.6). However, if the design temperature is 450°C, the capital cost will be 2.3 and 1.6 times greater than that of basic and regenerative cycle at 300°C, respectively. On the other hand, the payback period decreases significantly in case of regenerative cycles in which it has an average value of 4.6 years at 300°C and 3.7 years at 450°C. This makes the regenerative cycle more attractive than the basic ORC since the latter has a minimum expected payback period of 4.9 years. This is due to the drop in operating costs that have corresponding values of £0.165/kWh and £0.143/kWh. Therefore, the most preferable system is the regenerative cycle that is running at an expander inlet temperature of 450°C having an annual net profit of £9,546. The second attractive choice would be the regenerative cycle with a design temperature of 300°C. This choice could also be considered as the best option if there is a budget constraint.

Table 7.6: Final estimates for the regenerative organic Rankine cycles' capital and operating cost

| **Parameter** | **Expander inlet temperature** | |
|---|---|---|
| | 300°C | 450°C |
| **Organic Rankine cycle (£)** | 12,335-16,446 | 23,765-31,686 |
| **High density polyethylene (£)** | 1,782 | 1,854 |
| **Groundwork (£)** | 2,945-7,364 | 3,064-7,659 |
| **Total capital cost (£)** | 17,062-25,592 | 28,682-41,199 |
| **Operating cost (£/kWh)** | 0.168 | 0.143 |
| **Diesel consumption (L/kWh)** | 0.32 | 0.28 |
| **Net profit (£/year)** | 4,640 | 9,546 |
| **Payback period (years)** | 3.7-5.5 | 3-4.3 |

## 7.6 Conclusion

In this chapter, the proposed system was applied as a waste heat recovery system on the exhaust of a diesel generator with a capacity of 30 kW. Based on the design conditions, it was found that the best operating temperature of the basic ORC is 300°C. This cycle was able to enhance the output power by 7.98%. However, this value can increase up to 15.31% when it is replaced by the regenerative ORC. Furthermore, the enhancement could reach a value of 31.5% if the turbine inlet temperature in the regenerative ORC increases to 450°C. This system has a capital cost and payback period ranges of £23,765-31,686 and 3-4.3 years.

# Chapter 8. Conclusions and Future Work

In this work, a new system was proposed combining organic Rankine cycle, ground-cooled condenser, and primary heat rejector. Experimental, analytical, and numerical studies were carried out to assess the thermodynamic performance and economic feasibility of the proposed system. The system was used as an enhancement for the ORC based on a waste heat recovery application. However, the presented parametric studies covered a wide range of heat source conditions in order to provide a guide for researchers working on waste heat recovery systems for low, medium, and high grades. The upcoming sections present the main outcomes of this research.

## 8.1 Ground-Cooled Condenser

- The investigation of using the ground as a heat sink for enhancing the efficiency of an organic Rankine cycle was successfully achieved. The use of a ground-cooled condenser helps decreasing the condensation temperature and hence increasing the expansion in the expander.
- Parametric studies were carried out on the $CO_2$-based transcritical Rankine cycle involving the variation of mass flow rates, temperatures and pressures of all states, and heat exchangers dimensions. The grade of energy source, expander inlet conditions (temperature and pressure), condensation temperature and pipe diameter were found to be the most effective parameters. It was found that the net output power of the cycle can be increased by 1 kW if the underground water temperature is lower than that of the ambient air by 10˚C.
- It necessary to replace the turbo expander with a scroll expander since the current study focuses on small scale power cycles which can be noticed from the resulting low net output power. This is crucial to avoid inefficient expansions in small turbines that operate at very high rotational speeds.

## 8.2 Experimental Study on Shallow Geothermal Energy in Bekaa-Lebanon

- Six thermocouples were inserted at depths of 0.3, 0.6, 1, 1.3, 1.6 and 2 m to measure the ground temperatures in Bekaa-Lebanon and compare them with the lowest, highest, and average ambient air temperatures.
- The maximum differences between highest and lowest temperatures during 2020 were 40°C, 33°C and 7°C for ambient high, ambient low and ground temperature at 2 m, respectively. The corresponding average values were 22.83°C, 8.87°C and 15.51°C. All ground temperatures were more stable than that of ambient such that as the depth increased the stability increased.
- Based on the comparison between daily ambient air and ground temperatures, it was found that there are three different operating cases. The first two cases represent the days where the ambient air temperature is higher or lower than that of the ground. However, the third case refer to the days when the ambient air temperature is fluctuating around that of the ground.
- The potential of using shallow geothermal energy for cooling was found to be significant since a considerable decrease in the average effective cooling source temperature was achieved due to the incorporation of ground-cooled condenser. Additionally, the ground cooling system can operate 207 days/year with full operations of 51 days. This was based on the potential of operating between 06:00 and 24:00 in which this was considered as the maximum duration since the ORC is always turned off during night hours.

## 8.3 Ground Based-Cooling System Configurations

- Based on the comparison between direct and indirect ground cooling systems, it was found that pressure drop has a huge impact on the net output power under the investigated conditions.

Thus, it was recommended to use the indirect cooling strategy to avoid the mentioned drawback, ensure stability and make the system more controllable.

- A primary heat rejector was introduced to reduce the amount of heat rejected to the ground and provide coolth compensation during off-periods. Thus, the modified condenser was regarded as a hybrid-cooled condenser.
- Based on the instantaneous ambient air and ground temperatures, it was found that it is necessary to use four different operating modes to manage the flowing paths of water. The operating modes aimed to allow the water either to flow into or overtake the GHE, primary heat rejector and cycle's condenser.

## 8.4 Working Fluid Selection

- A comparison between four working fluids was carried out that are $CO_2$, R123, R124 and R245fa. Among these fluids, R123 showed the best performance in terms of net output power.
- Each working fluid has an optimal operating temperature at a given expander inlet pressure. It was shown that as the critical temperature increased the best point temperature also increased. As the pressure changed from 3 MPa to 6 MPa, the optimal expander inlet temperature for R123 was shifted from 184.2°C to 263.2°C.
- The effect of decreasing the condensation temperature was more considerable for low expander inlet pressures and working fluids with low critical temperatures in case of basic ORC. At 3 MPa, as the condensation temperature was decreased from 25°C to 15°C the enhancements in net output power were 7.35%, 12.13% and 8.77% for R123, R124 and R245fa, respectively. However, an opposite relation was recorded for the regenerative cycle.

### 8.5 Cost Assessment and Payback Period

- To study the economic feasibility of the proposed system, a numerical study was carried out to investigate the effect of using the heat wasted from a diesel engine generator. The capacity of generator was 30 kW with exhaust mass flow rate and temperature of 150 kg/hr and 500°C.
- The total average power of the plant (basic ORC) was increased to 32.395 kW which corresponds to an enhancement of 7.98%. This has helped reducing the fuel consumption per unit of energy and decreasing the operating cost from 0.37 L/kWh to 0.34 L/kWh and £0.188/kWh to £0.173/kWh, respectively.
- The total capital cost of the proposed system was estimated between £11,945-18,770. Considering the decreased operating cost and high levelized cost of electricity (£0.35/kWh), the payback period was expected to be varying between 4.9 and 7.8 years according to the shallow geothermal conditions. However, this may change depending on the total annual operating hours.
- The average total capital cost of the system based on the regenerative ORC was estimated as £21,327 and £34,941 for an expander inlet temperature of 300°C and 450°C, respectively. The corresponding net output power enhancements are 15.31% and 31.5% and the estimated payback periods are 4.6 and 3.7 years.

### 8.6 Future Work

- The system can be further improved by using the heat rejected from the cycle. This can be mainly applied to the sensible part of heat rejection since the fluid exiting the expander is still carrying a considerable amount of energy. In the current thesis, this was addressed by adding a regenerator which is one of the possible heat recovery options.

- The feasibility of using the proposed system in other regions needs to be investigated. This is very crucial since the system is highly affected by the ambient air and ground temperatures which indeed vary based on the location. This work would help encouraging the use of shallow geothermal energy systems.
- The proposed system was applied on a specific case study (diesel generator) in this thesis. Testing this system on further applications is critical allowing to figure out the limitations of the system and determine where it can be feasible.
- The effect of using mixture of different working fluids could be investigated. This can be also applied to the coolant which is flowing in the primary heat rejector and GHE. It is always essential to investigate new working fluids due to the critical drawbacks and restrictions. Thus, searching for alternative working fluids in such a system will continually remain a major concern in order to improve the cycle in terms of performance, capital cost and environmental impact.
- A detailed study on the selection of underground storage material could be carried out to enhance the cooling capacity of the ground. Based on the literature, there are various types of materials that could be used to store and release energy in shallow geothermal energy applications. It would be beneficial to compare the two types of thermal energy storage materials (sensible and latent) because the storage capacity and charging/discharging duration are crucial factors in the proposed system.
- According to the literature, geothermal energy has presented significant contributions to develop hybrid energy systems. Thus, it is recommended to integrate the proposed system into existing energy systems and mainly into RES-based systems in order to increase the penetration of renewable energy.

## References


[1] B. Mullan, J. Haqq-Misra, Population growth, energy use, and the implications for the search for extraterrestrial intelligence, Futures, Volume 106, 2019, Pages 4-17, ISSN 0016-3287, https://doi.org/10.1016/j.futures.2018.06.009.

[2] Montaser Mahmoud, Mohamad Ramadan, Sumsun Naher, Keith Pullen, Abdul-Ghani Olabi, The impacts of different heating systems on the environment: A review, Science of The Total Environment, Volume, 766, 2021, 142625, ISSN 0048-9697, https://doi.org/10.1016/j.scitotenv.2020.142625.

[3] Montaser Mahmoud, Mohamad Ramadan, Sumsun Naher, Keith Pullen and Abdul-Ghani Olabi. An investigation on the environmental impact of different heating systems: A review, 12th International conference on Sustainable Energy and Environmental Protection, 18-21 November 2019, Sharjah university, UAE.

[4] World Heath Organization, "WHO News Release," 02 05 2018. [Online]. Available: https://www.who.int/news-room/detail/02-05-2018-9-out-of-10-people-worldwide-breathe-polluted-air-but-more-countries-are-taking-action. [Accessed 13 01 2019].

[5] Montaser Mahmoud, Mohamad Ramadan, Sumsun Naher, Keith Pullen and Abdul-Ghani Olabi. An investigation on the effect of burning coal, natural gas and wood on the environment, 6th International conference on material science and smart materials, July 2019 23-26, Aston University, UK.

[6] Montaser Mahmoud, Mohamad Ramadan, Abdul-Ghani Olabi, Keith Pullen, Sumsun Naher, A review of mechanical energy storage systems combined with wind and solar applications, Energy Conversion and Management, Volume 210, 2020, 112670, ISSN 0196-8904, https://doi.org/10.1016/j.enconman.2020.112670.

[7] Montaser Mahmoud, Mohamad Ramadan, Sumsun Naher, Keith Pullen and Abdul-Ghani Olabi. A review on mechanical energy storage systems combined with wind and solar applications, 12th International conference on Sustainable Energy and Environmental Protection, 18-21 November 2019, Sharjah University, UAE.

[8] Montaser Mahmoud, Mohamad Ramadan, Sumsun Naher, Keith Pullen, Ahmad Baroutaji, Abdul-Ghani Olabi, Recent advances in district energy systems: A review, Thermal Science and Engineering Progress, Volume 20, 2020, 100678, ISSN 2451-9049, https://doi.org/10.1016/j.tsep.2020.100678.

[9] Dan Sui, Vebjørn Haraldstad Langåker, Zhixin Yu, Investigation of Thermophysical Properties of Nanofluids for Application in Geothermal Energy, Energy Procedia, Volume 105, 2017, Pages 5055-5060, ISSN 1876-6102, https://doi.org/10.1016/j.egypro.2017.03.1021.

[10] Alena Bleicher, Matthias Gross, Geothermal heat pumps and the vagaries of subterranean geology: Energy independence at a household level as a real world experiment, Renewable

and Sustainable Energy Reviews, Volume 64, 2016, Pages 279-288, ISSN 1364-0321, https://doi.org/10.1016/j.rser.2016.06.013.

[11] Peter Bayer, Guillaume Attard, Philipp Blum, Kathrin Menberg, The geothermal potential of cities, Renewable and Sustainable Energy Reviews, Volume 106, 2019, Pages 17-30, ISSN 1364-0321, https://doi.org/10.1016/j.rser.2019.02.019.

[12] Yuanlong Cui, Jie Zhu, Ssennoga Twaha, Junze Chu, Hongyu Bai, Kuo Huang, Xiangjie Chen, Stamatis Zoras, Zohreh Soleimani, Techno-economic assessment of the horizontal geothermal heat pump systems: A comprehensive review, Energy Conversion and Management, Volume 191, 2019, Pages 208-236, ISSN 0196-8904, https://doi.org/10.1016/j.enconman.2019.04.018.

[13] Daniel Adamovský, Pavel Neuberger, Radomír Adamovský, Results of operational verification of vertical ground heat exchangers, Energy and Buildings, Volume 152, 2017, Pages 185-193, ISSN 0378-7788, https://doi.org/10.1016/j.enbuild.2017.07.015.

[14] Kejuan Wei, Wenxin Li, Jiarong Li, Yong Wang, Lu Zhang, Study on a design method for hybrid ground heat exchangers of ground-coupled heat pump system, International Journal of Refrigeration, Volume 76, 2017, Pages 394-405, ISSN 0140-7007, https://doi.org/10.1016/j.ijrefrig.2016.12.020.

[15] Montaser Mahmoud, Mohamad Ramadan, Sumsun Naher, Keith Pullen, Abdul-Ghani Olabi, Advances in Grout Materials in Borehole Heat Exchangers, Encyclopedia of Smart Materials, Elsevier, Volume 4, 2022, Pages 334-342, ISBN 9780128157336, https://doi.org/10.1016/B978-0-12-815732-9.00053-X.

[16] Montaser Mahmoud, Mohamad Ramadan, Keith Pullen, Mohammad Ali Abdelkareem, Tabbi Wilberforce, Abdul-Ghani Olabi, Sumsun Naher, A review of grout materials in geothermal energy applications, International Journal of Thermofluids, 2021, 100070, ISSN 2666-2027, https://doi.org/10.1016/j.ijft.2021.100070.

[17] Juan Carlos Ríos Fernández, Integration capacity of geothermal energy in supermarkets through case analysis, Sustainable Energy Technologies and Assessments, Volume 34, 2019, Pages 49-55, ISSN 2213-1388, https://doi.org/10.1016/j.seta.2019.04.007.

[18] Bobo Zheng, Jiuping Xu, Ting Ni, Meihui Li, Geothermal energy utilization trends from a technological paradigm perspective, Renewable Energy, Volume 77, 2015, Pages 430-441, ISSN 0960-1481, https://doi.org/10.1016/j.renene.2014.12.035.

[19] John W. Lund, Tonya L. Boyd, Direct utilization of geothermal energy 2015 worldwide review, Geothermics, Volume 60, 2016, Pages 66-93, ISSN 0375-6505, https://doi.org/10.1016/j.geothermics.2015.11.004.

[20] Hyeongjin Moon; Hongkyo Kim; Yujin Nam, Study on the Optimum Design of a Ground Heat Pump System Using Optimization Algorithms, Energies 2019, 12(21), 4033; https://doi.org/10.3390/en12214033 - 23 Oct 2019.

[21] Ahmed A. Serageldin, Ali K. Abdelrahman, Shinichi Ookawara, Parametric study and optimization of a solar chimney passive ventilation system coupled with an earth-to-air heat exchanger, Sustainable Energy Technologies and Assessments, Volume 30, 2018, Pages 263-278, ISSN 2213-1388, https://doi.org/10.1016/j.seta.2018.10.010.

[22] Issam M. Ali Aljubury, Hind Dhia'a Ridha, Enhancement of evaporative cooling system in a greenhouse using geothermal energy, Renewable Energy, Volume 111, 2017, Pages 321-331, ISSN 0960-1481, https://doi.org/10.1016/j.renene.2017.03.080.

[23] B. L. Avanthi Isaka, P.G. Ranjith, T.D. Rathnaweera, The use of super-critical carbon dioxide as the working fluid in enhanced geothermal systems (EGSs): A review study, Sustainable Energy Technologies and Assessments, Volume 36, 2019, 100547, ISSN 2213-1388, https://doi.org/10.1016/j.seta.2019.100547.

[24] Dongdong Liu; Yanyong Xiang, A Semi-Analytical Method for Three-Dimensional Heat Transfer in Multi-Fracture Enhanced Geothermal Systems, Energies 2019, 12(7), 1211; https://doi.org/10.3390/en12071211 - 28 Mar 2019.

[25] Diego Moya, Juan Paredes, Prasad Kaparaju, Technical, financial, economic and environmental pre-feasibility study of geothermal power plants by RETScreen – Ecuador's case study, Renewable and Sustainable Energy Reviews, Volume 92, 2018, Pages 628-637, ISSN 1364-0321, https://doi.org/10.1016/j.rser.2018.04.027.

[26] Francesco Tinti, Alberto Barbaresi, Daniele Torreggiani, Davide Brunelli, Marco Ferrari, Andrea Verdecchia, Emanuele Bedeschi, Patrizia Tassinari, Roberto Bruno, Evaluation of efficiency of hybrid geothermal basket/air heat pump on a case study winery bas ed on experimental data, Energy and Buildings, Volume 151, 2017, Pages 365-380, ISSN 0378-7788, https://doi.org/10.1016/j.enbuild.2017.

[27] Benjamin Hénault, Philippe Pasquier, Michaël Kummert, Financial optimization and design of hybrid ground-coupled heat pump systems, Applied Thermal Engineering, Volume 93, 2016, Pages 72-82, ISSN 1359-4311, https://doi.org/10.1016/j.applthermaleng.2015.09.088.

[28] Montaser Mahmoud, Mohamad Ramadan, Sumsun Naher, Keith Pullen, Mohammad Ali Abdelkareem, Abdul-Ghani Olabi, A review of geothermal energy-driven hydrogen production systems, Thermal Science and Engineering Progress, Volume 22, 2021, 100854, ISSN 2451-9049, https://doi.org/10.1016/j.tsep.2021.100854.

[29] Emilio Hernández Martínez, M.C. Patricia Avitia Carlos, José Isaac Cisneros Solís, M.C. María del Carmen Prieto Avalos, Thermodynamic simulation and mathematical model for single and double flash cycles of Cerro Prieto geothermal power plants, Geothermics, Volume 83, 2020, 101713, ISSN 0375-6505, https://doi.org/10.1016/j.geothermics.2019.101713.

[30] Matthew J. Proctor, Wei Yu, Robert D. Kirkpatrick, Brent R. Young, Dynamic modelling and validation of a commercial scale geothermal organic rankine cycle power plant,

Geothermics, Volume 61, 2016, Pages 63-74, ISSN 0375-6505, https://doi.org/10.1016/j.geothermics.2016.01.007.

[31] Noémie Chagnon-Lessard, François Mathieu-Potvin, Louis Gosselin, Geothermal power plants with maximized specific power output: Optimal working fluid and operating conditions of subcritical and transcritical Organic Rankine Cycles, Geothermics, Volume 64, 2016, Pages 111-124, ISSN 0375-6505, https://doi.org/10.1016/j.geothermics.2016.04.002.

[32] A.H. Mosaffa, A. Zareei, Proposal and thermoeconomic analysis of geothermal flash binary power plants utilizing different types of organic flash cycle, Geothermics, Volume 72, 2018, Pages 47-63, ISSN 0375-6505, https://doi.org/10.1016/j.geothermics.2017.10.011.

[33] Chayadit Pumaneratkul, Haruhiko Yamasaki, Hiroshi Yamaguchi, Shinichi Kitamura, Yoshihiro Sako, Supercritical CO2 Rankine Cycle System with Low-Temperature Geothermal Heat Pipe, Energy Procedia, Volume 105, 2017, Pages 1029-1036, ISSN 1876-6102, https://doi.org/10.1016/j.egypro.2017.03.448.

[34] pp. Tomasz Kujawa, Władysław Nowak, Aleksander A. Stachel, Heat-flow characteristics of one-hole and two-hole systems for winning geothermal heat, Applied Energy, Volume 74, Issues 1–2, 2003, Pages 21-31, ISSN 0306-2619,, https://doi.org/10.1016/S0306-2619(02)00127-7.

[35] Peixue Jiang, Xiaolu Li, Ruina Xu, Fuzhen Zhang, Heat extraction of novel underground well pattern systems for geothermal energy exploitation, Renewable Energy, Volume 90, 2016, Pages 83-94, ISSN 0960-1481, https://doi.org/10.1016/j.renene.2015.12.062.

[36] Ceyhun Yilmaz, Ismail Koyuncu, Murat Alcin, Murat Tuna, Artificial Neural Networks based thermodynamic and economic analysis of a hydrogen production system assisted by geothermal energy on Fiel Programmable Gate Array, International Journal of Hydrogen Energy, Volume 44, Issue 33, 2019, Pages 17443-17459, ISSN 0360-3199, https://doi.org/10.1016/j.ijhydene.2019.05.049.

[37] Ceyhun Yilmaz, Mehmet Kanoglu, Thermodynamic evaluation of geothermal energy powered hydrogen production by PEM water electrolysis, Energy, Volume 69, 2014, Pages 592-602, ISSN 0360-5442, https://doi.org/10.1016/j.energy.2014.03.054.

[38] Liyan Cao, Juwei Lou, Jiangfeng Wang, Yiping Dai, Exergy analysis and optimization of a combined cooling and power system driven by geothermal energy for ice-making and hydrogen production, Energy Conversion and Management, Volume 174, 2018, Pages 886-896, ISSN 0196-8904, https://doi.org/10.1016/j.enconman.2018.08.067.

[39] Ceyhun Yilmaz, Mehmet Kanoglu, Aysegul Abusoglu, Thermoeconomic cost evaluation of hydrogen production driven by binary geothermal power plant, Geothermics, Volume 57, 2015, Pages 18-25, ISSN 0375-6505, https://doi.org/10.1016/j.geothermics.2015.05.005.

[40] Ceyhun Yilmaz, Mehmet Kanoglu, Aysegul Abusoglu, Exergetic cost evaluation of hydrogen production powered by combined flash-binary geothermal power plant, International Journal of Hydrogen Energy, Volume 40, Issue 40, 2015, Pages 14021-14030, ISSN 0360-3199, https://doi.org/10.1016/j.ijhydene.2015.07.031.

[41] Yunus Emre Yuksel, Murat Ozturk, Ibrahim Dincer, Energetic and exergetic performance evaluations of a geothermal power plant based integrated system for hydrogen production, International Journal of Hydrogen Energy, Volume 43, Issue 1, 2018, Pages 78-90, ISSN 0360-3199, https://doi.org/10.1016/j.ijhydene.2017.11.002.

[42] Mohammad Ebadollahi, Hadi Rostamzadeh, Mona Zamani Pedram, Hadi Ghaebi, Majid Amidpour, Proposal and assessment of a new geothermal-based multigeneration system for cooling, heating, power, and hydrogen production, using LNG cold energy recovery, Renewable Energy, Volume 135, 2019, Pages 66-87, ISSN 0960-1481, https://doi.org/10.1016/j.renene.2018.11.108.

[43] Ceyhun Yilmaz, Thermoeconomic modeling and optimization of a hydrogen production system using geothermal energy, Geothermics, Volume 65, 2017, Pages 32-43, ISSN 0375-6505, https://doi.org/10.1016/j.geothermics.2016.08.008.

[44] Aras Karapekmez, Ibrahim Dincer, Thermodynamic analysis of a novel solar and geothermal based combined energy system for hydrogen production, International Journal of Hydrogen Energy, Volume 45, Issue 9, 2020, Pages 5608-5628, ISSN 0360-3199, https://doi.org/10.1016/j.ijhydene.2018.12.046.

[45] Aras Karapekmez, Ibrahim Dincer, Modelling of hydrogen production from hydrogen sulfide in geothermal power plants, International Journal of Hydrogen Energy, Volume 43, Issue 23, 2018, Pages 10569-10579, ISSN 0360-3199, https://doi.org/10.1016/j.ijhydene.2018.02.020.

[46] Hatice Karakilcik, Mustafa Erden, Mehmet Karakilcik, Investigation of hydrogen production performance of chlor-alkali cell integrated into a power generation system based on geothermal resources, International Journal of Hydrogen Energy, Volume 44, Issue 27, 2019, Pages 14145-14150, ISSN 0360-3199, https://doi.org/10.1016/j.ijhydene.2018.09.095.

[47] Francesco Calise, Francesco Liberato Cappiello, Massimo Dentice d'Accadia, Maria Vicidomin, Thermo-economic analysis of hybrid solar-geothermal polygeneration plants in different configurations, 2020, Energies, Volume 13, https://doi.org/10.3390/en13092391.

[48] Rachana Vidhi, Pardeep Garg, Matthew S. Orosz, D. Yogi Goswami, Pramod Kumar, Ground cooling system for improving the efficiency of low temperature power generation, 2014, ASME 2014 8th International Conference on Energy Sustainability, ES 2014 Collocated with the ASME 2014 12th International Conference on Fuel Cell Science, Engineering and Technology, Volume 1, doi 10.1115/ES2014-6618.

[49] Rachana Vidhi, D. Yogi Goswami, Elias Stefanakos, Supercritical Rankine Cycle Coupled with Ground Cooling for Low Temperature Power Generation, Energy Procedia, Volume 57, 2014, Pages 524-532, ISSN 1876-6102, https://doi.org/10.1016/j.egypro.2014.10.206.

[50] Nicholas Charles Collier; Neil Brennan Milestone; Karl Patrick Travis, A Review of Potential Cementing Systems for Sealing and Support Matrices in Deep Borehole Disposal of Radioactive Waste, Energies 2019, 12(12), 2393; https://doi.org/10.3390/en12122393 - 21 Jun 2019.

[51] Zehao Lyu, Xianzhi Song, Gensheng Li, Yu Shi, Zihan Mu, Numerical analysis of characteristics of a single U-tube downhole heat exchanger in a geothermal well, Geothermics, Volume 72, 2018, Pages 15-23, ISSN 0375-6505, https://doi.org/10.1016/j.geothermics.2017.10.012.

[52] Jin Luo, Joachim Rohn, Wei Xiang, Manfred Bayer, Anna Priess, Lucas Wilkmann, Hagen Steger, Roman Zorn, Experimental investigation of a borehole field by enhanced geothermal response test and numerical analysis of performance of the borehole heat exchangers, Energy, Volume 84, 2015, Pages 473-484, ISSN 0360-5442, https://doi.org/10.1016/j.energy.2015.03.013.

[53] Zehao Lyu, Xianzhi Song, Gensheng Li, Xiaodong Hu, Yu Shi, Zhipeng Xu, Numerical analysis of characteristics of a single U-tube downhole heat exchanger in the borehole for geothermal wells, Energy, Volume 125, 2017, Pages 186-196, ISSN 0360-5442, https://doi.org/10.1016/j.energy.2017.02.125.

[54] Noori BniLam, Rafid Al-Khoury, A spectral model for heat transfer with friction heat gain in geothermal borehole heat exchangers, Applied Mathematical Modelling, Volume 40, Issues 15-16, 2016, Pages 7410-7421, ISSN 0307-904X, https://doi.org/10.1016/j.apm.2016.02.031.

[55] Liu Jun, Zhang Xu, Gao Jun, Yang Jie, Evaluation of heat exchange rate of GHE in geothermal heat pump systems, Renewable Energy, Volume 34, Issue 12, 2009, Pages 2898-2904, ISSN 0960-1481, https://doi.org/10.1016/j.renene.2009.04.009.

[56] Roque Borinaga-Treviño, Pablo Pascual-Muñoz, Daniel Castro-Fresno, Elena Blanco-Fernandez, Borehole thermal response and thermal resistance of four different grouting materials measured with a TRT, Applied Thermal Engineering, Volume 53, Issue 1, 2013, Pages 13-20, ISSN 1359-4311, https://doi.org/10.1016/j.applthermaleng.2012.12.036.

[57] Yong-Le Nian, Wen-Long Cheng, Analytical g-function for vertical geothermal boreholes with effect of borehole heat capacity, Applied Thermal Engineering, Volume 140, 2018, Pages 733-744, ISSN 1359-4311, https://doi.org/10.1016/j.applthermaleng.2018.05.086.

[58] Tianyuan Zheng, Haibing Shao, Sophie Schelenz, Philipp Hein, Thomas Vienken, Zhonghe Pang, Olaf Kolditz, Thomas Nagel, Efficiency and economic analysis of utilizing latent heat from groundwater freezing in the context of borehole heat exchanger coupled ground

source heat pump systems, Applied Thermal Engineering, Volume 105, 2016, Pages 314-326, ISSN 1359-4311, https://doi.org/10.1016/j.applthermaleng.2016.05.158.

[59] Cristina Sáez Blázquez, Arturo Farfán Martín, Ignacio Martín Nieto, Pedro Carrasco García, Luis Santiago Sánchez Pérez, Diego González-Aguilera, Analysis and study of different grouting materials in vertical geothermal closed-loop systems, Renewable Energy, Volume 114, Part B, 2017, Pages 1189-1200, ISSN 0960-1481, https://doi.org/10.1016/j.renene.2017.08.011.

[60] Daehoon Kim, Gyoungman Kim, Donghui Kim, Hwanjo Baek, Experimental and numerical investigation of thermal properties of cement-based grouts used for vertical ground heat exchanger, Renewable Energy, Volume 112, 2017, Pages 260-267, ISSN 0960-1481, https://doi.org/10.1016/j.renene.2017.05.045.

[61] T. Sliwa, M.A. Rosen, Efficiency analysis of borehole heat exchangers as grout varies via thermal response test simulations, Geothermics, Volume 69, 2017, Pages 132-138, ISSN 0375-6505, https://doi.org/10.1016/j.geothermics.2017.05.004.

[62] D. Pahud, B. Matthey, Comparison of the thermal performance of double U-pipe borehole heat exchangers measured in situ, Energy and Buildings, Volume 33, Issue 5, 2001, Pages 503-507, ISSN 0378-7788, https://doi.org/10.1016/S0378-7788(00)00106-7.

[63] Chulho Lee, Sangwoo Park, Dongseop Lee, In-Mo Lee, Hangseok Choi, Viscosity and salinity effect on thermal performance of bentonite-based grouts for ground heat exchanger, Applied Clay Science, Volume 101, 2014, Pages 455-460, ISSN 0169-1317, https://doi.org/10.1016/j.clay.2014.09.008.

[64] Wonjun Choi, Ryozo Ooka, Effect of natural convection on thermal response test conducted in saturated porous formation: Comparison of gravel-backfilled and cement-grouted borehole heat exchangers, Renewable Energy, Volume 96, Part A, 2016, Pages 891-903, ISSN 0960-1481, https://doi.org/10.1016/j.renene.2016.05.040.

[65] Roque Borinaga-Treviño, Pablo Pascual-Muñoz, Miguel Ángel Calzada-Pérez, Daniel Castro-Fresno, Freeze–thaw durability of cement-based geothermal grouting materials, Construction and Building Materials, Volume 55, 2014, Pages 390-397, ISSN 0950-0618, https://doi.org/10.1016/j.conbuildmat.2014.01.051.

[66] Selçuk Erol, Bertrand François, Efficiency of various grouting materials for borehole heat exchangers, Applied Thermal Engineering, Volume 70, Issue 1, 2014, Pages 788-799, ISSN 1359-4311, https://doi.org/10.1016/j.applthermaleng.2014.05.034.

[67] Fabien Delaleux, Xavier Py, Régis Olives, Antoine Dominguez, Enhancement of geothermal borehole heat exchangers performances by improvement of bentonite grouts conductivity, Applied Thermal Engineering, Volumes 33–34, 2012, Pages 92-99, ISSN 1359-4311, https://doi.org/10.1016/j.applthermaleng.2011.09.017.

[68] P. Pascual-Muñoz, I. Indacoechea-Vega, D. Zamora-Barraza, D. Castro-Fresno, Experimental analysis of enhanced cement-sand-based geothermal grouting materials,

Construction and Building Materials, Volume 185, 2018, Pages 481-488, ISSN 0950-0618, https://doi.org/10.1016/j.conbuildmat.2018.07.076.

[69] Daehoon Kim, Seokhoon Oh, Relationship between the thermal properties and degree of saturation of cementitious grouts used in vertical borehole heat exchangers, Energy and Buildings, Volume 201, 2019, Pages 1-9, ISSN 0378-7788, https://doi.org/10.1016/j.enbuild.2019.07.017.

[70] Jinsong Qian, Yiyun Hu, Jiake Zhang, Wenxin Xiao, Jianming Ling, Evaluation the performance of controlled low strength material made of excess excavated soil, Journal of Cleaner Production, Volume 214, 2019, Pages 79-88, ISSN 0959-6526, https://doi.org/10.1016/j.jclepro.2018.12.171.

[71] Tan Manh Do, Anh Ngoc Do, Gyeong-O Kang, Young-Sang Kim, Utilization of marine dredged soil in controlled low-strength material used as a thermal grout in geothermal systems, Construction and Building Materials, Volume 215, 2019, Pages 613-622, ISSN 0950-0618, https://doi.org/10.1016/j.conbuildmat.2019.04.255.

[72] Tan Manh Do, Hyeong-Ki Kim, Min-Jun Kim, Young-Sang Kim, Utilization of controlled low strength material (CLSM) as a novel grout for geothermal systems: Laboratory and field experiments, Journal of Building Engineering, Volume 29, 2020, 101110, ISSN 2352-7102, https://doi.org/10.1016/j.jobe.2019.101110.

[73] Young-sang Kim, Tan Manh Do, Min-Jun Kim, Bong-Ju Kim, Hyeong-Ki Kim, Utilization of by-product in controlled low-strength material for geothermal systems: Engineering performances, environmental impact, and cost analysis, Journal of Cleaner Production, Volume 172, 2018, Pages 909-920, ISSN 0959-6526, https://doi.org/10.1016/j.jclepro.2017.10.260.

[74] Tan Manh Do, Gyeong-O Kang, Young-Sang Kim, Thermal conductivity of controlled low strength material (CLSM) under various degrees of saturation using a modified pressure plate extractor apparatus – A case study for geothermal systems, Applied Thermal Engineering, Volume 143, 2018, Pages 607-613, ISSN 1359-4311, https://doi.org/10.1016/j.applthermaleng.2018.07.116.

[75] Jin Luo, Wei Xue, Tao Hu, Wei Xiang, Joachim Rohn, Thermo-economic analysis of borehole heat exchangers (BHE) grouted using drilling cuttings in a dolomite area, Applied Thermal Engineering, Volume 150, 2019, Pages 305-315, ISSN 1359-4311, https://doi.org/10.1016/j.applthermaleng.2018.12.130.

[76] Montaser Mahmoud, Mohamad Ramadan, Keith Pullen, Mohammad A. Abdelkareem, Abdul Ghani Olabi, Sumsun Naher, An Investigation on Nano-Enhanced Phase Change Materials: Carbon-Based Nanoparticles, Key Engineering Materials, Volume 922, 2022, ISSN 1662-9795, https://doi.org/10.4028/p-m17i9f.

[77] Montaser Mahmoud, Mohamad Ramadan, Keith Pullen, Mohammad A. Abdelkareem, Tabbi Wilberforce, Abdul-Ghani Olabi, Sumsun Naher, Waste Heat Recovery Applications Incorporating Phase Change Materials, Encyclopedia of Smart Materials, Elsevier, Volume

2, 2022, Pages 513-521, ISBN 9780128157336, https://doi.org/10.1016/B978-0-12-815732-9.00074-7.

[78] Montaser Mahmoud, Keith Pullen, Mohamad Ramadan, Ahmad Baroutaji, Mohammad A. Abdelkareem, Abdul-Ghani Olabi, Sumsun Naher, Phase Change Materials Integrated Into Solar Parabolic Collectors, Encyclopedia of Smart Materials, Elsevier, Volume 2, 2022, Pages 613-620, ISBN 9780128157336, https://doi.org/10.1016/B978-0-12-815732-9.00084-X.

[79] Montaser Mahmoud, Mohamad Ramadan, Keith Pullen, Mohammad A. Abdelkareem, Abdul Hai Alami, Abdul-Ghani Olabi, Sumsun Naher, Foam-Based Composite Phase Change Materials, Encyclopedia of Smart Materials, Elsevier, Volume 4, 2022, Pages 343-351, ISBN 9780128157336, https://doi.org/10.1016/B978-0-12-815732-9.00083-8.

[80] Montaser Mahmoud, Mohamad Ramadan, Keith Pullen, Mohammad A. Abdelkareem, Abdul Hai Alami, Abdul-Ghani Olabi, Sumsun Naher, Using Nanoparticles for Thermal Enhancement of Phase Change Materials, Encyclopedia of Smart Materials, Elsevier, Volume 3, 2022, Pages 281-287, ISBN 9780128157336, https://doi.org/10.1016/B978-0-12-815732-9.00111-X.

[81] Montaser Mahmoud, Mohamad Ramadan, Keith Pullen, Abdul-Ghani Olabi, Sumsun Naher, An investigation on nano-enhanced phase change materials: Carbon-based nanoparticles, 7th International Conference on Materials Science and Smart Materials, 4-6 August 2021, Brunel University London, UK.

[82] Montaser Mahmoud, Mohamad Ramadan, Keith Pullen, Mohammad A. Abdelkareem, Ahmad Baroutaji, Abdul-Ghani Olabi, Sumsun Naher, Advances in Shape-Stabilized Phase Change Materials, Encyclopedia of Smart Materials, Elsevier, Volume 4, 2022, Pages 326-333, ISBN 9780128157336, https://doi.org/10.1016/B978-0-12-815732-9.00094-2.

[83] Michele Bottarelli, Marco Bortoloni, Yuehong Su, Charles Yousif, Ahmet Alper Aydın, Aleksandar Georgiev, Numerical analysis of a novel ground heat exchanger coupled with phase change materials, Applied Thermal Engineering, Volume 88, 2015, Pages 369-375, https://doi.org/10.1016/j.applthermaleng.2014.10.016.

[84] Michel Bernier, Eslami-nejad P. A Preliminary Assessment on the Use of Phase Change Materials around Geothermal Boreholes. ASHRAE Trans 2013; 119:312.

[85] Fei Chen, Jinfeng Mao, Shangyuan Chen, Chaofeng Li, Pumin Hou, Lu Liao, Efficiency analysis of utilizing phase change materials as grout for a vertical U-tube heat exchanger coupled ground source heat pump system, Applied Thermal Engineering, Volume 130, 2018, Pages 698-709, ISSN 1359-4311, https://doi.org/10.1016/j.applthermaleng.2017.11.062.

[86] Fei Chen, Jinfeng Mao, Chaofeng Li, Pumin Hou, Yong Li, Zheli Xing, Shangyuan Chen, Restoration performance and operation characteristics of a vertical U-tube ground source heat pump system with phase change grouts under different running modes, Applied

Thermal Engineering, Volume 141, 2018, Pages 467-482, ISSN 1359-4311, https://doi.org/10.1016/j.applthermaleng.2018.06.009.

[87] Minsuk Kong, Jorge L. Alvarado, Curt Thies, Sean Morefield, Charles P. Marsh, Field evaluation of microencapsulated phase change material slurry in ground source heat pump systems, Energy, Volume 122, 2017, Pages 691-700, ISSN 0360-5442, https://doi.org/10.1016/j.energy.2016.12.092.

[88] Liang Pu, Lingling Xu, Shengqi Zhang, Yanzhong Li, Optimization of ground heat exchanger using microencapsulated phase change material slurry based on tree-shaped structure, Applied Energy, Volume 240, 2019, Pages 860-869, ISSN 0306-2619, https://doi.org/10.1016/j.apenergy.2019.02.088.

[89] Di Qi, Liang Pu, Futao Sun, Yanzhong Li, Numerical investigation on thermal performance of ground heat exchangers using phase change materials as grout for ground source heat pump system, Applied Thermal Engineering, Volume 106, 2016, Pages 1023-1032, ISSN 1359-4311, https://doi.org/10.1016/j.applthermaleng.2016.06.048.

[90] Weibo Yang, Rui Xu, Binbin Yang, Jingjing Yang, Experimental and numerical investigations on the thermal performance of a borehole ground heat exchanger with PCM backfill, Energy, Volume 174, 2019, Pages 216-235, ISSN 0360-5442, https://doi.org/10.1016/j.energy.2019.02.172.

[91] Na Zhu, Pingfang Hu, Yu Lei, Zhangning Jiang, Fei Lei, Numerical study on ground source heat pump integrated with phase change material cooling storage system in office building, Applied Thermal Engineering, Volume 87, 2015, Pages 615-623, ISSN 1359-4311, https://doi.org/10.1016/j.applthermaleng.2015.05.056.

[92] H.M. Teamah, M.F. Lightstone, Numerical study of the electrical load shift capability of a ground source heat pump system with phase change thermal storage, Energy and Buildings, Volume 199, 2019, Pages 235-246, ISSN 0378-7788, https://doi.org/10.1016/j.enbuild.2019.06.056.

[93] Mingkan Zhang, Xiaobing Liu, Kaushik Biswas, Joseph Warner, A three-dimensional numerical investigation of a novel shallow bore ground heat exchanger integrated with phase change material, Applied Thermal Engineering, Volume 162, 2019, 114297, ISSN 1359-4311, https://doi.org/10.1016/j.applthermaleng.2019.114297.

[94] Koon Beng Ooi;Masa Noguchi, Verification of the Performance of a Vertical Ground Heat Exchanger Applied to a Test House in Melbourne, Australia, Energies 2017, 10(10), 1558; https://doi.org/10.3390/en10101558 - 10 Oct 2017.

[95] Rahim Hassanzadeh, Mohsen Darvishyadegari, Samaneh Arman, A new idea for improving the horizontal straight ground source heat exchangers performance, Sustainable Energy Technologies and Assessments, Volume 25, 2018, Pages 138-145, ISSN 2213-1388, https://doi.org/10.1016/j.seta.2017.12.006.

[96] Reza Saeidi, Younes Noorollahi, Vahid Esfahanian, Numerical simulation of a novel spiral type ground heat exchanger for enhancing heat transfer performance of geothermal heat pump, Energy Conversion and Management, Volume 168, 2018, Pages 296-307, ISSN 0196-8904, https://doi.org/10.1016/j.enconman.2018.05.015.

[97] Kwang-Seob Lee; Eun-Chul Kang; Yu-Jin Kim; Euy-Joon Lee, Model Verification and Justification Study of Spirally Corrugated Pipes in a Ground-Air Heat Exchanger Application, Energies 2019, 12(21), 4047; https://doi.org/10.3390/en12214047 - 24 Oct 2019.

[98] Conrad Kunze, Mareen Hertel, Contested deep geothermal energy in Germany-The emergence of an environmental protest movement, Energy Research & Social Science, Volume 27, 2017, Pages 174-180, ISSN 2214-6296, https://doi.org/10.1016/j.erss.2016.11.007.

[99] J.D. Templeton, F. Hassani, S.A. Ghoreishi-Madiseh, Study of effective solar energy storage using a double pipe geothermal heat exchanger, Renewable Energy, Volume 86, 2016, Pages 173-181, ISSN 0960-1481, https://doi.org/10.1016/j.renene.2015.08.024.

[100] Zeyu Xiong, Daniel E. Fisher, Jeffrey D. Spitler, Development and validation of a Slinky™ ground heat exchanger model, Applied Energy, Volume 141, 2015, Pages 57-69, ISSN 0306-2619, https://doi.org/10.1016/j.apenergy.2014.11.058.

[101] Abdul Ghani Olabi, Montaser Mahmoud, Bassel Soudan, Tabbi Wilberforce, Mohamad Ramadan, Geothermal based hybrid energy systems, toward eco-friendly energy approaches, Renewable Energy, Volume 147, Part 1, 2020, Pages 2003-2012, ISSN 0960-1481, https://doi.org/10.1016/j.renene.2019.09.140.

[102] Tian You, Baolong Wang, Wei Wu, Wenxing Shi, Xianting Li, Performance analysis of hybrid ground-coupled heat pump system with multi-functions, Energy Conversion and Management, Volume 92, 2015, Pages 47-59, ISSN 0196-8904, https://doi.org/10.1016/j.enconman.2014.12.036.

[103] Joo Seong Lee, Honghee Park, Yongchan Kim, Transient performance characteristics of a hybrid ground-source heat pump in the cooling mode, Applied Energy, Volume 123, 2014, Pages 121-128, ISSN 0306-2619, https://doi.org/10.1016/j.apenergy.2014.02.056.

[104] Masih Alavy, Seth B. Dworkin, Wey H. Leong, A design methodology and analysis of combining multiple buildings onto a single district hybrid ground source heat pump system, Renewable Energy, Volume 66, 2014, Pages 515-522, ISSN 0960-1481, https://doi.org/10.1016/j.renene.2013.12.030.

[105] K. Allaerts, M. Coomans, R. Salenbien, Hybrid ground-source heat pump system with active air source regeneration, Energy Conversion and Management, Volume 90, 2015, Pages 230-237, ISSN 0196-8904, https://doi.org/10.1016/j.enconman.2014.11.009.

[106] Nima Bonyadi, Evan Johnson, Derek Baker,Technoeconomic and exergy analysis of a solar geothermal hybrid electric power plant using a novel combined cycle, Energy Conversion

and Management, Volume 156, 2018, Pages 542-554, ISSN 0196-8904, https://doi.org/10.1016/j.enconman.2017.

[107] Martina Ciani Bassetti, Daniele Consoli, Giovanni Manente, Andrea Lazzaretto, Design and off-design models of a hybrid geothermal-solar power plant enhanced by a thermal storage, Renewable Energy, 2017, , ISSN 0960-1481, https://doi.org/10.1016/j.renene.2017.05.078.

[108] Pei-Xue Jiang, Fu-Zhen Zhang, Rui-Na Xu, Thermodynamic analysis of a solar–enhanced geothermal hybrid power plant using CO2 as working fluid, Applied Thermal Engineering, Volume 116, 2017, Pages 463-472, ISSN 1359-4311, https://doi.org/10.1016/j.applthermaleng.2016.12.086.

[109] Hadi Ghasemi, Elysia Sheu, Alessio Tizzanini, Marco Paci, Alexander Mitsos, Hybrid solar–geothermal power generation: Optimal retrofitting, Applied Energy, Volume 131, 2014, Pages 158-170, ISSN 0306-2619, https://doi.org/10.1016/j.apenergy.2014.06.010.

[110] Álvaro Lentz, Rafael Almanza, Solar–geothermal hybrid system, Applied Thermal Engineering, Volume 26, Issues 14–15, 2006, Pages 1537-1544, ISSN 1359-4311, https://doi.org/10.1016/j.applthermaleng.2005.12.008.

[111] Mohammad Ayub, Alexander Mitsos, Hadi Ghasemi, Thermo-economic analysis of a hybrid solar-binary geothermal power plant, Energy, Volume 87, 2015, Pages 326-335, ISSN 0360-5442, https://doi.org/10.1016/j.energy.2015.04.106.

[112] A. Acuna, F. Lara, P. Rosales, J. Suastegui, N. Velazquez, A. Ruelas, Impact of a vertical geothermal heat exchanger on the solar fraction of a solar cooling system, International Journal of Refrigeration, Volume 76, 2017, Pages 63-72, ISSN 0140-7007, https://doi.org/10.1016/j.ijrefrig.2017.02.007.

[113] Min Guo, Nairen Diao, Yi Man, Zhaohong Fang, Research and development of the hybrid ground-coupled heat pump technology in China, Renewable Energy, Volume 87, Part 3, 2016, Pages 1033-1044, ISSN 0960-1481, https://doi.org/10.1016/j.renene.2015.08.021.

[114] Jérôme de La Bernardie, Jean-Raynald de Dreuzy, Olivier Bour, Hervé Lesueur, Synthetic investigation of thermal storage capacities in crystalline bedrock through a regular fracture network as heat exchanger, Geothermics, Volume 77, 2019, Pages 130-138, IS SN 0375-6505, https://doi.org/10.1016/j.geothermics.2018.08.010.

[115] José Miguel Cardemil, Felipe Cortés, Andrés Díaz, Rodrigo Escobar, Thermodynamic evaluation of solar-geothermal hybrid power plants in northern Chile, Energy Conversion and Management, Volume 123, 2016, Pages 348-361, ISSN 0196-8904, https://doi.org/10.1016/j.enconman.2016.06.032.

[116] Saeid Mohammadzadeh Bina, Saeid Jalilinasrabady, Hikari Fujii, Exergoeconomic analysis and optimization of single and double flash cycles for Sabalan geothermal power plant, Geothermics, Volume 72, 2018, Pages 74-82, ISSN 0375-6505, https://doi.org/10.1016/j.geothermics.2017.10.013.

[117] Zhequan Jin, Trygve M. Eikevik, Petter Nekså, Armin Hafner, Investigation on CO2 hybrid ground-coupled heat pumping system under warm climate, International Journal of Refrigeration, Volume 62, 2016, Pages 145-152, ISSN 0140-7007, https://doi.org/10.1016/j.ijrefrig.2015.10.005.

[118] Zhequan Jin, Trygve M. Eikevik, Petter Nekså, Armin Hafner, A steady and quasi-steady state analysis on the CO2 hybrid ground-coupled heat pumping system, International Journal of Refrigeration, Volume 76, 2017, Pages 29-41, ISSN 0140-7007, https://doi.org/10.1016/j.ijrefrig.2017.01.029.

[119] Francesco Calise, Massimo Dentice d'Accadia, Adriano Macaluso, Antonio Piacentino, Laura Vanoli, Exergetic and exergoeconomic analysis of a novel hybrid solar–geothermal polygeneration system producing energy and water, Energy Conversion and Management, Volume 115, 2016, Pages 200-220, ISSN 0196-8904, https://doi.org/10.1016/j.enconman.2016.02.029.

[120] Osamah Siddiqui, Haris Ishaq, Ibrahim Dincer, A novel solar and geothermal-based trigeneration system for electricity generation, hydrogen production and cooling, Energy Conversion and Management, Volume 198, 2019, 111812, ISSN 0196-8904, https://doi.org/10.1016/j.enconman.2019.111812.

[121] S. Andrew Putrayudha, Eun Chul Kang, E. Evgueniy, Y. Libing, Euy Joon Lee, A study of photovoltaic/thermal (PVT)-ground source heat pump hybrid system by using fuzzy logic control, Applied Thermal Engineering, Volume 89, 2015, Pages 578-586, ISSN 1359-4311, https://doi.org/10.1016/j.applthermaleng.2015.06.019.

[122] S. Antonov, L. Helsen, Robustness analysis of a hybrid ground coupled heat pump system with model predictive control, Journal of Process Control, Volume 47, 2016, Pages 191-200, ISSN 0959-1524, https://doi.org/10.1016/j.jprocont.2016.08.009.

[123] Valentin Trillat-Berdal, Bernard Souyri, Gilbert Achard, Coupling of geothermal heat pumps with thermal solar collectors, Applied Thermal Engineering, Volume 27, Issue 10, 2007, Pages 1750-1755, ISSN 1359-4311, https://doi.org/10.1016/j.applthermaleng.2006.07.022.

[124] Zongwei Han, Xiaomei Ju, Xiao Ma, Yanhong Zhang, Min Lin, Simulation of the performance of a hybrid ground-coupled heat pump system on the basis of wet bulb temperature control, Applied Thermal Engineering, Volume 108, 2016, Pages 980-988, ISSN 1359-4311, https://doi.org/10.1016/j.applthermaleng.2016.07.171.

[125] Wenzhi Cui, Shiyu Zhou, Xiangyang Liu, Optimization of design and operation parameters for hybrid ground-source heat pump assisted with cooling tower, Energy and Buildings, Volume 99, 2015, Pages 253-262, ISSN 0378-7788, https://doi.org/10.1016/j.enbuild.2015.04.034.

[126] Bin Hu, Yaoyu Li, Baojie Mu, Shaojie Wang, John E. Seem, Feng Cao, Extremum seeking control for efficient operation of hybrid ground source heat pump system, Renewable

Energy, Volume 86, 2016, Pages 332-346, ISSN 0960-1481, https://doi.org/10.1016/j.renene.2015.07.092.

[127] Joo Seong Lee, Kang Sub Song, Jae Hwan Ahn, Yongchan Kim, Comparison on the transient cooling performances of hybrid ground-source heat pumps with various flow loop configurations, Energy, Volume 82, 2015, Pages 678-685, ISSN 0360-5442, https://doi.org/10.1016/j.energy.2015.01.076.

[128] Rui Fan, Yan Gao, Li Hua, Xiaoxi Deng, Jie Shi, Thermal performance and operation strategy optimization for a practical hybrid ground-source heat-pump system, Energy and Buildings, Volume 78, 2014, Pages 238-247, ISSN 0378-7788, https://doi.org/10.1016/j.enbuild.2014.04.041.

[129] Jing Yang, Linghong Xu, Pingfang Hu, Na Zhu, Xuepeng Chen, Study on intermittent operation strategies of a hybrid ground-source heat pump system with double-cooling towers for hotel buildings, Energy and Buildings, Volume 76, 2014, Pages 506-512, ISSN 0378-7788, https://doi.org/10.1016/j.enbuild.2014.02.061.

[130] Wenjie Gang, Jinbo Wang, Predictive ANN models of ground heat exchanger for the control of hybrid ground source heat pump systems, Applied Energy, Volume 112, 2013, Pages 1146-1153, ISSN 0306-2619, https://doi.org/10.1016/j.apenergy.2012.12.031.

[131] Jin Luo, Haifeng Zhao, Jia Jia, Wei Xiang, Joachim Rohn, Philipp Blum, Study on operation management of borehole heat exchangers for a large-scale hybrid ground source heat pump system in China, Energy, Volume 123, 2017, Pages 340-352, ISSN 0360-5442, https://doi.org/10.1016/j.energy.2017.01.136.

[132] Qiang Liu, Linlin Shang, Yuanyuan Duan, Performance analyses of a hybrid geothermal–fossil power generation system using low-enthalpy geothermal resources, Applied Energy, Volume 162, 2016, Pages 149-162, ISSN 0306-2619, https://doi.org/10.1016/j.apenergy.2015.10.078.

[133] Zhijian Liu, Wei Xu, Xue Zhai, Cheng Qian, Xi Chen, Feasibility and performance study of the hybrid ground-source heat pump system for one office building in Chinese heating dominated areas, Renewable Energy, Volume 101, 2017, Pages 1131-1140, ISSN 0960-1481, https://doi.org/10.1016/j.renene.2016.10.006.

[134] Kathrin Menberg, Yeonsook Heo, Wonjun Choi, Ryozo Ooka, Ruchi Choudhary, Masanori Shukuya, Exergy analysis of a hybrid ground-source heat pump system, Applied Energy, Volume 204, 2017, Pages 31-46, ISSN 0306-2619, https://doi.org/10.1016/j.apenergy.2017.06.076.

[135] Aleksandra Borsukiewicz-Gozdur, Dual-fluid-hybrid power plant co-powered by low-temperature geothermal water, Geothermics, Volume 39, Issue 2, 2010, Pages 170-176, ISSN 0375-6505, https://doi.org/10.1016/j.geothermics.2009.10.004.

[136] Muhsen Habka, Salman Ajib, Investigation of novel, hybrid, geothermal-energized cogeneration plants based on organic Rankine cycle, Energy, Volume 70, 2014, Pages 212-222, ISSN 0360-5442, https://doi.org/10.1016/j.energy.2014.03.114.

[137] Koenraad F. Beckers; Gloria A. Aguirre; Jefferson W. Tester, Hybrid Ground-Source Heat Pump Systems for Cooling-Dominated Applications: Experimental and Numerical Case-Study of Cooling for Cellular Tower Shelters, Energy & Buildings, doi:10.1016/j.enbuild.2018.08.005.

[138] Yi Man, Hongxing Yang, Jeffrey D. Spitler, Zhaohong Fang, Feasibility study on novel hybrid ground coupled heat pump system with nocturnal cooling radiator for cooling load dominated buildings, Applied Energy, Volume 88, Issue 11, 2011, Pages 4160-4171, ISSN 0306-2619, https://doi.org/10.1016/j.apenergy.2011.04.035.

[139] Ping Cui, Hongxing Yang, Jeffrey D. Spitler, Zhaohong Fang, Simulation of hybrid ground-coupled heat pump with domestic hot water heating systems using HVACSIM+, Energy and Buildings, Volume 40, Issue 9, 2008, Pages 1731-1736, ISSN 0378-7788, https://doi.org/10.1016/j.enbuild.2008.03.001.

[140] Hiep V. Nguyen, Ying Lam E. Law, Xiaoyan Zhou, Philip R. Walsh, Wey H. Leong, Seth B. Dworkin, A techno-economic analysis of heat-pump entering fluid temperatures, and CO2 emissions for hybrid ground-source heat pump systems, Geothermics, Volume 61, 2016, Pages 24-34, ISSN 0375-6505, https://doi.org/10.1016/j.geothermics.2016.01.013.

[141] Honghee Park, Joo Seoung Lee, Wonuk Kim, Yongchan Kim, The cooling seasonal performance factor of a hybrid ground-source heat pump with parallel and serial configurations, Applied Energy, Volume 102, 2013, Pages 877-884, ISSN 0306-2619, https://doi.org/10.1016/j.apenergy.2012.09.035.

[142] Farzin M. Rad, Alan S. Fung, Solar community heating and cooling system with borehole thermal energy storage – Review of systems, Renewable and Sustainable Energy Reviews, Volume 60, 2016, Pages 1550-1561, ISSN 1364-0321, https://doi.org/10.1016/j.rser.2016.03.025.

[143] Seyed Ali Ghoreishi-Madiseh; Ali Fahrettin Kuyuk; Marco Antonio Rodrigues de Brito; Durjoy Baidya; Zahra Torabigoodarzi and Amir Safari, Application of Borehole Thermal Energy Storage in Waste Heat Recovery from Diesel Generators in Remote Cold Climate Locations, Energies 2019, 12(4), 656; https://doi.org/10.3390/en12040656.

[144] Abidur Rahman, Omar Farrok, Md Mejbaul Haque, Environmental impact of renewable energy source based electrical power plants: Solar, wind, hydroelectric, biomass, geothermal, tidal, ocean, and osmotic, Renewable and Sustainable Energy Reviews, Volume 161, 2022, 112279, ISSN 1364-0321, https://doi.org/10.1016/j.rser.2022.112279.

[145] Mirko Bravi, Riccardo Basosi, Environmental impact of electricity from selected geothermal power plants in Italy, Journal of Cleaner Production, Volume 66, 2014, Pages 301-308, ISSN 0959-6526, https://doi.org/10.1016/j.jclepro.2013.11.015.

[146] Spyridon Karytsas, Ioannis Choropanitis, Barriers against and actions towards renewable energy technologies diffusion: A Principal Component Analysis for residential ground source heat pump (GSHP) systems, Renewable and Sustainable Energy Reviews, Volume 78, 2017, Pages 252-271, ISSN 1364-0321, https://doi.org/10.1016/j.rser.2017.04.060.

[147] I. W. Johnston, G. A. Narsilio, S. Colls, Emerging Geothermal Energy Technologies, KSCE Journal of Civil Engineering, Volume 15, 2011, Pages 643–653, https://doi.org/10.1007/s12205-011-0005-7.

[148] Yasuhiro Fujimitsu, Koichiro Fukuoka, Sachio Ehara, Hiroto Takeshita, Fuminori Abe, Evaluation of subsurface thermal environmental change caused by a ground-coupled heat pump system, Current Applied Physics, Volume 10, Issue 2, Supplement, 2010, Pages S113-S116, ISSN 1567-1739, https://doi.org/10.1016/j.cap.2009.11.014.

[149] Montaser Mahmoud, Mohamad Ramadan, Sumsun Naher, Keith Pullen, Abdul-Ghani Olabi, CO2 – Based transcritical Rankine cycle coupled with a ground-cooled condenser, Thermal Science and Engineering Progress, Volume 25, 2021, 100948, ISSN 2451-9049, https://doi.org/10.1016/j.tsep.2021.100948.

[150] Mehran Abdolalipouradl, Farzad Mohammadkhani, Shahram Khalilarya, A comparative analysis of novel combined flash-binary cycles for Sabalan geothermal wells: Thermodynamic and exergoeconomic viewpoints, Energy, Volume 209, 2020, 118235, ISSN 0360-5442, https://doi.org/10.1016/j.energy.2020.118235.

[151] Yuhong Zhou, Shanshan Li, Lei Sun, Shupeng Zhao, Seyed Saman Ashraf Talesh, Optimization and thermodynamic performance analysis of a power generation system based on geothermal flash and dual-pressure evaporation organic Rankine cycles using zeotropic mixtures, Energy, Volume 194, 2020, 116785, ISSN 0360-5442, https://doi.org/10.1016/j.energy.2019.116785.

[152] Sebastian Eyerer, Fabian Dawo, Christoph Wieland, Hartmut Spliethoff, Advanced ORC architecture for geothermal combined heat and power generation, Energy, Volume 205, 2020, 117967, ISSN 0360-5442, https://doi.org/10.1016/j.energy.2020.117967.

[153] Shabnam Kazemi, Mohamad Iskandr Mohamad Nor, Wen Hui Teoh, Thermodynamic and economic investigation of an ionic liquid as a new proposed geothermal fluid in different organic Rankine cycles for energy production, Energy, Volume 193, 2020, 116722, ISSN 0360-5442, https://doi.org/10.1016/j.energy.2019.116722.

[154] Frank P. Incropera, David P. Dewitt, Theodore L. Bergman, Adrienne S. Lavine, Fundamentals of Heat and Mass Transfer, 8e, New York: Wiley, 2017.

[155] Ehsan Izadpanah, Ahmad Zarei, Saeed Akhavan, Marzie Babaie Rabiee, An experimental investigation of natural convection heat transfer from a helically coiled heat exchanger, International Journal of Refrigeration, Volume 93, 2018, Pages 38-46, ISSN 0140-7007, https://doi.org/10.1016/j.ijrefrig.2018.06.008.

[156] Gequn Shu, Lingfeng Shi, Hua Tian, Shuai Deng, Xiaoya Li, Liwen Chang, Configurations selection maps of CO2-based transcritical Rankine cycle (CTRC) for thermal energy management of engine waste heat, Applied Energy, Volume 186, Part 3, 2017, Pages 423-435, ISSN 0306-2619, https://doi.org/10.1016/j.apenergy.2016.03.049.

[157] Jian Li, Zhen Yang, Shuozhuo Hu, Yuanyuan Duan, Influences of fluid corrosivity and heat exchanger materials on design and thermo-economic performance of organic Rankine cycle systems, Energy, Volume 228, 2021, 120589, ISSN 0360-5442, https://doi.org/10.1016/j.energy.2021.120589.

[158] Kiyarash Rahbar, Saad Mahmoud, Raya K. Al-Dadah, Nima Moazami, Seyed A. Mirhadizadeh, Review of organic Rankine cycle for small-scale applications, Energy Conversion and Management, Volume 134, 2017, Pages 135-155, ISSN 0196-8904, https://doi.org/10.1016/j.enconman.2016.12.023.

[159] Montaser Mahmoud, Mohammad Alkhedher, Mohamad Ramadan, Keith Pullen, Abdul-Ghani Olabi, Sumsun Naher, Experimental investigation into the potential of using a shallow ground-cooled condenser in Lebanon, Energy Conversion and Management, Volume 264, 2022, 115729, ISSN 0196-8904, https://doi.org/10.1016/j.enconman.2022.115729.

[160] Montaser Mahmoud, Mohammad Alkhedher, Mohamad Ramadan, Sumsun Naher, Keith Pullen, An investigation on organic Rankine cycle incorporating a ground-cooled condenser: Working fluid selection and regeneration, Energy, Volume 249, 2022, 123742, ISSN 0360-5442, https://doi.org/10.1016/j.energy.2022.123742.

[161] Robert W. Fox, Alan T. McDonald, Philip J. Pritchard, Introduction to Fluid Mechanics, 6e, Wiley, 2003.

[162] Hikari Fujii, Keita Nishi, Yoshihito Komaniwa, Naokatsu Chou, Numerical modeling of slinky-coil horizontal ground heat exchangers, Geothermics, Volume 41, 2012, Pages 55-62, ISSN 0375-6505, https://doi.org/10.1016/j.geothermics.2011.09.002.

[163] Roberto Capata, Gustavo Hernandez, Preliminary Design and Simulation of a Turbo Expander for Small Rated Power Organic Rankine Cycle (ORC), Energies, Volume 7, 2014, 7067-7093, https://doi:10.3390/en7117067.

[164] Montaser Mahmoud, Mohamad Ramadan, Keith Pullen, Abdul-Ghani Olabi, Sumsun Naher, An investigation on the effect of configuration on the performance of organic Rankine cycle incorporating a ground-cooled condenser, 13th International Conference on Sustainable Energy & Environmental Protection, SEEP, 13-16 September 2021, University of Natural Resources and Life Science, Vienna (BOKU), Austria.

[165] Montaser Mahmoud, Keith Pullen, Mohamad Ramadan, Abdul-Ghani Olabi, Sumsun Naher, Optimizing ground-cooled condenser in a Rankine cycle using phase change materials, 7th International Conference on Materials Science and Smart Materials, 4-6 August 2021, Brunel University London, UK.

[166] Montaser Mahmoud, Mohamad Ramadan, Sumsun Naher, Keith Pullen, Mohammad A. Abdelkareem, Ahmad Baroutaji, Abdul-Ghani Olabi, Investigation on the Use of Phase Change Materials in Geothermal Energy Applications, Encyclopedia of Smart Materials, Elsevier, Volume 4, 2022, Pages 352-361, ISBN 9780128157336, https://doi.org/10.1016/B978-0-12-815732-9.00059-0.

[167] Russell Charles Hibbeler, Mechanics of materials, Book, Pearson Educación, 2005, ISBN 013191345X.

[168] Tocci, L., Pal, T., Pesmazoglou, I. and Franchetti, B., 2017. Small scale Organic Rankine Cycle (ORC): A techno-economic review. Energies, 10(4), p.413, doi:10.3390/en10040413.

# Appendix A. Engineering Equations Solver

## A.1 Basic model

```
etta_p=0.8        "Pump Efficiency"
etta_t=0.7        "Turbine Efficiency"
etta_g=0.9        "generator efficiency"
g=9.81
R$='CarbonDioxide'

"Gas"
m_dot_g=mg/3600
T_gi=Tgi
T_go=Tgo
T_g_avg=(Tgi+Tgo)/2
cp_g=Cp(CarbonDioxide,T=T_g_avg,P=101)*0.1984+Cp(Water,T=T_g_avg,P=101)*0.0826+Cp(Nitrogen,
T=T_g_avg,P=101)*0.7149
K_g=(Conductivity(CarbonDioxide,T=T_g_avg,P=101)*0.1984+Conductivity(Water,T=T_g_avg,P=101)*0.
0826+Conductivity(Nitrogen,T=T_g_avg,P=101)*0.7149)/1000
mu_g=Viscosity(CarbonDioxide,T=T_g_avg,P=101)*0.1984+Viscosity(Water,T=T_g_avg,P=101)*0.0826+
Viscosity(Nitrogen,T=T_g_avg,P=101)*0.7149
Pr_g=Prandtl(CarbonDioxide,T=T_g_avg,P=101)*0.1984+Prandtl(Water,T=T_g_avg,P=101)*0.0826+Pra
ndtl(Nitrogen,T=T_g_avg,P=101)*0.7149

"CO_2"
P_1=P1
T_1=T1
h_1=Enthalpy(R$,T=T_1,P=P_1)
s_1=Entropy(R$,T=T_1,P=P_1)

s_2=s_1
P_2=P_3
h_2s=Enthalpy(R$,s=s_2,P=P_2)
h_2=h_1-etta_t*(h_1-h_2s)
T_2=Temperature(R$,P=P_2,h=h_2)


T_3=T_w+pinch
P_3=P_sat(R$,T=T_3)
h_3=Enthalpy(R$,T=T_3,x=0)
v_3=Volume(R$,T=T_3,x=0)

P_4=P_1
h_4=v_3*(P_4-P_3)/etta_p+h_3
T_4=Temperature(R$,h=h_4,P=P_4)

"Evaporator"
Q_in=m_dot_g*cp_g*(T_gi-T_go)
m_dot_CO2=Q_in/(h_1-h_4)

"Work Output"
W_t=m_dot_CO2*(h_1-h_2)
W_p=m_dot_CO2*(h_4-h_3)
W_net=W_t*etta_g-W_p
```

```
eff=W_net/Q_in*100

h_sat=Enthalpy(R$,x=1,P=P_2)

"Condenser1"
T_avg=(T_2+T_3)/2
mu_CO2_1=Viscosity(R$,T=T_avg,P=P_2)
Re_CO2_1=4*m_dot_CO2/(3.14*D*mu_CO2_1)
Pr_CO2_1=Prandtl(R$,T=T_avg,P=P_2)
Nu_CO2_1=0.023*Re_CO2_1^0.8*Pr_CO2_1^0.3
K_CO2_1=Conductivity(R$,T=T_avg,P=P_2)/1000
h_CO2_1=Nu_CO2_1*K_CO2_1/D


Pr_w=Prandtl(Water,T=T_w,P=101)
v=Viscosity(Water,T=T_w,P=101)/Density(Water,T=T_w,P=101)
T_s_1=(T_avg+T_w)/2
B_1=1/((T_s_1+T_w)/2+273)
K_w=Conductivity(Water,T=T_w,P=101)/1000

"Characteristic length: Coil length"
Ra_w_1=g*B_1*(T_s_1-T_w)*L_coil_1^3*Pr_w/v^2
Nu_w_1=(g*B_1*(T_s_1-T_w)*L_coil_1^3*Pr_w/v^2)^0.3071*(H_coil_1/D_coil)^(-0.1097)
h_w_1=Nu_w_1*K_w/L_coil_1

dtlm=(T_2-T_3)/(ln((T_2-T_w)/(T_3-T_w)))

Q_out_1=m_dot_CO2*(h_2-h_sat)

h_w_1*h_CO2_1/(h_w_1+h_CO2_1)*3.14*L_1*D*dtlm=Q_out_1

L_1=n_coil_1*D_coil
L_coil_1=n_coil_1*(p_coil^2+3.14^2*D_coil^2)^0.5
H_coil_1=(n_coil_1+1)*D+n_coil_1*p_coil

"Condenser2"
mu_CO2_L=Viscosity(R$,x=0,P=P_2)
mu_CO2_v=Viscosity(R$,x=1,P=P_2)
mu_CO2_2=(mu_CO2_L+mu_CO2_v)/2
Re_CO2_2=4*m_dot_CO2/(3.14*D*mu_CO2_2)
Pr_CO2_L=Prandtl(R$,x=0,P=P_2)
Pr_CO2_v=Prandtl(R$,x=1,P=P_2)
Pr_CO2_2=(Pr_CO2_L+Pr_CO2_v)/2
Nu_CO2_2=0.023*Re_CO2_2^0.8*Pr_CO2_2^0.3
K_CO2_L=Conductivity(R$,x=0,P=P_2)/1000
K_CO2_v=Conductivity(R$,x=1,P=P_2)/1000
K_CO2_2=(K_CO2_L+K_CO2_v)/2
h_CO2_2=Nu_CO2_2*K_CO2_2/D

T_s_2=(T_3+T_w)/2
B_2=1/((T_s_2+T_w)/2+273)

"Characteristic length: Coil length"
Ra_w_2=g*B_2*(T_s_2-T_w)*L_coil_2^3*Pr_w/v^2
Nu_w_2=(g*B_2*(T_s_2-T_w)*L_coil_2^3*Pr_w/v^2)^0.3071*(H_coil_2/D_coil)^(-0.1097)
h_w_2=Nu_w_2*K_w/L_coil_2
```

```
Q_out_2=m_dot_CO2*(h_sat-h_3)

h_w_2*h_CO2_2/(h_w_2+h_CO2_2)*3.14*L_2*D*(T_3-T_w)=Q_out_2

L_2=n_coil_2*D_coil
L_coil_2=n_coil_2*(p_coil^2+3.14^2*D_coil^2)^0.5
H_coil_2=(n_coil_2+1)*D+n_coil_1*p_coil

L_con=L_1+L_2

"Evaporator"
d_h=(D_g^2-D^2)/(D_g+D)
Re_g=4*m_dot_g/(3.14*d_h*mu_g)
Nu_g=0.023*Re_g^0.8*Pr_g^0.3
h_g=Nu_g*K_g/d_h

mu_CO2_e_1=Viscosity(R$,P=P_1,T=T_4)
mu_CO2_e_2=Viscosity(R$,P=P_1,T=T_1)
mu_CO2=(mu_CO2_e_1+mu_CO2_e_2)/2
Re_CO2=4*m_dot_CO2/(3.14*D*mu_CO2)
Pr_e_1=Prandtl(R$,P=P_1,T=T_4)
Pr_e_2=Prandtl(R$,P=P_1,T=T_1)
Pr_CO2=(Pr_e_1+Pr_e_2)/2
Nu_CO2=0.023*Re_CO2^0.8*Pr_CO2^0.4
K_CO2_e_1=Conductivity(R$,P=P_1,T=T_4)/1000
K_CO2_e_2=Conductivity(R$,P=P_1,T=T_1)/1000
K_CO2=(K_CO2_e_1+K_CO2_e_2)/2
h_CO2=Nu_CO2*K_CO2/D

U_e=h_g*h_CO2/(h_g+h_CO2)
dt1=T_gi-T_1
dt2=T_go-T_4
dtlm_e=(dt1-dt2)/ln(dt1/dt2)
A_e=3.14*D*L_evap
Q_in=U_e*A_e*dtlm_e

H_coil=H_coil_1+H_coil_2
```

## A.2 Effect of pressure drop

### A.2.1 Ideal direct ground cooling

```
etta_p=0.8        "Pump Efficiency"
etta_t=0.7        "Turbine Efficiency"
etta_g=0.9      "generator efficiency"
g=9.81
R$='CarbonDioxide'

"Gas"
m_dot_g=mg/3600
T_gi=Tgi
T_go=Tgo
T_g_avg=(Tgi+Tgo)/2
```

```
cp_g=Cp(CarbonDioxide,T=T_g_avg,P=101)*0.1984+Cp(Water,T=T_g_avg,P=101)*0.0826+Cp(Nitrogen,
T=T_g_avg,P=101)*0.7149
K_g=(Conductivity(CarbonDioxide,T=T_g_avg,P=101)*0.1984+Conductivity(Water,T=T_g_avg,P=101)*0.
0826+Conductivity(Nitrogen,T=T_g_avg,P=101)*0.7149)/1000
mu_g=Viscosity(CarbonDioxide,T=T_g_avg,P=101)*0.1984+Viscosity(Water,T=T_g_avg,P=101)*0.0826+
Viscosity(Nitrogen,T=T_g_avg,P=101)*0.7149
Pr_g=Prandtl(CarbonDioxide,T=T_g_avg,P=101)*0.1984+Prandtl(Water,T=T_g_avg,P=101)*0.0826+Pra
ndtl(Nitrogen,T=T_g_avg,P=101)*0.7149

"CO_2"
P_1=P1
T_1=T1
h_1=Enthalpy(R$,T=T_1,P=P_1)
s_1=Entropy(R$,T=T_1,P=P_1)

s_2=s_1
P_2=P_3
h_2s=Enthalpy(R$,s=s_2,P=P_2)
h_2=h_1-etta_t*(h_1-h_2s)
T_2=Temperature(R$,P=P_2,h=h_2)

T_3=T3
P_3=P_sat(R$,T=T_3)
h_3=Enthalpy(R$,T=T_3,x=0)
v_3=Volume(R$,T=T_3,x=0)

P_4=P_1
h_4=v_3*(P_4-P_3)/etta_p+h_3
T_4=Temperature(R$,h=h_4,P=P_4)

"Boiler"
Q_in=m_dot_g*cp_g*(T_gi-T_go)
m_dot_CO2=Q_in/(h_1-h_4)

"Work Output"
W_t=m_dot_CO2*(h_1-h_2)
W_p=m_dot_CO2*(h_4-h_3)
W_net=(W_t-W_p)*etta_g
eff=W_net/Q_in*100

h_sat=Enthalpy(R$,x=1,P=P_2)

"Condenser1"
T_avg=(T_2+T_3)/2
mu_CO2_1=Viscosity(R$,T=T_avg,P=P_2)
Re_CO2_1=4*m_dot_CO2/(3.14*D*mu_CO2_1)
Pr_CO2_1=Prandtl(R$,T=T_avg,P=P_2)
Nu_CO2_1=0.023*Re_CO2_1^0.8*Pr_CO2_1^0.3
K_CO2_1=Conductivity(R$,T=T_avg,P=P_2)/1000
h_CO2_1=Nu_CO2_1*K_CO2_1/D

T_s_1=(T_2+T_g)/2
T_s_2=(T_3+T_g)/2

"Horizontal"
dtlm=(T_2-T_s_1-T_3+T_s_2)/(ln((T_2-T_s_1)/(T_3-T_s_2)))
Q_out_1=m_dot_CO2*(h_2-h_sat)
```

```
h_CO2_1*3.14*L_h_1*D*dtlm=Q_out_1

"Condenser2"
mu_CO2_L=Viscosity(R$,x=0,P=P_2)
mu_CO2_v=Viscosity(R$,x=1,P=P_2)
mu_CO2_2=(mu_CO2_L+mu_CO2_v)/2
Re_CO2_2=4*m_dot_CO2/(3.14*D*mu_CO2_2)
Pr_CO2_L=Prandtl(R$,x=0,P=P_2)
Pr_CO2_v=Prandtl(R$,x=1,P=P_2)
Pr_CO2_2=(Pr_CO2_L+Pr_CO2_v)/2
Nu_CO2_2=0.023*Re_CO2_2^0.8*Pr_CO2_2^0.3
K_CO2_L=Conductivity(R$,x=0,P=P_2)/1000
K_CO2_v=Conductivity(R$,x=1,P=P_2)/1000
K_CO2_2=(K_CO2_L+K_CO2_v)/2
h_CO2_2=Nu_CO2_2*K_CO2_2/D

"Horizontal"
Q_out_2=m_dot_CO2*(h_sat-h_3)
h_CO2_2*3.14*L_h_2*D*(T_3-T_s_2)=Q_out_2
L_h=L_h_1+L_h_2

"Evaporator"
d_h=(D_g^2-D^2)/(D_g+D)
Re_g=4*m_dot_g/(3.14*d_h*mu_g)
Nu_g=0.023*Re_g^0.8*Pr_g^0.3
h_g=Nu_g*K_g/d_h

mu_CO2_e_1=Viscosity(R$,P=P_1,T=T_4)
mu_CO2_e_2=Viscosity(R$,P=P_1,T=T_1)
mu_CO2=(mu_CO2_e_1+mu_CO2_e_2)/2
Re_CO2=4*m_dot_CO2/(3.14*D*mu_CO2)
Pr_e_1=Prandtl(R$,P=P_1,T=T_4)
Pr_e_2=Prandtl(R$,P=P_1,T=T_1)
Pr_CO2=(Pr_e_1+Pr_e_2)/2
Nu_CO2=0.023*Re_CO2^0.8*Pr_CO2^0.4
K_CO2_e_1=Conductivity(R$,P=P_1,T=T_4)/1000
K_CO2_e_2=Conductivity(R$,P=P_1,T=T_1)/1000
K_CO2=(K_CO2_e_1+K_CO2_e_2)/2
h_CO2=Nu_CO2*K_CO2/D

U_e=h_g*h_CO2/(h_g+h_CO2)
dt1=T_gi-T_1
dt2=T_go-T_4
dtlm_e=(dt1-dt2)/ln(dt1/dt2)
A_e=3.14*D*L_evap
Q_in=U_e*A_e*dtlm_e
```

### A.2.2 Considering pressure drop in the condenser

```
subprogram f(R$,s_2,P_3,P_2,P_2s,m_dot_CO2,Q_in,W_p,D,T_g,T_3,h_1,h_3,ee :
L_h,L_h_1,L_h_2,T_avg,W_net,T_2,fr1,fr2)

etta_t=0.7        "Turbine Efficiency"
etta_g=0.9     "generator efficiency"
g=9.81
```

```
h_2s=Enthalpy(R$,s=s_2,P=P_2)
h_2=h_1-etta_t*(h_1-h_2s)
T_2=Temperature(R$,P=P_2,h=h_2)

W_t=m_dot_CO2*(h_1-h_2)
W_net=(W_t-W_p)*etta_g
eff=W_net/Q_in*100

T_2s=T_sat(R$,P=P_2s)
h_sat=Enthalpy(R$,x=1,P=P_2s)

"Condenser1"
T_avg=(T_2+T_2s)/2
Pavg=(P_2+P_2s)/2
mu_CO2_1=Viscosity(R$,T=T_avg,P=Pavg)
Re_CO2_1=4*m_dot_CO2/(3.14*D*mu_CO2_1)
Pr_CO2_1=Prandtl(R$,T=T_avg,P=Pavg)
Nu_CO2_1=0.023*Re_CO2_1^0.8*Pr_CO2_1^0.3
K_CO2_1=Conductivity(R$,T=T_avg,P=Pavg)/1000
h_CO2_1=Nu_CO2_1*K_CO2_1/D

T_s_1=(T_2+T_g)/2
T_s_2=(T_2s+T_g)/2
T_s_3=((T_2s+T_3)/2+T_g)/2

"Horizontal"
dtlm=(T_2-T_s_1-T_2s+T_s_2)/(ln((T_2-T_s_1)/(T_2s-T_s_2)))
Q_out_1=m_dot_CO2*(h_2-h_sat)
h_CO2_1*3.14*L_h_1*D*dtlm=Q_out_1

"Condenser2"
Pavg2=(P_2s+P_3)/2
mu_CO2_L=Viscosity(R$,x=0,P=P_3)
mu_CO2_v=Viscosity(R$,x=1,P=P_2s)
mu_CO2_2=(mu_CO2_L+mu_CO2_v)/2
Re_CO2_2=4*m_dot_CO2/(3.14*D*mu_CO2_2)
Pr_CO2_L=Prandtl(R$,x=0,P=P_3)
Pr_CO2_v=Prandtl(R$,x=1,P=P_2s)
Pr_CO2_2=(Pr_CO2_L+Pr_CO2_v)/2
Nu_CO2_2=0.023*Re_CO2_2^0.8*Pr_CO2_2^0.3
K_CO2_L=Conductivity(R$,x=0,P=P_3)/1000
K_CO2_v=Conductivity(R$,x=1,P=P_2s)/1000
K_CO2_2=(K_CO2_L+K_CO2_v)/2
h_CO2_2=Nu_CO2_2*K_CO2_2/D

Q_out_2=m_dot_CO2*(h_sat-h_3)
h_CO2_2*3.14*L_h_2*D*(T_3-T_s_3)=Q_out_2

L_h=L_h_1+L_h_2
fr1=0.316/Re_CO2_1^0.25
fr2=0.316/Re_CO2_2^0.25
end

Procedure g(R$,s_2,P_3,m_dot_CO2,Q_in,W_p,D,T_g,T_3,h_1,h_3,ee : L_h,dp,W_net,P_2,T_2)
P_2=P_3
P_2s=P_3
Lr=0
```

```
Repeat
call f(R$,s_2,P_3,P_2,P_2s,m_dot_CO2,Q_in,W_p,D,T_g,T_3,h_1,h_3,ee :
L_h,L_h_1,L_h_2,T_avg,W_net,T_2,fr1,fr2)
v_CO2_1=m_dot_CO2/(Density(CarbonDioxide,P=(P_2s+P_3)/2,x=0.5)*3.14*D^2/4)
dp1=Density(CarbonDioxide,P=(P_2s+P_3)/2,x=0.5)*fr1*L_h_1*v_CO2_1^2/(2*D)
v_CO2_2=m_dot_CO2/(Density(CarbonDioxide,P=(P_2+P_2s)/2,T=T_avg)*3.14*D^2/4)
dp2=Density(CarbonDioxide,P=(P_2+P_2s)/2,T=T_avg)*fr2*L_h_1*v_CO2_2^2/(2*D)
dp=dp1+dp2
dl=Lr-L_h
Lr=L_h
P_2s=P_3+dp1/1000
P_2=P_2s+dp2/1000
until (dl<0.01) and (dl>0)
end

etta_p=0.8        "Pump Efficiency"
g=9.81
R$='CarbonDioxide'

"Gas"
m_dot_g=mg/3600
T_gi=Tgi
T_go=Tgo
T_g_avg=(Tgi+Tgo)/2
cp_g=Cp(CarbonDioxide,T=T_g_avg,P=101)*0.1984+Cp(Water,T=T_g_avg,P=101)*0.0826+Cp(Nitrogen,
T=T_g_avg,P=101)*0.7149
K_g=(Conductivity(CarbonDioxide,T=T_g_avg,P=101)*0.1984+Conductivity(Water,T=T_g_avg,P=101)*0.
0826+Conductivity(Nitrogen,T=T_g_avg,P=101)*0.7149)/1000
mu_g=Viscosity(CarbonDioxide,T=T_g_avg,P=101)*0.1984+Viscosity(Water,T=T_g_avg,P=101)*0.0826+
Viscosity(Nitrogen,T=T_g_avg,P=101)*0.7149
Pr_g=Prandtl(CarbonDioxide,T=T_g_avg,P=101)*0.1984+Prandtl(Water,T=T_g_avg,P=101)*0.0826+Pra
ndtl(Nitrogen,T=T_g_avg,P=101)*0.7149

"CO_2"
P_1=P1
T_1=T1
h_1=Enthalpy(R$,T=T_1,P=P_1)
s_1=Entropy(R$,T=T_1,P=P_1)

s_2=s_1

T_3=T3
P_3=P_sat(R$,T=T_3)
h_3=Enthalpy(R$,T=T_3,x=0)
v_3=Volume(R$,T=T_3,x=0)

P_4=P_1
h_4=v_3*(P_4-P_3)/etta_p+h_3
T_4=Temperature(R$,h=h_4,P=P_4)

"Boiler"
Q_in=m_dot_g*cp_g*(T_gi-T_go)
m_dot_CO2=Q_in/(h_1-h_4)

ee=0
call g(R$,s_2,P_3,m_dot_CO2,Q_in,W_p,D,T_g,T_3,h_1,h_3,ee : L_h,dp,W_net,P_2,T_2)
W_p=m_dot_CO2*(h_4-h_3)
```

```
Wreal=W_net
Lcondenser=L_h
eff=W_net/Q_in*100

"Evaporator"
d_h=(D_g^2-D^2)/(D_g+D)
Re_g=4*m_dot_g/(3.14*d_h*mu_g)
Nu_g=0.023*Re_g^0.8*Pr_g^0.3
h_g=Nu_g*K_g/d_h

mu_CO2_e_1=Viscosity(R$,P=P_1,T=T_4)
mu_CO2_e_2=Viscosity(R$,P=P_1,T=T_1)
mu_CO2=(mu_CO2_e_1+mu_CO2_e_2)/2
Re_CO2=4*m_dot_CO2/(3.14*D*mu_CO2)
Pr_e_1=Prandtl(R$,P=P_1,T=T_4)
Pr_e_2=Prandtl(R$,P=P_1,T=T_1)
Pr_CO2=(Pr_e_1+Pr_e_2)/2
Nu_CO2=0.023*Re_CO2^0.8*Pr_CO2^0.4
K_CO2_e_1=Conductivity(R$,P=P_1,T=T_4)/1000
K_CO2_e_2=Conductivity(R$,P=P_1,T=T_1)/1000
K_CO2=(K_CO2_e_1+K_CO2_e_2)/2
h_CO2=Nu_CO2*K_CO2/D

U_e=h_g*h_CO2/(h_g+h_CO2)
dt1=T_gi-T_1
dt2=T_go-T_4
dtlm_e=(dt1-dt2)/ln(dt1/dt2)
A_e=3.14*D*L_evap
Q_in=U_e*A_e*dtlm_e
```

### A.2.3 Direct ground cooling

```
subprogram f(R$,P_3,P_2,P_2s,Q_in,D,T_g,T_3,h_3,ee,P_1,Tgi,Tgo,m_dot_g,D_g,h_4,T_1,T_4,P_4 :
L_h,L_h_1,L_h_2,T_avg,W_net,T_2,fr1,fr2,fre,L_evap,m_dot_CO2)

T_g_avg=(Tgi+Tgo)/2
cp_g=Cp(CarbonDioxide,T=T_g_avg,P=101)*0.1984+Cp(Water,T=T_g_avg,P=101)*0.0826+Cp(Nitrogen,
T=T_g_avg,P=101)*0.7149
K_g=(Conductivity(CarbonDioxide,T=T_g_avg,P=101)*0.1984+Conductivity(Water,T=T_g_avg,P=101)*0.
0826+Conductivity(Nitrogen,T=T_g_avg,P=101)*0.7149)/1000
mu_g=Viscosity(CarbonDioxide,T=T_g_avg,P=101)*0.1984+Viscosity(Water,T=T_g_avg,P=101)*0.0826+
Viscosity(Nitrogen,T=T_g_avg,P=101)*0.7149
Pr_g=Prandtl(CarbonDioxide,T=T_g_avg,P=101)*0.1984+Prandtl(Water,T=T_g_avg,P=101)*0.0826+Pra
ndtl(Nitrogen,T=T_g_avg,P=101)*0.7149

h_1=Enthalpy(R$,T=T_1,P=P_1)
s_1=Entropy(R$,T=T_1,P=P_1)

s_2=s_1
m_dot_CO2=Q_in/(h_1-h_4)
W_p=m_dot_CO2*(h_4-h_3)
etta_t=0.7          "Turbine Efficiency"
etta_g=0.9      "generator efficiency"
g=9.81
```

```
h_2s=Enthalpy(R$,s=s_2,P=P_2)
h_2=h_1-etta_t*(h_1-h_2s)
T_2=Temperature(R$,P=P_2,h=h_2)

W_t=m_dot_CO2*(h_1-h_2)
W_net=(W_t-W_p)*etta_g
eff=W_net/Q_in*100

T_2s=T_sat(R$,P=P_2s)
h_sat=Enthalpy(R$,x=1,P=P_2s)

"Condenser1"
T_avg=(T_2+T_2s)/2
Pavg=(P_2+P_2s)/2
mu_CO2_1=Viscosity(R$,T=T_avg,P=Pavg)
Re_CO2_1=4*m_dot_CO2/(3.14*D*mu_CO2_1)
Pr_CO2_1=Prandtl(R$,T=T_avg,P=Pavg)
Nu_CO2_1=0.023*Re_CO2_1^0.8*Pr_CO2_1^0.3
K_CO2_1=Conductivity(R$,T=T_avg,P=Pavg)/1000
h_CO2_1=Nu_CO2_1*K_CO2_1/D

T_s_1=(T_2+T_g)/2
T_s_2=(T_2s+T_g)/2
T_s_3=((T_2s+T_3)/2+T_g)/2

"Horizontal"
dtlm=(T_2-T_s_1-T_2s+T_s_2)/(ln((T_2-T_s_1)/(T_2s-T_s_2)))
Q_out_1=m_dot_CO2*(h_2-h_sat)
h_CO2_1*3.14*L_h_1*D*dtlm=Q_out_1

"Condenser2"
Pavg2=(P_2s+P_3)/2
mu_CO2_L=Viscosity(R$,x=0,P=P_3)
mu_CO2_v=Viscosity(R$,x=1,P=P_2s)
mu_CO2_2=(mu_CO2_L+mu_CO2_v)/2
Re_CO2_2=4*m_dot_CO2/(3.14*D*mu_CO2_2)
Pr_CO2_L=Prandtl(R$,x=0,P=P_3)
Pr_CO2_v=Prandtl(R$,x=1,P=P_2s)
Pr_CO2_2=(Pr_CO2_L+Pr_CO2_v)/2
Nu_CO2_2=0.023*Re_CO2_2^0.8*Pr_CO2_2^0.3
K_CO2_L=Conductivity(R$,x=0,P=P_3)/1000
K_CO2_v=Conductivity(R$,x=1,P=P_2s)/1000
K_CO2_2=(K_CO2_L+K_CO2_v)/2
h_CO2_2=Nu_CO2_2*K_CO2_2/D

Q_out_2=m_dot_CO2*(h_sat-h_3)
h_CO2_2*3.14*L_h_2*D*(T_3-T_s_3)=Q_out_2

L_h=L_h_1+L_h_2
fr1=0.316/Re_CO2_1^0.25
fr2=0.316/Re_CO2_2^0.25

"Evaporator"
d_h=(D_g^2-D^2)/(D_g+D)
Re_g=4*m_dot_g/(3.14*d_h*mu_g)
Nu_g=0.023*Re_g^0.8*Pr_g^0.3
h_g=Nu_g*K_g/d_h
```

```
mu_CO2_e_1=Viscosity(R$,P=P_4,T=T_4)
mu_CO2_e_2=Viscosity(R$,P=P_1,T=T_1)
mu_CO2=(mu_CO2_e_1+mu_CO2_e_2)/2
Re_CO2=4*m_dot_CO2/(3.14*D*mu_CO2)
Pr_e_1=Prandtl(R$,P=P_4,T=T_4)
Pr_e_2=Prandtl(R$,P=P_1,T=T_1)
Pr_CO2=(Pr_e_1+Pr_e_2)/2
Nu_CO2=0.023*Re_CO2^0.8*Pr_CO2^0.4
K_CO2_e_1=Conductivity(R$,P=P_4,T=T_4)/1000
K_CO2_e_2=Conductivity(R$,P=P_1,T=T_1)/1000
K_CO2=(K_CO2_e_1+K_CO2_e_2)/2
h_CO2=Nu_CO2*K_CO2/D

U_e=h_g*h_CO2/(h_g+h_CO2)
dt1=Tgi-T_1
dt2=Tgo-T_4
dtlm_e=(dt1-dt2)/ln(dt1/dt2)
A_e=3.14*D*L_evap
Q_in=U_e*A_e*dtlm_e

fre=0.316/Re_CO2^0.25
end

Procedure g(R$,P_3,Q_in,D,T_g,T_3,h_3,ee,Tgi,Tgo,m_dot_g,D_g,h_4,P_4,T_1,T_4 :
L_h,dp,W_net,P_2,T_2,L_evap,m_dot_CO2)
P_2=P_3
P_2s=P_3
P_1=P_4
Lr=0
Repeat
call f(R$,P_3,P_2,P_2s,Q_in,D,T_g,T_3,h_3,ee,P_1,Tgi,Tgo,m_dot_g,D_g,h_4,T_1,T_4,P_4 :
L_h,L_h_1,L_h_2,T_avg,W_net,T_2,fr1,fr2,fre,L_evap,m_dot_CO2)
v_CO2_1=m_dot_CO2/(Density(CarbonDioxide,P=(P_2s+P_3)/2,x=0.5)*3.14*D^2/4)
dp1=Density(CarbonDioxide,P=(P_2s+P_3)/2,x=0.5)*fr1*L_h_1*v_CO2_1^2/(2*D)
v_CO2_2=m_dot_CO2/(Density(CarbonDioxide,P=(P_2+P_2s)/2,T=T_avg)*3.14*D^2/4)
dp2=Density(CarbonDioxide,P=(P_2+P_2s)/2,T=T_avg)*fr2*L_h_1*v_CO2_2^2/(2*D)
dp=dp1+dp2
v_CO2_e=m_dot_CO2/(Density(CarbonDioxide,P=(P_1+P_4)/2,T=(Tgi+Tgo)/2)*3.14*D^2/4)
dpe=Density(CarbonDioxide,P=(P_1+P_4)/2,T=(Tgi+Tgo)/2)*fre*L_evap*v_CO2_e^2/(2*D)
dl=Lr-L_h
Lr=L_h
P_2s=P_3+dp1/1000
P_2=P_2s+dp2/1000
P_1=P_4-dpe/1000
until (dl<0.01) and (dl>0)
end

etta_p=0.8        "Pump Efficiency"
g=9.81
R$='CarbonDioxide'

"Gas"
m_dot_g=mg/3600
T_gi=Tgi
T_go=Tgo
T_g_avg=(Tgi+Tgo)/2
```

```
cp_g=Cp(CarbonDioxide,T=T_g_avg,P=101)*0.1984+Cp(Water,T=T_g_avg,P=101)*0.0826+Cp(Nitrogen,
T=T_g_avg,P=101)*0.7149

"CO_2"
P_4=P1
T_1=T1
T_3=T3
P_3=P_sat(R$,T=T_3)
h_3=Enthalpy(R$,T=T_3,x=0)
v_3=Volume(R$,T=T_3,x=0)

"P_4=P_1"
h_4=v_3*(P_4-P_3)/etta_p+h_3
T_4=Temperature(R$,h=h_4,P=P_4)

"Boiler"
Q_in=m_dot_g*cp_g*(T_gi-T_go)
ee=0
call g(R$,P_3,Q_in,D,T_g,T_3,h_3,ee,Tgi,Tgo,m_dot_g,D_g,h_4,P_4,T_1,T_4 :
L_h,dp,W_net,P_2,T_2,L_evap,m_dot_CO2)
Wreal=W_net
Lcondenser=L_h
eff=W_net/Q_in*100
```

## A.3 Working fluid selection

### A.3.1 Basic organic Rankine cycle

```
etta_p=0.8        "Pump Efficiency"
etta_t=0.7        "Turbine Efficiency"
etta_g=0.9      "generator efficiency"
g=9.81
"R$='Fluid'"

"Gas"
m_dot_g=mg/3600
T_gi=Tgi
T_go=Tgo
T_g_avg=(Tgi+Tgo)/2
cp_g=Cp(CarbonDioxide,T=T_g_avg,P=101)*0.1984+Cp(Water,T=T_g_avg,P=101)*0.0826+Cp(Nitrogen,
T=T_g_avg,P=101)*0.7149

"R$"
P_1=P1
T_1=T1
h_1=Enthalpy(R$,T=T_1,P=P_1)
s_1=Entropy(R$,T=T_1,P=P_1)

s_2=s_1
P_2=P_3
h_2s=Enthalpy(R$,s=s_2,P=P_2)
h_2=h_1-etta_t*(h_1-h_2s)
T_2=Temperature(R$,P=P_2,h=h_2)
```

```
T_3=T_w+pinch
P_3=P_sat(R$,T=T_3)
h_3=Enthalpy(R$,T=T_3,x=0)
v_3=Volume(R$,T=T_3,x=0)

P_4=P_1
h_4=v_3*(P_4-P_3)/etta_p+h_3
T_4=Temperature(R$,h=h_4,P=P_4)

"Evaporator"
Q_in=m_dot_g*cp_g*(T_gi-T_go)
m_dot_f=Q_in/(h_1-h_4)

"Work Output"
W_t=m_dot_f*(h_1-h_2)
W_p=m_dot_f*(h_4-h_3)
W_net=W_t*etta_g-W_p
eff=W_net/Q_in*100

Q_rej=m_dot_f*(h_2-h_3)
```

### A.3.2 Regenerative cycle

```
etta_p=0.8        "Pump Efficiency"
etta_t=0.7        "Turbine Efficiency"
etta_g=0.9      "generator efficiency"
etta_r=0.8
g=9.81
"R$='Fluid'"

"Gas"
m_dot_g=mg/3600
T_gi=Tgi
T_go=Tgo
T_g_avg=(Tgi+Tgo)/2
cp_g=Cp(CarbonDioxide,T=T_g_avg,P=101)*0.1984+Cp(Water,T=T_g_avg,P=101)*0.0826+Cp(Nitrogen,
T=T_g_avg,P=101)*0.7149

"R$"
P_1=P1
T_1=T1
h_1=Enthalpy(R$,T=T_1,P=P_1)
s_1=Entropy(R$,T=T_1,P=P_1)

s_2=s_1
P_2=P_3
h_2s=Enthalpy(R$,s=s_2,P=P_2)
h_2=h_1-etta_t*(h_1-h_2s)
T_2=Temperature(R$,P=P_2,h=h_2)

T_3=T_w+pinch
P_3=P_sat(R$,T=T_3)
h_3=Enthalpy(R$,T=T_3,x=0)
v_3=Volume(R$,T=T_3,x=0)
```

```
P_4=P_1
h_4=v_3*(P_4-P_3)/etta_p+h_3
T_4=Temperature(R$,h=h_4,P=P_4)

"Regenerator"
T_44=T_2-30
h_44=Enthalpy(R$, T=T_44, P=P_1)
h_22=h_2-etta_r*(h_44-h_4)
T_22=Temperature(R$, h=h_22, P=P_2)


"Evaporator"
Q_in=m_dot_g*cp_g*(T_gi-T_go)
m_dot_f=Q_in/(h_1-h_44)

"Work Output"
W_t=m_dot_f*(h_1-h_2)
W_p=m_dot_f*(h_4-h_3)
W_net=W_t*etta_g-W_p
eff=W_net/Q_in*100

Q_rej=m_dot_f*(h_22-h_3)
```

## A.4 Ground loop sizing

```
P_w=101
cp_w=Cp(Water,T=T_wa,P=P_w)
mu_w1=Viscosity(Water,T=T_wa,P=P_w)
Re_w1=4*m_w/(3.14*Dh*mu_w1)
Pr_w1=Prandtl(Water,T=T_wa,P=P_w)
Nu_w1=0.023*Re_w1^0.8*Pr_w1^0.4
K_w1=Conductivity(Water,T=T_wa,P=P_w)/1000
h_w1=Nu_w1*K_w1/Dh

kp=0.5
kpcm=0.2
ks=2

rin=0.032/2
ro=rin+0.0023
roo=ro+0.0023
rooo=0.32

R1=1/(h_w1*3.14*Dh*L*1000)
R2=ln(ro/rin)/(2*3.14*kp*L)
R3=ln(roo/ro)/(2*3.14*kpcm*L)
R4=ln(rooo/roo)/(2*3.14*ks*L)

Req=R1+R2+R3+R4

dt1=6
dt2=2
dtlm=(dt1-dt2)/ln(dt1/dt2)
```

```
Qrej=m_w*cp_w*4
dtlm/Req=Qrej*1000
```

## A.5 Application

### A.5.1 Basic organic Rankine cycle

```
etta_p=0.9        "Pump Efficiency"
etta_t=0.7        "Turbine Efficiency"
etta_g=0.9      "generator efficiency"
g=9.81
"R$='Fluid'"

"Gas"
m_dot_g=mg/3600
T_gi=Tgi
T_go=Tgo
cp_g=1.063

"R123"
P_1=P1
T_1=T1
h_1=Enthalpy(R$,T=T_1,P=P_1)
s_1=Entropy(R$,T=T_1,P=P_1)

s_2=s_1
P_2=P_3
h_2s=Enthalpy(R$,s=s_2,P=P_2)
h_2=h_1-etta_t*(h_1-h_2s)
T_2=Temperature(R$,P=P_2,h=h_2)


T_3=T_w+pinch
P_3=P_sat(R$,T=T_3)
h_3=Enthalpy(R$,T=T_3,x=0)
v_3=Volume(R$,T=T_3,x=0)
h_31=Enthalpy(R$,T=T_3,x=1)

P_4=P_1
h_4=v_3*(P_4-P_3)/etta_p+h_3
T_4=Temperature(R$,h=h_4,P=P_4)

"Evaporator"
Q_in=m_dot_g*cp_g*(T_gi-T_go)
m_dot_f=Q_in/(h_1-h_4)

"Work Output"
W_t=m_dot_f*(h_1-h_2)
rho_2=Density(R$,P=P_2,h=h_2)
Q_2=m_dot_f/rho_2
sH=(h_1-h_2)*1000
Ns=0.58
N=60*Ns*sH^(3/4)/(2*3.14*Q_2^0.5)
```

```
W_p=m_dot_f*(h_4-h_3)
W_net=W_t*etta_g-W_p-Wpump
eff=W_net/Q_in*100

Q_rej=m_dot_f*(h_2-h_3)

T_w_1=T_3-2
T_w_2=T_3-6
Q_rej=m_dot_w*4.18*(T_w_1-T_w_2)

D=0.032
A=3.14*D^2/4
v=m_dot_w/(1000*A)
Vis=Viscosity(Water,T=T_w+4,P=101)

Re=1000*v*D/Vis
f=0.316/Re^0.25
l=1423    "GHE Length"
dP=f*l*v^2/(2*D)
Wpump=dP*v*A
Q=v*A
```

### A.5.2 Regenerative cycle

```
etta_p=0.9        "Pump Efficiency"
etta_t=0.7        "Turbine Efficiency"
etta_g=0.9      "generator efficiency"
etta_r=0.8
g=9.81
"R$='Fluid'"

"Gas"
m_dot_g=mg/3600
T_gi=Tgi
T_go=Tgo
T_g_avg=(Tgi+Tgo)/2
cp_g=1.063

"R123"
P_1=P1
T_1=T1
h_1=Enthalpy(R$,T=T_1,P=P_1)
s_1=Entropy(R$,T=T_1,P=P_1)

s_2=s_1
P_2=P_3
h_2s=Enthalpy(R$,s=s_2,P=P_2)
h_2=h_1-etta_t*(h_1-h_2s)
T_2=Temperature(R$,P=P_2,h=h_2)

T_3=T_w+pinch
P_3=P_sat(R$,T=T_3)
h_3=Enthalpy(R$,T=T_3,x=0)
v_3=Volume(R$,T=T_3,x=0)

P_4=P_1
```

```
h_4=v_3*(P_4-P_3)/etta_p+h_3
T_4=Temperature(R$,h=h_4,P=P_4)

"Regenerator"
T_44=T_2-30
h_44=Enthalpy(R$, T=T_44, P=P_1)
h_22=h_2-etta_r*(h_44-h_4)
T_22=Temperature(R$, h=h_22, P=P_2)


"Evaporator"
Q_in=m_dot_g*cp_g*(T_gi-T_go)
m_dot_f=Q_in/(h_1-h_44)

"Work Output"
W_t=m_dot_f*(h_1-h_2)
W_p=m_dot_f*(h_4-h_3)
W_net=W_t*etta_g-W_p-Wpump
eff=W_net/Q_in*100

Q_rej=m_dot_f*(h_22-h_3)

D=0.032
A=3.14*D^2/4
v=m_dot_w/(1000*A)
Vis=Viscosity(Water,T=T_w+4,P=101)

Re=1000*v*D/Vis
f=0.316/Re^0.25
l=1423     "GHE length"
dP=f*l*v^2/(2*D)
Wpump=dP*v*A
Q=v*A

T_w_1=T_3-2
T_w_2=T_3-6
Q_rej=m_dot_w*4.18*(T_w_1-T_w_2)
```

# Appendix B. Visual Basic

```
Private Sub Click_Click()
For i = 2 To 367
tmax = Cells(i, "B")
tmin = Cells(i, "C")
tg = Cells(i, "D")
t1 = 25
t2 = 25

'T3'
x = (tmax - tmin) / 17
t3 = 6 * x + tmin
Cells(i, "E") = t3

aa1 = (tmax + tmin) * 7 / 2
aa2 = (tmax + t3) * 11 / 2
tavamb = (aa1 + aa2) / 18
Cells(i, "I") = tavamb

If tg < tmin Then
teff = tg
t1 = 6
t2 = 24
ElseIf tg > tmax Then
teff = tavamb
Else
't1'
a1 = (tmax - tmin) / 7
b1 = tmin - 6 * a1
```

```
t1 = (tg - b1) / a1

't2'
a2 = (t3 - tmax) / 11
b2 = (tmax - 13 * a2)
t2 = (tg - b2) / a2
ar1 = (tg + tmin) * (t1 - 6) / 2
ar2 = tg * (t2 - t1)
ar3 = (tg + t3) * (24 - t2) / 2
ar = ar1 + ar2 + ar3
teff = ar / 18
End If
Cells(i, "J") = teff

If t1 < 13 Then
Cells(i, "F") = t1
Else
Cells(i, "F") = ""
End If
If t1 < 13 And t2 <= 24 Then
Cells(i, "G") = t2
Else
Cells(i, "G") = ""
End If

deltat = Cells(i, "G") - Cells(i, "F")
If deltat = 0 Then
Cells(i, "H") = 0
ElseIf deltat < 0 Then
Cells(i, "H") = 24 - Cells(i, "F")
```

```
Else
Cells(i, "H") = Cells(i, "G") - Cells(i, "F")
End If
Next i
End Sub
```

# Appendix C. ANSYS

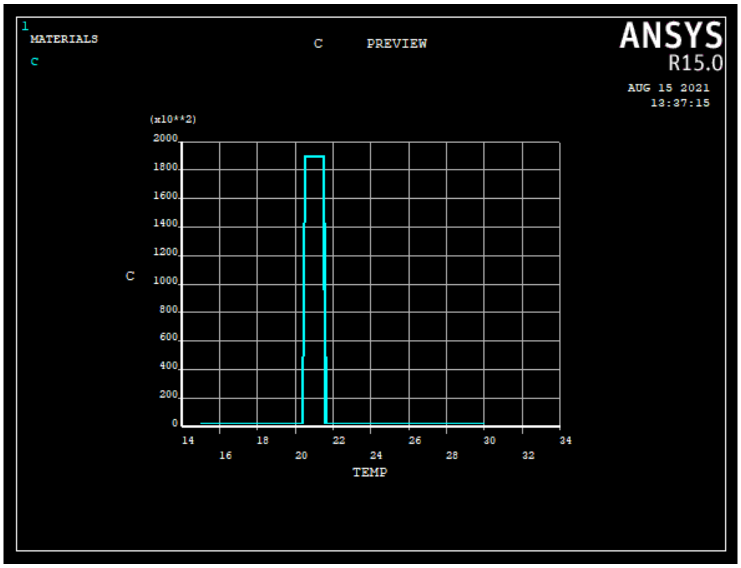


Figure C.1: The variation of RT 21HC specific heat with respect to the temperature and change of phase

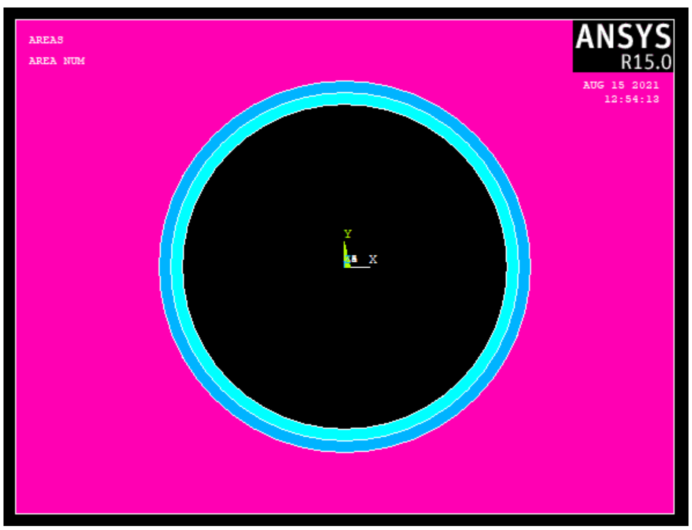


(a)

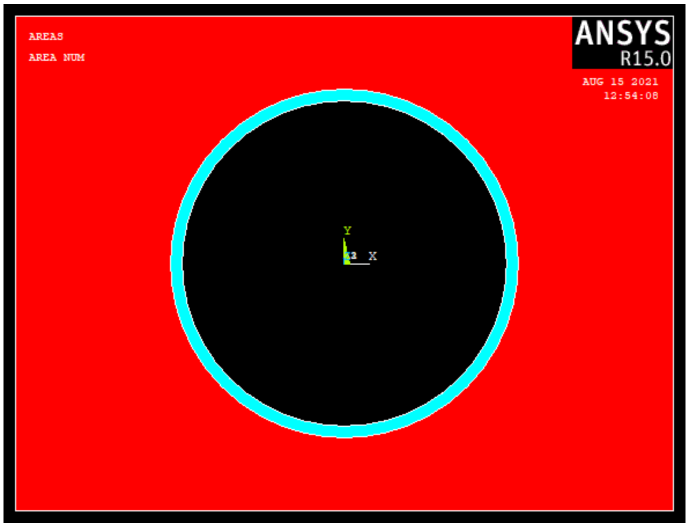


(b)

Figure C.2: The areas created in ANSYS (a) with and (b) without phase change materials